This dissertation has been 64–13,350
microfilmed exactly as received

LANE, Neal Francis, 1938–
A STUDY OF CERTAIN INELASTIC
ELECTRON–ATOM COLLISION PROCESSES.

The University of Oklahoma, Ph.D., 1964
Physics, general

University Microfilms, Inc., Ann Arbor, Michigan

Downloaded from SHAREOK. Persistent Handle URL: https://hdl.handle.net/11244/1815

THE UNIVERSITY OF OKLAHOMA

GRADUATE COLLEGE

A STUDY OF CERTAIN INELASTIC ELECTRON-ATOM COLLISION PROCESSES

A DISSERTATION

SUBMITTED TO THE GRADUATE FACULTY

in partial fulfillment of the requirements for the

degree of

DOCTOR OF PHILOSOPHY

BY

NEAL FRANCIS LANE

Norman, Oklahoma

1964

A STUDY OF CERTAIN INELASTIC ELECTRON-ATOM

COLLISION PROCESSES

A DISSERTATION

APPROVED FOR THE DEPARTMENT OF PHYSICS

BY

Chun C. Lin

J. Kurt Nielsen

[illegible] Fowler

Robert M. St. John

William N. Huff

DISSERTATION COMMITTEE

ACKNOWLEDGEMENTS

The author wishes to express his sincere appreciation to Professor Chun C. Lin for suggesting the research problems, and for his continued interest and invaluable advice.

It is also desired to thank Professor R. G. Fowler for enlightening discussions concerning certain aspects of the hydrogen problem, and Sydney Hamberger for helpful information regarding the experimental background.

Thanks are due George Shelton, Barbra Lafon, and Larry Barnes for aiding in the computations and coding many of the troublesome functions for the computer.

It is a pleasure to acknowledge my wife Joni Sue, whose continued support, both moral and financial, was a most important factor in the completion of this work. In a more direct way, she assisted in the research by coding a considerable amount of the numerical work for the computer. For these things and an uncountable number of others, the author is deeply grateful.

TABLE OF CONTENTS

		Page
LIST OF TABLES		vi
LIST OF ILLUSTRATIONS		ix
INTRODUCTION		1
Chapter		
I.	ELECTRON-ATOM COLLISIONS	4
	Strong Coupling	8
	Exact Resonance	9
	Near Resonance	10
	Approximate Forms of the Interaction Potential	11
	Schematic Model	16
II.	BORN AND BETHE APPROXIMATIONS	32
	Bethe Approximation	36
	Partial Wave Formulation of the Bethe Approximation	40
III.	METHOD OF RESONANCE DISTORTION	47
	Differential Equations	50
	Zeroth-Order Approximation (Exact Resonance)	53
	Resonance Distortion Approximation	56
IV.	GENERAL RESULTS	59
	Effect of the Magnitude of Coupling	59
	Effect of ΔE	61
	Comparison with Other Methods	65
V.	APPLICATION - $3^2S \rightarrow 3^2P$ TRANSITION OF Na BY ELECTRON IMPACT	73
VI.	TWO-CHANNEL APPROXIMATION FOR ELECTRON-ATOM COLLISION	84
VII.	DISCUSSION	96

TABLE OF CONTENTS (CONTINUED)

Chapter		Page
VIII.	THE CONTINUUM OF ATOMIC HYDROGEN	102
	Electron-Proton, Radiative Recombination . .	103
	Lowering of the Ionization Potential	105
	Electron-Proton Bremsstrahlung	121
IX.	THE CONTINUUM OF THE NEGATIVE HYDROGEN ION . .	127
	The Affinity Spectrum	128
	Free-Free Transitions in H^-	135
	Calculation of the Transition Probability .	137
	The Dipole Matrix Element	143
	Emission Spectrum	151
	Electron-Hydrogen, Elastic Scattering Cross Sections	153
	Integration over the Boltzmann Distribution	155
X.	COMPARISON OF RADIATIVE PROCESSES	160
	Emission Spectrum	161
	Dependence on Electron Temperature and Electron Density	163
	The Free-Bound H^- Continuum	164
	The Free-Free Continuum	166
XI.	TRANSITIONS BETWEEN FINE-STRUCTURE LEVELS IN MERCURY RESULTING FROM ELECTRON IMPACT . . .	195
	Wave Functions for the $6^3P_{0,1,2}$ States of Mercury	196
	Radial Functions	199
	Electron-Collision Problem	201
	Two-Channel Approximation	204
	Solution of the Differential Equations . . .	209
	Bethe I Approximation	211
	Exact-Resonance Results	213
APPENDIX I	. . . . .	216
APPENDIX II	. . . . .	225
LIST OF REFERENCES	. . . . .	227

LIST OF TABLES

Table		Page
I.	Values of ΔE(eV) Corresponding to Given Values of E(eV) and z	67
II.	Partial Cross Sections in Units of πa_o^2 of the 3s→3p Transitions of Na, Calculated by the Method of Resonance Distortion	75
III.	Partial Cross Sections in Units of πa_o^2 of the 3s→3p Transitions of Na, Calculated by the B'II Method	76
IV.	Total Cross Sections in Units of πa_o^2 and Partial Sums of Q_ℓ for the 3s → 3p Transition of Na	81
V.	Integrals of Three Normalized Associated Legendre Polynomials	89
VI.	Calculated Rates of Emission from Proton-Electron Recombination ($N_e = 10^{15}$ cm^{-3}), 1	109
VII.	Calculated Rates of Emission from Proton-Electron Recombination ($N_e = 10^{15}$ cm^{-3}), 2	110
VIII.	Calculated Rates of Emission from Proton-Electron Recombination ($N_e = 10^{15}$ cm^{-3}), 3	111
IX.	Calculated Rates of Emission from Proton-Electron Recombination ($N_e = 10^{16}$ cm^{-3}), 1	112
X.	Calculated Rates of Emission from Proton-Electron Recombination ($N_e = 10^{16}$ cm^{-3}), 2	113
XI.	Calculated Rates of Emission from Proton-Electron Recombination ($N_e = 10^{16}$ cm^{-3}), 3	114
XII.	Calculated Rates of Emission from Proton-Electron Recombination ($N_e = 10^{17}$ cm^{-3}), 1	115
XIII.	Calculated Rates of Emission from Proton-Electron Recombination ($N_e = 10^{17}$ cm^{-3}), 2	116

LIST OF TABLES (CONTINUED)

Table		Page
XIV.	Calculated Rates of Emission from Proton-Electron Recombination ($N_e = 10^{17}$ cm^{-3}), 3	117
XV.	Calculated Rates of Emission from Proton-Electron Recombination ($N_e = 10^{18}$ cm^{-3}), 1	118
XVI.	Calculated Rates of Emission from Proton-Electron Recombination ($N_e = 10^{18}$ cm^{-3}), 2	119
XVII.	Calculated Rates of Emission from Proton-Electron Recombination ($N_e = 10^{18}$ cm^{-3}), 3	120
XVIII.	Calculated Rates of Emission from Proton-Electron Bremsstrahlung, 1	124
XIX.	Calculated Rates of Emission from Proton-Electron Bremsstrahlung, 2	125
XX.	Calculated Rates of Emission from Proton-Electron Bremsstrahlung, 3	126
XXI.	Photodetachment and Attachment Cross Sections for H^-	130
XXII.	Calculated Rates of Emission from Free-Bound Transitions of H^-, 1	132
XXIII.	Calculated Rates of Emission from Free-Bound Transitions of H^-, 2	133
XXIV.	Calculated Rates of Emission from Free-Bound Transitions of H^-, 3	134
XXV.	Angular Integrals	147
XXVI.	The Elastic Cross Section σ_o	154
XXVII.	Calculated Rates of Emission from Free-Free Transitions in H^-, 1	158
XXVIII.	Calculated Rates of Emission from Free-Free Transitions in H^-, 2	159
XXIX.	Eigenfunctions Ψ_{LSJM} in Terms of $LmSm_s$ Basis Functions (written as ψ_{mm_s}) for $L = S = 1$.	198
XXX.	The Matrix $U_{JM,J'M'}$	205

LIST OF TABLES (CONTINUED)

Table		Page
XXXI.	Partial Cross Sections (units of πa_o^2) for the $6^3P_1 \rightarrow 6^3P_2$ Transition in Mercury in the Two Channel, and Bethe I, Exact-Resonance, Approximations	214
XXXII.	Total Cross Sections (units of πa_o^2) for the $6^3P_1 \rightarrow 6^3P_2$ Transitions in Mercury in the Two-Channel, Exact-Resonance, Approximation	214
A.	Calculated Values of (EE), (EB), (AB), and Percentage Differences for a = 1.0 a_o, and k_o^2 = 2.3 a.u., 1	222
B.	Calculated Values of (EE), (EB), (AB), and Percentage Differences for a = 1.0 a_o and k_o^2 = 2.3 a.u., 2	223
C.	A Comparison of (EE), (EB), and (AB) for Several Choices of the Radius a and Depth k_o^2	224

LIST OF ILLUSTRATIONS

Figure		Page
1.	Matrix Elements for 2s → 2p(m) in Hydrogen . .	15
2.	Partial Cross Sections Q_ℓ^{SMRD} (ΔE) for Different Values of ΔE(eV) with E = 13.6 eV and A = 3.0, Calculated by Using the Schematic Model (units πa_o^2)	28
3.	Partial Cross Sections Q_ℓ^{SMRD} (ΔE = 0) for Different Values of A, and E = 13.6 eV (units πa_o^2)	30
4.	Partial Cross Sections Q_ℓ^{SMRD} (ΔE = 1.144 eV) for Different Values of A, and E = 13.6 eV (units πa_o^2)	31
5.	Orientation of Momentum Vectors	35
6.	Orientation of Position and Momentum Vectors .	42
7.	Collision Strengths Ω_ℓ^{RD} in the Case of Exact Resonance for Several Values of the Line Strength s^2	60
8.	Values of $\Omega_\ell^{RD}/(2\ell + 1)$ for Different ℓ and ΔE = 0 in Terms of the Line Strength s^2	62
9.	Values of $\Omega_\ell^{RD}/(2\ell + 1)$ for Different ℓ and ΔE = 2.0 eV in Terms of the Line Strength s^2 . . .	63
10.	Collision Strengths Ω_ℓ^{RD} with s^2 = 19.3 for Several Values of ΔE (eV)	64
11.	Values of $\Omega_\ell^{RD}/(2\ell + 1)$ for Different ℓ and s^2 = 19.3 in Terms of ΔE $(eV)^{-1}$	66
12.	Bethe II Collision Strengths $\Omega_\ell^{B'II}$ with s^2 = 19.3 for Several Values of ΔE (eV)	70

LIST OF ILLUSTRATIONS (CONTINUED)

Figure		Page
13.	Collision Strengths Ω_ℓ^{RD} for ΔE = 0, 0.5, 3.0 eV, and $\Omega_\ell^{B'II}$ for ΔE = 0.5, 3.0 eV. (The upper of the two solid and of the two dashed curves correspond to the Bethe II method, and the lower, the Resonance-Distortion method.)	71
14.	Partial Cross Sections Q_ℓ^{RD}, $Q_\ell^{B'I}$, $Q_\ell^{B'II}$, and $\frac{1}{2} Q_\ell^{max}$ for Na, $3^2s \rightarrow 3^2p$, by Electron Impact, with ΔE = 2.104 eV and s^2 = 19.0 for an Incident Energy E = 10.520 eV	77
15.	Partial Cross Sections Q_ℓ^{RD}, $Q_\ell^{B'I}$, $Q_\ell^{B'II}$, and $\frac{1}{2} Q_\ell^{max}$ for Na, $3^2s \rightarrow 3^2p$, by Electron Impact, with ΔE = 2.104 eV and s^2 = 19.0 for an Incident Energy E = 33.660 eV	78
16.	Total Cross Sections Q^{RD}, $Q^{B'I}$, $Q^{B'II}$, and Q^{CC} for Na, $3^2s \rightarrow 3^2p$, by Electron Impact. (The open circles refer to the absolute measurements of Christoph and the solid curve marked EXPT represents the relative measurements of Haft. The dashed curve represents Seaton's Close-Coupling Approximation Q^{CC}	80
17.	Collision Strengths Ω_ℓ^{RD} (s^2 = 19.0) and Ω_ℓ (2-Channel, A = 2.9, 4.0, 5.0) for Na, $3^2s \rightarrow 3^2p$, by Electron Impact, with ΔE = 2.104 eV. (The value of A = 2.9 corresponds to the relation $\|A\| = 2\|s\|/3$)	95
18.	Orientation of the Polarization and Propagation Vectors	140
19.	Orientation of the Electron Position Vector and the Final Momentum Vector	144
20.	Continuum Spectrum, T = 10,000°K	168
21.	Continuum Spectrum, T = 15,000°K	169
22.	Continuum Spectrum, T = 20,000°K	170
23.	Continuum Spectrum, T = 25,000°K	171
24.	Continuum Spectrum, T = 30,000°K	172
25.	Continuum Spectrum, T = 35,000°K	173

LIST OF ILLUSTRATIONS (CONTINUED)

Figure		Page
26.	Continuum Spectrum, T = 40,000°K	174
27.	Continuum Spectrum, T = 45,000°K	175
28.	Continuum Spectrum, T = 50,000°K	176
29.	Continuum Spectrum, T = 55,000°K	177
30.	Continuum Spectrum, T = 60,000°K	178
31.	Continuum Spectrum, T = 65,000°K	179
32.	Continuum Spectrum, T = 70,000°K	180
33.	Continuum Spectrum, T = 75,000°K	181
34.	Continuum Spectrum, T = 80,000°K	182
35.	Continuum Spectrum, T = 85,000°K	183
36.	Continuum Spectrum, T = 90,000°K	184
37.	Continuum Spectrum, T = 95,000°K	185
38.	Continuum Spectrum, T = 100,000°K	186
39.	Continuum Emission for λ = 3000 A°, T = 25,000°K	187
40.	Continuum Emission for λ = 5000 A°, T = 25,000°K	188
41.	Continuum Emission for λ = 3000 A°, T = 50,000°K	189
42.	Continuum Emission for λ = 5000 A°, T = 50,000°K	190
43.	Continuum Emission for λ = 3000 A°, T = 75,000°K	191
44.	Continuum Emission for λ = 5000 A°, T = 75,000°K	192
45.	Continuum Emission for λ = 3000 A°, T = 100,000°K	193
46.	Continuum Emission for λ = 5000 A°, T = 100,000°K	194
47.	Energy Levels of Mercury	196
48.	Comparison of r R_{6s} Calculated by Hartree's Function (solid curve) and a Nodeless Orbital (dashed curve)	202

INTRODUCTION

It is well known that in atomic processes where the interaction between, say, a free (i.e., unbound) electron and an atom gives rise to an internal atomic transition, the probabilities (related to the inelastic-collision cross sections) of possible transitions depend not only on the properties of the initial and final atomic states, but on the properties of all other atomic states as well. Thus, an exact treatment of such a problem is a hopelessly complicated application of quantum mechanics to an infinity of interacting (i.e., coupled) states. Fortunately, however, it often happens that only a small number of states are strongly coupled (i.e., only the influence of a small number of states appreciably affects the transition probability between two particular states). In fact, there are many instances when only the initial and final atomic states are strongly coupled. This often occurs when the two states are in near resonance (i.e., the energy separation of the two states is small).

Collision problems involving near resonance and strong coupling are found to be somewhat troublesome since the standard weak-coupling, approximate methods such as Born

Approximation, and the Method of Distorted Waves give poor results. In fact, in the partial wave analysis, the Born Approximation is found to give partial cross sections in excess of the limits imposed by conservation. Two methods have been proposed which satisfy conservation. However, both of these methods consist in modification of the standard Born Approximation. It would seem more desirable to have a method of solution which incorporates the two distinguishing characteristics of the problem (i.e., near resonance and strong coupling) in a more fundamental way.

A method (called the method of resonance distortion) is developed in this thesis to handle electron-collision-induced atomic transitions under conditions of near resonance and strong coupling between the initial and final states. The scheme involves an iteration procedure based on the zeroth-order solution for the case of exact resonance. In cases where the coupling is weak, the resonance-distortion results are found to reduce to those of the Method of Distorted Waves.

Electron-atom collisions accompanied by the emission of radiation are handled in a distinctly different way. With the particles and the radiation field taken together as the system, one may employ the standard time-dependent perturbation approach in determining cross sections for various processes.

For hydrogen, four radiative processes are possible:

two-body recombination of protons and electrons, proton-electron bremsstrahlung, free-bound transitions causing the formation of H^-, and free-free transitions in H^-. Because of the importance of hydrogen in plasma research, it is important to be able to analyze the continuous emission spectrum with respect to these processes. The least familiar of the four, free-free transitions in H^-, is investigated, and the resulting emission compared with that due to recombination, bremsstrahlung, and free-bound of H^-. It is found that in cases where the degree of ionization of hydrogen remains small, the free-free process becomes significant for large temperatures, say $T = 50{,}000^\circ K$. Such conditions may be found in cases where thermal equilibrium is absent (i.e. Saha equation invalid), or where other gases are present, ensuring charge neutrality without a necessarily high proton density.

Finally, cross sections are calculated for the $6^3P_1 \rightarrow 6^3P_2$ transition in mercury under the assumption of exact resonance. Such cross sections are important in establishing the population densities of these states. The energy dependence of the cross sections is found to be consistent with the experimental determination.

CHAPTER I

ELECTRON-ATOM COLLISIONS

The theoretical approach to scattering phenomena is basically quite simple. One need only obtain the wave function Ψ which describes the whole system (this includes the atomic system and scattered particles). A detailed analysis of the properties of this function will yield all information necessary to the determination of cross sections for particular internal processes. Essential to the interpretation of this function are, of course, the boundary conditions imposed on it. These conditions specify, for example, the form of the continuum parts of Ψ for large separations of the atomic and scattered systems, and the flux of incident particles, relative to which the cross sections are determined; as in other wave mechanics problems, it is necessary to assume regularity of all solutions at the origin chosen. One is, however, unable to solve such a problem exactly, and it becomes necessary to resort to one's own physical intuition as well as the invaluable experience of others in order to find acceptable, approximate descriptions of the phenomena.

The problem to be dealt with most extensively in

this work is that of one electron, having linear momentum $\hbar\vec{k}_o$, incident upon an atomic system centered at $r = 0$[1-3]. Referring to the atomic coordinates as $\vec{r}_1$, $\vec{r}_2$, ..., $\vec{r}_z$ and those of the incident electron as $\vec{r}$, we find the hamiltonian for the system to be given by (atomic units, $e = m = \hbar = 1$)

$$H = -\tfrac{1}{2}\sum_i \nabla_i^2 - \tfrac{1}{2}\nabla^2 + H_e(\vec{r}_i,\vec{r}), \tag{1.1}$$

where

$$H_e(r_i,r) = -\sum_i \frac{z}{r_i} + \sum'_{ij} \frac{1}{r_{ij}} - \frac{z}{r} + \sum_i \frac{1}{|\vec{r} - \vec{r}_i|} . \tag{1.2}$$

It is then necessary to solve the Schroedinger equation

$$(H - E)\Psi(\vec{r}_i,\vec{r}) = 0 , \tag{1.3}$$

where E represents the total energy of the system

$$E = E_o + \frac{\hbar^2}{2m} k_o^2 , \tag{1.4}$$

E_o representing the energy of the atomic state prior to the scattering, and where $\vec{r}_i$ appearing as an argument represents the entire collection of atomic coordinates. The last two terms in Eq. (1.2) represent the interaction between the incident electron and the atomic system. When the scattered electron is close to the atomic system, this interaction could cause considerable distortion of the atomic system resulting in a polarization effect. However, since the r_i are bound within a small region of space ($\sim 10^{-8}$ cm), the two terms nearly cancel for large r; we have

$$-\frac{z}{r}+\sum_i^z \frac{1}{|\vec{r}_i-\vec{r}|}\sim -\frac{z}{r}+\sum_i^z \frac{1}{r}\sim 0\ . \qquad (1.5)$$

Since in the limiting case where the cancellation is exact, the wave function becomes

$$\Psi(\vec{r}_i,\vec{r}) \to F_m(\vec{r})\Psi_m(\vec{r}_i)\ , \qquad (1.6)$$

a logical manner in which to represent $\Psi(\vec{r}_i,\vec{r})$ is by means of the expansion[1]

$$\Psi(\vec{r}_i,\vec{r}) = \sum_m F_m(\vec{r})\Psi_m(\vec{r}_i)\ , \qquad (1.7)$$

where the functions Ψ_m form a complete set over the space $\vec{r}_i$ and the $\vec{r}$ dependence is carried in the coefficients F_m. Substitution of Ψ as given by Eq. (1.7) into Eq. (1.3) yields

$$\sum_m F_m(\vec{r})\left\{-\tfrac{1}{2}\sum_i \nabla_i^2-\sum_i\frac{z}{r_i}+\sum_{ij}{}'\frac{1}{r_{ij}}\right\}\Psi_m(\vec{r}_i)$$
$$=\sum_m\left(\tfrac{1}{2}\nabla^2+\frac{z}{r}-\sum_i\frac{1}{|\vec{r}_i-\vec{r}|}\right\}F_m(\vec{r})\,\Psi_m(\vec{r}_i)\ , \qquad (1.8)$$

which upon multiplication by $-2\Psi_{m'}^*(\vec{r}_i)d\vec{r}_i$ and integration over all of the atomic coordinates becomes

$$(\nabla^2+k_{m'}^2)F_{m'}(\vec{r}) = \sum_m U_{m'm}(\vec{r})F_m(\vec{r})\ , \qquad (1.9)$$

where

$$U_{m'm}(\vec{r}) = \frac{2M}{\hbar^2}V_{m'm}(\vec{r}) = \frac{2M}{\hbar^2}\int \Psi_{m'}^*(\vec{r}_i)V(\vec{r}_i,\vec{r})\Psi_m(\vec{r}_i)d\vec{r}_i, \qquad (1.10)$$

$$V(\vec{r}_i,\vec{r}) = -\frac{z}{r} + \sum_i \frac{1}{|\vec{r}_i - \vec{r}|}, \tag{1.11}$$

$$k_{m'}^2 = k_o^2 + \frac{2M}{\hbar^2}(E_o - E_{m'}) . \tag{1.12}$$

It may be seen from Eq. (1.7) that the function $F_m(\vec{r})$ describes completely the behavior of the scattered electron for the atom in state m, and that the asymptotic behavior of this function will indicate the flux distribution of the outgoing electrons and thus the cross section for a process in which the final atomic state is represented by m. For a problem in which the initial state is represented by o, the functions $F_m(\vec{r})$ must satisfy the conditions

$$\begin{aligned} F_o(\vec{r}) &\sim \exp(i\vec{k}_o\cdot\vec{r}) + \frac{1}{r} f_o(\theta,\varphi) \exp(ik_o r), \\ F_m(\vec{r}) &\sim \frac{1}{r} f_m(\theta,\varphi) \exp(ik_m r),\ m \neq 0 . \end{aligned} \tag{1.13}$$

It is assumed that Ψ is normalized such that the number of scattered electrons per unit volume at $\vec{r}$ coming off with the atomic system left in the mth state is $|F_m(\vec{r})|^2$. We obtain, then, the outgoing flux of such electrons for large r into solid angle $d\Omega$ as

$$v_n \frac{1}{r^2} |f_m(\theta,\varphi)|^2 (r^2 d\Omega) . \tag{1.14}$$

If in the incident beam, the density of particles is held at $1/cm^3$, then the incident flux is simply v_o. The

differential cross section $I_m d\Omega$ is defined as the number of particles per unit area per unit time which come off within $d\Omega$ having given rise to a transition o→m, per unit incident intensity. Thus we have[1]

$$I_m(\theta,\varphi)d\Omega = \frac{k_m}{k_o} |f_m(\theta,\varphi)|^2 d\Omega \ ; \qquad (1.15)$$

similarly for the elastic cross section

$$I_o(\theta,\varphi)d\Omega = |f_o(\theta,\varphi)|^2 d\Omega \ . \qquad (1.16)$$

It should be pointed out that the plane wave part of $F_o(\vec{r})$ is not considered here since in actuality it should be replaced by a wave packet of width large compared to the region of interaction but negligible compared to the separation of atomic system and measuring apparatus. In other words, except for a very small region surrounding the $\vec{k}_o$ axis, only the second term in $F_o(\vec{r})$ is significant. The total cross section is obtained by integrating the differential cross section over all space as

$$Q(o\to m) = \int I_m(\theta,\varphi)d\Omega \ . \qquad (1.17)$$

Strong Coupling

It is often the case that for certain transitions the coupling between two states is so strong that the influence of all other states may be neglected. Say o and n represent two such strongly coupled states, where o refers to the initial atomic state. It is then possible to consider

in Eq. (1.9) only the two coupled equations[4]

$$(\nabla^2 + k_o^2 - U_{oo})F_o = U_{on}F_n \ , \tag{1.18}$$

$$(\nabla^2 + k_n^2 - U_{nn})F_n = U_{no}F_o \ . \tag{1.19}$$

In cases where U_{oo}, U_{nn}, and U_{on} are small, it is sometimes valid to set $U_{oo} = U_{nn} = 0$ and solve Eq. (1.19) for F_n, having replaced F_o by $\exp(i\vec{k}_o \cdot \vec{r})$. This is the familiar First Born Approximation[1-3] (BI), the validity of which depends on the matrix elements being small as compared to the incident energy of the electron. The Born approximation is usually good only for relatively large incident energies. Often the situation arises where U_{on} is small but U_{oo} and U_{nn} are not. A method suitable in this case is that of Distorted Waves[1-2], in which U_{oo} and U_{nn} are retained. The function F_o is first determined from Eq. (1.18), neglecting the term $U_{on}F_n$. This function is then inserted in Eq. (1.19) which is solved for F_n. Again, the validity of this method depends on U_{on} being small.

Exact Resonance

In cases where U_{on} is not small, neither of the two previous methods is satisfactory and it is necessary to treat the coupling in a more balanced manner. In the case of exact resonance (i.e., $k_n = k_o$, $U_{nn} = U_{oo}$), Eqs. (1.18) and (1.19) may be uncoupled exactly giving[4]

$$(\nabla^2 + k_o^2 - U_{oo} \mp U_{on})(F_o \pm F_n) = 0. \tag{1.20}$$

Defining, in the usual way, the phase shifts η_ℓ and δ_ℓ for $F_o + F_n$ and $F_o - F_n$ respectively, we obtain for F_n (assuming spherically symmetric potentials)

$$F_n \sim r^{-1} \exp(ik_o r) \frac{1}{4ik_o} \sum_\ell (2\ell + 1)(e^{2i\eta_\ell} - e^{2i\delta_\ell}) P_\ell(\cos\theta). \tag{1.21}$$

The differential cross section for the transition o→n is then given by

$$I_n(\theta)d\Omega = \frac{1}{16k_o^2} \left| \sum_\ell (e^{2i\eta_\ell} - e^{2i\delta_\ell})(2\ell + 1) P_\ell(\cos\theta) \right|^2 d\Omega , \tag{1.22}$$

and the total cross section becomes

$$Q(o\to n) = \frac{\pi}{k_o^2} \sum_\ell (2\ell + 1) \sin^2(\eta_\ell - \delta_\ell) . \tag{1.23}$$

Near Resonance

When exact resonance is not present, there is no exact way to decouple the equations, and a more complicated method of solution must be invoked. In some instances[2] numerical methods have been tried, however in most cases these are quite complicated and do not lend themselves to very extensive physical interpretation. A new method for this type of problem has been developed. It consists of first solving the exact resonance problem for the function F_o, which will be called $F_o^{(o)}$; then Eq. (1.19) is solved for F_n, replacing F_o by $F_o^{(o)}$. The method, called resonance-distortion, is similar to the method of distorted waves in

that the former method assumes close coupling in the zeroth order while the latter starts with zero coupling. In the following chapters the resonance-distortion method is discussed in detail. Along with the description are included applications and detailed comparisons with other methods.

Approximate Forms of the Interaction Potential

In the present work, we will be concerned primarily with the special class of electron-atom collisions which involve (i) strong coupling, (ii) a long-range interaction potential, and (iii) near resonance; however, the resonance-distortion method is not restricted to such problems.

It has been known for some time[3] that several collision-induced atomic transitions show strong coupling, for example, 2s→2p of Hydrogen (It was found that the coupling here was so strong that the consideration of these states considerably reduced the 1s→2p cross section in agreement with experiment), $2^1s \rightarrow 2^1p$, $2^3s \rightarrow 2^3p$ of Helium, 4s→4p, 3d→4p of Ca^+ and 3s→3p of Sodium. This last transition will be used as an application of resonance distortion. These transitions are all optically allowed and of the form $n',\ell,m' \rightarrow n,\ell\pm1,m$; such transitions have long-range interactions[5], which in the partial wave picture render several partial waves important.

In many instances, if we are dealing only with single excitation, the wave function of the atom can be represented approximately by the one-electron orbital of the

excited electron $\psi_{n\ell m}(\vec{r}_1) = R_{n\ell}(r_1)Y_{\ell m}(\hat{r}_1)$. (This is, of course, not always valid, especially for cases where the exchange effects of the atomic electrons must be considered, e.g., He(2^3s-2^3p)). However, extension of the treatment in this section to these cases can be made very easily and will not be considered here. In Eq. (1.11) this amounts to considering z - 1 electrons along with the nucleus as making up the core of charge +1; the remaining electron (coordinate $\vec{r}_1$) along with the core represents the scattering field seen by the incident electron. We have, then, for the coupling matrix element

$$U_{no}(\vec{r}) = 2 \int \psi^*_{n\ell m}(\vec{r}_1) \left[\frac{1}{|\vec{r}_1 - \vec{r}|} - \frac{1}{r} \right] \psi_{n'\ell'm'}(\vec{r}_1)d\vec{r}_1$$

$$= \sum_{\lambda=0}^{\infty} \left(\frac{8\pi}{2\lambda + 1} \right) y_\lambda(n\ell,n'\ell'|r) \sum_{\mu=-\lambda}^{\lambda} h_{\lambda\mu}(\ell m,\ell'm')Y^*_{\lambda\mu}(\hat{r}), \qquad (1.24)$$

where

$$h_{\lambda\mu} = \int Y^*_{\ell m}(\hat{r}_1)\ Y_{\lambda\mu}(\hat{r}_1)\ Y_{\ell'm'}(\hat{r}_1)d\hat{r}_1$$

$$= \left(\frac{2\lambda + 1}{4\pi} \right)^{\frac{1}{2}} C^\lambda(\ell m,\ell'm'), \qquad (1.25)$$

$$y_\lambda(n\ell,n'\ell'|r) = \frac{1}{r^{\lambda+1}} \int_0^r R_{n\ell}(r_1)r_1^{\lambda+2}R_{n'\ell'}(r_1)dr_1$$

$$+ r^\lambda \int_r^\infty R_{n\ell}(r_1)r_1^{1-\lambda}\ R_{n'\ell'}(r_1)dr_1 \sim \frac{s_\lambda(n\ell,n'\ell')}{r^{\lambda+1}}, \qquad (1.26)$$

and where we have made use of the multipole expansion

$$\frac{1}{|\vec{r}_1 - \vec{r}|} = \sum_{\lambda=0}^{\infty} \frac{4\pi r_<^{\lambda}\, r_>^{-(\lambda+1)}}{2\lambda+1} \sum_{\mu=-\lambda}^{\lambda} Y_{\lambda\mu}(\hat{r}_1)\, Y^*_{\lambda\mu}(\hat{r}) \ . \qquad (1.27)$$

The long-range behavior of U_{no} for optically allowed transitions (i.e., $\ell \to \ell \pm 1$) follows from the fact[5] that for large r

$$y_1(n\ \ell\pm1,\ n'\ell\,|r) \sim \frac{s_1(n\ \ell\pm1, n'\ell)}{r^2} \ , \qquad (1.28)$$

where s_1^2 is the line strength for the transition given by

$$s_1(n\ \ell\pm1,\ n'\ell) = \int_0^{\infty} R_{n\ \ell\pm1}(r_1)\, R_{n'\ell}(r_1) r_1^3 dr_1 \ . \qquad (1.29)$$

The line strength is related to the oscillator strength f by[6]

$$f = \frac{8\pi^2 mc}{3he^2} \frac{1}{g_1 \lambda} s_1^2 \ , \qquad (1.30)$$

where λ is the wave length corresponding to the energy separation, and g_1 is the statistical weight of the lower state. We see from Eq. (1.28) that for large r the line strength is a measure of the strength of coupling of the two states. The diagonal elements U_{oo} and U_{nn} can be calculated similarly, however they are found to fall off exponentially for large r. In problems involving allowed transitions, where the coupling is long-range, these short range functions are of minor importance.

In order to illustrate the behavior of these matrix

elements, we may consider a simple example such as the 2s→2p(m) transition in Hydrogen. The matrix elements are easily found to be (in Slater atomic units)

$$U_{oo} = -\tfrac{1}{4} e^{-r}(r^2 + 2r + 6 + \frac{8}{r}) , \qquad (1.31)$$

$$\overline{U_{nn}} = -\frac{1}{12} e^{-r}(r^2 + 6r + 18 + \frac{24}{r}) , \qquad (1.32)$$

$$(U_{on}) = \frac{4\sqrt{\pi}}{3} U(r)\, Y_1^m(\theta,\varphi) \quad (m=0, \pm 1) , \qquad (1.33)$$

where

$$\overline{U_{nn}} = \frac{1}{4\pi} \int U_{nn}(\vec{r})\, d\hat{r} , \qquad (1.34)$$

and

$$U(r) = \frac{1}{8\sqrt{3}} e^{-r}(3r^2 + 12r + 36 + \frac{72}{r} + \frac{72}{r^2}) - \frac{9}{\sqrt{3}\, r^2} , \qquad (1.35)$$

the averaging having been done merely to remove the angular dependence for comparison. Similarly, we employ

$$(U_{on})_{rms} = \left\{ \frac{1}{4\pi} \int |U_{on}^{m=o}(\vec{r})|^2 d\hat{r} \right\} = \frac{2}{3} U(r) . \qquad (1.36)$$

The behavior of these functions is illustrated in Figure 1, where the function $-2\sqrt{3}/r^2$ has been included to show the importance of the exponential part of U_{on}.

Near resonance often occurs for transitions between the same n, i.e., $n\ell \to n\,\ell\pm 1$. Here, a significant contribution to the total cross section comes from the partial waves of large ℓ, and the effects of U_{on} at small distances are

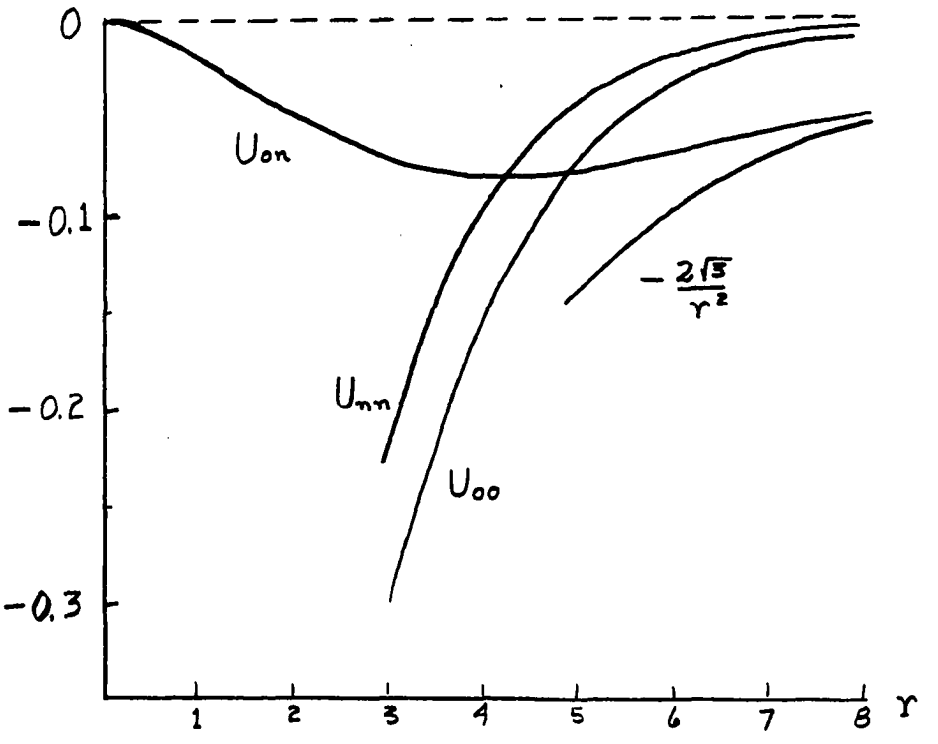

Figure 1

unimportant. Thus in the ns→np transition we shall make the simplification of replacing the true interaction potentials by

$$U_{oo} = U_{nn} = 0,$$

$$U_{on} = \frac{2M}{\hbar^2} \cdot \frac{2}{3}\sqrt{\pi}\ Y_{1m}(\theta,\varphi)\ \frac{s}{r^2} = U_{no}^{*}\ , \qquad (1.37)$$

The same set of potential functions was used by Seaton[7] in deriving the close-coupling formula and the modified version of the Bethe approximation. Throughout the calculation, the exchange between the incident and atomic electrons has been ignored; this is justifiable for collisions with

long-range interactions. However, the effect of electron exchange can be readily incorporated into the general formulation of the resonance-distortion method (see Ch. VII).

Schematic Model

The effects of using potential functions of the form given in Eqs. (1.37) can be illustrated to some extent by means of a schematic model (denoted by SM) in which it is assumed that

$$U_{oo} = U_{nn} = 0 \ , \qquad U_{on} = - A/r^2 \ , \tag{1.38}$$

A being an adjustable parameter. The advantage of treating such a model is the simplicity of solution. U_{on} in the schematic model may be thought of as representing some kind of angular average of U_{on} in Eqs. (1.37). We will consider the results of the Born approximation (same as Distorted waves for schematic model), exact resonance, and the resonance-distortion method.

In the Born approximation it is assumed that the wave function representing the incident particles is not distorted by the scattering center. This amounts to setting $F_o = \exp\ (i\vec{k}_o \cdot \vec{r})$ in Eq. (1.19) which then becomes

$$(\nabla^2 + k_n^2) F_n(\vec{r}) = - \frac{A}{r^2} \exp\ (i\vec{k}_o \cdot \vec{r}) \ . \tag{1.39}$$

We expand $\exp\ (i\vec{k}_o \cdot \vec{r})$ and $F_n(\vec{r})$ in terms of Legendre

polynomials as[1]

$$\exp\ (i\vec{k}_o\cdot\vec{r}) = \frac{1}{r}\sum_{\ell=0}^{\infty} i^{\ell}(2\ell+1)P_{\ell}(\cos\theta)j_{\ell}(k_o r), \qquad (1.40)$$

where

$$j_{\ell}(k_o r) = \left(\frac{\pi r}{2k_o}\right)^{\frac{1}{2}} J_{\ell+\frac{1}{2}}(k_o r)\ , \qquad (1.41)$$

and

$$F_n(\vec{r}) = \frac{1}{r}\sum_{\ell=0}^{\infty} i^{\ell}(2\ell+1)P_{\ell}(\cos\theta)\ F_{n,\ell}(r)\ . \qquad (1.42)$$

Eq. (1.39) then breaks up into an infinity of ordinary differential equations

$$\left[\frac{d^2}{dr^2} + k_n^2 - \frac{\ell(\ell+1)}{r^2}\right] F_{n,\ell}(r) = -\frac{A}{r^2}\left(\frac{\pi r}{2k_o}\right)^{\frac{1}{2}} J_{\ell+\frac{1}{2}}(k_o r)\ . \qquad (1.43)$$

This equation can be solved by the standard variation of parameters procedure.[8] The asymptotic form of $F_{n,\ell}$ is found to be

$$F_{n,\ell} \sim \frac{\pi A}{2(k_o k_n)^{\frac{1}{2}}}(-i)^{\ell}\exp\ (ik_n r)\int_o^{\infty} J_{\ell+\frac{1}{2}}(k_o r)\ J_{\ell+\frac{1}{2}}(k_n r)\ \frac{dr}{r}\ . \qquad (1.44)$$

From Eqs. (1.42) and (1.44) we see that the amplitude $f_n(\theta)$ is given by

$$f_n(\theta) = \frac{A\pi}{2(k_o k_n)^{\frac{1}{2}}}\sum_{\ell=o}^{\infty}(2\ell+1)P_{\ell}(\cos\theta)\int_o^{\infty} J_{\ell+\frac{1}{2}}(k_o r)\ J_{\ell+\frac{1}{2}}(k_n r)\ \frac{dr}{r}, \qquad (1.45)$$

which, when squared (absolute) and multiplied by $(k_n/k_o)d\Omega$

yields the differential cross section

$$I_n(\theta)d\Omega =$$

$$\frac{1}{k_o^2}\left(\frac{\pi A}{2}\right)^2 \left| \sum_\ell (2\ell + 1)P_\ell(\cos\theta) \int_o^\infty J_{\ell+\frac{1}{2}}(k_o r)\, J_{\ell+\frac{1}{2}}(k_n r)\, \frac{dr}{r} \right|^2 d\Omega. \tag{1.46}$$

Upon integration over θ and φ, we obtain the total cross section

$$Q(o\to n) = \frac{\pi}{k_o^2}(\pi A)^2 \sum_\ell (2\ell + 1) \left| \int_o^\infty J_{\ell+\frac{1}{2}}(k_o r)\, J_{\ell+\frac{1}{2}}(k_n r)\, \frac{dr}{r} \right|^2 , \tag{1.47}$$

which, making use of the relation[9]

$$\int_o^\infty J_{\ell+\frac{1}{2}}(k_o r)\, J_{\ell+\frac{1}{2}}(k_n r)\, \frac{dr}{r} = \frac{1}{2\ell + 1}\left(\frac{k_n}{k_o}\right)^{\ell+\frac{1}{2}} , \tag{1.48}$$

we may write as

$$Q^{SMBI}(o\to n) = \sum_{\ell=o}^\infty Q_\ell^{SMBI}(o\to n) = \frac{\pi}{k_o^2}\frac{(\pi A)^2}{2} \ln\left(\frac{1 + \sqrt{z}}{1 - \sqrt{z}}\right) , \tag{1.49}$$

where

$$z = k_n^2/k_o^2 = (E - \Delta E)/E , \tag{1.50}$$

and where the partial cross section $Q_\ell^{SMBI}(o\to n)$ is given by

$$Q_\ell^{SMBI}(o\to n) = \frac{\pi}{k_o^2}\,\frac{(\pi A)^2}{2\ell + 1}\left(\frac{k_n}{k_o}\right)^{2\ell+1} . \tag{1.51}$$

Eq. (1.49) is of the same form as the total Born cross

section obtained using the angular dependent potentials (see Eq. 2.23) and in fact the two give the same result if we set $A = 4s/\pi\sqrt{3}$, s^2 being the line strength for the transition o→n.[7]

For the case of exact resonance, Eqs. (1.18) and (1.19) may be uncoupled exactly by introducing

$$F^{\pm} = F_o \pm F_n \ . \tag{1.52}$$

These functions satisfy the uncoupled equations

$$(\nabla^2 + k_o^2 \pm A/r^2)F^{\pm} = 0 \ , \tag{1.53}$$

which, upon substitution of the usual partial wave expansion

$$F^{\pm}(\vec{r}) = \frac{1}{r}\sum_{\ell=o}^{\infty} i^{\ell}(2\ell + 1)F_{\ell}^{\pm}(r)P_{\ell}(\cos\theta) \ , \tag{1.54}$$

become

$$\left[\frac{d^2}{dr^2} + k_o^2 - (P_{\pm}^2 - \tfrac{1}{4})/r^2\right] F_{\ell}^{\pm}(r) = 0 \ , \tag{1.55}$$

where

$$P_{\pm} = [(\ell + \tfrac{1}{2})^2 \mp A]^{\frac{1}{2}} \ , \tag{1.56}$$

and thus

$$F_{\ell}^{\pm} = a_{\pm}\left(\frac{\pi r}{2k_o}\right)^{\frac{1}{2}} J_{P_{\pm}}(k_o r) \tag{1.57}$$

Here $J_{P_{\pm}}(k_o r)$ is the Bessel function of the first kind of

order $P_{\pm}$ and is the solution regular at the origin; the $a_{\pm}$ are constant coefficients. Considering the asymptotic conditions for F_o and F_n, which are given in Eqs. (1.13), the partial wave expansion of exp $(i\vec{k}_o \cdot \vec{r})$ given in Eq. (1.40), and the relation

$$\left(\frac{\pi r}{2k_o}\right)^{\frac{1}{2}} J_{\ell+\frac{1}{2}}(k_o r) \sim \frac{1}{k_o} \sin\,(k_o r - \ell\pi/2)\ , \qquad (1.58)$$

we find the asymptotic conditions for $F_{o,\ell}$ and $F_{n,\ell}$ to take the form

$$F_{o,\ell} = \tfrac{1}{2}(F_\ell^+ + F_\ell^-) \sim \frac{1}{k_o} \sin\,(k_o r - \ell\pi/2) + c_{o,\ell} \exp\,(ik_o r), \qquad (1.59)$$

$$F_{n,\ell} = \tfrac{1}{2}(F_\ell^+ - F_\ell^-) \sim c_{n,\ell} \exp\,(ik_o r)\ ; \qquad (1.60)$$

the collision amplitude $f_n(\theta)$ is then expressed as

$$f_n(\theta) = \sum_{\ell=0}^{\infty} i^\ell (2\ell + 1)\, c_{n,\ell}\ P_\ell(\cos\,\theta)\ . \qquad (1.61)$$

In order to determine the coefficients $a_{\pm}$, we must examine the asymptotic behavior of $F_{o,\ell}$ and $F_{n,\ell}$. For the elastic scattering function we have

$$F_{o,\ell} = \tfrac{1}{2}\left(\frac{\pi r}{2k_o}\right)^{\frac{1}{2}} [a_+ J_{P_+}(k_o r) + a_- J_{P_-}(k_o r)] \sim$$

$$\frac{1}{2k_o} [a_+ \cos\,(k_o r - \pi/4 - P^+\pi/2) + a_- \cos\,(k_o r - \pi/4 - P^-\pi/2)] \qquad (1.62)$$

$$= \frac{1}{4k_o} \{a_+ \exp i(k_o r - \pi/4 - P^+\pi/2) + a_+ \exp [-i(k_o r - \pi/4 - P^-\pi/2)] + a_- \exp i(k_o r - \pi/4 - P^-\pi/2) + a_- \exp [-i(k_o r - \pi/4 - P^-\pi/2)]\} + \frac{1}{k_o} \sin (k_o r - \ell\pi/2) - \frac{1}{2ik_o} \exp i(k_o r - \ell\pi/2) + \frac{1}{2ik_o} \exp [-i(k_o r - \ell\pi/2)] = \frac{1}{k_o} \sin (k_o r - \ell\pi/2) + \frac{1}{4k_o} \exp ik_o r \{a^+ \exp [-i(\pi/4 + P^+\pi/2)] + a_- \exp [-i(\pi/4 + P^-\pi/2) - \frac{2}{i} \exp (-i\pi/2)\} + \frac{1}{4k_o} \exp (-ik_o r) \{a_+ \exp i(\pi/4 + P^+\pi/2) + a^- \exp i(\pi/4 + P^-\pi/2) + \frac{2}{i} \exp (i\ell\pi/2)\} . \quad (1.63)$$

Comparing Eqs. (1.59) and (1.63) we see that the first term of Eq. (1.63) represents the incident wave part; the remainder, then, should represent only scattered waves (i.e., outgoing waves). Thus the coefficient of $\exp (-ik_o r)$ must vanish, yielding

$$a_+ \exp (iP^+\pi/2) + a_- \exp (iP^-\pi/2) = 2i \exp i(\ell\pi/2 - \pi/4). \quad (1.64)$$

Similarly, the asymptotic form of $F_{n,\ell}$ is found to be

$$F_{n,\ell} = \tfrac{1}{2} \left(\frac{\pi r}{2k_o} \right)^{\frac{1}{2}} [a_+ J_{P_+}(k_o r) - a_- J_{P_-}(k_o r)] \sim \frac{1}{4k_o} \{a_+ \exp i(k_o r - \pi/4 - P^+\pi/2) + a_+ \exp [-i(k_o r - \pi/4 - P^+\pi/2)] - a_- \exp i(k_o r - \pi/4 - P^-\pi/2) - a_- \exp [-i(k_o r -$$

$$\pi/4 - P^-\pi/2)]\} = \frac{1}{4k_o} \exp ik_o r \{a_+ \exp [-i(\pi/4 + P^+\pi/2)] - a_- \exp [-i(\pi/4 + P^-\pi/2)]\} + \frac{1}{4k_o} \exp (-ik_o r)\{a_+ \exp i(\pi/4 + P^+\pi/2) - a^- \exp i(\pi/4 + P^-\pi/2)\} . \quad (1.65)$$

The asymptotic form of $F_{n,\ell}$ must contain outgoing waves only; thus the coefficient of $\exp (-ik_o r)$ must vanish, yielding

$$a_- = a_+ \exp [i(P_+ - P_-) \frac{\pi}{2}] . \quad (1.66)$$

Combining Eqs. (1.64) and (1.66), we find

$$\begin{aligned} a_+ &= i^{\ell+1} \exp [-i(P^+ + \tfrac{1}{2}) \frac{\pi}{2}] , \\ a_- &= i^{\ell+1} \exp [-i(P^- + \tfrac{1}{2}) \frac{\pi}{2}] . \end{aligned} \quad (1.67)$$

From Eqs. (1.62) and (1.67), we may write $F_{o,\ell}$ as

$$F_{o,\ell}(r) = \frac{i^{\ell+1}}{2} \left(\frac{\pi r}{2k_o} \right)^{\frac{1}{2}} \exp (-i\pi/4) \left[J_{P_+}(k_o r) \exp (-iP_+\pi/2) + J_{P_-}(k_o r) \exp (-iP_-\pi/2) \right] ; \quad (1.68)$$

this function will be used in the iteration method which follows. In order to determine the exact-resonance cross section for the schematic model, we must examine the asymptotic behavior of $F_{n,\ell}$. Comparing Eqs. (1.60) and (1.65) we observe that

$$c_{n,\ell} = \frac{1}{4k_o}\{a_+ \exp[-i(\pi/4 + P^+\pi/2)] - a_- \exp[-i(\pi/4 + P^-\pi/2)]\} = \frac{i^\ell}{4k_o}[\exp(-iP^+\pi/2) - \exp(-iP^-\pi/2)] . \quad (1.69)$$

From Eqs. (1.15) and (1.61) it follows that the total exact-resonance cross section for the schematic model is given by

$$Q^{SMEX}(o\to n) = 4\pi \sum_\ell (2\ell + 1)|c_{n,\ell}|^2 , \quad (1.70)$$

which by means of Eq. (1.69) becomes

$$Q^{SMEX}(o\to n) = \frac{\pi}{k_o^2} \sum_\ell (2\ell + 1) \sin^2 (P_+ - P_-)\frac{\pi}{2} . \quad (1.71)$$

Here, $P^+\pi/2$ and $P^-\pi/2$ may be identified with the standard partial phase shifts given in Eq. (1.23). It should be mentioned that the above treatment is invalid if P_+ becomes imaginary[10], i.e., if $A > (\ell + \frac{1}{2})^{\frac{1}{2}}$; thus for small ℓ the partial cross sections may have to be calculated by some other means. For the schematic model under exact-resonance conditions, the total cross section is found to diverge, as may be seen by examining $\sin^2[(P_+ - P_-)\pi/2]$ for large ℓ in Eq. (1.71). This model is, however, only for illustrative purposes and the divergence is of little concern. It is found, nevertheless that upon introduction of the inexactness (i.e., $E_o - E_n \neq 0$) the divergence disappears.

When $k_o \neq k_n$, we are faced with the task of treating the coupled equations

$$(\nabla^2 + k_o^2)F_o = -\frac{A}{r^2} F_n \ , \tag{1.72}$$

$$(\nabla^2 + k_n^2)F_n = -\frac{A}{r^2} F_o \ . \tag{1.73}$$

The resonance-distortion method, briefly described earlier, consists, in the case of the schematic model, of solving Eq. (1.73) for F_n in terms of F_o which is then replaced by $F_o^{(o)}$, the solution obtained under exact-resonance conditions. Expanding F_o in terms of partial waves in the form

$$F_o = \frac{1}{r} \sum_\ell i^\ell (2\ell + 1) P_\ell(\cos\theta)\ F_{o,\ell}(r) \ , \tag{1.74}$$

as was done for F_n in Eq. (1.42), we obtain for $F_{n,\ell}$

$$\left[\frac{d^2}{dr^2} + k_n^2 - \frac{\ell(\ell+1)}{r^2} \right] F_{n,\ell} = -\frac{A}{r^2} F_{o,\ell} \ . \tag{1.75}$$

Making use of the standard variation of parameters method of solution, we obtain for the asymptotic form

$$F_{n,\ell} \sim \frac{\pi A}{2(k_o k_n)^{\frac{1}{2}}} (-i)^\ell \exp(ik_n r) \int_o^\infty J_{\ell+\frac{1}{2}}(k_n r)$$

$$\times \left(\frac{2k_o}{\pi r} \right)^{\frac{1}{2}} F_{o,\ell}(r)\ \frac{dr}{r} \ . \tag{1.76}$$

It is interesting at this point to compare the above equation with the SM Born result given by Eq. (1.44). In the latter, one has within the integral the function $J_{\ell+\frac{1}{2}}(k_o r)$ in place of $(2k_o/\pi r)^{\frac{1}{2}} F_{o,\ell}(r)$ found in Eq. (1.76). The pure Bessel

function results from the plane wave assumption for the elastic function, which is inherent in the Born approximation. In line with the resonance-distortion approximation, we replace $F_{o,\ell}$ in Eq. (1.76) by $F^{(o)}_{o,\ell}$ of Eq. (1.68) which was calculated for the case of exact resonance and is given by

$$\left(\frac{2k_o}{\pi r}\right)^{\frac{1}{2}} F^{(o)}_{o,\ell}(r) = \tfrac{1}{2}\, i^{\ell+1} \exp\,(-\tfrac{1}{4}\pi i)[J_{P_+}(k_o r) \exp\,(-iP_+\pi/2) + J_{P_-}(k_o r) \exp\,(-iP_-\pi/2)] \,. \qquad (1.77)$$

From Eqs. (1.76) and (1.77) we obtain for the collision amplitude

$$f_n(\theta) = \frac{\pi A}{4(k_o k_n)^{\frac{1}{2}}} \exp\,(-i\pi/4) \sum_{\ell=0}^{\infty} i^{\ell}(2\ell + 1)[I^{+}_{\ell} \exp\,(-iP_+\pi/2) + I^{-}_{\ell} \exp\,(-iP_-\pi/2)]P_{\ell}(\cos\,\theta) \,, \qquad (1.78)$$

where

$$I^{\pm}_{\ell} = \int_0^{\infty} J_{\ell+\frac{1}{2}}(k_n r)\, J_{P_{\pm}}(k_o r)\, \frac{dr}{r} \,. \qquad (1.79)$$

Considering Eq. (1.78), it follows in a straightforward manner that the resonance-distortion partial cross sections for the schematic model under conditions of near-resonance are given by

$$Q^{\mathrm{SMRD}}_{\ell}(o\to n) = \frac{\pi}{k_o^2} (\tfrac{1}{2}\pi A)^2 (2\ell + 1)[\, |I^{+}_{\ell}|^2 + |I^{-}_{\ell}|^2 + 2I^{+}_{\ell} I^{-}_{\ell} \cos\,\tfrac{1}{2}(P_+ - P_-)\pi] \,, \qquad (1.80)$$

where the superscript SMRD refers to schematic model (resonance-distortion). It may be easily shown that, as should of course be expected, Q_ℓ^{SMRD} reduces to Q_ℓ^{SMEX} of Eq. (1.71) in the limit of $k_n = k_o$. It is of interest to point out that the resonance-distortion method does not appear to be limited to cases of strong coupling since for small A, Q_ℓ^{SMRD} reduces to the Born approximation result Q_ℓ^{SMBI} given in Eq. (1.49), which should be valid in such a case. One finds that for any magnitude of A, $Q_\ell^{SMRD} \to Q_\ell^{SMBI}$ for large ℓ; the coupling, then, is said to be weak for large ℓ.

The radial integrals present in Eq. (1.80) may be evaluated in terms of the hypergeometric functions ${}_2F_1$, which in turn may be determined by their power series representation[11]

$$ {}_2F_1\ (a,b;c;z) = \sum_{P=0}^{\infty} \frac{(a)_P (b)_P}{(c)_P} \frac{(z)^P}{P!} , \tag{1.81} $$

where

$$ (a)_P = a(a+1) \ldots (a+P-1) . $$

We have then[9]

$$ I_\ell^{\pm} = \tfrac{1}{2} \left(\frac{k_n}{k_o} \right)^{\ell+\frac{1}{2}} \frac{\Gamma(a_\pm)}{\Gamma(1-b_\pm)\Gamma(a_\pm + b_\pm + 1)}\ {}_2F_1[a_\pm, b_\pm; a_\pm + b_\pm + 1; z], \tag{1.82} $$

where

$$ a_\pm = \tfrac{1}{2}(P_\pm + \ell + \tfrac{1}{2}) , $$

$$b_{\pm} = \tfrac{1}{2}(\ell + \tfrac{1}{2} - P_{\pm}) ,$$

$$a_{\pm} + b_{\pm} + 1 = \ell + \frac{3}{2} ,$$

$$Z = (k_n/k_o)^2 .$$

The variation of Q_ℓ^{SMRD} with ΔE is given in Figure 2. for several values of ℓ. The partial cross section for each ℓ is seen to increase steadily with decreasing ΔE, reaching a maximum for $\Delta E = 0$. Also plotted in Figure 2. is the maximum partial cross section allowed by conservation limits[1]

$$Q_\ell^{max}(o \to n) = \frac{\pi}{k_o^2} \Omega_\ell^{max} = \frac{\pi}{k_o^2} (2\ell + 1) . \qquad (1.83)$$

It is seen that the resonance-distortion partial cross sections satisfy conservation requirements even for $\Delta E = 0$. It is interesting to notice that the distribution in ℓ does not differ greatly for different ΔE.

The dependence of Q_ℓ^{SMRD} $(\Delta E = 0)$ on the coupling parameter A is given in Figure 3. There are two important things to notice here; first, for each different value of ℓ there is a clustering of points (and for some cases even oscillation) as the coupling A is increased, and secondly, the distribution in ℓ is sensitive to the degree of coupling. The clustering is evidence of a saturation of Q_ℓ with increasing A. This effect is intimately connected with particle conservation and is not present in the Born

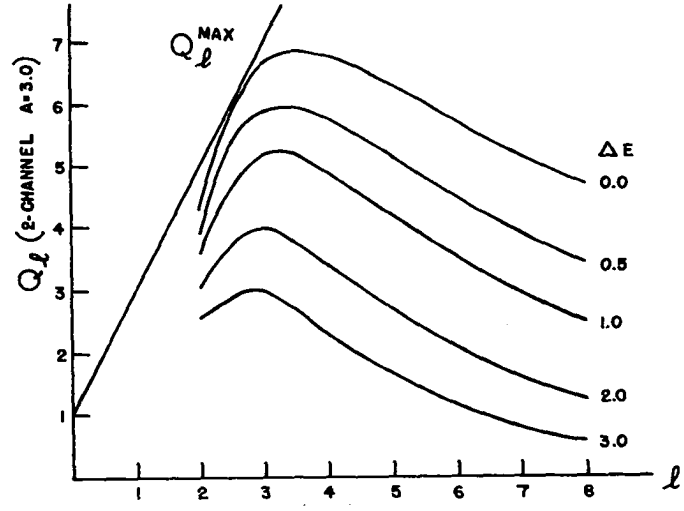

Figure 2. Partial Cross Sections Q_ℓ^{SMRD} (ΔE) for Different Values of ΔE(eV) with E = 13.6 eV and A = 3.0, Calculated by Using the Schematic Model (units πa_o^2).

approximation, sometimes causing the latter to actually exceed Q_ℓ^{max} for large values of A. This saturation effect will be discussed more in detail when the angular dependent potential functions are considered. The distribution in ℓ of the partial cross sections is related to the applicability of Born approximation, which is most suitable for problems in which many partial waves, all making small contributions, are necessary. We see from Figure 3 that the distribution is most uniform and the partial cross sections smallest for small A; this is in agreement with our analytic result that $Q_\ell^{SMRD} \rightarrow Q_\ell^{SMBI}$ for small A.

Introduction of the inexactness correction ΔE appears to decrease the cross sections in general as shown by Figure 4. The saturation effect is present just as in the exact-resonance case, and the distribution remains somewhat sensitive to the magnitude of the coupling parameter A. A careful comparison of Figures 3 and 4 shows that in the case of $\Delta E = 3eV$, the maxima of the inexact-resonance partial cross sections are shifted inward slightly as compared with those of the exact-resonance case. The various properties mentioned above have been pointed out so that when results of the more involved methods are analyzed, one may sort out which of these properties, for example, are related to the angular dependence of the coupling matrix element U_{on}.

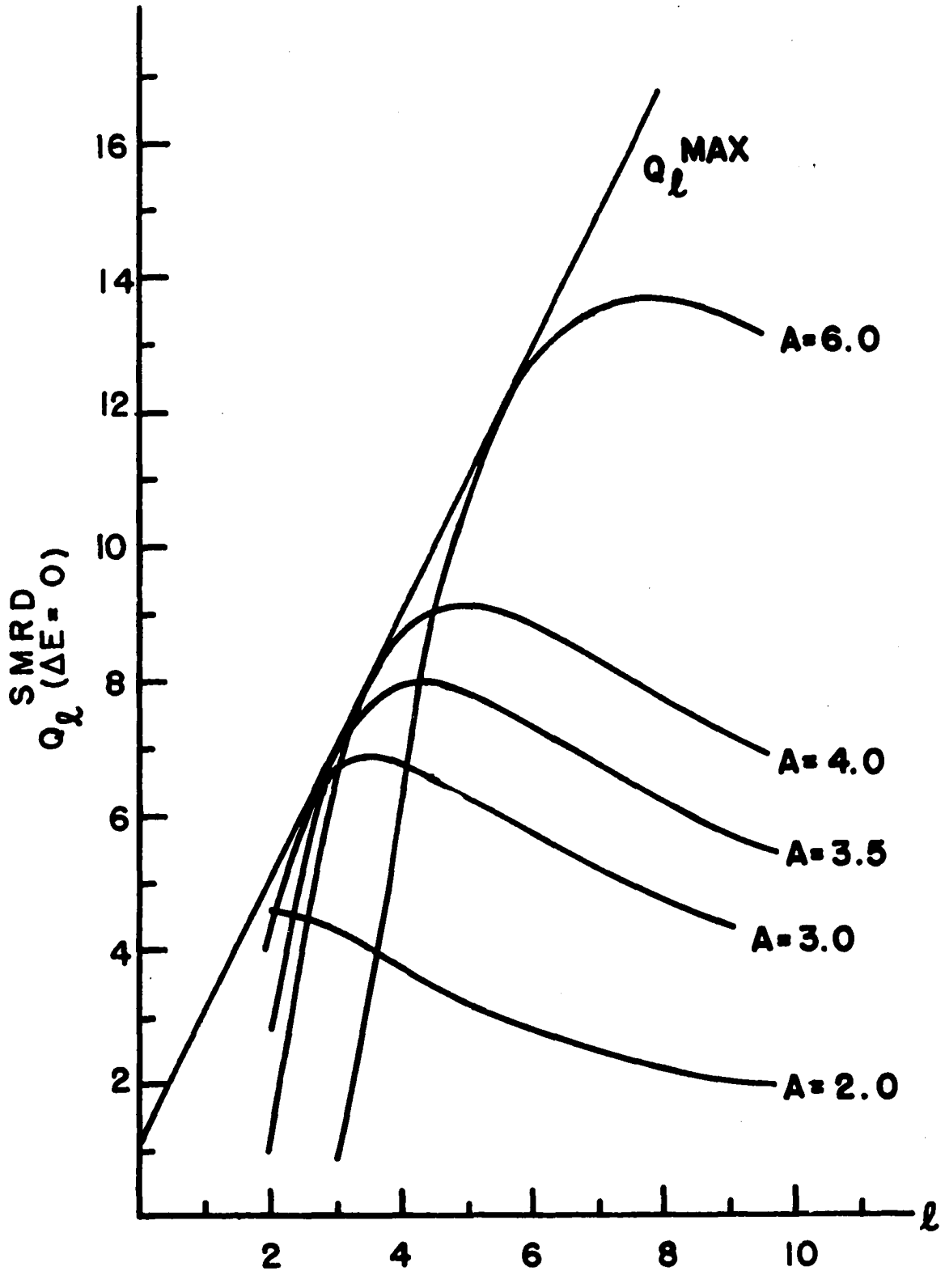

Figure 3. Partial Cross Sections Q_ℓ^{SMRD} ($\Delta E = 0$) for Different Values of A, and E = 13.6 eV (units of πa_o^2).

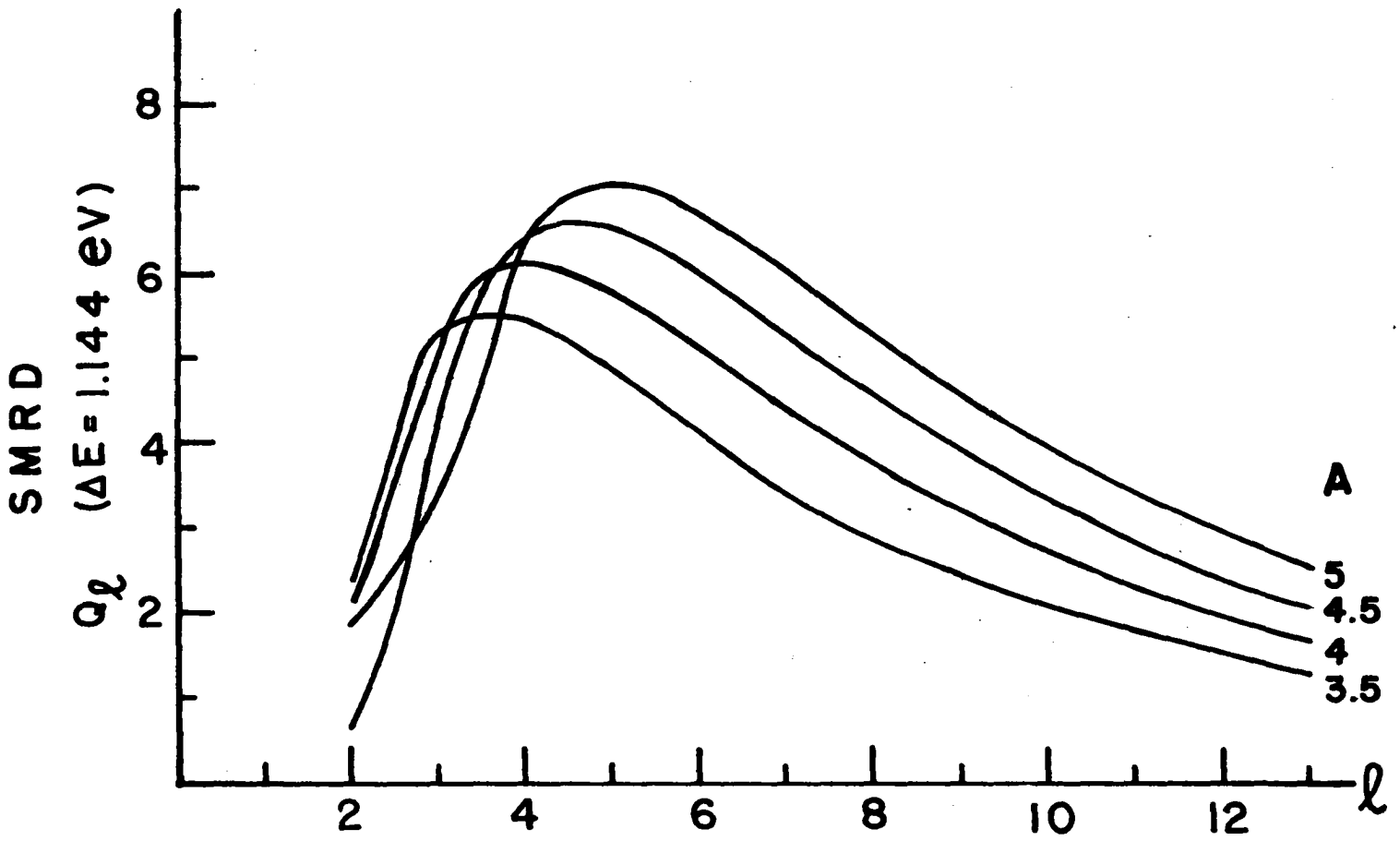

Figure 4. Partial Cross Sections Q_ℓ^{SMRD} ($\Delta E = 1.144$ eV) for Different Values of A, and E = 13.6 eV (units of πa_o^2).

CHAPTER II

BORN AND BETHE APPROXIMATIONS

As was mentioned in the previous chapter, there are several instances in electron-atom scattering where the coupling between the two states of interest is not strong and where one is interested in incident energies large enough so that it may be assumed the incident plane wave is not appreciably distorted by the scatterer and hence, to a zeroth-order approximation the elastic scattering function may be represented by

$$F_o(\vec{r}) = \exp\ (i\vec{k}_o \cdot \vec{r}) \ . \tag{2.1}$$

This amounts to neglecting the terms $U_{oo}F_o$ and $U_{on}F_n$ in Eq. (1.18). In keeping with the degree of approximation, one neglects $U_{nn}F_n$ in Eq. (1.19), which then becomes

$$(\nabla^2 + k_n^2)F_n = U_{no} \exp\ (i\vec{k}_o \cdot \vec{r}) \ . \tag{2.2}$$

Solving Eq. (2.2) then results in the first Born approximation (will be denoted as BI) for F_n and thus for the cross section. The Born approximation has for some time been a popular research tool, and an abundant supply of calculations is available in the literature.[1,2,3,11] However, in regard

to problems involving strong coupling and near resonance, with which we are primarily concerned here, the Born approximation is inadequate and usually gives a cross section very much larger than experiment.[3,7] A detailed derivation of the Born approximation will be presented here in order to illustrate a useful fact concerning choice of the axis of quantization, and to compare two methods of obtaining the Bethe approximation, which will be discussed.

We consider as before an electron having linear momentum $\hbar\vec{k}_o$ incident upon an atomic system consisting of one electron outside a core of charge +1. The total wave function is expanded in terms of atomic wave functions as in Eq. (1.7), and the scattered electron is described by F_n which, rewriting Eq. (2.2), is found to satisfy

$$(\nabla^2 + k_n^2)F_n(\vec{r}) = 2 \exp(i\vec{k}_o\cdot\vec{r}) \int \psi_n^*(\vec{r}_1)\, V(\vec{r}_1,\vec{r})\, \psi_o(\vec{r}_1)d\vec{r}_1 , \tag{2.3}$$

where $V(\vec{r}_1,\vec{r})$ is given in Eq. (1.11) with z = 1. A solution to this equation is easily obtained by means of the Green's function for the operator $\nabla^2 + k_n^2$, which is given by[1]

$$K(\vec{r},\vec{r}_2) = \frac{1}{4\pi}\frac{\exp(ik_n|\vec{r} - \vec{r}_2|)}{|\vec{r} - \vec{r}_2|} = K(\vec{r}_2,\vec{r}) . \tag{2.4}$$

Thus we have

$$F_n(\vec{r}) =$$

$$\frac{1}{2\pi}\int \exp(i\vec{k}_o\cdot\vec{r}_2)\left\{\frac{\exp(ik_n|\vec{r} - \vec{r}_2|)}{|\vec{r} - \vec{r}_2|}\right\}d\vec{r}_2 \int \psi_n^*(\vec{r}_1)V(\vec{r}_1,\vec{r}_2)\psi_o(\vec{r}_1)d\vec{r}_1 \tag{2.5}$$

For large values of r (r represents the distance of scattered electron from atom) one has the relation

$$|\vec{r} - \vec{r}_2| \sim r - \hat{n}\cdot\vec{r}_2 \ ,$$

where (2.6)

$$\hat{n} = \vec{r}/r \cong \vec{k}_n/k_n \ ,$$

and thus

$$K(\vec{r},\vec{r}_2) \underset{r\to\infty}{\sim} \frac{1}{4\pi r} \exp\ (ik_n r) \exp\ (-i\vec{k}_n\cdot\vec{r}_2) \ . \tag{2.7}$$

Asymptotically, then, we have that

$$F_n(\vec{r}) \sim \frac{\exp\ (ik_n r)}{2\pi r} \int \exp\ [i(\vec{k}_o - \vec{k}_n)\cdot\vec{r}_2]\ d\vec{r}_2$$
$$\times \int \psi_n^*(\vec{r}_1)\ V(\vec{r}_1,\vec{r}_2)\ \psi_o(\vec{r}_1)\ d\vec{r}_1 \tag{2.8}$$

Comparing Eqs. (1.13) and (2.8) one obtains

$$I_n(\theta,\varphi) = \frac{k_n}{4\pi^2 k_o} \left| \int \exp\ [i(\vec{k}_o - \vec{k}_n)\cdot\vec{r}_2] d\vec{r}_2 \right.$$
$$\left. \times \int \psi_n^*(\vec{r}_1)\ V(\vec{r}_1,\vec{r}_2)\ \psi_o(\vec{r}_1)\ d\vec{r}_1 \right|^2 . \tag{2.9}$$

To facilitate calculation of the total cross section, it is convenient to introduce the relative momentum coordinates $\vec{K}$, where

$$K^2 = |\vec{k}_o - \vec{k}_n|^2 = k_o^2 + k_n^2 - 2k_o k_n \cos\theta \ , \tag{2.10}$$

and where θ is the scattering angle, i.e., $\vec{k}_o\cdot\vec{k}_n = k_o k_n \cos\theta$ (see Figure 5).

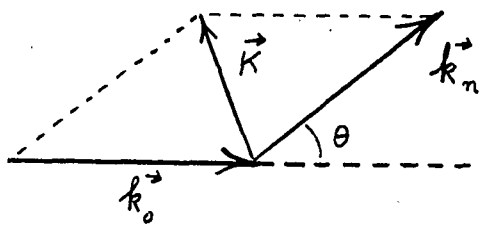

Figure 5

Differentiating Eq. (2.10) we obtain

$$K\, dK = k_o k_n \sin\theta\, d\theta \,. \tag{2.11}$$

The total cross section is given according to Eq. (1.17) as

$$Q(o\to n) = \int_0^{2\pi}\int_0^{\pi} I_n(\theta,\varphi) \sin\theta\, d\theta\, d\varphi \,. \tag{2.12}$$

We now choose to define

$$I_n(K,\varphi)\, dK\, d\varphi = I_n(\theta,\varphi)\, \frac{K\, dK\, d\varphi}{k_o k_n} \,, \tag{2.13}$$

and consequently

$$Q(o\to n) = \int_0^{2\pi}\int_{|k_o-k_n|}^{k_o+k_n} I_n(K,\varphi)\, dK\, d\varphi \,. \tag{2.14}$$

The potential according to Eq. (1.11) is given as

$$V(\vec{r}_1,\vec{r}) = \frac{1}{|\vec{r}_1 - \vec{r}|} - \frac{1}{r} ; \qquad (2.15)$$

the second term, however, makes no contribution to the integral because of the orthogonality of ψ_n and ψ_o. Making use of an expression due to Bethe,

$$\int \frac{\exp\ (i\vec{K}\cdot\vec{r}_1)}{|\vec{r} - \vec{r}_1|}\, d\vec{r}_1 = \frac{4\pi}{K^2} \exp\ (i\vec{K}\cdot\vec{r}) , \qquad (2.16)$$

we obtain

$$I_n(K,\varphi)\ dK\ d\varphi = \frac{4}{k_o^2}\frac{dK\ d\varphi}{K^3} \left| \int \exp\ (i\vec{K}\cdot\vec{r}_1)\ \psi_n(\vec{r}_1)\ \psi_o(\vec{r}_1)\ d\vec{r}_1 \right|^2 . \qquad (2.17)$$

Bethe Approximation

The standard Bethe approximation (will be denoted as B'I)[1] is obtained by expanding the function exp $(i\vec{K}\cdot\vec{r}_1)$ in Eq. (2.17) and retaining only the first two terms $1 + i\vec{K}\cdot\vec{r}_1$. This is valid for K small relative to r^{-1}, for r in the region of overlap of the atomic wave functions. In situations where K is not small (i.e., close encounters), this approximation may be expected to produce too large a cross section. In the past, several methods of correcting the Bethe approximation have been devised, including a reasonably successful scheme by Seaton.[7] This technique, called the close-coupling method, will be discussed in Chapter V.

We take γ as the angle between $\vec{n}$ and $\vec{r}$, i.e.,

$$\vec{K}\cdot\vec{r}_1 = Kr_1 \cos\gamma \,, \tag{2.18}$$

where $\cos\gamma$ may be expanded in spherical harmonics as

$$\cos\gamma = \frac{4\pi}{3} \sum_{m=-1}^{1} Y_{1,m}(\theta_1,\varphi_1)\, Y^*_{1,m}(\theta',\varphi') \,, \tag{2.19}$$

where θ_1,φ_1 are atomic electron coordinates and θ',φ' give the orientation of $\vec{K}$ referred to the atomic coordinate system (the z-axis is taken as the axis of quantization). Thus we have for an ns→npm transition

$$\int \vec{K}\cdot\vec{r}_1\, \psi^*_n(\vec{r}_1)\, \psi_o(\vec{r}_1)\, d\vec{r}_1 = \frac{4\pi K}{3} \sum_{m=-1}^{1} Y^*_{1,m}(\theta'\varphi') \int r_1 Y_{1,m}(\theta_1,\varphi_1)$$

$$\times\, \psi^*_n(\vec{r}_1)\, \psi_o(\vec{r}_1)\, d\vec{r}_1 = \frac{4\pi K}{3} \sum_{m=-1}^{1} Y^*_{1,m}(\theta',\varphi') \int Y_{1,m}(\theta_1,\varphi_1)$$

$$\times\, Y_{o,o}(\theta_1,\varphi_1)\, Y^*_{1,m}(\theta_1,\varphi_1)\, d\hat{r}_1 \int_o^\infty R_{ns}(r_1)\, R_{np}(r_1)\, r_1^3\, dr_1 =$$

$$\frac{\sqrt{4\pi}\, K}{3} Y^*_{1,m}(\theta',\varphi')\; s_1(np,ns) \,. \tag{2.20}$$

The first term in the expansion of $\exp(i\vec{K}\cdot\vec{r}_1)$ makes no contribution because of the orthogonality of ψ_o and ψ_n. The differential cross section in K becomes

$$I_n(K,\varphi)\, dK\, d\varphi = \left(\frac{\pi}{k_o^2}\right) \frac{8 s_1^2(np,ns)}{9\pi} \frac{dK\, d\varphi}{K} \left|\theta_{1,m}(\theta')\right|^2, \tag{2.21}$$

which is independent of φ. In the case of transitions

involving a degenerate final state, such as the ns→np transition considered here, the total cross section is obtained by summing over the degenerate states. Thus for a beam of electrons incident on an unpolarized group of atoms, we have

$$Q(ns\rightarrow np) = \overset{m=0}{Q}(ns\rightarrow np) + \overset{m=1}{Q}(ns\rightarrow np) + \overset{m=-1}{Q}(ns\rightarrow np). \qquad (2.22)$$

We may choose to identify $\vec{k}_o$ as the axis of quantization (z axis) for the atomic system. The cross section becomes

$$Q(ns\rightarrow np) = \left(\frac{\pi}{k_o^2}\right)\frac{16}{9}\int \sum_{m=-1}^{1} |\Theta_{1,m}(\theta')|^2 \frac{dK}{K}$$

$$= \left(\frac{\pi}{k_o^2}\right)\frac{8}{3} s_1^2(np,ns)\ \ln\left(\frac{k_o + k_n}{|k_o - k_n|}\right). \qquad (2.23)$$

If, on the other hand, $\vec{K}$ is chosen as the z axis, we see immediately that $\theta' = 0$ and noticing that

$$\Theta_{1,\pm1}(0) = 0, \quad \Theta_{1,0}(0) = \sqrt{3/2},$$

we find that Q(ns→np) is identical to Eq. (2.23). Thus if one can choose an axis of quantization such that two of the three degenerate states produce zero cross sections, then the cross section due to the third does indeed represent the total ns→np cross section. There is a related theorem[12] due to Oppenheimer to the effect that for a degenerate level, the sum of transition probabilities from one state to each

of the degenerate states is invariant for all choices of the axis of quantization. Thus if one can find an axis such that only one transition probability does not vanish, then this does indeed represent the total transition probability.

The Bethe approximation can also be obtained by a different approach, in which one does not expand the function $\exp(i\vec{K}\cdot\vec{r})$, but rather replaces the matrix element $U_{no}(\vec{r}) = 2\int \psi_n^* V \psi_o \, d\vec{r}_1$ in Eq. (2.3) by its asymptotic form. From Eq. (1.37) we have (in Slater atomic units)

$$U_{no}(\vec{r}_1) = \frac{4\sqrt{\pi}}{3} Y_{1,m}^*(\hat{r}_1) \frac{s_1(np,ns)}{r_1^2}, \qquad (2.24)$$

for the special case of an ns→np transition. One can see a basic similarity in the two approaches in that both overemphasize the degree of interaction for close encounters (see Figure 1), and thus predict too large a cross section. Choosing $\vec{K} = \vec{k}_o - \vec{k}_n$ as the axis of quantization, we have from Eq. (2.9)

$$I_n(\theta,\varphi) = \frac{k_n}{4\pi k_o} \left| \int \exp\left[i(Kr_2 \cos\theta_2)\right] \frac{2\sqrt{\pi}}{3} \right.$$
$$\left. \times Y_{1,0}^*(\hat{r}_2) \frac{s_1(np,ns)}{r_2^2} d\vec{r}_2 \right|^2 . \qquad (2.25)$$

The integral may be written

$$\frac{2\pi}{\sqrt{3}} s_1(np,ns) \int_0^\infty dr_2 \int_0^\pi \exp(iKr_2 \cos\theta_2) \cos\theta_2 \sin\theta_2 \, d\theta_2$$

$$= \frac{4\pi i s_1(np,ns)}{\sqrt{3}\,K^2} \left\{ -K \int_o^\infty \cos\,(Kr_2)\,\frac{dr_2}{r_2} + \int_o^\infty \sin\,(Kr_2)\frac{dr_2}{r_2^2} \right\} . \tag{2.26}$$

One can easily verify, using integration by parts, that

$$\int \sin\,(Kr)\,\frac{dr}{r^2} - K \int \cos\,(Kr)\,\frac{dr}{r} = -\frac{\sin\,(Kr)}{r} , \tag{2.27}$$

and since

$$\lim_{r\to o} \frac{\sin Kr}{r} = K , \tag{2.28}$$

we obtain

$$\int \exp\,(iKr_2\cos\theta_2)\,\frac{2\sqrt{\pi}}{3}\,Y^*_{1,0}(\hat{r}_2)\,s_1(np,ns)\,\frac{d\vec{r}_2}{r_2^2} = \frac{4\pi i s_1}{\sqrt{3}\,K} . \tag{2.29}$$

The differential cross section in K becomes

$$I_n(K,\varphi)\,dK\,d\varphi = \frac{k_n}{4\pi^2 k_o} \cdot \frac{K\,dK\,d\varphi}{k_o k_n} \cdot \frac{16\pi^2 s_1^2}{3K^2} , \tag{2.30}$$

and from this the total cross section is found to be identical to that given in Eq. (2.23). Thus with respect to the total Bethe approximation, the technique of expanding $\exp\,(i\vec{K}\cdot\vec{r}_1)$ and that of using the asymptotic form of U_{no} appear to be identical. It is found that the latter approach is more convenient in the Bethe partial-wave development.

Partial Wave Formulation of the Bethe Approximation

In many methods of treating inelastic scattering it is not possible to obtain a closed-form expression for the

total cross section, as was done for the Bethe approximation in the previous section; such is the case, for instance, in the resonance-distortion method, to be discussed in more detail in Chapter III. In such instances it is necessary to resort to a partial wave formulation in which the incident plane wave is analyzed in terms of its spherical-wave components, each having angular momentum ℓ. The total cross section is then determined as the sum of the partial cross sections, each of which corresponds to a particular value of ℓ. This technique was used in the schematic model discussed in Chapter I. The partial wave procedure is, in spite of its complexity, an extremely valuable means of investigating the validity of certain approximations, since unlike the total cross section, the partial cross section is subject to certain conservation laws such as that given in Eq. (1.83). We will make direct use of the partial Bethe cross sections for large ℓ in calculating total cross sections, since it is found, as will be discussed later, that for large values of ℓ the Bethe approximation is quite good.

In Eq. (2.9) for the differential cross section, we expand $\exp(i\vec{k}_o\cdot\vec{r}_2)$ and $\exp[-i(\vec{k}_n\cdot\vec{r}_2)]$ according to Eq. (1.40) as

$$\exp(i\vec{k}_o\cdot\vec{r}_2) = \frac{1}{r_2}\sum_{\ell=0}^{\infty} i^{\ell}(2\ell+1)P_{\ell}(\cos\theta_2)j_{\ell}(k_o r_2)\ ,$$

$$\exp(-i\vec{k}_n\cdot\vec{r}_2) = \frac{1}{r_2}\sum_{\ell'=0}^{\infty}(-1)^{\ell'}(2\ell'+1)P_{\ell'}(\cos\theta_n)j_{\ell'}(k_n r_2), \tag{2.31}$$

where

$$j_\ell(kr) = \left(\frac{\pi r}{2k}\right)^{\frac{1}{2}} J_{\ell+\frac{1}{2}}(kr) \ . \qquad (2.32)$$

The angles are identified in Figure 6, where the x-axis is taken in the plane of $\vec{k}_o$ and $\vec{k}_n$. Making use of the addition

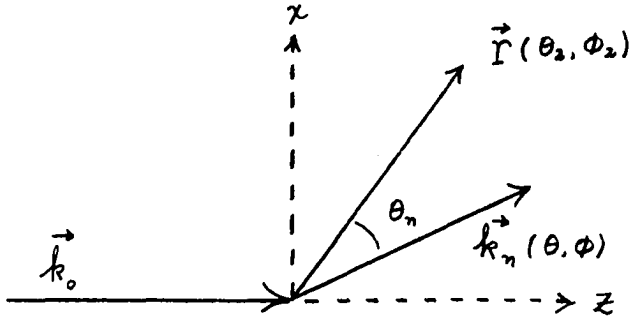

Figure 6

theorem of spherical harmonics, we have that[13]

$$P_{\ell'}(\cos\theta_n) = \frac{4\pi}{2\ell'+1} \sum_{m'=-\ell'}^{\ell'} Y_{\ell',m'}(\theta_2,\varphi_2)\, Y^*_{\ell',m'}(\theta,\varphi) \ . \qquad (2.33)$$

For an ns→npm transition, the interaction matrix element is gotten from Eq. (2.24) (in Slater atomic units) as

$$U_{no}(\vec{r}_2) = \frac{4\sqrt{\pi}}{3} Y^*_{1,m}(\hat{r}_2)\, y_1(np,ns|r_2) \ . \qquad (2.34)$$

When these expressions are inserted into Eq. (2.9), the resultant Born differential cross section is

$$I_n(\theta,\varphi) = \frac{k_n}{4\pi^2 k_o} \left| \sum_{\ell=0}^{\infty} \sum_{\ell'=0}^{\infty} i^{\ell}(-i)^{\ell'}(2\ell+1)(2\ell'+1) I^{BI}(\ell,\ell') \right.$$

$$\times \left\{ \sum_{m'=-\ell'}^{\ell'} \iint \frac{2\sqrt{\pi}}{3} Y^*_{1,m}(\theta_2,\varphi_2) P_\ell(\cos\theta_2) \frac{4\pi}{2\ell'+1} Y^*_{\ell',m'}(\theta_2,\varphi_2) \right.$$

$$\left. \times \sin\theta_2 \, d\theta_2 \, d\varphi_2 \, Y_{\ell',m'}(\theta,\varphi) \right\} |^2 , \qquad (2.35)$$

where we have defined

$$I^{BI}(\ell,\ell') = \int_0^\infty j_\ell(k_o r) j_{\ell'}(k_n r) y_1(np,ns|r) \, dr . \qquad (2.36)$$

We consider first the angular integral

$$\frac{2\sqrt{\pi}}{3} \cdot \frac{4\pi}{2\ell'+1} \iint Y^*_{1,m}(\theta_2,\varphi_2) \left(\frac{2}{2\ell+1}\right)^{\frac{1}{2}} \Theta^o_\ell(\theta_2) \, Y^*_{\ell',m'}(\theta_2,\varphi_2)$$

$$\times \sin\theta_2 \, d\theta_2 \, d\varphi_2 = \frac{8\pi^{3/2}}{3(2\ell'+1)} \left(\frac{2}{2\ell+1}\right)^{\frac{1}{2}} \int \Theta_{1,m}(\theta_2) \; \Theta_{\ell,o}(\theta_2)$$

$$\times \Theta_{\ell',m'}(\theta_2) \sin\theta_2 \, d\theta_2 , \qquad (2.37)$$

where $\ell' = \ell \pm 1$, and $m' = -m$ are the only ℓ', m' giving non-vanishing results. The angular integrals are evaluated by means of Gaunt's formula and found to be[13]

$$\int \Theta_{1,1}\Theta_{\ell,0}\Theta_{\ell+1,-1} = -\tfrac{1}{2}\left[\frac{3(\ell+1)(\ell+2)}{(2\ell+1)(2\ell+3)}\right]^{\frac{1}{2}} ,$$

$$\int \Theta_{1,1}\Theta_{\ell,0}\Theta_{\ell-1,-1} = \tfrac{1}{2}\left[\frac{3\ell(\ell-1)}{(2\ell+1)(2\ell-1)}\right]^{\frac{1}{2}} ,$$

$$\int \Theta_{1,0}\Theta_{\ell,0}\Theta_{\ell+1,0} = \left(\frac{3}{2}\right)^{\frac{1}{2}} \frac{(\ell+1)}{[(2\ell+3)(2\ell+1)]^{\frac{1}{2}}} , \qquad (2.38)$$

$$\int \Theta_{1,0}\Theta_{\ell,0}\Theta_{\ell-1,0} = \left(\frac{3}{2}\right)^{\frac{1}{2}} \frac{\ell}{[(2\ell+1)(2\ell-1)]^{\frac{1}{2}}} .$$

Thus, we have

$$I_n^m(\theta,\varphi) = \frac{k_n}{k_o}\frac{16\pi}{9}\Big|\sum_{\ell=0}^{\infty} i^{\ell}(2\ell+1)\left(\frac{2}{2\ell+1}\right)^{\frac{1}{2}}\Big\{(-1)^{\ell+1}I^{BI}_{I(\ell,\ell+1)}$$

$$\times\int\Theta_{1,m}\Theta_{\ell,0}\Theta_{\ell+1,m'}\,Y_{\ell+1,m'}(\theta,\varphi) + (-1)^{\ell-1}I^{BI}_{I(\ell,\ell-1)}$$

$$\times\int\Theta_{1,m}\Theta_{\ell,0}\Theta_{\ell-1,m'}\,Y_{\ell-1,m'}(\theta,\varphi)\Big\}\Big|^2 . \qquad (2.39)$$

Making use of Eqs. (2.38), we find for $m = 0$

$$I_n^{m=0}(\theta,\varphi) = \frac{k_n}{k_o}\frac{16\pi}{3}\Big|\sum_{\ell=0}^{\infty}\frac{\ell+1}{(2\ell+3)^{\frac{1}{2}}}I^{BI}_{I(\ell,\ell+1)}\,Y_{\ell+1,0}(\theta,\varphi)$$

$$-\frac{\ell}{(2\ell-1)^{\frac{1}{2}}}I^{BI}_{I(\ell,\ell-1)}\,Y_{\ell-1,0}(\theta,\varphi)\Big|^2 , \qquad (2.40)$$

and similarly for $m = \pm 1$,

$$I_n^{m=\pm1}(\theta,\varphi) = \frac{k_n}{k_o}\frac{16\pi}{3}\Big|\sum_{\ell=0}^{\infty}\Big\{\Big[\frac{3(\ell+1)(\ell+2)}{2(2\ell+3)}\Big]^{\frac{1}{2}}I^{BI}_{I(\ell,\ell+1)}$$

$$\times\,Y_{\ell+1,\mp1}(\theta,\varphi) + \Big[\frac{3\ell(\ell-1)}{2(2\ell-1)}\Big]^{\frac{1}{2}}I^{BI}_{I(\ell,\ell-1)}\,Y_{\ell-1,\mp1}(\theta,\varphi)\Big\}\Big|^2 . \qquad (2.41)$$

Integrating these differential cross sections over all orientations of the final momentum $\vec{k}_n$, one obtains

$$Q^{m=0}(2s\to2p) = \frac{k_n}{k_o}\frac{16\pi}{3}\sum_{\ell=0}^{\infty}\Big\{\frac{(\ell+1)^2}{2\ell+3}\Big[I^{BI}_{I(\ell,\ell+1)}\Big]^2$$

$$+ \frac{\ell^2}{2\ell - 1} \left[\overset{BI}{I}(\ell,\ell-1) \right]^2 - \frac{(\ell + 1)(\ell + 2)}{2\ell + 3} \overset{BI}{I}(\ell+2,\ell+1)\ \overset{BI}{I}(\ell,\ell+1)$$

$$- \frac{\ell(\ell - 1)}{2\ell - 1} \overset{BI}{I}(\ell-2,\ell-1)\ \overset{BI}{I}(\ell,\ell-1) \Big\} , \qquad (2.42)$$

and

$$\overset{m=\pm 1}{Q}(2s\to 2p) = \frac{k_n}{k_o} \frac{8\pi}{3} \sum_{\ell=0}^{\infty} \Big\{ \frac{(\ell + 1)(\ell + 2)}{2\ell + 3} \left[\overset{BI}{I}(\ell,\ell+1) \right]^2$$

$$+ \frac{\ell(\ell - 1)}{2\ell - 1} \left[\overset{BI}{I}(\ell,\ell-1) \right]^2 + \frac{(\ell + 1)(\ell + 2)}{2\ell + 3} \overset{BI}{I}(\ell+2,\ell+1)\ \overset{BI}{I}(\ell,\ell+1)$$

$$+ \frac{\ell(\ell - 1)}{2\ell - 1} \overset{BI}{I}(\ell-2,\ell-1)\ \overset{BI}{I}(\ell,\ell-1) \Big\} . \qquad (2.43)$$

The total cross section for an ns→np transition is obtained by summing over the three degenerate states; from Eqs. (2.42) and (2.43) we have

$$\overset{BI}{Q}(2s\to 2p) = \frac{k_n}{k_o} \frac{16\pi}{3} \sum_{\ell=0}^{\infty} \Big\{ (\ell + 1) \left[\overset{BI}{I}(\ell,\ell+1) \right]^2 + \ell \left[\overset{BI}{I}(\ell,\ell-1) \right]^2 \Big\} . \qquad (2.44)$$

The cross section given above is strictly that of the Born approximation (BI), since no approximation has been made in connection with the matrix element V_{no}.

The Bethe approximation (B'I) may now be obtained, as we have shown previously, by replacing $y_1(np,ns|r)$ in the radial integrals by

$$y_1(np,ns|r) \sim \frac{s_1(np,ns)}{r^2} . \qquad (2.45)$$

Renaming these integrals $I^{B'I}(\ell,\ell')$, we obtain

$$I^{B'I}(\ell,\ell\pm1) = \frac{\pi s_1}{2(k_o k_n)^{\frac{1}{2}}} \int_o^\infty J_{\ell+\frac{1}{2}}(k_o r)\, J_{\ell+\frac{1}{2}\pm1}(k_n r)\, \frac{dr}{r}\,, \qquad (2.46)$$

and then for the total cross section

$$Q^{B'I}(2s\rightarrow 2p) = \left(\frac{\pi}{k_o^2}\right)\frac{4}{3}(\pi s_1)^2 \sum_{\ell=o}^{\infty} \Big\{ (\ell+1) \Big| \int_o^\infty J_{\ell+\frac{1}{2}}(k_o r)$$

$$\times\, J_{\ell+3/2}(k_n r)\, \frac{dr}{r} \Big|^2 + \ell \Big| \int_o^\infty J_{\ell+\frac{1}{2}}(k_o r)\, J_{\ell-\frac{1}{2}}(k_n r)\, \frac{dr}{r} \Big|^2 \Big\}\,. \qquad (2.47)$$

This is the standard Bethe I cross section[7], which will be derived in another manner in Chapter VI.

CHAPTER III

METHOD OF RESONANCE DISTORTION

In the Born and Bethe approximations as well as the Method of Distorted Waves, validity requires that the coupling of the states of interest be weak (i.e., that the off-diagonal matrix element be relatively small). However, there are several instances, particularly in cases of near resonance, when the coupling is quite large. In such cases it is necessary to treat the off-diagonal elements as completely as possible. Percival and Seaton[14] have formulated the general partial wave theory for electron-Hydrogen atom collisions. Their formulation will be used below for electron-atom collisions where the atom is replaced by an electron outside a core of unit charge.

Consider an electron of linear momentum $\hbar\vec{k}'$ incident upon an atom in the state $n_1'\ell_1'$. We wish to obtain the cross section for a process in which the atom undergoes the transition $n_1'\ell_1' \rightarrow n_1\ell_1$ and the electron goes off with kinetic energy $\hbar^2k^2/2m$. Since U_{on} is in general angularly-dependent, the expansion of the amplitude functions F_o and F_n in terms of spherical harmonics, causes the two coupled, partial differential equations of Eqs. (1.18) and (1.19) to decompose

into an infinity of coupled differential equations in ℓ. For the case of an ns→np transition, the equation for the ℓ'th partial amplitude function couples with equations for $\ell \pm 1$. One must find a way to approximately decouple these equations in order to obtain a solution.

Seaton[5] has suggested a method of solution based on the fact that the total angular momentum of the electron-atom system must be conserved. We first describe the system by assigning quantum numbers n_1 ℓ_1 m_1 to the atom, and ℓm to the scattered electron, where $\ell_1 m_1$ represent the angular momentum of the atomic electron, and ℓ,m that of the scattered electron. (Or if one prefers, ℓ,m represent the angular momentum of one partial-wave component of the scattered electron, the solution for the scattering problem then requiring the results for all ℓm.) Then in order to obtain solutions to Schroedinger's equation

$$(H - E)\Psi = 0 \ , \tag{3.1}$$

we first construct eigenfunctions of the total angular momentum L,M as

$$\Phi_\nu(\vec{r}_1,\hat{r}) = \sum_{m_1 m} C^{\ell_1 \ell L}_{m_1 m M} \, \phi_{n_1 \ell_1 m_1}(\vec{r}_1) \, Y_{\ell m}(\hat{r}) \ , \tag{3.2}$$

where ν stands for the group of quantum numbers $n_1 \ell_1 \ell LM$, and C is the Clebsch-Gordon coefficient. Then the wave function for the whole system is expanded as

$$\Psi(\nu' | \vec{r}_1,\vec{r}) = r^{-1} \sum_\nu F_\nu(\nu' | r) \, \Phi_\nu(\vec{r}_1,\hat{r}) \ , \tag{3.3}$$

where the index ν' is included to remind us that the system was initially in the state characterized by ν'. In other words, the asymptotic form of $F_\nu(\nu'|r)$ for $r \to \infty$ is

$$F_\nu(\nu'|r) \sim k^{-\frac{1}{2}}\{\exp\,[-i(kr - \tfrac{1}{2}\ell\pi)]\delta_{\nu\nu'} - \exp\,[i(kr - \tfrac{1}{2}\ell\pi)]S_{\nu\nu'}\}\,, \tag{3.4}$$

in terms of the S-matrix, or alternatively

$$F_\nu(\nu'|r) \sim k^{-\frac{1}{2}}\{\sin\,(kr - \tfrac{1}{2}\ell\pi)\delta_{\nu\nu'} + \cos\,(kr - \tfrac{1}{2}\ell\pi)R_{\nu\nu'}\} \tag{3.5}$$

where the S- and R-matrices are related by the equation[5]

$$\underline{S} = (\underline{1} + i\underline{R})(\underline{1} - i\underline{R})^{-1}\,, \tag{3.6}$$

where the S-matrix is unitary and diagonal in L and M.

Upon introducing the T-matrix defined by

$$\underline{T} = \underline{1} - \underline{S} = -2i\underline{R}(\underline{1} - i\underline{R})^{-1}\,, \tag{3.7}$$

one can express the cross section for the $n_1'\ell_1' \to n_1\ell_1$ transition as

$$Q(n_1'\ell_1' \to n_1\ell_1) = [\pi/(k')^2(2\ell_1' + 1)]\Omega(n_1\ell_1, n_1'\ell_1')$$

$$= (\pi/(k')^2(2\ell_1' + 1)) \sum_{\ell\ell' L} (2L + 1)\,|T(n_1\ell_1\ell L, n_1'\ell_1'\ell' L)|^2\,, \tag{3.8}$$

where $\Omega(n_1\ell_1, n_1'\ell_1')$ is the collision strength for the transition $n_1'\ell_1' \to n_1\ell_1$.

Differential Equations

When the total wave function given in Eq. (3.3) is substituted into Schroedinger's equation, Eq. (3.1), one obtains, after multiplying by $\Psi_\nu^*(\vec{r}_1,\hat{r})\, d\vec{r}_1\, d\hat{r}$ and integrating,

$$\left[\frac{d^2}{dr^2} + k_\nu^2 - \ell(\ell+1)/r^2 \right] F_\nu(\nu'|r) = \sum_\mu F_\mu(\nu'|r)\, U(\nu,\mu|r) \tag{3.9}$$

where

$$U(\nu,\mu) = \iint \Psi_\nu^*(\vec{r}_1,\hat{r}) \left\{ \frac{2}{|\vec{r}_1 - \vec{r}|} - \frac{2}{r} \right\} \Psi_\mu(\vec{r}_1,\hat{r})\, d\vec{r}_1\, d\hat{r} ,$$

and where we have made use of the orthonormality relation

$$\iint \Psi_\mu^*(\vec{r}_1,\hat{r})\, \Psi_\nu(\vec{r}_1,\hat{r})\, d\vec{r}_1\, d\hat{r} = \delta_{\mu\nu} . \tag{3.10}$$

A multipole expansion of $U(\nu,\mu|r)$ may be obtained upon expanding $|\vec{r}_1 - \vec{r}|^{-1}$ in terms of spherical harmonics (see Eq. (1.27)); we obtain

$$U(\nu,\mu|r) = \sum_\lambda U_\lambda(\nu,\mu|r) \tag{3.11}$$

where

$$U_o(\nu,\mu|r) = 2\delta[(\ell_1)_\nu \ell_\nu, (\ell_1)_\mu \ell_\mu]\{-\delta[(n_1)_\nu, (n_1)_\mu] r^{-1} + y_o[(n_1)_\nu (\ell_1)_\nu, (n_1)_\mu (\ell_1)_\mu | r]\} ,$$

and

$$U_\lambda(\nu,\mu|r) = 2 f_\lambda[(\ell_1)_\nu \ell_\nu, (\ell_1)_\mu \ell_\mu; L] y_\lambda[(n_1)_\nu (\ell_1)_\nu\ (n_1)_\mu (\ell_1)_\mu | r] \tag{3.12}$$

for $\lambda > 0$, where $y_\lambda(\nu,\mu)$ is given in Eq. (1.26), and where

$$f_\lambda[(\ell_1)_\nu \ell_\nu, (\ell_1)_\mu \ell_\mu; L] = \langle (\ell_1)_\nu \ell_\nu L | P_\lambda(\hat{r}_1 \cdot \hat{r}) | (\ell_1)_\mu \ell_\mu L \rangle \ , \tag{3.13}$$

P_λ being the ordinary Legendre polynomial of order λ. Tables of f_λ for the cases of interest are available.[14] Let us now consider an ns→np transition and neglect interactions with all other states. To obtain a given total angular momentum L, one may choose three different combinations of ℓ_1 and ℓ as follows:

$$\begin{aligned} &(1) \quad \ell_1 = 0 \quad \ell = L \\ &(2) \quad \ell_1 = 1 \quad \ell = L - 1 \\ &(3) \quad \ell_1 = 1 \quad \ell = L + 1 \ , \end{aligned} \tag{3.14}$$

where the possibility $\ell_1 = 1$, $\ell = L$ has been ignored since there is no coupling between this state and the other three. We will designate the F functions of these three channels as F_1, F_2, and F_3, and matrix elements connecting channels i and j as U_{ij}. We have then

$$\begin{aligned} U_{12} &= 2f_1(1,2)\ y_1(np,ns|r) \sim 2f_1(0\ L,1\ L-1;L)\ s_1(np,ns)/r^2 \\ U_{13} &= 2f_1(1,3)\ y_1(np,ns|r) \sim 2f_1(0\ L,1\ L+1;L)\ s_1(np,ns)/r^2 \ , \end{aligned} \tag{3.15}$$

where the f_λ coefficients are found to be

$$\begin{aligned} f_1(0\ L,1\ L-1;L) &= [L/3(2L+1)]^{\frac{1}{2}} \ , \\ \text{and} \qquad & \\ f_1(0\ L,1\ L+1;L) &= -[(L+1)/3(2L+1)]^{\frac{1}{2}} \ . \end{aligned} \tag{3.16}$$

We have pointed out earlier (see Chapter I) that the diagonal elements fall off exponentially and for intermediate electron energies, have little effect on the cross section; also, it was mentioned that the behavior of the off-diagonal elements, for small r, was not important to the cross section for intermediate incident energies. Therefore, in the following we keep only the asymptotic parts of the off-diagonal elements and ignore the diagonal ones completely. Thus, with

$$U_{11} = U_{22} = U_{33} = U_{23} = 0 \ , \tag{3.17}$$

and

$$\begin{aligned} U_{12} &= L^{\frac{1}{2}}\beta/r^2 \ , \\ U_{13} &= -(L+1)^{\frac{1}{2}}\beta/r^2 \ , \end{aligned} \tag{3.18}$$

we obtain for the differential equations

$$\left[\frac{d^2}{dr^2} + k_o^2 - L(L+1)/r^2 \right] F_1 = L^{\frac{1}{2}}\beta r^{-2} F_2 - (L+1)^{\frac{1}{2}}\beta r^{-2} F_3 \ , \tag{3.19}$$

$$\left[\frac{d^2}{dr^2} + k_n^2 - L(L-1)/r^2 \right] F_2 = L^{\frac{1}{2}}\beta r^{-2} F_1 \ , \tag{3.20}$$

and

$$\left[\frac{d^2}{dr^2} + k_n^2 - (L+1)(L+2)/r^2 \right] F_3 = -(L+1)^{\frac{1}{2}}\beta r^{-2} F_1 \ , \tag{3.21}$$

where

$$\beta = \frac{2s_1(np,ns)}{[3(2L+1)]^{\frac{1}{2}}} \tag{3.22}$$

and

$$\frac{\hbar^2}{2m} k_o^2 + E_{ns} = \frac{\hbar^2}{2m} k_n^2 + E_{np} .$$

The collision strength, then, according to Eq. (3.8) is

$$\Omega(np,ns) = \sum_L (2L + 1) \left\{ |T_{12}|^2 + |T_{13}|^2 \right\} , \qquad (3.23)$$

where the indices 1, 2, 3 refer to the respective channels.

Zeroth-Order Approximation (Exact Resonance)

In the resonance-distortion method, the zeroth-order approximation is obtained by solving for the case of exact-resonance, i.e., $k_o = k_n$. Under this condition, the coupled equations may be decoupled by forming suitable linear combinations of F_1, F_2 and F_3.[5] This can be seen more clearly by writing Eqs. (3.19), (3.20) and (3.21) in the form of a matrix equation

$$r^2 \left(\frac{d^2}{dr^2} + k_o^2 \right) \underline{F} = \underline{A}\, \underline{F} , \qquad (3.24)$$

where $\underline{F}$ is a column vector with components F_1, F_2, F_3 and $\underline{A}$ is the square matrix

$$\underline{A} = \begin{bmatrix} L(L+1) & L^{\frac{1}{2}}\beta & -(L+1)^{\frac{1}{2}}\beta \\ L^{\frac{1}{2}}\beta & L(L-1) & 0 \\ -(L+1)^{\frac{1}{2}}\beta & 0 & (L+1)(L+2) \end{bmatrix} . \qquad (3.25)$$

Thus to obtain the solutions, we merely diagonalize $\underline{A}$ by means of the orthogonal transformation $\underline{X}$ so that Eq. (3.24)

becomes

$$r^2 \left(\frac{d^2}{dr^2} + k_o^2 \right) \underline{G} = \underline{a}\ \underline{G} \ , \tag{3.26}$$

where $\underline{a} = \underline{X}^{-1}\ \underline{A}\ \underline{X}$, and $\underline{G} = \underline{X}^{-1}\ \underline{F}$. The eigenvalues of $\underline{a}$ are

$$\begin{aligned} a_1 &= L(L+1), \\ a_2 &= L^2 + L + 1 - (2L+1)x, \\ a_3 &= L^2 + L + 1 + (2L+1)x, \end{aligned} \tag{3.27}$$

where

$$x = [1 + \beta^2/(2L+1)]^{\frac{1}{2}}, \tag{3.28}$$

and thus the transformation matrix is given by

$$\underline{X} = \begin{bmatrix} \xi_1 & \xi_2 & \xi_3 \\ \dfrac{L^{\frac{1}{2}}\beta\xi_1}{2L} & \dfrac{L^{\frac{1}{2}}\beta\xi_2}{(2L+1)(1-x)} & \dfrac{L^{\frac{1}{2}}\beta\xi_3}{(2L+1)(1+x)} \\ \dfrac{(L+1)^{\frac{1}{2}}\beta\xi_1}{2(L+1)} & \dfrac{(L+1)^{\frac{1}{2}}\beta\xi_2}{(2L+1)(1+x)} & \dfrac{(L+1)^{\frac{1}{2}}\beta\xi_3}{(2L+1)(1-x)} \end{bmatrix} \tag{3.29}$$

where

$$\begin{aligned} \xi_1^2 &= 4L(L+1)/[4L(L+1) + \beta^2(2L+1)] \ , \\ \xi_2^2 &= \beta^2/2(\beta^2 + 2L + 1 - x) \ , \\ \xi_3^2 &= \beta^2/2(\beta^2 + 2L + 1 + x) \ . \end{aligned} \tag{3.30}$$

The procedure now is to choose solutions of the decoupled

equations having the proper asymptotic behavior, and then transform back to $\underline{F}$. To investigate the asymptotic behavior, we note that

$$G_i = \sum_j (\underline{X}^{-1})_{ij} F_j = \sum_j X_{ji} F_j \ . \tag{3.31}$$

Considering the asymptotic form of F_j, we find that

$$\begin{aligned} G_i \sim k_o^{-\frac{1}{2}} \{ & X_{1i}(-2i) \sin (k_o r - \tfrac{1}{2}\ell\pi) \\ & + X_{1i} T_{1l} \exp [i(k_o r - \tfrac{1}{2}\ell\pi)] \\ & + X_{2i} T_{2l} \exp [i(k_o r - \tfrac{1}{2}\ell\pi)] \\ & + X_{3i} T_{3l} \exp [i(k_o r - \tfrac{1}{2}\ell\pi)]] \ . \end{aligned} \tag{3.32}$$

Thus, the solutions of G_i which conform to the proper boundary conditions are

$$\begin{aligned} G_1 &= -2iX_{11}(\tfrac{1}{2}\pi r)^{\frac{1}{2}} J_{L+\frac{1}{2}}(k_o r) \ , \\ G_2 &= -2iX_{12} \exp [\tfrac{1}{2}i\pi(L - \mu_2)](\tfrac{1}{2}\pi r)^{\frac{1}{2}} J_{\mu_2+\frac{1}{2}}(k_o r) \ , \\ G_3 &= -2iX_{13} \exp [\tfrac{1}{2}i\pi(L - \mu_3)](\tfrac{1}{2}\pi r)^{\frac{1}{2}} J_{\mu_3+\frac{1}{2}}(k_o r) \ . \end{aligned} \tag{3.33}$$

Here we have used the abbreviations

$$\begin{aligned} \mu_2 &= -\tfrac{1}{2} + [(L - \tfrac{1}{2})^2 - C]^{\frac{1}{2}} \ , \\ \mu_3 &= -\tfrac{1}{2} + [(L + \tfrac{3}{2})^2 + C]^{\frac{1}{2}} \ , \end{aligned} \tag{3.34}$$

where

$$C = (2L + 1)(x - 1), \quad C \geq (L - \tfrac{1}{2})^2 . \tag{3.35}$$

The phase factors are due to the assignment of phase in the definition of the S-matrix (see Eq. (3.4)).

The functions F_1, F_2, F_3 may now be determined by transforming from $\underline{G}$ to $\underline{F}$. In particular, for F_1 we obtain

$$\begin{aligned} F_1(r) = -2i(\tfrac{1}{2}\pi r)^{\frac{1}{2}}\{&X_{11}^2 J_{L+\frac{1}{2}}(k_o r) \\ &+ X_{12}^2 J_{\mu_2+\frac{1}{2}}(k_o r) \exp[\tfrac{1}{2}\pi i(L - \mu_2)] \\ &+ X_{13}^2 J_{\mu_3+\frac{1}{2}}(k_o r) \exp[\tfrac{1}{2}\pi i(L - \mu_3)]\} . \end{aligned} \tag{3.36}$$

The above results have been checked by ensuring that they do indeed yield the exact resonance cross section given by Seaton.[5]

Resonance Distortion Approximation

The resonance-distortion approximation, as outlined earlier, consists of replacing the F function describing the elastic scattering by the function obtained assuming exact resonance. The functions F_2 and F_3 can be determined in terms of F_1 by solving Eqs. (3.20) and (3.21) by the variation of parameters technique.[8] We have asymptotically

$$\begin{aligned} F_2 \sim k_n^{-1} &\exp[i(k_n r - \tfrac{1}{2}\pi(L - 1)] \\ &\times \int_0^\infty (\tfrac{1}{2}\pi k_n r)^{\frac{1}{2}} J_{L-\frac{1}{2}}(k_n r)\ (L^{\frac{1}{2}}\beta r^{-2} F_1)\, dr , \end{aligned} \tag{3.37}$$

$$F_3 \sim k_n^{-1} \exp\left[i(k_n r - \tfrac{1}{2}\pi(L+1)\right]$$

$$\times \int_0^\infty (\tfrac{1}{2}\pi k_n r)^{\frac{1}{2}} J_{L+3/2}(k_n r) \left(-(L+1)^{\frac{1}{2}}\beta r^{-2} F_1\right) dr. \quad (3.38)$$

According to the definition of the S-matrix in Eq. (3.4), we have

$$F_\nu(\nu'|r) \sim k_n^{-\frac{1}{2}} \exp\left[i(k_n r - \tfrac{1}{2}\pi L)\right] S_{\nu\nu'} \; ; \quad (3.39)$$

thus one obtains

$$S_{21} = i(\pi/2)^{\frac{1}{2}} L^{\frac{1}{2}} \beta \int_0^\infty J_{L-1/2}(k_n r)\, F_1(r)\, r^{-3/2}\, dr \; , \quad (3.40)$$

$$S_{31} = i(\pi/2)^{\frac{1}{2}} (L+1)^{\frac{1}{2}} \beta \int_0^\infty J_{L+3/2}(k_n r)\, F_1(r)\, r^{-3/2}\, dr \; . \quad (3.41)$$

Introducing into Eqs. (3.40) and (3.41) the exact resonance expression for F_1, given by Eq. (3.36), and recalling that $|T_{ij}|^2 = |S_{ij}|^2$, one finds the resonance-distortion collision strength to be given by

$$\Omega^{RD}(np,ns) = \frac{4}{3}(\pi s_1)^2 \sum_L \{L|I(L,L-1)|^2 + (L+1)|I(L,L+1)|^2\} \; , \quad (3.42)$$

where

$$I(L,L\pm1) = \xi_1^2 H^{(1)}(L,L\pm1) + \xi_2^2 H^{(2)}(L,L\pm1) \exp\left[\tfrac{1}{2}i\pi(L-\mu_2)\right]$$

$$+ \xi_3^2 H^{(3)}(L,L\pm1) \exp\left[\tfrac{1}{2}i\pi(L-\mu_3)\right] \; , \quad (3.43)$$

and

$$H^{(i)}(L,L\pm1) = \int_0^\infty J_{P_i}(k_o r)\, J_{L\pm1+\frac{1}{2}}(k_n r)\, r^{-1}\, dr \; , \quad (3.44)$$

$$P_i = \mu_i + \tfrac{1}{2} \qquad (\mu_1 \equiv L) \ .$$

The integrals $H^{(i)}(L,L\pm1)$ may be expressed in terms of hypergeometric functions as[9]

$$H^{(i)}(L,L\pm1) = \tfrac{1}{2}(k_n/k_o)^{L\pm1+\frac{1}{2}}\{\Gamma[a_i(L \pm 1)]/\Gamma[c_i(L \pm 1)]$$

$$\times\ \Gamma[1 - b_i(L \pm 1)]\}\ {}_2F_1[a_i(L\pm1),b_i(L\pm1);c_i(L\pm1);(k_n/k_o)^2] \ , \tag{3.45}$$

where

$$a_i(L\pm1) = \tfrac{1}{2}[(L \pm 1) + P_i + \tfrac{1}{2}] \ ,$$

$$b_i(L\pm1) = \tfrac{1}{2}[(L \pm 1) - P_i + \tfrac{1}{2}] \ ,$$

$$c_i(L\pm1) = L \pm 1 + 3/2 \ .$$

It has been verified that in the limit of exact resonance ($k_o = k_n$), the collision strength given in Eq. (3.42) does agree exactly with that determined by Seaton's formulas. It is also found that for large values of L, the resonance-distortion cross section approaches that of the Bethe approximation (B'I). Again, all of the above results are valid only for those values of L which satisfy the inequality in Eqs. (3.35).

CHAPTER IV

GENERAL RESULTS

In the previous chapter a technique was presented whereby inelastic cross sections for collision-induced transitions under near-resonance conditions could be determined. It is now wished to investigate the general behavior of these cross sections for different degrees of coupling and resonance and to compare them with the results obtained from other methods of calculation.

Effect of the Magnitude of Coupling

In Figure 7, the collision strength for ns-np transition with exact resonance is given for several values of the line strength s^2 (s^2 is a measure of the strength of coupling). The cross sections with $\ell = 0$ and 1 cannot be calculated by the scheme outlined in the previous section, since they violate the inequality in Eqs. (3.35). It has been shown that for exact-resonance collisions, as one increases the strength of coupling (from weak coupling), the transfer probability first increases rapidly, then reaches a certain saturation stage, and finally behaves in an oscillatory manner.[15] For a given ℓ, such saturation and oscillation

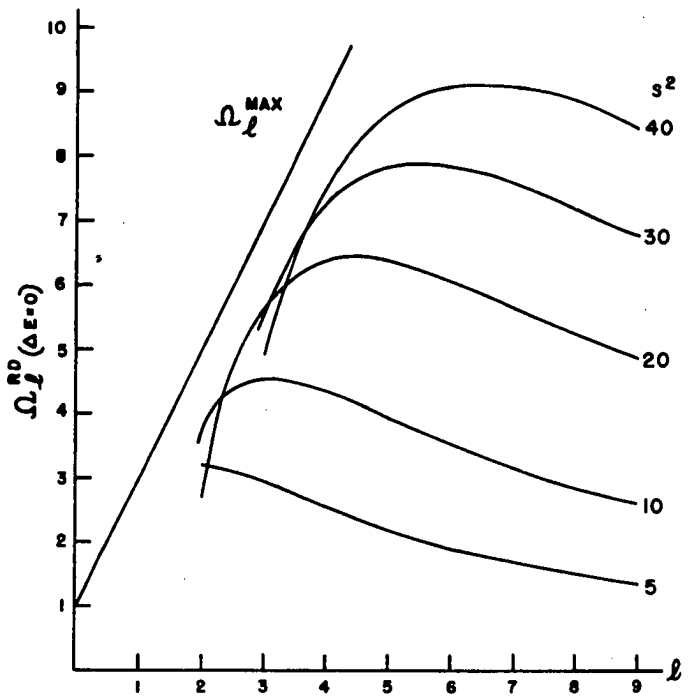

Figure 7. Collision Strengths Ω_ℓ^{RD} in the Case of Exact Resonance for Several Values of the Line Strength s^2.

behavior can be seen from the convergence of the points corresponding to larger values of s along each vertical line in Figure 7. (Here we have replaced the expansion index L by ℓ in order to facilitate comparisons with other works.) This can be illustrated more clearly in Figure 8, where $\Omega_{\ell}^{RD}(2\ell + 1)$ is plotted against s^2 for $\ell = 2, 3, \ldots, 6$. The saturation effect is more pronounced for low values of ℓ since partial waves with small ℓ correspond classically to a small impact parameter and therefore stronger interaction. Thus the curve for $\ell = 2$ in Figure 8 passes through a maximum around $s^2 = 10$, while the $\ell = 3$ collision strength does not reach the highest value until $s^2 = 25$, and the collision strengths for higher ℓ require even stronger coupling for complete saturation. This saturation effect is also responsible for keeping the collision strengths below the conservation limit (see Figure 7).

For the case of near (but not exact) resonance, the qualitative behavior of the partial collision strengths with respect to the degree of coupling is similar to that of exact resonance. Figure 9 shows the variation of $\Omega_{\ell}^{RD}/(2\ell + 1)$ with respect to s^2 for an energy separation of the initial and final states (ΔE) of 2.0 eV.

Effect of ΔE

In Figure 10 is displayed the collision strength Ω_{ℓ}^{RD} in terms of ℓ for several different ΔE with $s^2 = 19.3$. As ΔE is decreased, the collision strength curves are found to

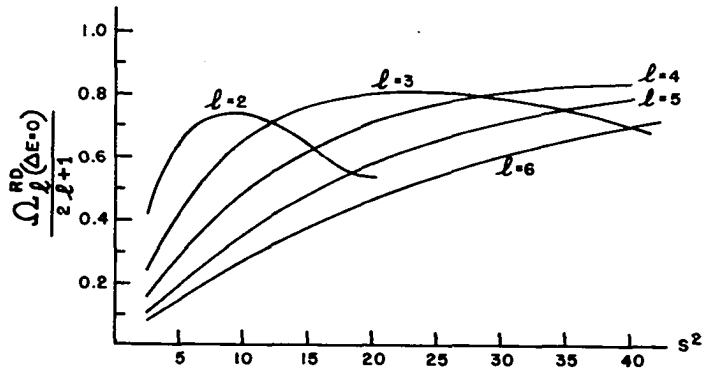

Figure 8. Values of $\Omega_\ell^{RD}/(2\ell + 1)$ for Different ℓ and $\Delta E = 0$ in Terms of the Line Strength s^2.

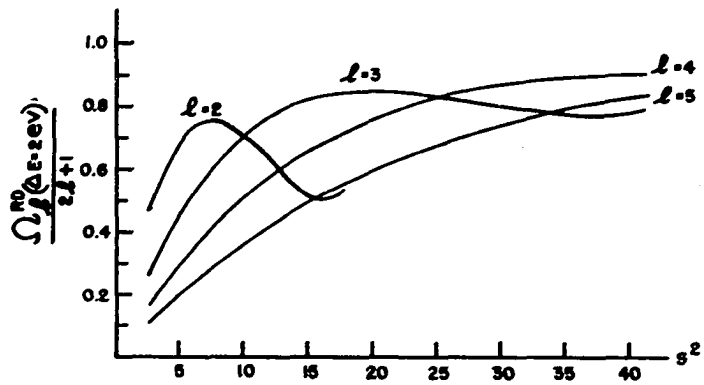

Figure 9. Values of $\Omega_{\ell}^{RD}/(2\ell + 1)$ for Different ℓ and ΔE = 2.0 eV in Terms of the Line Strength s^2.

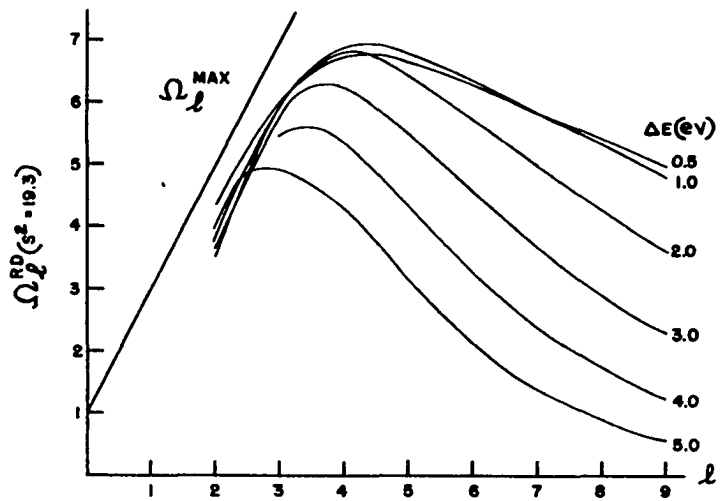

Figure 10. Collision Strengths Ω_ℓ^{RD} with $s^2 = 19.3$ for Several Values of ΔE (eV).

move up steadily, at first, and finally converge upon the $\Delta E = 0$ curve in an oscillatory fashion. Vertical sections of these curves are plotted against $(\Delta E)^{-1}$ in Figure 11. All the computations were made for a particular value of E of 13.6 eV; in general, the collision strengths depend on E and ΔE solely through $z = (k_n/k_o)^2 = (E - \Delta E)/E$. This fact enables us to use Figures 10 and 11 for several different sets of E and ΔE by means of Table I. Figure 11 illustrates that for low values of ℓ, reduction of ΔE leads to saturation and oscillatory behavior of Ω_ℓ^{RD} analogous to Figure 8.

Comparison with Other Methods

The standard approximate methods for systems with weak coupling, such as Born approximation and the Method of Distorted Waves, break down in the region where saturation is important (i.e., large s^2 or $z \approx 1$), since they give an accurate estimation of the cross sections only along the initial rise of the curves[15] of $\Omega_\ell/(2\ell + 1)$ vs. s^2. Thus when these methods are used for cases with strong coupling, they may produce partial cross sections which violate the conservation limit[5,7]

$$Q_\ell \leq \pi k_o^{-2}(2\ell + 1). \qquad (4.1)$$

It may be seen in Figure 8 that a weak coupling approximation applied to $\ell = 2$ is valid only for relatively small line strengths ($s^2 = 7.5$ is considered small for near-resonance optically allowed transitions).[6]

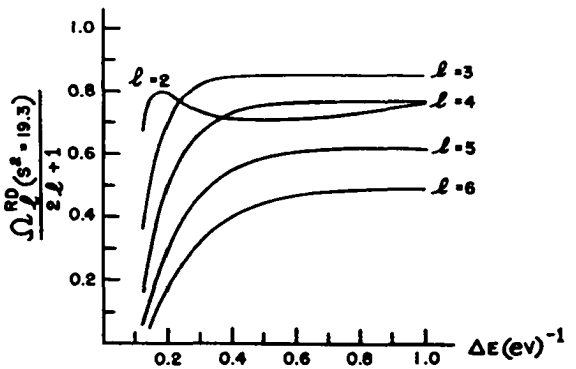

Figure 11. Values of $\Omega_\ell^{RD}/(2\ell + 1)$ for Different ℓ and $s^2 = 19.3$ in Terms of ΔE $(eV)^{-1}$.

TABLE I

VALUES OF ΔE(eV) CORRESPONDING TO GIVEN VALUES OF E(eV) AND z

	E(eV)							
z	3.4	6.8	10.2	13.6	17.0	20.4	23.8	27.2
.9632	.125	.25	.375	.50	.625	.75	.875	1.0
.9265	.25	.50	.75	1.0	1.25	1.5	1.75	2.0
.8897	.375	.75	1.125	1.5	1.875	2.25	2.625	3.0
.8529	.5	1.0	1.5	2.0	2.5	3.0	3.5	4.0
.8162	.625	1.25	1.875	2.5	3.125	3.75	4.375	5.0
.7794	.75	1.5	2.25	3.0	3.75	4.5	5.25	6.0
.7426	.875	1.75	2.625	3.5	4.375	5.25	6.125	7.0
.7059	1.0	2.0	3.0	4.0	5.0	6.0	7.0	8.0
.6324	1.25	2.5	3.75	5.0	6.25	7.5	8.75	10.0
.5588	1.5	3.0	4.5	6.0	7.5	9.0	10.5	12.0
.4853	1.75	3.5	5.25	7.0	8.75	10.5	12.5	14.0
.4118	2.0	4.0	6.0	8.0	10.0	12.0	14.0	16.0

One method which has been devised so as to satisfy the conservation rule is that of Born II.[5] The method consists of replacing the R-matrix, which was defined in Eq. (3.5), by the B-matrix, which for the particular case of three channels is given in atomic units by[5]

$$B_{ij} = -\tfrac{1}{2}\pi \int_0^\infty J_{\ell+\frac{1}{2}}(k_i r)\, U_{ij}(r)\, J_{\ell'+\frac{1}{2}}(k_j r)\, r\, dr \,, \tag{4.2}$$

where

$$\begin{aligned} U_{12} &= 2f_1(0\ \ell\ 1\ \ell\text{-}1;\ell)\ y_1(np,\ ns) \,, \\ U_{13} &= 2f_1(0\ \ell\ 1\ \ell\text{+}1;\ell)\ y_1(np,\ ns) \,, \end{aligned} \tag{4.3}$$

and

$$\begin{aligned} f_1(0\ \ell\ 1\ \ell\text{-}1;\ell) &= [\ell/3(2\ell+1)]^{\frac{1}{2}} \,, \\ f_1(0\ \ell\ 1\ \ell\text{+}1;\ell) &= -[(\ell+1)/3(2\ell+1)]^{\frac{1}{2}} \,. \end{aligned} \tag{4.4}$$

In the approximation of keeping only the asymptotic parts of the potentials (corresponding to the Bethe Approximation), we have

$$\begin{aligned} U_{11} = U_{22} = U_{33} &= 0 \,, \\ U_{12} = \ell^{\frac{1}{2}}\beta/r^2 \,, \quad U_{13} &= -(\ell+1)^{\frac{1}{2}}\beta/r^2 \end{aligned} \tag{4.5}$$

and

$$B_{12} = -\tfrac{1}{2}\pi\ell^{\frac{1}{2}}\beta \int_0^\infty J_{\ell+\frac{1}{2}}(k_o r)\, J_{\ell-\frac{1}{2}}(k_n r)\, r^{-1}\, dr \,, \tag{4.6}$$

$$B_{13} = -\tfrac{1}{2}\pi(\ell+1)^{\frac{1}{2}}\beta \int_0^\infty J_{\ell+\frac{1}{2}}(k_o r)\, J_{\ell+3/2}(k_n r)\, r^{-1}\, dr \,, \tag{4.7}$$

where

$$\beta = 2s_1(np, ns)/[3(2\ell + 1)]^{\frac{1}{2}} . \qquad (4.8)$$

Accordingly, the partial collision strength will be denoted by $\Omega_\ell^{B'II}$,

$$\Omega_\ell^{B'II} = 4(2\ell + 1)\{[(B_{12})^2 + (B_{13})^2]/[1 + (B_{12})^2 + (B_{13})^2]\} . \qquad (4.9)$$

The B'I (usual Bethe approximation) partial cross section may be expressed in terms of these matrix elements as

$$Q_\ell^{B'I} = \pi k_o^{-2}\, 4(2\ell + 1)[(B_{12})^2 + (B_{13})^2] . \qquad (4.10)$$

For purposes of comparison, Calculations of $\Omega_\ell^{B'II}$ have been made for E = 13.6 eV, s^2 = 19.3, and several values of the energy separation ΔE. The results are shown in Figure 12. From Figure 13 we see that for $\ell > 3$, the partial cross sections calculated by the resonance-distortion method and by B'II agree quite well with each other for ΔE as large as 3.0 eV. However, for $\ell = 2$ and $\ell = 3$, they are found to differ considerably. This can be ascribed to the fact that the method B'II tends to overestimate the collision strength for small ℓ, since in the limit of $\Delta E = 0$, $Q_\ell^{B'II}$ does exceed the corresponding partial cross section obtained from the exact calculation for $\ell = 2$ and 3.[5] Furthermore Figure 10 shows that for these low values of ℓ and for $\Delta E < 3.0$, Ω_ℓ^{RD} is quite insensitive to ΔE. Because of the insensitivity of the collision strength with respect to ΔE and the fact that for $\Delta E = 0$ the resonance-distortion result is exact for the

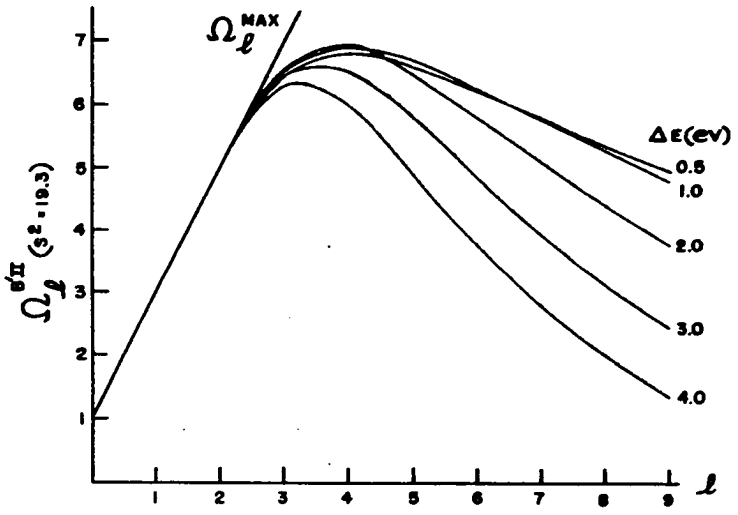

Figure 12. Bethe II Collision Strengths $\Omega_\ell^{B'II}$ with $s^2 = 19.3$ for Several Values of ΔE (eV).

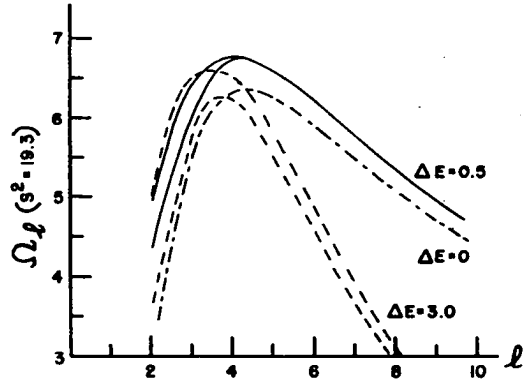

Figure 13. Collision Strengths Ω_ℓ^{RD} for $\Delta E = 0$, 0.5, 3.0 eV, and $\Omega_\ell^{B'II}$ for $\Delta E = 0.5$, 3.0 eV. (The upper of the two solid and of the two dashed curves correspond to the Bethe II method, and the lower, the Resonance-Distortion method.)

particular potentials chosen, it appears likely that the resonance-distortion method gives more accurate partial cross sections for small ℓ than does B'II.

CHAPTER V

APPLICATION - 3^2S-3^2P TRANSITION OF Na BY ELECTRON IMPACT

An excellent example of a near-resonance and strong-coupling situation is the 3^2S-3^2P transition in Na, which has an energy separation $\Delta E = 2.104$ eV and a rather large line strength $s^2 = 19.0$. Since this transition is optically allowed, the coupling matrix element V_{on} becomes proportional to $1/r^2$ asymptotically, and because of this long-range interaction it is expected that many partial waves will contribute to the total cross section. Salmona and Seaton[16] have discussed this problem and made calculations based on the modified Bethe approximations B'II and B'III, which are found to satisfy conservation conditions. Previously, Seaton had investigated, by a close coupling technique,[7] proton and electron impact on Na, giving rise to this transition; the results were found to be quite good for high energies. Cross sections for this transition have been determined experimentally and found to be large.[17]

Partial cross sections have been calculated for several values of the incident electron energy k_o^2 using the resonance-distortion method, Bethe I, and Bethe II approximations. Since for large values of ℓ, say $\ell > \ell_o$, the

coupling is weak, we find that the partial cross sections Q_ℓ^{RD}, $Q_\ell^{B'I}$ and $Q_\ell^{B'II}$ all coincide. The total cross sections may then be determined by utilizing the "tail" of B'I as

$$Q^{RD} = Q^{B'I} - \sum_{\ell=0}^{\ell_o} Q_\ell^{B'I} + \sum_{\ell=2}^{\ell_o} Q_\ell^{RD} + Q', \tag{5.1}$$

$$Q^{B'II} = Q^{B'I} - \sum_{\ell=0}^{\ell_o} Q_\ell^{B'I} + \sum_{\ell=0}^{\ell_o} Q_\ell^{B'II}, \tag{5.2}$$

where

$$Q_\ell^{B'I} = \pi k_o^{-2}(8s^2/3)\ \ell n\ [(k_o + k_n)/|k_o - k_n|], \tag{5.3}$$

and Q' represents the sum of the s and p cross sections, which must be determined in some other manner. Numerical values for Q_ℓ^{RD} and $Q_\ell^{B'II}$ are given in Tables II and III for several values of the incident energy and several ℓ; all cross sections are in units of πa_o^2. A comparison of the partial cross sections Q_ℓ^{RD}, $Q_\ell^{B'I}$, $Q_\ell^{B'II}$ and $\frac{1}{2}Q_\ell^{max}$ is given in Figures 14 and 15 for incident electron energies 10.520 eV and 33.660 eV, respectively. As is, of course, to be expected, the major contribution to the cross section in the case of E = 10.520 eV is due to a few intermediate values of ℓ; while for E = 33.660 eV, the contribution is more uniformly distributed among several different ℓ. One may also notice that Q_ℓ^{RD}, $Q_\ell^{B'I}$, and $Q_\ell^{B'II}$ all approach the same value for large ℓ, the convergence being faster for small E.

In calculating cross sections by the resonance-

TABLE II

PARTIAL CROSS SECTIONS IN UNITS OF πa_o^2 OF THE 3s→3p TRANSITION OF Na CALCULATED BY THE METHOD OF RESONANCE DISTORTION

	E(eV)					
ℓ	4.210	7.364	10.520	16.832	23.144	33.660
2	11.79	6.54	4.31	2.69	2.04	1.51
3	11.44	10.17	7.58	4.80	3.49	2.40
4	7.84	10.03	8.25	5.50	4.02	2.74
5	4.52	8.18	7.44	5.29	3.93	2.70
6	2.45	6.26	6.29	4.80	3.65	2.54
7	1.29	4.65	5.18	4.25	3.32	2.34
8	0.66	3.40	4.21	3.72	2.98	2.15
9	0.34	2.46	3.39	3.24	2.68	1.96
10	0.17	1.77	2.72	2.82	2.40	1.79
11	0.09	1.27	2.18	2.45	2.15	1.64
12	0.04	0.91	1.74	2.12	1.92	1.50
13	0.02	0.65	1.39	1.84	1.72	1.38
14	0.01	0.47	1.11	1.60	1.55	1.27
15	0.006	0.33	0.89	1.39	1.39	1.17

TABLE III

PARTIAL CROSS SECTIONS IN UNITS OF πa_o^2 OF THE 3s-3p TRANSITIONS OF Na CALCULATED BY B'II METHOD

	E(eV)					
ℓ	4.210	7.364	10.520	16.832	23.144	33.660
0	3.18	1.50	0.93	0.51	0.35	0.23
1	6.19	3.64	2.62	1.68	1.24	0.86
2	16.14	9.17	6.41	4.02	2.93	2.01
3	16.43	11.67	8.37	5.26	3.81	2.61
4	10.83	11.08	8.52	5.52	4.02	2.75
5	5.98	9.13	7.73	5.27	3.89	2.67
6	3.08	7.01	6.61	4.81	3.62	2.51
7	1.55	5.18	5.47	4.29	3.30	2.32
8	0.77	3.76	4.46	3.78	2.98	2.13
9	0.38	2.70	3.59	3.30	2.69	1.95
10	0.19	1.93	2.88	2.88	2.41	1.79
11	0.10	1.37	2.30	2.50	2.16	1.64
12	0.05	0.98	1.83	2.17	1.94	1.50
13	0.02	0.69	1.46	1.89	1.74	1.38
14	0.01	0.49	1.16	1.64	1.57	1.27
15	0.006	0.35	0.92	1.42	1.41	1.17

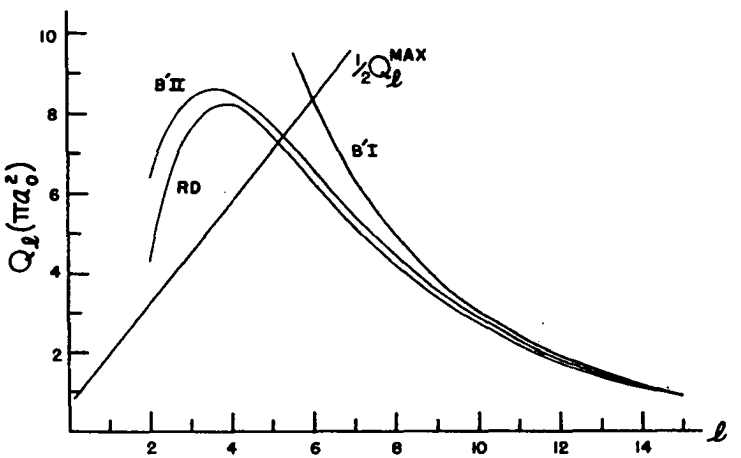

Figure 14. Partial Cross Sections Q_ℓ^{RD}, $Q_\ell^{B'I}$, $Q_\ell^{B'II}$, and $\frac{1}{2} Q_\ell^{max}$ for Na, $3^2s \rightarrow 3^2p$, by Electron Impact, with $\Delta E = 2.104$ eV and $s^2 = 19.0$ for an Incident Energy $E = 10.520$ eV

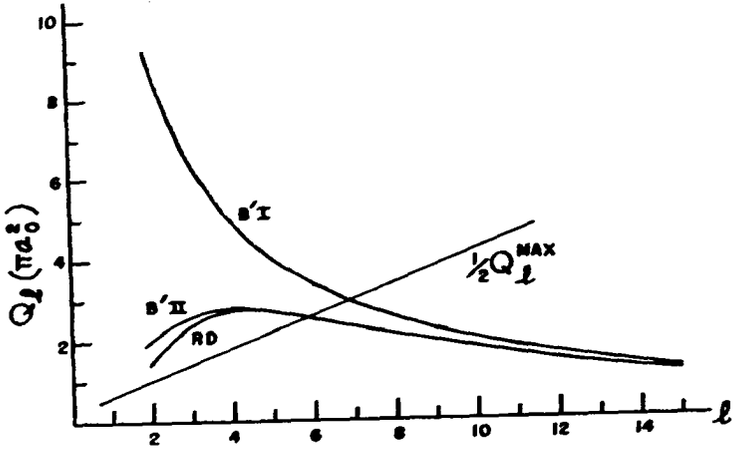

Figure 15. Partial Cross Sections Q_ℓ^{RD}, $Q_\ell^{B'I}$, $Q_\ell^{B'II}$, and $\frac{1}{2} Q_\ell^{max}$ for Na, $3^2s \rightarrow 3^2p$, by Electron Impact, with $\Delta E = 2.104$ eV and $s^2 = 19.0$ for an Incident Energy $E = 33.660$ eV.

distortion and Bethe methods, all of the hypergeometric functions needed, except those for E = 33.66 eV, were evaluated by means of the series representation[11]

$$ {}_2F_1(a;\ b;\ c;\ z) = \sum_{n=0}^{\infty} [(a)_n\ (b)_n/(c)_n\ n!]z^n, \qquad (5.4) $$

where

$$ (\rho)_n = (\rho + 1)(\rho + 2)\ \ldots\ (\rho + n - 1), \qquad (5.5) $$

and

$$ |z| \leq 1. $$

For the higher energy, use was made of a formula given by Seaton.[7]

The total resonance-distortion and Bethe II cross sections calculated by means of Eqs. (5.1) and (5.2) are given in Table IV. The cut-off value for the tail is ℓ_o = 15 and the percentage contributions from the tail, the intermediate values of ℓ, and ℓ = 0 and ℓ = 1 are also given in the table (i.e. % relative to Q^{RD}); the s and p cross sections were arbitrarily taken as $\frac{1}{2}Q_\ell^{max}$. In Figure 16, these cross sections are compared with Born approximation as well as absolute measurements of Christoph and relative measurements of Haft (as quoted by Bates, et al.).[18] The relative curve has been adjusted according to the absolute measurements. It is important to note that some freedom remains in the adjustment of Haft's relative measurements. Each resonance-distortion cross section in Figure 16 is accompanied by a bar indicating the maximum and

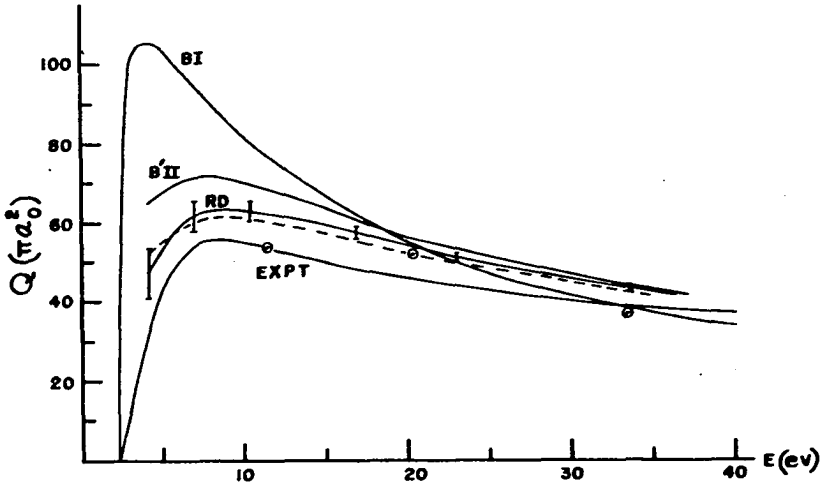

Figure 16. Total Cross Sections Q^{RD}, $Q^{B'I}$, $Q^{B'II}$, and Q^{CC} for Na, $3^2s \rightarrow 3^2p$, by Electron Impact. (The open circles refer to the absolute measurements of Christoph and the solid curve marked EXPT represents the relative measurements of Haft. The dashed curve represents Seaton's Close-Coupling Approximation Q^{CC}.)

TABLE IV

TOTAL CROSS SECTIONS IN UNITS OF πa_o^2 AND PARTIAL SUMS OF Q_ℓ FOR THE 3s→3p TRANSITION OF Na.

E(eV)	$Q^{B'I}$	$Q^{B'II}$	Q^{RD}	Q'	$\sum_{\ell=16}^{\infty} Q_\ell^{B'I}$	$\sum_{\ell=2}^{15} Q_\ell^{RD}$
4.210	288.63	64.9	47.1	6.5(13.7%)	0.0(0%)	40.66(86.3%)
7.364	231.87	71.6	61.7	3.7(6.0%)	0.9(1.5%)	57.10(92.5%)
10.520	189.12	68.9	62.9	2.6(4.1%)	3.6(5.7%)	56.69(90.2%)
16.832	139.19	60.5	57.7	1.6(2.8%)	9.6(16.6%)	46.50(80.6%)
23.144	111.26	53.3	51.6	1.2(2.3%)	13.2(25.6%)	37.24(72.1%)
33.660	84.48	44.4	43.5	0.8(1.8%)	15.6(35.9%)	27.10(62.3%)

minimum values obtained by taking $Q' = 0$ and $Q' = Q'_{max}$ respectively. (One may recall that in Table IV the value $\frac{1}{2}Q'_{max}$ was used.) It is clear that the form of the resonance-distortion curve is in reasonable agreement with that of the experimental curve, however we should not place too much faith in our results for small E, since in such cases, $k_o^2 - k_n^2$ is no longer very small compared to k_o^2 (i.e., the kinetic energy of relative motion changes considerably during the collision), and thus our assumption of exact resonance in the zeroth order is no longer justified. It is also likely that distortion effects due to the diagonal elements U_{oo}, U_{nn} will come in. Exchange effects have been neglected completely, and are expected to be important only for small ℓ; however, since for small E, the effect of small ℓ becomes significant, one might then expect exchange to be important.

A close coupling technique was devised by Seaton[7] specifically for cases where exceptionally strong coupling causes the weak coupling approximations to give much too large cross sections. In such cases, one may find a value ℓ_o of ℓ, such that

$$Q_\ell^{BI} \approx \tfrac{1}{2}\pi k_o^{-2}(2\ell_o + 1). \qquad (5.6)$$

It is found that a reasonably good approximation is

$$Q_\ell^{CC} = \begin{cases} \frac{1}{2}\pi k_o^{-2}(2\ell + 1), & \ell < \ell_o \\ Q_\ell^{BI}, & \ell \geq \ell_o \end{cases} \qquad (5.7)$$

It is known that for large ℓ, Q_ℓ^{BI} and $Q_\ell^{B'I}$ (standard Bethe approximation) coincide. Thus, if ℓ_o is suitably large, one may simplify calculation by replacing Q_ℓ^{BI} above by $Q_\ell^{B'I}$. Despite the simplicity of this approach, it is actually found to give satisfactory results. Cross sections calculated by this method (denoted by CC) are included in Figure 16. It should be pointed out that this method is strictly limited to cases of strong coupling, its failure in other cases having been clearly demonstrated.[7]

CHAPTER VI

TWO-CHANNEL APPROXIMATION FOR ELECTRON-ATOM COLLISION

Attempts have been made to devise a simplified procedure for the calculation of the collision strength by the resonance-distortion method, particularly to avoid the task of solving the three-channel, coupled differential equations. Here the zeroth-order solution of F_o (denoted by $F_o^{(o)}$ is again obtained from the limiting exact-resonance case, i.e., $F_o^{(o)}$ and $F_n^{(o)}$ satisfy the equations

$$(\nabla^2 + k_o^2)\, F_o^{(o)} = U_{on}\, F_n^{(o)} \,, \tag{6.1}$$

$$(\nabla^2 + k_o^2)\, F_n^{(o)} = U_{no}\, F_o^{(o)} \,. \tag{6.2}$$

At this point we introduce an additional approximation of replacing the angular dependent $U_{on}(\vec{r})$ by an angular independent potential of the form $-A/r^2$. This eliminates the three-channel coupling for the zeroth order equations and $F_o^{(o)}$ can be obtained by a procedure analogous to that given in Sec. III. We then solve for F_n by using this form of $F_o^{(o)}$ and the original angular dependent U_{on}. At first thought, this procedure might seem inconsistent in that we use an angular independent interaction potential to calculate

$F_o^{(o)}$, and an angular dependent one for F_n. However, it must be remembered that $F_o^{(o)}$ can be regarded as a first-step trial function. It need not be the solution of the problem corresponding to the true potentials as long as it has sufficient resemblence to the actual solution F_o of Eqs. (1.18) and (1.19).

The first task is to select a suitable value of A, so that $F_o^{(o)}$ gotten here will produce a satisfactory result for F_n. As suggested before, the potential $-A/r^2$ represents some kind of average of U_{on}. Considering Eqs. (1.37), we can write down the asymptotic form of U_{on} for the transitions ns→npm, as

$$U_{on} = (4/3)\sqrt{\pi}\, Y_1^m(\theta,\varphi)\, s/r^2 = U_{no}^*(\vec{r}) \qquad (6.3)$$

where θ, φ give the orientation of the incident particle in the atomic coordinate system. We recall that when one considers the cross section for transition to a degenerate level, one must sum the cross sections over each of the degenerate states of the level. This fact leads us to consider two averaging techniques in order to obtain an appropriate value of A. It should be remembered that the zeroth order function $F_o^{(o)}$ need only represent one of the three degenerate states ($m = 0, \pm 1$), since in performing the iteration it will be used to calculate the cross section for each of the degenerate states, separately. We first take A to be determined by averaging the modulus squared of $U_{on}^o(\vec{r})$

over all space as

$$(U_{on})_{rms} = -A/r^2 = \frac{4}{3}\sqrt{\pi}\left\{\frac{1}{4\pi}\int |Y_1^o(\hat{r})|^2\, d\hat{r}\right\}^{\frac{1}{2}} sr^{-2} = \frac{2}{3}\, s/r^2 , \tag{6.4}$$

thus

$$-A = \frac{2}{3}\, s.$$

Alternatively, we can average the square of the matrix elements over all the m values, i.e.,

$$(U_{on})_{rms} = \left\{\frac{1}{3}\left(|U_{on}^o|^2 + |U_{on}^{+1}|^2 + |U_{on}^{-1}|^2\right)\right\}^{\frac{1}{2}} = \frac{2}{3}\, s/r^2, \tag{6.5}$$

giving the same result as Eq. (6.4).

Next we shall determine F_n from

$$(\nabla^2 + k_n^2)\, F_n(\vec{r}) = U_{no}(\vec{r})\, F_o(\vec{r}) , \tag{6.6}$$

where U_{no} is given by Eq. (1.10). It is not permissible to expand $F_n(\vec{r})$ in terms of Legendre Polynomials since such an expansion implies cylindrical symmetry. Rather, the spherical harmonics must be used, i.e.,

$$F_n(\vec{r}) = r^{-1} \sum_{\ell g} F_{n,\ell g}(r)\, Y_{\ell g}(\hat{r}) . \tag{6.7}$$

The differential equation for the partial wave amplitudes is

$$\left[\frac{d^2}{dr^2} + k_n^2 - \ell(\ell+1)/r^2\right] F_{n,\ell g}(r) = \sum_{\ell' g'} \int Y_{\ell g}^*(\hat{r})\, U_{no}(\vec{r})$$

$$X\ Y_{\ell'g'}(\hat{r})\ F_{o,\ell'g'}(r)\ d\hat{r}. \qquad (6.8)$$

The desired solution may be found by the standard variation of parameters technique, in which the wronskian of the homogeneous solutions is chosen to be equal to one.[8] Thus we have for the partial wave amplitudes, the asymptotic result

$$F_{n,\ell g}(r) \sim (-1)^{\ell} \exp(ik_n r) \sum_{\ell'g'} \int_o^\infty r j_\ell(k_n r)\ F_{o,\ell'g'}(r)\ dr$$

$$X \int Y^*_{\ell g}(\hat{r})\ U_{no}(\vec{r})\ Y_{\ell'g'}(\hat{r})\ d\hat{r}\ , \qquad (6.9)$$

where

$$j_\ell(kr) = (\pi/2kr)^{\frac{1}{2}} J_{\ell+\frac{1}{2}}(kr)\ ,$$

and for the total inelastic function

$$F_n(\vec{r}) \sim r^{-1} \exp(ik_n r) \sum_{\ell g, \ell' g'} (-1)^{\ell} \int_o^\infty r j_\ell(k_n r)\ F_{o,\ell'g'}(r)\ dr$$

$$X \int Y^*_{\ell g}(\hat{r})\ U_{no}(\vec{r})\ Y_{\ell'g'}(\hat{r})\ d\hat{r}\ Y_{\ell g}(\hat{r})\ . \qquad (6.10)$$

In the case of optically allowed transitions, which are often accompanied by strong coupling, $U_{no}(\vec{r})$ will always include a dipole term i.e., a term given by

$$b_\mu(\ell\pm1\ m, \ell m')\ Y^*_{1\mu}(\hat{r})\ y_1(n\ \ell\pm1,\ n\ell|r)\ , \qquad (6.11)$$

where for ns→np transitions we have

$$b_m(pm,\ so) = (4/3)\sqrt{\pi}\ , \qquad (6.12)$$

and for large r

$$y_1(np,\ ns \mid r) \sim s_1(np,\ ns)/r^2 \ . \qquad (6.13)$$

We replace $U_{no}(\vec{r})$ in Eq. (6.10) by its asymptotic form, and noticing that as a result of the angular integration, $g = g' - m$ and $\ell = \ell' \pm 1$, we obtain for the total collision amplitude

$$\begin{aligned} f_n^m(\theta,\varphi) = \tfrac{4}{3}\sqrt{\pi}\ s \sum_{\ell' g'} (-1)^{\ell'} \Big\{ & \int_0^\infty j_{\ell'+1}(k_n r)\ F_{o,\ell' g'}(r)\ r^{-1}\,dr \\ & \times \int Y_{\ell'+1,g'-m}(\hat{r})\ Y_{1m}(\hat{r})\ Y_{\ell' g'}(\hat{r})\,d\hat{r} \cdot Y_{\ell'+1\ g'-m}(\hat{r}) \\ & - \int_0^\infty j_{\ell'-1}(k_n r)\ F_{o,\ell' g'}(r)\ r^{-1} dr \int Y^*_{\ell'-1\ g'-m}(\hat{r}) \\ & \times Y_{1m}(\hat{r})\ Y_{\ell' g'}(\hat{r})\,d\hat{r}\ Y_{\ell'-1\ g'-m}(\hat{r}) \Big\} \qquad (6.14) \\ = -2s \sum_{\ell g} (-1)^{\ell} \{ & I(\ell+1,\ell\ g)\ c^1(\ell\ g;\ \ell+1\ g-m) \\ & \times Y_{\ell+1\ g-m}(\hat{r}) + I(\ell-1,\ell\ g)\ c^1(\ell\ g;\ \ell-1\ g-m) \\ & \times Y_{\ell-1\ g-m}(\hat{r}) \} \ , \end{aligned}$$

where we have employed the Condon and Shortley notation,[13] (see Table V)

$$c^k(\ell m;\ell' m') = (2/2k+1)^{\frac{1}{2}} \int_0^\pi \Theta(k,m-m')\ \Theta(\ell,m)\ \Theta(\ell',m')\ \sin\theta\ d\theta, \qquad (6.15)$$

TABLE V

INTEGRALS OF THREE NORMALIZED ASSOCIATED LEGENDRE POLYNOMIALS.

$$c^1(\ell, 0; \ell + 1, \pm 1) = -[(\ell + 2)(\ell + 1)/2(2\ell + 3)(2\ell + 1)]^{\frac{1}{2}}$$

$$c^1(\ell, 0; \ell - 1, \pm 1) = [\ell(\ell - 1)/2(2\ell + 1)(2\ell - 1)]^{\frac{1}{2}}$$

$$c^1(\ell + 2, 0; \ell + 1, \pm 1) = [(\ell + 2)(\ell + 1)/2(2\ell + 5)(2\ell + 3)]^{\frac{1}{2}}$$

$$c^1(\ell - 2, 0; \ell - 1, \pm 1) = -[\ell(\ell - 1)/2(2\ell - 1)(2\ell - 3)]^{\frac{1}{2}}$$

$$c^1(\ell, 0; \ell + 1, 0) = (\ell + 1)/[(2\ell + 3)(2\ell + 1)]^{\frac{1}{2}}$$

$$c^1(\ell, 0; \ell - 1, 0) = \ell/[(2\ell + 1)(2\ell - 1)]^{\frac{1}{2}}$$

and where we have defined

$$I(\ell' \pm 1,\ \ell' g') \equiv \int_0^\infty j_{\ell' \pm 1}(k_n r)\ F_{o,\ell' g'}(r)\ r^{-1}\ dr. \qquad (6.16)$$

The total cross section for the transition ns→npm, is given by

$$\begin{aligned} Q(ns\to npm) &= (k_n/k_o) \int |f_n^m(\theta,\varphi)|^2\ d\Omega \\ &= (k_n/k_o)\ \frac{4}{3}\ s^2 \sum_{\ell g} \{ |I(\ell+1,\ell\ g)\ c^1(\ell\ g;\ \ell+1\ g-m)|^2 \\ &+ |I(\ell-1,\ell\ g)\ c^1(\ell\ g;\ell-1\ g-m)|^2 + I^*(\ell+1,\ell\ g) \\ &X\ I(\ell+1,\ell+2\ g)\ c^1(\ell\ g;\ell+1\ g-m)\ c^1(\ell+2\ g;\ell+1\ g-m) \\ &+ I^*(\ell-1,\ell\ g)\ I(\ell-1,\ell-2\ g)\ c^1(\ell\ g;\ell-1\ g-m) \\ &X\ c^1(\ell-2\ g;\ell-1\ g-m)\} . \end{aligned} \qquad (6.17)$$

In evaluating the radial integrals $I(\ell',\ell\ g)$, we use $F^{(o)}_{o,\ell g}(r)$ as determined for the case of exact resonance. In this section, we have made use of the expansion

$$F_o(\vec{r}) = r^{-1} \sum_{\ell g} F_{o,\ell g}(r)\ Y_{\ell g}(\hat{r}) . \qquad (6.18)$$

Comparing this with Eq. (1.68) for $F_{o,\ell}$, we find that

$$F_{o,\ell g}(r) = 2i^{\ell}[\pi(2\ell+1)]^{\frac{1}{2}}\ F_{o,\ell}(r)\ \delta_{g,o} \qquad (6.19)$$

where $\delta_{g,o}$ is the usual Kronecker delta. The radial integrals

are found to be given by

$$I(\ell\pm1,\ell\ 0) = i\pi^{3/2}(-1)^{\ell}(2\ell+1)^{\frac{1}{2}}(k_o k_n)^{-\frac{1}{2}} \exp(-\tfrac{1}{4}\pi i)$$
$$\times [H^{+}(\ell\pm1,\ell) \exp(-\tfrac{1}{2}ip_{+}\pi)$$
$$+ H^{-}(\ell\pm1,\ell) \exp(-\tfrac{1}{2}ip_{-}\pi)] , \qquad (6.20)$$

where we have defined

$$H^{+}(\ell\pm1,\ell) \equiv \tfrac{1}{2}\int_0^\infty J_{p_+}(k_o r)\, J_{\ell\pm1+\frac{1}{2}}(k_n r)\, r^{-1}\, dr ,$$
$$H^{-}(\ell\pm1,\ell) \equiv \tfrac{1}{2}\int_0^\infty J_{p_-}(k_o r)\, J_{\ell\pm1+\frac{1}{2}}(k_n r)\, r^{-1}\, dr . \qquad (6.21)$$

Making use of the coefficients given in Table V, we find for the total cross sections

$$Q(ns\to np(\pm1)) = \pi k_o^{-2}(4/3)(\pi s)^2 \sum_{\ell} \Big\{ \frac{(\ell+2)(\ell+1)}{2(2\ell+3)}$$
$$\times |G(\ell+1,\ell)|^2 + \frac{\ell(\ell-1)}{2(2\ell-1)} |G(\ell-1,\ell)|^2$$
$$- \frac{(\ell+2)(\ell+1)}{2(2\ell+3)} G^{*}(\ell+1,\ell)\, G(\ell+1,\ell+2) \qquad (6.22)$$
$$- \frac{\ell(\ell-1)}{2(2\ell-1)} G^{*}(\ell-1,\ell)\, G(\ell-1,\ell-2) ,$$

and

$$Q(ns\to npo) = \pi k_o^{-2}(4/3)(\pi s)^2 \sum_{\ell} \Big\{ \frac{(\ell+1)^2}{2\ell+3} |G(\ell+1,\ell)|^2$$
$$+ \frac{\ell^2}{2\ell-1} |G(\ell-1,\ell)|^2 + \frac{(\ell+2)(\ell+1)}{2\ell+3} G^{*}(\ell+1,\ell)$$

$$x\ G(\ell+1,\ell+2) + \frac{\ell(\ell-1)}{2(2\ell-1)} G^*(\ell-1,\ell)\ G(\ell-1,\ell-2)\ \Big\}\ , \tag{6.23}$$

where we have defined

$$G(\ell\pm1,\ell) \equiv H^+(\ell\pm1,\ell)\ \exp\ (-\tfrac{1}{2}\ ip_+\pi) + H^-(\ell\pm1,\ell)\ \exp\ (-\tfrac{1}{2}ip_-\pi). \tag{6.24}$$

Since the initial state is non-degenerate, we need only sum the three cross sections above to obtain the total ns→np cross section; one finds

$$Q(ns\to np) = \pi k_o^{-2}(4/3)(\pi s)^2 \sum_\ell \Big\{(\ell+1)|G(\ell+1,\ell)|^2 + \ell|G(\ell-1,\ell)|^2\Big\}\ . \tag{6.25}$$

The radial integrals given in Eqs. (6.24) may be readily evaluated in terms of hypergeometric functions[9] as

$$\begin{aligned} H^\pm(\ell+1,\ell) &= \tfrac{1}{2}\int_0^\infty J_{p_\pm}(k_o r)\ J_{\ell+3/2}(k_n r)\ r^{-1}\ dr \\ &= \tfrac{1}{4}(k_n/k_o)^{\ell+3/2}\{\Gamma(a_\pm)/\Gamma(c_\pm)\ \Gamma(1-b_\pm)\} \\ &\quad x\ {}_2F_1\ [a_\pm,\ b_\pm;\ c_\pm;\ (k_n/k_o)^2]\ , \end{aligned} \tag{6.26}$$

where

$$\begin{aligned} a_\pm &= \tfrac{1}{2}(p_\pm + \ell + 3/2)\ , \\ b_\pm &= \tfrac{1}{2}(\ell + 3/2 - p_\pm)\ , \\ c_\pm &= \ell + 5/2\ , \end{aligned} \tag{6.27}$$

and

$$H^{\pm}(\ell-1,\ell) = \tfrac{1}{2}\int_0^{\infty} J_{p_\pm}(k_o r)\, J_{\ell-\frac{1}{2}}(k_n r)\, r^{-1}\, dr$$

$$= \tfrac{1}{4}(k_n/k_o)^{\ell-\frac{1}{2}}\{\Gamma(a'_\pm)/\Gamma(c'_\pm)\,\Gamma(1-b'_\pm)\} \qquad (6.28)$$

$$\times\ {}_2F_1\,[a'_\pm,\ b'_\pm;\ c'_\pm;\ (k_n/k_o)^2]\ ,$$

with

$$a'_\pm = \tfrac{1}{2}(p_\pm + \ell + 3/2)\ ,$$

$$b'_\pm = \tfrac{1}{2}(\ell + 3/2 - p_\pm)\ , \qquad (6.29)$$

$$c'_\pm = \ell + 5/2\ .$$

We notice that Eq. (6.25) is of precisely the same form as the Born cross section given by Eq. (2.47), except that the radial integrals are different and in the iteration result, contain the A dependence. It can be shown that for a given A and large values of ℓ, or for small A and any values of ℓ, the two results coincide. This is to be expected since A is a measure of the distortion of F_o, and its effect becomes much less pronounced for large ℓ; we also find that for A→0 we have $F_o^{(o)}(\vec{r}) \to \exp\,(i\vec{k}_o\cdot\vec{r})$.

The criterion by which we chose the constant A is, of course, somewhat intuitive. It is based on the well-known idea that transitions in an atomic system are governed by the absolute square of the matrix elements of the external perturbation connecting the initial and the final state.

Since the cross sections calculated from Eq. (6.25) do depend appreciably on A, the use of the two-channel approximation does introduce some uncertainty to the cross sections. Nevertheless, this "two-channel" scheme may be used as an approximate method for calculating the cross sections where more detailed calculations are impractical. Figure 17 shows reasonable agreement between the collision strengths calculated by the three-channel coupling equations and by the two-channel approximation with $A = -\frac{2}{3}s$. Also is shown the variation of the collision strengths with respect to A.

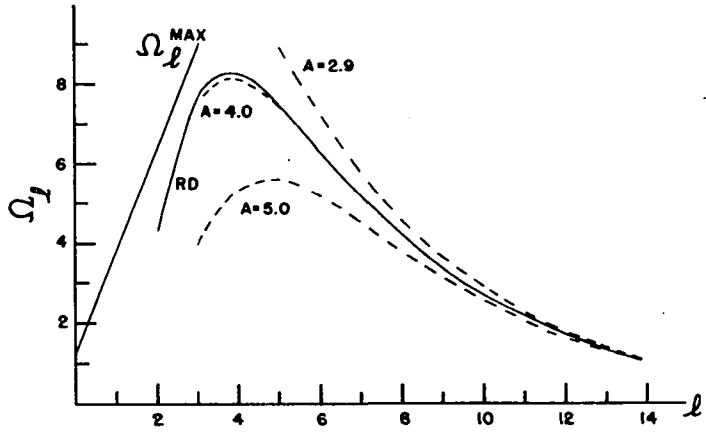

Figure 17. Collision Strengths Ω_ℓ^{RD} (s^2 = 19.0) and Ω_ℓ (2-Channel, A = 2.9, 4.0, 5.0) for Na, $3^2s \rightarrow 3^2p$, by Electron Impact, with ΔE = 2.104 eV. (The value of A = 2.9 corresponds to the relation $|A| = 2|s|/3$).

CHAPTER VII

DISCUSSION

In the calculations presented in the previous chapters, we have made the approximation of using a special set of potential functions as given in Eqs. (1.37) and of neglecting the effect of exchange between the colliding and the atomic electrons. For transitions with long-range coupling, where the total cross section is distributed over a large number of Q_ℓ, these approximations can be justified on the basis that they affect only the partial cross sections corresponding to small values of ℓ. The use of the approximate potential functions is merely to simplify the calculation of the cross sections, and is not essential to the method of resonance-distortion. In case U_{oo} and U_{nn} are not set to zero, our zeroth order solution, in the uncoupled representation,[19] is taken as the solution of

$$(\nabla^2 + k_o^2 - U_{oo})\, F_o^{(o)} = U_{on}\, F_n^{(o)} \,, \qquad (7.1)$$

$$(\nabla^2 + k_o^2 - U_{oo})\, F_n^{(o)} = U_{no}\, F_o^{(o)} \,,$$

and the first approximation of F_n is gotten by solving

$$(\nabla^2 + k_n^2 - U_{nn})\, F_n = U_{no}\, F_o^{(o)} \,. \qquad (7.2)$$

We have investigated, to a certain extent, the effects of the parts of the potential functions which were neglected in Eqs. (1.37), on the cross sections. For electron-atom collisions, U_{oo} and U_{nn} behave like $-r^{-1}\exp(-ar)$ near the origin and decay rapidly on account of the exponential factor. The radial part of $-U_{on}$ is proportional to r^{-2} at large distances (ns→np), but attains a maximum and eventually passes through the origin as r is decreased to zero. Even for elastic collision problems, the functional form of U_{oo} is so complicated as to make exact solution impractical. In their studies of elastic collisions between electrons and atoms of the rare gases, Allis and Morse[20] used a potential of the form

$$\begin{aligned} V &= Z(1/r_o - 1/r), && r < r_o, \\ &= 0, && r \geq r_o, \end{aligned} \tag{7.3}$$

which makes possible an analytic solution of the Schroedinger equation. As a trial calculation we have considered a modified schematic model with the following interaction terms:

$$\left.\begin{aligned} U_{oo} &= U_{nn} = 2Z(1/r_o - 1/r) \\ U_{on} &= 0 \end{aligned}\right\} \quad r < r_o, \tag{7.4}$$

$$\left.\begin{aligned} U_{oo} &= U_{nn} = 0 \\ U_{on} &= -A/r^2 \end{aligned}\right\} \quad r \geq r_o\ . \tag{7.5}$$

We chose the parameter r_o so that at $r = r_o$, U_{oo} and U_{nn} are

both very small and U_{on} has deviated appreciably from its asymptotic inverse-square form. Once r_o is fixed, z can be determined in the same manner as was done by Allis and Morse.[20] For the case of <u>exact</u> resonance, the solutions of F_o and F_n can be expressed in terms of the coulomb wave functions[20] ($r < r_o$) and Bessel functions ($r \geq r_o$). We have calculated the partial cross sections (exact resonance) for the 2s→2p transitions of H at an electron energy of 13.6 eV using the two-region interaction potentials of Eqs. (7.4) and (7.5), and have repeated the same calculation with the one-region asymptotic form of Eqs. (1.38). It is found that the results of these two cases are different only for small ℓ. For instance, the sum of Q_ℓ from $\ell = 2$ to $\ell = 7$ varies by about 10%. Thus for transitions involving a long-range interaction, the introduction of the two-region potential alters the total cross section only slightly.

The exchange effect of the electrons can be incorporated into the formulation of the method of resonance distortion. If we consider only the interaction of two states, ψ_o and ψ_n, the total wave function is now expanded as

$$\Psi(1,2) = F_o(\vec{r})\,\psi_o(\vec{r}') + F_n(\vec{r})\,\psi_n(\vec{r}') + G_o(\vec{r}')\,\psi_o(\vec{r}) + G_n(\vec{r}')\,\psi_n(\vec{r}) \,, \tag{7.6}$$

in the uncoupled representation. Upon introducing

$$\begin{aligned} F_{o,\pm} &= F_o \pm G_o \,, \\ F_{n,\pm} &= F_n \pm G_n \,, \end{aligned} \tag{7.7}$$

we obtain the differential equations for the scattering amplitudes as[2]

$$[\nabla^2 + k_o^2 - U_{oo}]\, F_{o,\pm}(\vec{r}) \pm \int K_{oo}(\vec{r},\vec{r}')\, F_{o,\pm}(\vec{r}')\, d\vec{r}' = U_{on} F_{n,\pm}(\vec{r}) \mp \int K_{on}(\vec{r},\vec{r}')\, F_{n,\pm}(\vec{r}')\, d\vec{r}' \,, \tag{7.8}$$

$$[\nabla^2 + k_n^2 - U_{nn}]\, F_{n,\pm}(\vec{r}) \pm \int K_{nn}(\vec{r},\vec{r}')\, F_{n,\pm}(\vec{r}')\, d\vec{r}' = U_{no} F_{o,\pm}(\vec{r}) \mp \int K_{no}(\vec{r},\vec{r}')\, F_{o,\pm}(\vec{r}')\, d\vec{r}' \,, \tag{7.9}$$

where U_{oo}, U_{nn}, and U_{on} are given by Eq. (1.24), and

$$K_{oo}(\vec{r}_1,\vec{r}_2) = \psi_o^*(\vec{r}_1)\, \psi_o(\vec{r}_2)\, (k_o^2 - 2/r_{12} - 2E_o) \,,$$

$$K_{nn}(\vec{r}_1,\vec{r}_2) = \psi_n^*(\vec{r}_1)\, \psi_n(\vec{r}_2)\, (k_n^2 - 2/r_{12} - 2E_n) \,, \tag{7.10}$$

$$K_{on}(\vec{r}_1,\vec{r}_2) = \psi_n^*(\vec{r}_1)\, \psi_o(\vec{r}_2)\, (k_n^2 - 2/r_{12} - 2E_o) = K_{no}^*(\vec{r}_2,\vec{r}_1) \,.$$

The zeroth order solutions, which will be denoted as $F^{(o)}_{o,\pm}$ and $F^{(o)}_{n,\pm}$, are taken as the solutions of the limiting exact-resonance problem, ignoring exchange. Under these limiting conditions, Eqs. (7.8) and (7.9) reduce to Eqs. (7.1) and $F^{(o)}_{o,\pm}$ and $F^{(o)}_{n,\pm}$ become identical to the functions $F^{(o)}_o$ and $F^{(o)}_n$, respectively. We then replace $F_{o,\pm}$ in Eq. (7.9) by $F^{(o)}_{o,\pm}$ and solve for $F_{n,\pm}$. A similar iteration procedure can be used if one expands $\Psi(1,2)$ in terms of basis functions of the coupled representation.[14]

Finally we wish to discuss the applicability of the method of resonance distortion and its relation to other

approximate methods of solving collision problems. First of all, the method of resonance distortion is restricted to problems involving near resonance, since the limiting case of exact resonance is taken as the zeroth-order approximation. This method is most suitable for cases where the coupling between the initial and final states is strong. We can illustrate the nature of this method through a partial wave analysis. The partial cross sections corresponding to large ℓ for the strong coupling case reduce to the Born partial cross sections, because partial waves of large ℓ are classically equivalent to distant impacts and at large distances, U_{oo}, U_{nn}, and U_{on} are sufficiently small so that the Born Approximation is applicable. At lower ℓ the "effective" coupling becomes so large that the use of the Born Approximation and the Method of Distorted Waves, which are valid for weak coupling, is not always justifiable. It is in this region of ℓ (called "low ℓ region") that the method of resonance distortion is useful. For collision-induced transitions with a long-range interaction potential, where the contribution from the partial cross sections in the "low ℓ region" constitutes a substantial part of the total cross section (e.g., Table IV), we may expect the method of resonance distortion to yield more accurate results than the usual Born Approximation.

For very weak coupling, the results of the method of resonance distortion approach those of the Method of Distorted Waves. This can be seen from Eqs. (7.1) and (7.2). When U_{on}

becomes very small, $F_o^{(o)}$ in Eq. (7.2) is nearly equal to the zeroth order solution in the Method of Distorted Waves, which is defined by

$$(\nu^2 + k_o^2 - U_{oo})(F_o^{(o)})_{DW} = 0.$$

The difference in F_n as calculated by these two zeroth order functions should be small compared to F_n itself.

CHAPTER VIII

THE CONTINUUM OF ATOMIC HYDROGEN

For some time, researchers have been aware of the existence of a strong continuum in hydrogen arcs, sparks, and of particular interest in the expansion from an electric shock tube;[21] the continuum radiation is of particular interest in the visible region, and hence this investigation will concern, primarily, wavelengths in the range 2000 to 6000 A°.

It was generally believed that this continuum was due to recombination (i.e., radiation resulting from the combining of a free electron with a proton), and proton-electron bremsstrahlung, however it was often found that the measured intensity was too strong to be explained by these alone.[21] In high-pressure hydrogen-arc experiments,[22] it was shown that a large part of the continuum was due to the free-bound transition of the negative hydrogen ion (i.e., the attachment of a free electron onto a neutral hydrogen atom). The importance of the reverse process of photodetachment of H^-, as an absorption mechanism in the atmosphere of the sun, had been realized for some time,[23] and much work had already been done on the calculation of absorption coefficients.[24]

In electrically energized shocks, it is possible to

have conditions in which local thermodynamic equilibrium is not present[25] (e.g. populations of excited levels are not related by the Boltzmann factors, and the Saha equation doesn't apply) and hence, such properties as electron density and electron temperature are not simply related. Since measurements of such properties are often quite uncertain, it was felt that a comparison of measured continuum intensities with those calculated under an array of different conditions, could be helpful in determining characteristics of the plasma. With this in mind, then, we determine contributions to the hydrogen continuum from several processes, assuming only that the electrons themselves are in thermal equilibrium (i.e. an electron temperature T may be defined).

Electron-Proton, Radiative Recombination

Whenever a free electron is located in the proximity of a proton, there exists a finite probability that the two will combine to form a bound state (say, n, ℓ) of the hydrogen atom. In so doing, an amount of energy $h\nu$ is emitted, where

$$h\nu = E + I_{n,\ell} \,, \tag{8.1}$$

E being the initial kinetic energy of the electron and $I_{n,\ell}$ the ionization potential of the level n,ℓ. In the following, we shall neglect the lifting of the ℓ-degeneracy in hydrogen (i.e. $I_{n,\ell} \rightarrow I_n$). The cross section for such a process is well known and is given by[22,26,27]

$$\sigma_R = \frac{32\pi}{3\sqrt{3}} \frac{e^2\hbar}{m^2c^3} \frac{\nu_1^2}{\nu(\nu - \nu_n)} \frac{g_{II}}{n^3} \tag{8.2}$$

where g_{II} is the Gaunt factor for the free-bound transition[28] and

$$\nu_n = \frac{\nu_1}{n^2}, \quad \nu_1 = Rc, \tag{8.3}$$

where R is the Rydberg constant. Gaunt factors have been calculated and tables are available,[29] however for most cases one finds $g_{II} \cong 1$.[28-30]

The cross section given in Eq. (8.2) is for a process in which a free electron of kinetic energy $E = h(\nu - \nu_n) = \frac{1}{2}mv^2$ is captured into the nth quantum state of a hydrogen atom. In general, we do not have a beam of monoenergetic electrons but rather a maxwellian energy distribution, where the number of electrons per unit volume in the energy range E, E + dE is given by

$$N_e \frac{2}{\sqrt{\pi}} (kT)^{-3/2} e^{-E/kT} E^{1/2} dE,$$

where N_e is the electron number density. Combining with Eq. (8.2) and multiplying by $v N_1 h\nu$, we obtain the energy per unit volume, per unit time, per unit solid angle emitted from a system of electrons and protons having densities N_e and N_i respectively, for recombination into the nth state; thus

$$\epsilon_{\nu,n} d\nu = C \frac{4\pi^2 e^4 m}{h^2 n^3} \frac{N_e N_i}{(kT)^{3/2}} e^{h(\nu_n - \nu)/kT} \tag{8.4}$$

where

$$C = \frac{32\,\pi^2 e^6}{3\sqrt{3}\,c^3\,(2\pi m)^{3/2}} .$$

In order to obtain the total power emitted per unit volume, one must sum Eq. (8.4) over all values of n such that $E = h(\nu - \nu_n) > 0$. It has been a standard practice to sum over n up to, say $n = 4$, and then integrate from $n = 5$ to ∞, thus taking advantage of the nearness of levels for high n values.[22] However, consideration of the stark broadening of higher levels suggests that only a finite number of discrete states be considered,[31-33] the cut-off being taken when the broadening becomes of the same order as the level separation, i.e.

$$\Delta E_m \cong Rhc \left[\frac{1}{m^2} + \frac{1}{(m+1)^2} \right] , \qquad (8.5)$$

where ΔE_m is the spread of the mth level due to the perturbation of the microfield.

Lowering of the Ionization Potential

Several researchers have considered this problem of determining to what extent the presence of electrons and ions in the proximity of a hydrogen atom causes the ionization potential to decrease and the corresponding series limits to shift toward larger wave lengths.[33-35] However, the most straightforward theory is probably that of Unsöld,[36] in which he considers only nearest neighbor interactions which is valid for not too high densities.[35] His result for the

lowering of the ionization potential $\Delta\chi$ is given by

$$\log\ (\Delta\chi) = -\ 6.158 + \frac{1}{3}\log\ N_e\ , \tag{8.6}$$

where N_e is the electron density. The principal quantum number corresponding to this energy is determined from

$$\Delta\chi = \frac{e^2}{2a_o}\frac{1}{n^2}\ , \tag{8.7}$$

and hence

$$\log\ n = 3.645 - \frac{1}{6}\log\ N_e\ . \tag{8.8}$$

This equation is found to give roughly the same value of n, for a given electron density, as the value, obtained by Inglis and Teller,[31] for which the levels begin to overlap due to Stark broadening; they obtained

$$7.5\ \log\ n = 23.26 - \log\ N\ , \tag{8.9}$$

where

$$\begin{aligned} N &= 2N_e\ , \qquad T \leq (10^5/n)^\circ K\ , \\ N &= N_e\ , \qquad T > (10^5/n)^\circ K\ . \end{aligned} \tag{8.10}$$

According to Eq. (8.10), only the ions are effective at larger temperatures.

Since we are not striving for high accuracy in this investigation, we choose to take advantage of the simplicity of Unsöld's results. It is convenient to consider the rate of photon emissions (i.e. number of photons/cm^3-sec-cm wavelength), which is related to the emission coefficient by

$$R_n = \frac{dn}{d\lambda} = \frac{4\pi}{h\lambda}\,\epsilon_{\nu,n} \,. \tag{8.11}$$

Thus we have

$$R_n = N_e N_i \;\frac{3.2594 \times 10^{27}}{\lambda T^{3/2} n^3}\;\exp\left\{-\frac{14.3867}{T}\left(\frac{1}{\lambda} - \frac{1}{\lambda_n}\right)\right\} \text{cm}^{-3}\ \text{sec}^{-1}\ \text{cm}^{-1} \,, \tag{8.12}$$

where

$$\lambda_n = (.911)\,\frac{p^2 n^2}{p^2 - n^2} \,, \tag{8.13}$$

$$p = 5612.1\left(\frac{3}{4\pi N_e}\right)^{1/6} \,, \tag{8.14}$$

and where λ and T are in units of 10^3 A° and 10^4°K, respectively, and N_e and N_i are in units of 10^{17} cm^{-3}. The parameter p is a measure of the shift of the ionization potential. The total rate of photon emission for a given wavelength is given by

$$R_r = \sum_{n=\ell}^{m} R_n \,, \tag{8.15}$$

where m is the largest integer contained in p, and ℓ is the smallest integer such that $\lambda \leq \lambda_\ell$. Of course, Eq. (8.14) is equivalent to Unsöld's result given in Eq. (8.8). The net effect of including the lowering of the ionization potential is to decrease somewhat the contribution from recombination

and to shift the discontinuity, due to passing over the Balmer series limit, toward higher wavelengths.

It should be pointed out here that we have made a rather arbitrary choice in shifting the ionization potential by $\Delta\chi$. Actually, the effects of the merging of higher levels and the lowering of the ionization potential are inseparable, and each plays a part in the apparent shift of the Balmer series limit. However, since the pseudo-continuum resulting from the overlapping of higher levels joins smoothly onto the real continuum, the net result will be approximately the same regardless of the degree of participation by each of the two effects.

In Tables VI-XVII are given calculated values of the rates of emission from proton-electron recombination (i.e., number of photons emitted per cm^3 per sec per cm of wavelength), which are obtained with the aid of Eqs. 8.12 - 8.15. Results are given for four arbitrarily chosen electron densities; the electron density, of course, enters the calculation through the shift of the ionization potential. It should be pointed out that the number of significant figures in all of the tables to be presented is in no way indicative of the accuracy; one should recall that in all cases, we have taken the gaunt factors as unity, which may cause errors ranging from about 1% for recombination to possibly as high as 15% for bremsstrahlung.

TABLE VI

CALCULATED RATES OF EMISSION FROM PROTON-ELECTRON RECOMBINATION

(units of $n_e^2 \times 10^{22}$ cm^{-3} sec^{-1} cm^{-1}

$n_e = .01$ ($N_e = 10^{15}$ cm^{-3})*, p = 13.98, λ (limit) = 3722 A°

	T (10^4 °K)									
λ (10^3 A°)	.50	.55	.60	.65	.70	.75	.80	.85	.90	.95
1.0	.0001	.0005	.0021	.0074	.0210	.0519	.1137	.2261	.4148	.7114
1.5	.8220	2.023	4.239	7.859	13.24	20.69	30.40	42.50	57.00	73.85
2.0	74.58	118.7	172.9	235.8	305.3	379.5	456.7	535.2	613.7	691.1
2.5	1060.	1298.	1522.	1725.	1907.	2067.	2207.	2326.	2428.	2514.
3.0	6015.	6189.	6271.	6288.	6256.	6189.	6099.	5992.	5874.	5749.
3.5	20292.	18434.	16838.	15462.	14268.	13225.	12308.	11498.	10779.	10136.
4.0	211.0	265.5	318.6	369.1	415.9	458.6	497.0	531.2	561.2	587.2
4.5	417.2	488.0	551.3	606.7	654.3	694.5	728.1	755.6	777.6	795.0
5.0	711.7	785.4	845.3	892.9	929.7	957.3	977.2	990.5	998.4	1002.
5.5	1092.	1149.	1188.	1214.	1228.	1234.	1232.	1225.	1214.	1199.
6.0	1548.	1565.	1567.	1556.	1537.	1512.	1483.	1451.	1417.	1383.
6.5	2066.	2021.	1967.	1908.	1847.	1785.	1724.	1664.	1606.	1550.
7.0	2632.	2501.	2377.	2259.	2149.	2046.	1950.	1861.	1778.	1700.
7.5	3230.	2995.	2787.	2603.	2440.	2293.	2161.	2041.	1932.	1833.
8.0	3849.	3491.	3191.	2935.	2714.	2522.	2353.	2203.	2069.	1949.
8.5	4476.	3983.	3582.	3251.	2971.	2733.	2528.	2348.	2191.	2051.
9.0	625.9	633.0	632.6	626.8	617.3	605.1	591.3	576.3	560.7	544.9
9.5	701.6	698.8	689.5	675.9	659.5	641.3	622.2	602.8	583.3	564.0
10.0	775.5	761.8	743.1	721.4	698.1	674.0	649.8	626.0	602.7	580.3

*Here, n_e is the electron density N_e, in units of 10^{17} cm^{-3}.

TABLE VII

CALCULATED RATES OF EMISSION FROM PROTON-ELECTRON RECOMBINATION

(units of $n_e^2 \times 10^{22}$ cm^{-3} sec^{-1} cm^{-1})

$n_e = .01$ ($N_e = 10^{15}$ cm^{-3}, p = 13.98, λ (limit) = 3722 A°

	T (10^4 °K)								
λ (10^3 A°)	1.0	1.5	2.0	2.5	3.0	3.5	4.0	4.5	5.0
1.0	1.152	22.11	87.06	185.6	293.8	394.8	480.4	548.7	600.6
1.5	92.93	360.5	638.4	842.4	968.8	1036.	1062.	1062.	1045.
2.0	766.6	1337.	1588.	1649.	1616.	1541.	1451.	1357.	1266.
2.5	2585.	2792.	2608.	2345.	2088.	1860.	1663.	1494.	1350.
3.0	5621.	4409.	3511.	2868.	2396.	2038.	1761.	1541.	1363.
3.5	9558.	5967.	4239.	3233.	2580.	2125.	1792.	1538.	1340.
4.0	609.6	694.	658.0	592.9	526.7	467.2	416.0	372.2	335.0
4.5	808.1	805.2	714.3	618.3	534.8	465.6	408.6	361.6	322.6
5.0	1001.	896.8	754.3	632.4	535.5	459.1	398.3	349.4	309.5
5.5	1182.	970.6	781.5	638.3	531.2	449.7	386.6	336.7	296.4
6.0	1348.	1029.	798.9	638.4	523.6	438.7	374.2	323.9	283.9
6.5	1496.	1074.	808.7	634.5	514.0	426.9	361.7	311.5	271.9
7.0	1627.	1108.	812.7	627.6	503.1	414.7	349.4	299.6	260.6
7.5	1742.	1133.	812.3	618.8	491.5	402.5	337.5	288.3	249.9
8.0	1841.	1151.	808.6	608.6	479.5	390.5	326.0	277.6	240.0
8.5	1926.	1162.	802.4	597.5	467.5	378.8	315.1	267.4	230.7
9.0	529.0	390.4	296.1	232.8	188.6	156.6	132.6	114.1	99.54
9.5	545.2	391.2	292.6	228.1	183.8	152.0	128.3	110.2	95.90
10.0	558.6	390.9	288.7	223.3	179.0	147.5	124.2	106.4	92.50

TABLE VIII

CALCULATED RATES OF EMISSION FROM PROTON-ELECTRON RECOMBINATION

(units of $n_e^2 \times 10^{22}$ cm^{-3} sec^{-1} cm^{-1})

$n_e = .01$ ($N_e = 10^{15}$ cm^{-3}), p = 13.98, λ (limit) = 3722 A°

	T (10^4 °K)									
λ (10^3 A°)	5.5	6.0	6.5	7.0	7.5	8.0	8.5	9.0	9.5	10.0
1.0	638.3	664.1	680.4	689.0	691.8	690.0	684.6	676.6	666.7	655.3
1.5	1018.	984.6	948.6	911.4	874.2	837.7	802.4	768.6	736.3	705.7
2.0	1180.	1101.	1029.	962.8	902.6	847.8	797.9	752.4	710.8	672.7
2.5	1227.	1120.	1027.	945.9	874.8	811.9	756.1	706.2	661.6	621.4
3.0	1217.	1095.	991.9	904.0	828.4	762.8	705.3	654.7	609.9	570.0
3.5	1181.	1052.	944.7	854.6	778.0	712.2	655.3	605.6	561.9	523.2
4.0	303.2	275.9	252.3	231.7	213.7	197.9	183.9	171.5	160.4	150.4
4.5	289.8	262.1	238.4	218.1	200.4	185.0	171.4	159.4	148.7	139.1
5.0	276.4	248.8	225.4	205.4	188.2	173.2	160.1	148.6	138.4	129.3
5.5	263.6	236.3	213.3	193.9	177.2	162.7	150.1	139.1	129.3	120.6
6.0	251.4	224.6	202.2	183.3	167.2	153.3	141.2	130.6	121.3	113.0
6.5	239.9	213.8	192.0	173.7	158.2	144.8	133.2	123.1	114.2	106.3
7.0	229.3	203.8	182.7	165.0	150.0	137.1	126.0	116.3	107.8	100.3
7.5	219.4	194.6	174.2	157.1	142.6	130.2	119.5	110.2	102.1	94.86
8.0	210.2	186.1	166.3	149.8	135.8	123.9	113.6	104.7	96.89	90.00
8.5	201.7	178.3	159.1	143.1	129.7	118.2	108.3	99.72	92.22	85.61
9.0	87.80	78.18	70.20	63.48	57.77	52.86	48.61	44.90	41.63	38.75
9.5	84.46	75.12	67.37	60.87	55.34	50.61	46.51	42.93	39.79	37.02
10.0	81.35	72.27	64.75	58.45	53.11	48.53	44.58	41.13	38.11	35.43

TABLE IX

CALCULATED RATES OF EMISSION FROM PROTON-ELECTRON RECOMBINATION

(units of $n_e^2 \times 10^{22}$ cm^{-3} sec^{-1} cm^{-1})

$n_e = 0.1$ ($N_e = 10^{16}$ cm^{-3}), $p = 9.52$, λ (limit) = 3814 A°

	T (10^4 °K)									
λ (10^3 A°)	.50	.55	.60	.65	.70	.75	.80	.85	.90	.95
1.0	.0001	.0004	.0018	.0064	.0185	.0459	.1015	.2032	.3753	.6473
1.5	.6828	1.709	3.635	6.822	11.62	18.32	27.14	38.21	51.57	67.19
2.0	61.95	100.3	148.3	204.7	267.8	336.1	407.7	481.2	555.3	628.8
2.5	880.5	1097.	1305.	1498.	1673.	1831.	1970.	2092.	2197.	2287.
3.0	4996.	5230.	5378.	5458.	5488.	5480.	5444.	5387.	5314.	5231.
3.5	16855.	15579.	14438.	13422.	12518.	11710.	10987.	10337.	9752.	9222.
4.0	179.4	229.5	279.2	327.0	371.9	413.4	450.9	484.6	514.4	540.6
4.5	354.6	421.9	483.1	537.6	585.2	626.0	660.6	689.3	712.9	731.8
5.0	605.0	679.0	740.8	791.2	831.5	862.9	886.6	903.7	915.3	922.2
5.5	928.0	993.1	1041.	1076.	1098.	1112.	1118.	1118.	1113.	1104.
6.0	1315.	1353.	1373.	1379.	1375.	1363.	1345.	1324.	1299.	1273.
6.5	1756.	1747.	1723.	1690.	1652.	1609.	1564.	1518.	1472.	1427.
7.0	2237.	2162.	2083.	2002.	1922.	1844.	1770.	1698.	1630.	1565.
7.5	2746.	2589.	2442.	2307.	2182.	2067.	1960.	1862.	1771.	1687.
8.0	3272.	3018.	2796.	2601.	2428.	2273.	2135.	2010.	1897.	1795.
8.5	3805.	3443.	3139.	2880.	2658.	2464.	2293.	2142.	2008.	1888.
9.0	4337.	3858.	3468.	3144.	2871.	2637.	2436.	2260.	2106.	1969.
9.5	608.2	612.1	608.8	600.6	589.0	575.2	560.0	544.1	527.8	511.4
10.0	672.3	667.3	656.1	641.0	623.5	604.5	584.9	565.0	545.4	526.2

TABLE X

CALCULATED RATES OF EMISSION FROM PROTON-ELECTRON RECOMBINATION

(units of $n_e^2 \times 10^{22}$ cm^{-3} sec^{-1} cm^{-1})

$n_e = 0.1$ ($N_e = 10^{16}$ cm^{-3}), p = 9.52, λ (limit) = 3814 A°

	T (10^4 °K)								
$(10^3 \lambda$ A°)	1.0	1.5	2.0	2.5	3.0	3.5	4.0	4.5	5.0
1.0	1.054	20.87	83.40	179.2	285.1	384.3	468.7	536.3	587.7
1.5	84.99	340.3	611.5	813.4	940.0	1008.	1036.	1038.	1022.
2.0	701.1	1262.	1521.	1592.	1568.	1500.	1415.	1326.	1239.
2.5	2364.	2635.	2498.	2264.	2026.	1811.	1623.	1461.	1321.
3.0	5141.	4162.	3363.	2769.	2325.	1984.	1718.	1506.	1334.
3.5	8742.	5633.	4060.	3122.	2504.	2069.	1748.	1503.	1311.
4.0	563.3	654.2	625.3	565.5	503.5	447.4	398.7	357.0	321.5
4.5	746.7	759.1	678.7	589.8	511.4	445.8	391.6	346.8	309.5
5.0	925.2	845.4	716.7	603.3	512.0	439.5	381.8	335.1	297.0
5.5	1093.	915.0	742.6	608.9	507.8	430.6	370.5	322.9	284.5
6.0	1245.	970.0	759.1	609.0	500.6	420.1	358.7	310.7	272.4
6.5	1382.	1012.	768.4	605.2	491.4	408.7	346.7	298.8	260.9
7.0	1504.	1045.	772.2	598.7	481.0	397.1	334.9	287.3	250.0
7.5	1609.	1068.	771.9	590.3	470.0	385.4	323.5	276.5	239.8
8.0	1701.	1085.	768.3	580.6	458.5	373.9	312.5	266.2	230.3
8.5	1780.	1096.	762.4	570.0	447.0	362.7	302.0	256.5	221.4
9.0	1846.	1102.	754.7	559.0	435.6	351.9	292.0	247.4	213.1
9.5	495.2	358.8	269.3	210.3	169.6	140.3	118.5	101.8	88.64
10.0	507.5	358.5	265.7	205.9	165.2	136.2	114.8	98.35	85.49

TABLE XI

CALCULATED RATES OF EMISSION FROM PROTON-ELECTRON RECOMBINATION

(units of $n_e^2 \times 10^{22}$ cm^{-3} sec^{-1} cm^{-1})

$n_e = 0.1$ ($N_e = 10^{16}$ cm^{-3}), $p = 5.92$, λ (limit) = 3814 A°

	T (10^4 °K)									
λ (10^3 A°)	5.5	6.0	6.5	7.0	7.5	8.0	8.5	9.0	9.5	10.0
1.0	625.2	651.0	667.3	676.2	679.2	677.6	672.6	664.9	655.3	644.2
1.5	996.8	965.1	930.4	894.3	858.2	822.7	788.3	755.2	723.7	693.7
2.0	1156.	1079.	1009.	944.8	886.1	832.6	783.9	739.3	698.6	661.3
2.5	1201.	1098.	1007.	928.3	858.8	792.4	742.8	694.0	650.3	610.9
3.0	1192.	1073.	972.8	887.2	813.3	749.1	692.9	643.4	599.5	560.3
3.5	1157.	1031.	926.6	838.6	763.8	699.5	643.8	595.1	552.2	514.3
4.0	291.1	264.9	242.3	222.6	205.4	190.2	176.8	164.8	154.2	144.6
4.5	278.2	251.7	229.0	209.5	192.6	177.7	164.7	153.2	142.9	133.8
5.0	265.4	238.9	216.5	197.4	180.8	166.5	153.9	142.8	133.0	124.3
5.5	253.0	226.9	204.9	186.2	170.2	156.4	144.3	133.7	124.3	116.0
6.0	241.3	215.7	194.2	176.1	160.7	147.3	135.7	125.6	116.6	108.7
6.5	230.3	205.3	184.5	166.9	152.0	139.1	128.0	118.3	109.7	102.2
7.0	220.1	195.7	175.5	158.5	144.1	131.8	121.1	111.8	103.6	96.38
7.5	210.6	186.9	167.3	150.9	137.0	125.1	114.9	105.9	98.11	91.20
8.0	201.8	178.7	159.8	143.9	130.5	119.1	109.2	100.7	93.15	86.53
8.5	193.6	171.2	152.8	137.5	124.6	113.6	104.1	95.85	88.65	82.31
9.0	186.0	164.3	146.4	131.6	119.1	108.5	99.39	91.48	84.56	78.47
9.5	78.07	69.44	62.29	56.28	51.18	46.80	43.01	39.71	36.81	34.24
10.0	75.20	66.81	59.87	54.05	49.11	44.88	41.23	38.04	35.24	32.77

TABLE XII

CALCULATED RATES OF EMISSION FROM PROTON-ELECTRON RECOMBINATION

(units of $n_e^2 \times 10^{22}$ cm^{-3} sec^{-1} cm^{-1})

$n_e = 1.0$ ($N_e = 10^{17}$ cm^{-3}), $p = 6.49$, λ (limit) = 4028 A°

	T (10^4 °K)									
10^3 λ A°	.50	.55	.60	.65	.70	.75	.80	.85	.90	.95
1.0	.0000	.0003	.0013	.0047	.0139	.0354	.0795	.1617	.3028	.5286
1.5	.4581	1.191	2.612	5.035	8.774	14.11	21.27	30.41	41.60	54.87
2.0	41.56	69.85	106.6	151.1	202.2	258.8	319.5	382.9	448.0	513.6
2.5	590.8	764.3	937.6	1105.	1263.	1410.	1544.	1665.	1772.	1868.
3.0	3352.	3643.	3864.	4028.	4144.	4221.	4267.	4287.	4288.	4272.
3.5	11309.	10850.	10376.	9906.	9452.	9019.	8611.	8227.	7868.	7532.
4.0	27651.	24164.	21376.	19107.	17230.	15657.	14321.	13176.	12184.	11318.
4.5	252.0	310.0	364.7	414.9	459.9	499.5	533.9	563.3	588.1	608.7
5.0	429.9	498.9	559.2	610.6	653.4	688.5	716.6	738.5	755.0	767.0
5.5	659.4	729.8	786.2	830.1	863.2	887.1	903.4	913.2	917.9	918.3
6.0	934.8	994.3	1036.	1064.	1080.	1087.	1087.	1082.	1072.	1059.
6.5	1248.	1284.	1301.	1305.	1298.	1284.	1264.	1241.	1215.	1187.
7.0	1590.	1589.	1572.	1545.	1511.	1472.	1430.	1388.	1344.	1302.
7.5	1951.	1902.	1844.	1780.	1715.	1649.	1584.	1522.	1461.	1403.
8.0	2325.	2218.	2111.	2007.	1908.	1814.	1725.	1643.	1565.	1493.
8.5	2704.	2530.	2370.	2223.	2088.	1966.	1853.	1751.	1657.	1570.
9.0	3082.	2835.	2618.	2426.	2256.	2104.	1969.	1847.	1737.	1637.
9.5	3455.	3130.	2853.	2616.	2410.	2230.	2072.	1932.	1807.	1695.
10.0	3819.	3412.	3075.	2792.	2551.	2344.	2164.	2006.	1867.	1744.

TABLE XIII

CALCULATED RATES OF EMISSION FROM PROTON-ELECTRON RECOMBINATION

(units of $n_e^2 \times 10^{22}$ cm^{-3} sec^{-1} cm^{-1})

$n_e = 1.0$ ($N_e = 10^{17}$ cm^{-3}), $p = 6.49$, λ (limit) = 4028 A°

λ (10^3 A°)	T (10^4 °K)								
	1.0	1.5	2.0	2.5	3.0	3.5	4.0	4.5	5.0
1.0	.8700	18.43	75.95	166.0	266.8	362.1	443.7	509.4	559.7
1.5	70.17	300.5	556.9	753.4	879.7	950.0	981.0	985.8	973.7
2.0	578.8	1115.	1385.	1474.	1467.	1414.	1340.	1260.	1180.
2.5	1952.	2327.	2275.	2097.	1896.	1706.	1536.	1387.	1258.
3.0	4244.	3675.	3063.	2565.	2175.	1870.	1627.	1431.	1270.
3.5	7217.	4974.	3698.	2892.	2343.	1949.	1655.	1428.	1249.
4.0	10557.	6130.	4183.	3107.	2433.	1975.	1646.	1401.	1211.
4.5	625.5	661.8	601.3	526.9	459.0	401.4	353.4	313.5	280.2
5.0	775.0	737.1	635.0	538.9	459.6	395.8	344.6	302.9	268.8
5.5	915.2	797.7	657.9	544.0	455.9	387.8	334.4	291.9	257.5
6.0	1043.	845.6	672.6	544.1	449.4	378.3	323.7	280.8	246.5
6.5	1158.	882.7	680.8	540.7	441.1	368.1	312.9	270.1	236.1
7.0	1259.	910.8	684.2	534.8	431.8	357.6	302.3	259.8	226.3
7.5	1348.	931.4	683.8	527.3	421.8	347.1	292.0	249.9	217.1
8.0	1425.	945.8	680.7	518.6	411.6	336.7	282.0	240.6	208.5
8.5	1491.	955.2	675.5	509.2	401.3	326.7	272.6	231.9	200.4
9.0	1547.	960.5	668.6	499.3	391.1	316.9	263.5	223.6	192.9
9.5	1594.	962.4	660.7	489.3	381.0	307.5	255.0	215.9	185.8
10.0	1633.	961.7	651.9	479.1	371.2	298.5	246.9	208.5	179.2

TABLE XIV

CALCULATED RATES OF EMISSION FROM PROTON-ELECTRON RECOMBINATION

(units of $n_e^2 \times 10^{22}$ cm^{-3} sec^{-1} cm^{-1})

$n_e = 1.0$ ($N_e = 10^{17}$ cm^{-3}), $p = 6.49$, λ (limit) = 4028 A°

	T (10^4 °K)									
$10^3\lambda$ A°	5.5	6.0	6.5	7.0	7.5	8.0	8.5	9.0	9.5	10.0
1.0	596.6	622.2	638.7	647.9	651.4	650.4	646.0	639.0	630.0	619.6
1.5	941.2	922.5	890.5	856.9	823.0	789.6	757.1	725.8	695.8	667.3
2.0	1103.	1032.	965.8	905.3	849.8	799.2	752.9	710.5	671.7	636.1
2.5	1146.	1049.	964.1	889.4	823.6	765.3	713.4	666.9	625.2	587.6
3.0	1137.	1026.	931.1	850.0	780.0	719.0	665.5	618.3	576.4	539.0
3.5	1104.	985.6	886.8	803.5	732.5	671.4	618.3	571.9	531.0	494.7
4.0	1061.	939.5	839.8	756.6	686.4	626.4	574.7	529.8	490.4	455.7
4.5	252.0	228.2	207.8	190.2	174.9	161.5	149.7	139.3	130.0	121.6
5.0	240.4	216.6	196.4	179.2	164.2	151.3	139.9	129.9	121.0	113.0
5.5	229.2	205.7	185.9	169.1	154.6	142.1	131.1	121.5	113.0	105.5
6.0	218.6	195.5	176.2	159.9	145.9	133.8	123.3	114.1	106.0	98.83
6.5	208.7	186.1	167.4	151.5	138.0	126.4	116.3	107.5	99.79	92.92
7.0	199.4	177.5	159.2	143.9	130.9	119.7	110.1	101.6	94.22	87.66
7.5	190.8	169.5	151.8	137.0	124.4	113.7	104.4	96.31	89.21	82.95
8.0	182.8	162.1	144.9	130.6	118.5	108.2	99.26	91.50	84.70	78.70
8.5	175.4	155.2	138.7	124.8	113.1	103.2	94.59	87.14	80.61	74.86
9.0	168.5	148.9	132.9	119.5	108.2	98.60	90.33	83.16	76.89	71.37
9.5	162.1	143.1	127.5	114.6	103.7	94.40	86.43	79.52	73.49	68.18
10.0	156.2	137.7	122.6	110.0	99.48	90.53	82.84	76.18	70.37	65.27

TABLE XV

CALCULATED RATES OF EMISSION FROM PROTON-ELECTRON RECOMBINATION

(units of $n_e^2 \times 10^{22}$ cm^{-3} sec^{-1} cm^{-1})

$n_e = 10.0$ ($N_e = 10^{18}$ cm^{-3}), $p = 4.42$, λ (limit) = 4584 A°

	T (10^4 °K)									
λ (10^3 A°)	.50	.55	.60	.65	.70	.75	.80	.85	.90	.95
1.0	.0000	.0001	.0007	.0025	.0077	.0203	.0473	.0994	.1916	.3433
1.5	.1949	.5493	1.290	2.633	4.820	8.089	12.66	18.69	26.33	35.64
2.0	17.68	32.23	52.61	78.99	111.1	148.4	190.1	235.4	283.5	333.5
2.5	251.3	352.6	463.0	578.0	694.0	808.3	918.6	1023.	1122.	1213.
3.0	1426.	1681.	1908.	2106.	2276.	2420.	2539.	2636.	2714.	2774.
3.5	4811.	5006.	5123	5180.	5192.	5170.	5123.	5058.	4979.	4891.
4.0	11764.	11149.	10554.	9992.	9465.	8975.	8521.	8101.	7711.	7350.
4.5	23256.	20495.	18262.	16425.	14891.	13593.	12482.	11523.	10686.	9951.
5.0	209.2	257.0	301.7	342.1	378.0	409.2	435.8	458.2	476.8	491.8
5.5	320.9	375.9	424.1	465.1	499.3	527.2	549.4	566.7	579.6	588.8
6.0	454.9	512.2	559.0	596.2	624.9	646.3	661.4	671.3	676.9	679.0
6.5	607.2	661.2	701.8	731.0	750.8	762.9	768.8	769.8	767.0	761.1
7.0	773.5	818.4	848.1	865.7	873.8	874.6	869.9	861.0	848.9	834.7
7.5	949.6	979.9	994.6	997.5	991.9	979.9	963.6	944.1	922.6	899.9
8.0	1132.	1142.	1139.	1125.	1104.	1078.	1049.	1019.	988.2	957.1
8.5	1316.	1303.	1278.	1246.	1208.	1168.	1127.	1086.	1046.	1007.
9.0	1500.	1460.	1412.	1359.	1305.	1251.	1197.	1146.	1097.	1050.
9.5	1681.	1612.	1539.	1466.	1394.	1325.	1260.	1199.	1141.	1087.
10.0	1858.	1758.	1659.	1565.	1476.	1393.	1316.	1245.	1179.	1118.

TABLE XVI

CALCULATED RATES OF EMISSION FROM PROTON-ELECTRON RECOMBINATION

(units of $n_e^2 \times 10^{22}$ cm^{-3} sec^{-1} cm^{-1})

$n_e = 10.0$ ($N_e = 10^{18}$ cm^{-3}), $p = 4.42$, λ (limit) = 4584 A°

	T (10^4 °K)								
λ (10^3 A°)	1.0	1.5	2.0	2.5	3.0	3.5	4.0	4.5	5.0
1.0	.5782	14.10	61.93	140.2	230.3	317.0	392.5	454.0	501.8
1.5	46.63	229.8	454.1	636.3	759.2	831.8	867.8	878.6	872.9
2.0	384.7	852.6	1130.	1245.	1266.	1238.	1185.	1123.	1058.
2.5	1297.	1780.	1855.	1771.	1636.	1494.	1359.	1237.	1128.
3.0	2821.	2811.	2497.	2166.	1877.	1637.	1439.	1275.	1139.
3.5	4796.	3804.	3015.	2442.	2022.	1707.	1464.	1273.	1120.
4.0	7016.	4689.	3411.	2624.	2100.	1729.	1456.	1248.	1086.
4.5	9300.	5440.	3703.	2737.	2132.	1723.	1431.	1213.	1045.
5.0	503.8	519.9	464.9	403.1	348.5	303.0	265.6	234.8	209.2
5.5	594.9	562.7	481.7	406.8	345.7	296.8	257.8	226.2	200.4
6.0	678.2	596.4	492.4	406.9	340.7	289.6	249.5	217.6	191.9
6.5	752.8	622.6	498.5	404.4	334.5	281.8	241.2	209.3	183.8
7.0	818.8	642.4	500.9	400.0	327.4	273.7	233.0	201.3	176.1
7.5	876.4	656.9	500.7	394.4	319.8	265.7	225.0	193.7	168.9
8.0	926.3	667.1	498.4	387.9	312.1	257.8	217.4	186.5	162.2
8.5	969.1	673.7	494.6	380.8	304.3	250.0	210.1	179.7	155.9
9.0	1005.	677.5	489.6	373.5	296.5	242.6	203.1	173.3	150.1
9.5	1036.	678.8	483.7	365.9	288.9	235.4	196.5	167.3	144.6
10.0	1062.	678.3	477.3	358.3	281.5	228.5	190.3	161.6	139.5

TABLE XVII

CALCULATED RATES OF EMISSION FROM PROTON-ELECTRON RECOMBINATION

(units of $n_e^2 \times 10^{22}$ cm^{-3} sec^{-1} cm^{-1})

$n_e = 10.0$ ($N_e = 10^{18}$ cm^{-3}), $p = 4.42$, λ (limit) = 4584 A°

	T (10^4 °K)									
λ (10^3 A°)	5.5	6.0	6.5	7.0	7.5	8.0	8.5	9.0	9.5	10.0
1.0	537.3	562.5	579.1	588.9	593.3	593.5	590.4	584.8	577.4	568.5
1.5	856.7	833.9	807.4	778.9	749.7	720.6	692.0	664.3	637.7	612.2
2.0	993.6	932.7	875.7	822.8	774.1	729.3	688.1	650.3	615.6	583.6
2.5	1033.	948.3	874.1	808.5	750.2	698.4	652.0	610.4	573.0	539.1
3.0	1024.	927.2	844.2	772.7	710.5	656.1	608.3	565.9	528.2	494.5
3.5	994.5	890.9	804.1	730.4	667.2	612.7	565.1	523.4	486.6	453.9
4.0	955.4	849.3	761.4	687.7	625.2	571.6	525.3	484.9	449.4	418.1
4.5	913.2	806.9	719.7	642.2	586.2	534.2	489.4	450.6	416.7	386.8
5.0	187.8	169.6	154.2	140.9	129.4	119.4	110.5	102.7	95.79	89.60
5.5	179.0	161.1	145.9	133.0	121.8	112.1	103.6	96.14	89.52	83.62
6.0	170.7	153.1	138.3	125.8	115.0	105.6	97.45	90.29	83.96	78.34
6.5	163.0	145.8	131.4	119.2	108.8	99.76	91.93	85.07	79.02	73.66
7.0	155.7	139.0	125.0	113.2	103.1	94.48	86.97	80.40	74.61	69.49
7.5	149.0	132.7	119.1	107.7	98.04	89.71	82.49	76.19	70.65	65.75
8.0	142.8	126.9	113.8	102.7	93.39	85.37	78.43	72.38	67.07	62.38
8.5	137.0	121.6	108.8	98.18	89.15	81.42	74.74	68.93	63.84	59.34
9.0	131.6	116.6	104.3	93.98	85.26	77.80	71.38	65.79	60.89	56.57
9.5	126.6	112.1	100.1	90.11	81.68	74.49	68.29	62.91	58.20	54.05
10.0	121.9	107.8	96.20	86.53	78.38	71.44	65.46	60.27	55.73	51.73

Electron-Proton Bremsstrahlung

An electron in the proximity of a proton may, instead of combining to form a hydrogen atom, lose part of its energy to the radiation field and remain unbound. The process is called bremsstrahlung and often constitutes a significant portion of the H-continuum. This phenomenon has been of interest for some time and has been widely investigated.[30,37-42]

It is found, as in the case of recombination, that the cross section may be written as the classical form multiplied by a correction factor g_{III} (i.e. Gaunt factor for free-free transitions).[28] Thus, we have[42]

$$\sigma(\nu)\, d\nu = \frac{16\pi\alpha^3 a_o^2}{3\sqrt{3}\,\nu}\left(\frac{hcR}{E}\right) g_{III}\, d\nu \,, \qquad (8.16)$$

where R is the Rydberg constant, α the fine structure constant, and E the initial electron energy. In calculating the emission coefficient, we must integrate $v\sigma(\nu)$ over the distribution function, which is proportional to $v^2 e^{-E/kT}\, dv$. Since the only quantity in $\sigma(\nu)$ which is velocity dependent is g_{III}/E, it is convenient to define a weighted average gaunt factor[30]

$$\bar{g}_{III} = e^{h\nu/kT} \int_{h\nu}^{\infty} g_{III}(E,\nu)\, e^{-E/kT}\, d\left(\frac{E}{kT}\right).$$

Average gaunt factors have been calculated for ranges of T and ν, and are tabulated.[29,30]

The emission coefficient for free-free transitions of an electron in the field of a proton, is given as[22]

$$\epsilon_\nu = \bar{g}_{III}\, C\, \frac{N_e N_i}{(kT)^{1/2}}\, e^{-h\nu/kT}\ , \qquad (8.17)$$

where

$$C = \frac{32\,\pi^2\, e^6}{3\,\sqrt{3}\, c^3 (2\pi m)^{3/2}}\ ,$$

and where N_i is the ion density, which for the case of a pure hydrogen plasma, in the absence of external fields, must be equal to the electron density N_e in order to produce charge neutrality. Thus making use of Eq. (8.11) the rate of photon emission becomes

$$R_b = \left(\frac{dn}{d\lambda}\right)_b = \bar{g}_{III}\, N_e N_i\, \frac{32\,\sqrt{\pi}}{3\,\sqrt{6}}\, \frac{\alpha\, e^4}{c^2 m^{3/2}}\, \frac{1}{\lambda (kT)^{1/2}}\, e^{-hc/\lambda kT}\ , \qquad (8.18)$$

where α is the fine structure constant (i.e., $\alpha = 7.29720 \times 10^{-3}$). Rewriting Eq. (8.18) with λ in units of 10^3 A°, T in units of 10^4°K, and n_i and n_e in units of 10^{17} cm^{-3}, we have

$$R_b = \bar{g}_{III}\, (1.03237 \times 10^{26})\, \frac{n_e n_i}{\lambda T^{1/2}}\, e^{\frac{-14.3867}{\lambda T}}\ cm^{-3}\ sec^{-1}\ cm^{-1}\ . \qquad (8.19)$$

The factor $\bar{g}_{III}$ for the free-free transition is also found to be close to unity.[28-30]

Since the rates and emission coefficients of the recombination and bremsstrahlung processes possess the same density dependence, they are often combined into one expression which is then simply said to represent the rate, or

emissivity for the hydrogen continuum. Simplification is then possible if one integrates over higher states in the recombination part. However, since we wish to examine relative contributions, we shall continue to distinguish between the two.

Tables XVIII - XX give values of rates of emission (i.e. number of photons emitted per cm^3 per sec per cm of wavelength) resulting from proton-electron bremsstrahlung, which were calculated using Eq. (8.19) with $\bar{g}_{III}$ set equal to unity.

TABLE XVIII

CALCULATED RATES OF EMISSION FROM PROTON-ELECTRON BREMSSTRAHLUNG

(units of $n_e^2 \times 10^{22}$ cm^{-3} sec^{-1} cm^{-1})

	T (10^4 °K)									
λ (10^3 A°)	.50	.55	.60	.65	.70	.75	.80	.85	.90	.95
1.0	.0000	.0000	.0000	.0000	.0000	.0001	.0002	.0005	.0012	.0028
1.5	.0000	.0002	.0010	.0033	.0092	.0222	.0478	.0939	.1708	.2913
2.0	.0041	.0145	.0414	.1000	.2125	.4073	.7182	1.182	1.839	2.726
2.5	.0586	.1591	.3643	.7319	1.327	2.219	3.470	5.139	7.275	9.914
3.0	.3325	.7583	1.501	2.668	4.354	6.642	9.590	13.24	17.60	22.68
3.5	1.122	2.259	4.031	6.560	9.931	14.19	19.35	25.40	32.29	39.98
4.0	2.743	5.030	8.305	12.65	18.10	24.64	32.19	40.68	50.01	60.07
4.5	5.423	9.246	14.37	20.80	28.48	37.31	47.15	57.87	69.31	81.33
5.0	9.250	14.88	22.03	30.61	40.47	51.43	63.29	75.86	88.98	102.5
5.5	14.19	21.77	30.98	41.62	53.46	66.26	79.78	93.82	108.2	122.7
6.0	20.11	29.66	40.84	53.35	66.91	81.23	96.04	111.1	126.3	141.5
6.5	26.85	38.29	51.26	65.41	80.38	95.88	111.6	127.5	143.1	158.6
7.0	34.21	47.39	61.95	77.46	93.56	109.9	126.3	142.5	158.4	173.9
7.5	41.99	56.74	72.65	89.26	106.2	123.2	139.9	156.3	172.2	187.5
8.0	50.03	66.15	83.17	100.6	118.2	135.5	152.4	168.7	184.4	199.4
8.5	58.18	75.47	93.37	111.5	129.4	146.8	163.7	179.9	195.2	209.8
9.0	66.32	84.56	103.1	121.6	139.7	157.2	173.9	189.7	204.7	218.8
9.5	74.34	93.35	112.4	131.2	149.3	166.6	183.0	198.4	212.9	226.4
10.0	82.17	101.8	121.2	140.0	158.0	175.1	191.1	206.1	220.0	233.0

TABLE XIX

CALCULATED RATES OF EMISSION FROM PROTON-ELECTRON BREMSSTRAHLUNG

(units of $n_e^2 \times 10^{22}$ cm^{-3} sec^{-1} cm^{-1})

	T (10^4 °K)								
λ (10^3 A°)	1.0	1.5	2.0	2.5	3.0	3.5	4.0	4.5	5.0
1.0	.0058	.5760	5.486	20.68	49.27	90.50	141.5	199.0	259.9
1.5	.4703	9.393	40.23	93.89	162.5	237.5	312.9	385.0	452.0
2.0	3.879	34.84	100.1	183.7	271.0	353.3	427.3	492.0	547.7
2.5	13.08	72.73	164.3	261.4	350.2	426.4	489.8	541.9	584.2
3.0	28.45	114.9	221.2	319.6	401.7	467.3	518.8	558.8	589.8
3.5	48.37	155.5	267.1	360.4	432.7	487.2	527.8	557.8	579.8
4.0	70.76	191.6	302.2	387.3	449.3	493.7	525.1	547.1	562.2
4.5	93.79	222.3	328.0	403.9	456.3	491.9	515.8	531.5	541.3
5.0	116.2	247.6	346.4	413.1	456.8	485.1	502.8	513.5	519.3
5.5	137.2	268.0	358.9	417.0	453.1	475.2	488.0	494.8	497.5
6.0	156.4	284.1	366.9	417.0	446.7	463.6	472.4	476.1	476.4
6.5	173.7	296.5	371.4	414.4	438.5	451.1	456.6	457.8	456.2
7.0	188.9	305.9	373.2	410.0	429.2	438.2	441.1	440.3	437.3
7.5	202.2	312.9	373.0	404.2	419.3	425.3	426.1	423.7	419.4
8.0	213.7	317.7	371.3	397.5	409.1	412.6	411.6	407.9	402.8
8.5	223.5	320.9	368.4	390.3	398.9	400.3	397.8	393.1	387.2
9.0	231.9	322.6	364.7	382.8	388.7	388.3	384.6	379.1	372.6
9.5	239.0	323.3	360.4	375.0	378.7	376.8	372.1	365.9	359.0
10.0	244.9	323.0	355.6	367.2	369.0	365.8	360.2	353.5	346.2

TABLE XX

CALCULATED RATES OF EMISSION FROM PROTON-ELECTRON BREMSSTRAHLUNG

(units of $n_e^2 \times 10^{22}$ cm^{-3} sec^{-1} cm^{-1})

	T (10^4 °K)									
λ (10^3 A°)	5.5	6.0	6.5	7.0	7.5	8.0	8.5	9.0	9.5	10.0
1.0	321.8	383.2	442.7	499.7	553.6	604.3	651.7	695.8	736.7	774.5
1.5	513.1	568.1	617.2	660.9	699.6	733.7	763.8	790.3	813.6	834.1
2.0	595.1	635.4	669.5	698.2	722.3	742.6	759.6	773.7	785.4	795.1
2.5	618.5	646.1	668.3	686.0	700.1	711.1	719.7	726.2	731.1	734.5
3.0	613.6	631.7	645.4	655.6	663.0	668.1	671.4	673.3	673.9	673.7
3.5	595.7	607.0	614.7	619.7	622.6	623.8	623.8	622.7	620.9	618.4
4.0	572.3	578.6	582.1	583.6	583.4	582.1	579.8	576.9	573.4	569.6
4.5	547.0	549.7	550.2	549.2	547.0	543.9	540.2	536.1	531.6	527.0
5.0	521.8	521.8	520.2	517.4	513.7	509.5	504.8	499.9	494.8	489.7
5.5	497.4	495.5	492.3	488.2	483.6	478.5	473.2	467.9	462.4	457.0
6.0	474.4	471.0	466.7	461.7	456.4	450.8	445.1	439.4	433.7	428.1
6.5	452.9	448.4	443.2	437.6	431.7	425.8	419.9	414.0	408.2	402.5
7.0	432.8	427.5	421.7	415.6	409.4	403.3	397.2	391.2	385.4	379.7
7.5	414.1	408.2	401.9	395.6	389.2	382.9	376.8	370.8	364.9	359.3
8.0	396.8	390.4	383.8	377.2	370.7	364.4	358.2	352.2	346.5	340.9
8.5	380.7	374.0	367.2	360.5	353.9	347.5	341.4	335.4	329.7	324.3
9.0	365.8	358.8	351.8	345.0	338.5	332.1	326.0	320.1	314.5	309.2
9.5	351.8	344.7	337.7	330.8	324.3	317.9	311.9	306.1	300.6	295.4
10.0	338.9	331.6	324.5	317.7	311.2	304.9	299.0	293.3	287.9	282.7

CHAPTER IX

THE CONTINUUM OF THE NEGATIVE HYDROGEN ION

The existence of a bound state of H^- was first confirmed by Bethe[43] and Hylleraas[44], when crude calculations were made for the wave function and the electron affinity (i.e. the binding energy of the electron to the hydrogen atom). The existence of such a bound state, then makes possible a radiative process analogous to recombination of electrons with protons; this process is called "attachment" and the resulting continuum is often referred to as the "affinity spectrum." This spectrum differs from that due to recombination in that H^- possesses only one bound state and thus only one series limit (i.e. threshold), located at $\lambda \cong 16{,}500$ A°. The inverse process, "photodetachment," has been found to be the dominant absorption mechanism in the atmospheres of the sun and similar stars at wavelengths $\lambda \lesssim 16{,}500$ A°.[24,45-47]

Another important continuous-emission process, is the free-free transition of H^- (i.e. a transition between two unbound states of the electron-hydrogen atom system). This process is analogous to bremsstrahlung resulting from electron-proton interactions, except, of course, that in the former the

long-range coulomb potential is not present; as a result of this rather significant difference, the behavior of the two is quite different. The inverse free-free process is also found to be an important absorption mechanism in the solar atmosphere for wavelengths $\lambda \gtrsim 16{,}500$ A°.[24,45-47]

The Affinity Spectrum

The calculation of the cross section for emission in a free-bound transition of H^- is extremely complicated. Since an electron approaching a hydrogen atom sees at large distances effectively a neutral atom, any chance for formation of a bound H^- system will have to result from the incomplete shielding of the nucleus by the atomic electron, as well as the re-orientation of the atomic electron density within the atom so that an attractive potential well of suitable depth may be formed for the incident electron. Thus it is found that correlation and polarization effects are important.[48]

Because of its importance in astrophysics, the absorption cross section of the corresponding bound-free transition has been investigated extensively, and quite accurate calculations have been made.[49-51] We will take advantage of this work by incorporating the principle of detailed balancing, which in quantum mechanics is simply a restatement of the fact that operators corresponding to observables are hermitian. The relation between the absorption (detachment) and emission (attachment) cross sections is given by Milne's formula[52-53]

$$Q_d = \frac{2m^2v^2c^2}{h^2\nu^2} Q_a \ , \qquad (9.1)$$

where ν is the frequency of the photon emitted in the capture. Rewriting Eq. (9.1), with λ in units of 10^3 A° and k^2 in units of 13.6 eV, we obtain

$$Q_a = \gamma \frac{(5.5230 \times 10^{-2})}{\lambda^2 k^2} Q_d \qquad (9.2)$$

where $\gamma = 4$ is a factor relating the total photon intensity to the flux passing perpendicularly through unit area (See Appendix II). Table XXI contains values of the photodetachment cross section obtained by Geltman, who used a rather complicated variational scheme[50]; also given are attachment cross sections calculated using Eq. (9.2). A slightly better fit to the experimental photodetachment cross sections[54] has been obtained by Armstrong,[49] using an empirical method based on effective range theory. However, his cross sections are in essential agreement with those of Geltman.

Now, assuming the population of free electron states to be given by a Maxwell-Boltzmann distribution, one obtains for the number of photons emitted per cm^3 per sec

$$dn(\lambda,T) = N_H N_e \ v \ dQ_a(\lambda,T) \ , \qquad (9.3)$$

where

$$dQ_a(\lambda,T) = Q_a \frac{2}{\sqrt{\pi}} (kT)^{-3/2} \ e^{-E/kT} \ E^{1/2} \ dE \ , \qquad (9.4)$$

and where N_H represents the density of hydrogen atoms. Thus

TABLE XXI

PHOTODETACHMENT AND ATTACHMENT CROSS SECTIONS FOR H^-

(units of 10^{-17} and 10^{-21} cm^2, respectively; See Appendix II)

λ (10^3 A°)	Q_d (10^{-17} cm^2)	Q_a (10^{-21} cm^2)
1.0	0.33	.085
1.5	0.57	.101
2.0	0.85	.117
2.5	1.17	.134
3.0	1.52	.150
3.5	1.89	.166
4.0	2.23	.178
4.5	2.55	.189
5.0	2.84	.197
5.5	3.11	.205
6.0	3.35	.212
6.5	3.56	.219
7.0	3.71	.223
7.5	3.83	.226
8.0	3.92	.230
8.5	3.95	.232
9.0	3.93	.232
9.5	3.85	.231
10.0	3.73	.229

making use of the relations

$$|dE| = |h\, d\nu| = \frac{hc\, d\lambda}{\lambda^2} ,$$

and

$$v = (2E/m)^{1/2} , \tag{9.5}$$

we obtain for the rate of photon emission per cm of wavelength as

$$R_a = \left(\frac{dn}{d\lambda}\right)_a = n_e n_H \frac{2}{\sqrt{\pi}} \left(\frac{2}{m}\right)^{1/2} Q_a \frac{hc}{\lambda^2} (kT)^{-3/2} e^{-E/kT} E , \tag{9.6}$$

or incorporating the units: n_H, n_e (10^{17} cm^{-3}), λ (10^{-5} cm), Q_a (10^{-21} cm^2), T (10^4 °K), E (eV), one obtains

$$R_a = (1.037 \times 10^{27}) \frac{n_H n_e Q_a}{\lambda^2 T^{3/2}} E\, e^{-1.161E/T} . \tag{9.7}$$

It is important to note here that R_a decreases rapidly with temperature as does R_r (Recombination), however the rate of emission due to attachment depends only linearly on the electron density N_e, while that due to recombination has a quadratic dependence. It is clear that by decreasing the degree of ionization, one may wash out the recombination contribution in favor of the affinity spectrum.

In Tables XXII - XXIV are given calculated values of rates of emission (i.e. number of photons emitted per cm^3 per sec per cm of wavelength), which were obtained from the

TABLE XXII

CALCULATED RATES OF EMISSION FROM FREE-BOUND TRANSITIONS OF H^-

(units of $n_e n_H \times 10^{22}$ cm^{-3} sec^{-1} cm^{-1}; See Appendix II)

	T (10^4 °K)									
λ (10^3 A°)	.50	.55	.60	.65	.70	.75	.80	.85	.90	.95
1.0	.0000	.0000	.0000	.0002	.0007	.0023	.0065	.0161	.0359	.0730
1.5	.0026	.0111	.0365	.0990	.2311	.4783	.8983	1.558	2.530	3.885
2.0	.1496	.4097	.9377	1.872	3.356	5.529	8.503	12.36	17.16	22.90
2.5	1.501	3.163	5.822	9.661	14.79	21.24	28.98	37.90	47.88	58.76
3.0	6.408	11.34	18.05	26.49	36.50	47.84	60.25	73.43	87.12	101.1
3.5	16.94	26.47	37.98	51.04	65.22	80.08	95.25	110.4	125.2	139.6
4.0	32.75	46.63	61.87	77.85	94.01	109.9	125.3	139.8	153.3	165.9
4.5	52.02	68.86	86.00	102.8	118.8	133.7	147.4	159.7	170.7	180.4
5.0	72.07	90.01	107.1	122.9	137.1	149.7	160.6	170.0	178.0	184.5
5.5	90.98	108.3	123.9	137.5	149.0	158.7	166.7	173.0	178.0	181.8
6.0	107.0	122.5	135.5	146.2	154.8	161.5	166.5	170.1	172.5	174.0
6.5	119.4	132.2	142.2	149.9	155.5	159.3	161.8	163.0	163.4	163.0
7.0	127.0	136.6	143.4	148.1	151.0	152.4	152.7	152.2	150.9	149.2
7.5	130.8	137.3	141.2	143.3	143.9	143.3	142.0	140.1	137.7	135.0
8.0	131.5	135.0	136.4	136.2	135.0	133.0	130.4	127.5	124.4	121.1
8.5	128.5	129.4	128.6	126.8	124.2	121.1	117.7	114.2	110.6	107.0
9.0	122.8	121.5	119.1	116.0	112.4	108.7	104.8	101.0	97.20	93.54
9.5	114.6	111.7	108.1	104.2	100.1	95.93	91.89	87.98	84.23	80.65
10.0	105.3	101.2	96.81	92.35	87.98	83.75	79.71	75.90	72.30	68.93

TABLE XXIII

CALCULATED RATES OF EMISSION FROM FREE-BOUND TRANSITIONS OF H^-

(units of $n_e n_H \times 10^{22}$ cm^{-3} sec^{-1} cm^{-1}; See Appendix II)

	T (10^4 °K)								
λ (10^3 A°)	1.0	1.5	2.0	2.5	3.0	3.5	4.0	4.5	5.0
1.0	.1376	6.798	42.06	116.4	218.1	329.5	437.2	533.4	615.1
1.5	5.695	56.82	158.0	270.6	368.3	442.8	495.0	528.6	547.9
2.0	29.59	132.7	247.4	333.3	386.6	414.7	425.4	425.0	417.7
2.5	70.37	195.3	286.5	334.2	352.2	352.7	343.7	330.0	314.1
3.0	115.1	232.0	290.0	307.4	303.8	290.7	273.7	255.9	238.4
3.5	153.3	245.9	274.2	271.4	256.2	237.3	218.1	200.0	183.5
4.0	177.3	239.6	245.2	230.5	210.4	190.1	171.5	155.1	140.7
4.5	188.8	223.3	213.8	193.1	171.6	152.1	135.3	121.0	108.8
5.0	189.9	202.0	183.3	160.4	139.5	121.8	107.1	94.91	84.73
5.5	184.6	179.8	156.3	133.2	113.8	98.17	85.52	75.24	66.78
6.0	174.6	158.2	132.6	110.5	93.10	79.46	68.69	60.06	53.06
6.5	162.0	138.0	112.2	91.81	76.39	64.63	55.50	48.28	42.47
7.0	147.0	118.8	94.06	75.78	62.39	52.39	44.74	38.75	33.97
7.5	132.1	102.0	78.91	62.71	51.16	42.68	36.27	31.29	27.35
8.0	117.7	87.36	66.25	52.02	42.10	34.92	29.55	25.41	22.15
8.5	103.5	74.12	55.22	42.91	34.48	28.46	23.99	20.57	17.89
9.0	90.00	62.47	45.82	35.27	28.17	23.14	19.44	16.63	14.43
9.5	77.26	52.14	37.71	28.78	22.86	18.71	15.67	13.37	11.58
10.0	65.76	43.28	30.91	23.41	18.50	15.08	12.60	10.73	9.276

TABLE XXIV

CALCULATED RATES OF EMISSION FROM FREE-BOUND TRANSITIONS OF H^-

(units of $n_e n_H \times 10^{22}$ cm^{-3} sec^{-1} cm^{-1}; See Appendix II)

	T (10^4 °K)									
λ (10^3 A°)	5.5	6.0	6.5	7.0	7.5	8.0	8.5	9.0	9.5	10.0
1.0	681.8	734.4	774.7	804.2	824.8	838.0	845.2	847.4	845.7	840.9
1.5	556.5	557.5	552.9	544.6	533.6	520.9	507.1	492.8	478.2	463.6
2.0	406.2	392.3	377.4	362.0	346.7	331.7	317.3	303.5	290.4	278.0
2.5	297.5	281.2	265.5	250.7	236.8	223.9	211.9	200.8	190.5	181.0
3.0	221.9	206.2	192.8	180.1	168.6	158.1	148.6	140.0	132.1	124.8
3.5	168.7	155.5	143.8	133.3	124.0	115.6	108.1	101.4	95.26	89.73
4.0	128.1	117.2	107.6	99.24	91.84	85.28	79.45	74.23	69.55	65.33
4.5	98.36	89.43	81.71	75.01	69.15	64.00	59.45	55.40	51.79	48.54
5.0	76.18	68.92	62.72	57.37	52.73	48.68	45.11	41.95	39.14	36.62
5.5	59.79	53.85	48.84	44.55	40.84	37.62	34.79	32.30	30.09	28.12
6.0	47.28	42.47	38.41	34.95	31.98	29.40	27.15	25.17	23.42	21.86
6.5	37.73	33.79	30.49	27.69	25.29	23.21	21.41	19.82	18.42	17.18
7.0	30.08	26.88	24.21	21.94	20.01	18.34	16.90	15.63	14.51	13.52
7.5	24.16	21.54	19.37	17.53	15.96	14.62	13.45	12.43	11.53	10.74
8.0	19.52	17.38	15.60	14.10	12.83	11.73	10.79	9.960	9.235	8.593
8.5	15.74	13.98	12.53	11.32	10.28	9.400	8.635	7.969	7.383	6.866
9.0	12.67	11.25	10.07	9.080	8.244	7.529	6.912	6.374	5.903	5.487
9.5	10.15	8.999	8.047	7.252	6.579	6.004	5.508	5.077	4.699	4.366
10.0	8.124	7.192	6.425	5.785	5.244	4.783	4.386	4.040	3.738	3.472

attachment cross sections given in Table XXI by means of Eq. (9.6).

Free-Free Transitions in H^-

Early attempts[55,56] to treat free-free transitions of H^- were rather unsuccessful since they incorporated the Born approximation, which is, of course, completely invalid for the conditions involved here. Considerable improvement was made by Chandrasekhar and Breen[57] who solved for the continuum states in a static Hartree field. More recently, Ohmura and Ohmura[58], realizing the possible importance of exchange and polarization, devised an approximate scheme which partially includes these effects. Finally, Firsov[59] and Hundley[60] have derived expressions for the emitted energy spectrum, both incorporating ideas similar to those of Ohmura and Ohmura. These expressions are actually intended for radiation emitted from electrons colliding with heavy atoms, and are not directly applicable to hydrogen. However, part of the present approach will parallel the work of Firsov.

In order to calculate the emission from the electron-hydrogen atom system interacting with the radiation field, we must first investigate the continuum states of H^-. The system is described by the hamiltonian

$$H = -\frac{\hbar^2}{2m}\nabla_1^2 - \frac{\hbar^2}{2m}\nabla_2^2 - \frac{e^2}{r_1} - \frac{e^2}{r_2} + \frac{e^2}{r_{12}}, \qquad (9.8)$$

which is helium-like, except that the nucleus has only a unit

charge. A crude choice for the total eigenfunction of (9.8) is

$$\Psi(\vec{r}_1,\vec{r}_2) = \psi_{1s}(\vec{r}_1)\ \varphi(\vec{k}|\vec{r}_2)\ , \qquad (9.9)$$

where $\psi_{1s}(\vec{r}_1)$ is the hydrogenic wavefunction for the ground state, and where $\varphi(\vec{k}|\vec{r}_2)$ represents the unbound state of momentum $\vec{k}\hbar$, and satisfies the asymptotic relation

$$\varphi(\vec{k}|\vec{r}_2) \sim e^{i\vec{k}\cdot\vec{r}_2} + \frac{1}{r^2}\, e^{ikr_2}\, f_{1s}(\hat{r}_2)\ . \qquad (9.10)$$

The asymptotic relation (9.10) is, of course, the familiar boundary condition for elastic scattering wave functions,[1] and the problem of obtaining the continuum-state functions reduces to that of solving the corresponding elastic scattering problem, except that in the latter, one is normally interested only in the asymptotic form of the wave functions, while here we wish the wave function in all regions of space. Ohmura and Ohmura[58] found, however, that for low energies it is possible to use the scattering cross-section results directly in determining the free-free absorption coefficients.

In the standard partial wave development, $\varphi(\vec{k}|\vec{r}_2)$ is expanded as[1]

$$\varphi(\vec{k}|\vec{r}_2) = \frac{1}{r_2} \sum_{\ell=0}^{\infty} i^{\ell}(2\ell + 1)P_{\ell}(\cos\theta_2)\, e^{i\eta_{\ell}(k)}\, f_{\ell}(kr_2), \qquad (9.11)$$

where

$$\vec{k}\cdot\vec{r}_2 = kr_2 \cos\theta_2 ,$$

and (9.12)

$$f_\ell(kr_2) \sim \frac{1}{k} \sin [kr_2 - \ell\pi/2 + \eta_\ell(k)] ,$$

where $\eta_\ell(k)$ is the elastic-scattering phase shift. When exchange effects are considered, i.e., when the total wave function is expressed, in the simplest case, as

$$\Psi(\vec{r}_1,\vec{r}_2) = \frac{1}{\sqrt{2}} \left\{ \psi_{1s}(\vec{r}_1)\, \varphi_\pm(\vec{r}_2) \pm \psi_{1s}(\vec{r}_2)\, \varphi_\pm(\vec{r}_1) \right\} , \quad (9.13)$$

one obtains two phase shifts η_ℓ^+ and η_ℓ^-, corresponding to the triplet and singlet states, respectively. Low energy electron-hydrogen collisions have been investigated extensively[61,62]; calculated cross sections are available which incorporate exchange, correlation, and strong coupling effects (e.g. influence of 2s, 2p states on 1s-elastic scattering). It is found that for rather low energies, say less than 13.6 eV, partial waves corresponding to $\ell \geq 2$ contribute only a small percentage to the total cross section, while for energies less than 4 eV, only the partial cross section corresponding to $\ell = 0$ is of great significance.

Calculation of the Transition Probability

In treating problems involving the radiation field, it is convenient to employ the standard technique of time dependent perturbation theory[63]. In this context, the particles are taken along with the quantized radiation field

to make up the complete system. As is well known, the transition probability per unit time (for times small compared to lifetimes of states but large relative to atomic periods) for a transition i → f, in which either the initial or final state is free, is given to first order by

$$W_{if} = \frac{2\pi}{\hbar} |H'_{if}|^2 \rho(E_f) , \tag{9.14}$$

where H'_{if} is the matrix element between initial and final states of the interaction part of the hamiltonian and $\rho(E_f)$ is the final state density. Thus, for a process in which a photon is emitted while a two-particle system undergoes a transition from state a to state b, we have

$$H'_{if} = \langle 00 \ldots 1 \ldots 0b | - \frac{e}{mc} (\vec{p}_1 + \vec{p}_2)\cdot\vec{A} | 00 \ldots 0 \ldots 0a \rangle , \tag{9.15}$$

where $\vec{A}$ is the vector-potential operator for the radiation field, and in terms of the individual quantum oscillators, is given by

$$\vec{A} = \sum_{\mu} (q_\mu \vec{A}_\mu + q^*_\mu \vec{A}^*_\mu) , \tag{9.16}$$

where

$$\vec{A}_\mu = \hat{e}_\mu (4\pi c^2)^{1/2} \exp (i\vec{K}_\mu \cdot \vec{r}) , \tag{9.17}$$

and where q_μ and q^*_μ are the familiar photon annihilation and creation operators, respectively. In Eq. (9.17), $\hat{e}_\mu$ and $\vec{K}_\mu$ represent the unit polarization vector, and the propagation vector (i.e. $|\vec{K}_\mu| = 2\pi/\lambda$) corresponding to the μth oscillator. Inherent in Eq. (9.14) is conservation of energy, viz.

$$E_a = E_b + h\nu \ . \tag{9.18}$$

Carrying out the integration over the field variables, we obtain

$$W_{\nu,j}\, d\Omega_{\hat{K}} = \frac{e^2\nu}{m^2c^3\hbar}\, d\Omega_{\hat{K}}\ |\ \langle b\,|\vec{p}\cdot\hat{e}_j e^{i\vec{K}\cdot\vec{r}}|a\rangle\ |^2 \ , \tag{9.19}$$

where $d\Omega_{\hat{K}}$ is the differential solid angle about the $\hat{K}$ axis, j designates the polarization (two possible), and where $\vec{p}$ is the total linear-momentum (i.e. $\vec{p} = \vec{p}_1 + \vec{p}_2$). In Eq. (9.19) we have included for $\rho(E_f)$, the photon state density (i.e. number of quantum oscillators per unit volume in the energy range ϵ, $\epsilon + d\epsilon$), which is given by

$$\rho_\epsilon\, d\epsilon = \frac{\nu^2}{hc^3}\, d\epsilon \ . \tag{9.20}$$

It is easily shown that

$$\langle b\,|\dot{\vec{r}}|a\rangle = -\,2\pi i\nu\ \langle b\,|\vec{r}\,|a\rangle \ ; \tag{9.21}$$

thus

$$W_{\nu,j}\, d\Omega_{\hat{K}} = \frac{4\pi^2e^2\nu^3}{c^3\,\hbar}\, d\Omega_{\hat{K}}\ |\vec{M}\cdot\hat{e}_j|^2 \ , \tag{9.22}$$

where, in the case where two electrons are involved,

$$\vec{M} = \langle b\,|\vec{r}_1 + \vec{r}_2|a\rangle \ , \tag{9.23}$$

and where we have dropped the retardation term exp $(i\vec{K}\cdot\vec{r})$, which is insignificant for problems involving nonrelativistic

energies.[64]

Since we are not interested in the probability of an event in which a photon is emitted having a particular polarization or direction of propagation, we sum over the two independent polarization directions and integrate over all directions of propagation. Referring to Figure 18, we have

$$W_\nu = \int_{\Omega_{\hat{K}}} (W_{\nu,1} + W_{\nu,2})\, d\Omega_{\hat{K}}$$

$$= \frac{4\pi^2 e^2 \nu^3}{c^3 \hbar} \int_{\Omega_{\hat{K}}} (|\vec{M}\cdot\hat{e}_1|^2 + |\vec{M}\cdot\hat{e}_2|^2)\, d\Omega_{\hat{K}} \qquad (9.24)$$

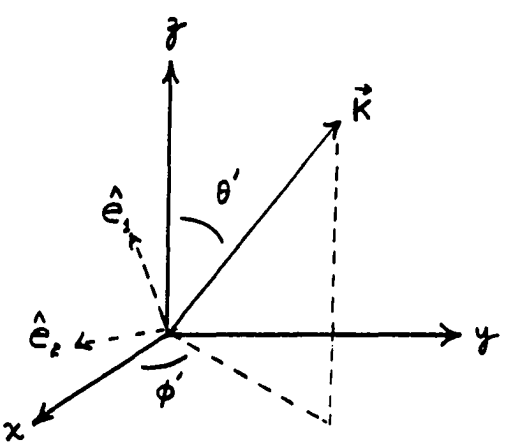

Figure 18. Orientation of the Polarization and Propagation Vectors.

Integrating first over φ', we obtain

$$\int_0^{2\pi} \left(|\vec{M}\cdot\hat{e}_1|^2 + |\vec{M}\cdot\hat{e}_2|^2\right) d\varphi' =$$

$$2\pi \left\{ |M_z|^2 \sin^2\theta' + \frac{1}{2}\left(|M_x|^2 + |M_y|^2\right)(1 + \cos^2\theta') \right\} ; \qquad (9.25)$$

the θ' integration then yields

$$\int_0^{\pi}\int_0^{2\pi} \left\{ |\vec{M}\cdot\hat{e}_1|^2 + |\vec{M}\cdot\hat{e}_2|^2 \right\} \sin\theta' \, d\theta' \, d\varphi' = \frac{8\pi}{3} |\vec{M}|^2 . \qquad (9.26)$$

Thus, for a process in which a particle state changes from a to b and a photon is emitted having energy $h\nu$, the transition probability per unit time is given by

$$W_\nu = \frac{64\,\pi^4 e^2 \nu^3}{3\,c^3\,h} |\vec{M}|^2 , \qquad (9.27)$$

and the energy radiated per unit time becomes

$$S_\nu = \frac{64\,\pi^4 e^2 \nu^4}{3\,c^3} |\vec{M}|^2 . \qquad (9.28)$$

It should be pointed out here, that although the previous development is located in the section concerning free-free transitions, it is perfectly general and Eqs. (9.27) and (9.28) apply to bound-bound and free-bound transitions as well. The derivations were placed in this section, rather than at the beginning of Chapter VII, partly because the

electron-proton, radiative processes are so well known that their derivations are unnecessary, and in order that a more continuous discussion of the electron-atom, free-free transitions might be presented.

The processes described by Eqs. (9.27) and (9.28) are distinguished by the form of the dipole matrix element $\vec{M}$. In the simplest case of bound-bound transitions, both initial and final state wave functions are normalized to unity. In the case of free-bound transitions, such as electron-recombination or attachment, the final state is still normalized to unity, while the normalization of the initial free state is left somewhat arbitrary depending on the interpretation of W_ν and S_ν. For instance, if the free state is normalized to a plane wave of unit amplitude at infinity, then W_ν simply represents the probability per unit time for the radiative process in which a beam of v electrons per cm^2 per sec is incident on the scatterer, however if one normalizes the free-state function so that it approaches a plane wave of amplitude $v^{-1/2}$ at infinity, then W_ν becomes σ_ν, the familiar cross section for the process. In the case of a free-free transition, the same discussion applies to the incident particle state, however the outgoing particle must be considered differently. We simply inquire as to what kind of phenomenon we wish W_ν to describe. For example, if we wish the cross section for a process in which the final state consists of a photon and an outgoing electron of a specific

energy E (i.e. in a range E, E + dE), we simply normalize the final free state to unit amplitude at infinity and multiply by the number of states per unit volume corresponding to the energy range E, E + dE. It should be clear then, that normalization of the wave functions appearing in $\vec{M}$ is indeed what indicates the nature of the process one is attempting to describe.

The Dipole Matrix Element

Specializing now to the particular process in which an electron is decelerated in the vicinity of a hydrogen atom and a photon emitted, we have from Eq. (9.23)

$$\vec{M} = \iint \Psi_b^*(\vec{r}_1,\vec{r}_2)\ (\vec{r}_1 + \vec{r}_2)\ \Psi_a(\vec{r}_1,\vec{r}_2)\ d\vec{r}_1\ d\vec{r}_2\ , \qquad (9.29)$$

which, in the case where Ψ takes on the simple form Eq. (9.13), becomes simply

$$\vec{M} = \int [\varphi_b^{\pm}(\vec{r})]^*\ \varphi_a^{\pm}(\vec{r})\ \vec{r}\ d\vec{r} \pm \int \psi^*(\vec{r})\ \varphi_b^{\pm}(\vec{r})\,\vec{r}\,d\vec{r} \int [\varphi_a^{\pm}(\vec{r})]^*$$

$$\times\ \psi(\vec{r})\ d\vec{r} \pm \int [\varphi_a^{\pm}(\vec{r})]^*\ \psi(\vec{r})\ \vec{r}\ d\vec{r} \int \psi^*(\vec{r})\ \varphi_b^{\pm}(\vec{r})\ d\vec{r}\ . \qquad (9.30)$$

If exchange is ignored in calculating the matrix element, then one no longer needs to distinguish between singlet and triplet states, and Eq. (9.30) becomes simply

$$\vec{M} = \int \varphi_b^*(\vec{r})\ \varphi_a(\vec{r})\ \vec{r}\ d\vec{r}\ , \qquad (9.31)$$

where $\varphi_a(\vec{r})$ and $\varphi_b(\vec{r})$ are as given in Eq. (9.11). Thus, we have

$$\varphi_a(\vec{r}) = \frac{1}{r} \sum_{\ell=0}^{\infty} i^{\ell}(2\ell + 1)\ e^{i\eta_\ell^a}\ P_\ell\ (\cos \alpha_a)\ f_\ell^a(r), \qquad (9.32)$$

$$\varphi_b(\vec{r}) = \frac{1}{r} \sum_{\ell'=0}^{\infty} i^{\ell'}(2\ell' + 1)\ e^{i\eta_{\ell'}^b}\ P_{\ell'}\ (\cos \alpha_b)\ f_\ell^b(r), \qquad (9.33)$$

where $\eta_\ell^a = \eta_\ell(k_a)$, and where the angles are defined in Figure 19. The z-axis here is the axis of quantization for the

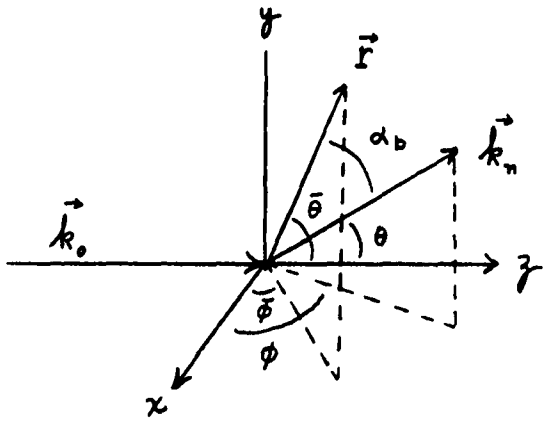

Figure 19. Orientation of the Electron Position Vector and the Final Momentum Vector.

hydrogen atom. From the addition theorem for spherical harmonics, one can express α_b in terms of θ, φ and $\bar{\theta}$, $\bar{\varphi}$ (of

course $\alpha_a = \bar{\theta}$) as

$$P_{\ell'}(\cos \alpha_b) = \frac{4\pi}{2\ell' + 1} \sum_{g=-\ell'}^{\ell'} Y^*_{\ell',g'}(\bar{\theta},\bar{\varphi})\, Y_{\ell',g'}(\theta,\varphi) \ . \qquad (9.34)$$

If we define

$$M_z = \int \varphi^*_b(\vec{r})\, \varphi_a(\vec{r})\, z\, d\vec{r} \ ,$$

and (9.35)

$$M_\pm = \int \varphi^*_b(\vec{r})\, \varphi_a(\vec{r})\, \sin\theta\, e^{\pm i\varphi}\, d\vec{r} \ ,$$

then clearly

$$|\vec{M}|^2 = |M_z|^2 + |M_+|^2 \ . \qquad (9.36)$$

Considering Eqs. (8.32) - (8.35), we find for the matrix elements

$$M_z = 4\pi e \sum_{\ell=0}^{\infty} i^{\ell}(2\ell + 1) \Big\{ i^{-(\ell+1)} \int Y_{\ell+1,o}(\bar{\theta},\bar{\varphi}) \cos\bar{\theta}$$

$$\times P_\ell(\cos\bar{\theta})\, d\bar{\Omega}\ Y_{\ell+1,o}(\theta,\varphi) \int_0^{\infty} f^b_{\ell+1}(r)\, f^a_\ell(r)\, dr$$

$$+ i^{-(\ell-1)} \int Y_{\ell-1,o}(\bar{\theta},\bar{\varphi}) \cos\bar{\theta}\, P_\ell\,(\cos\bar{\theta})\, d\bar{\Omega}\, Y_{\ell-1,o}(\theta,\varphi)$$

$$\times \int_0^{\infty} f^b_{\ell-1}(r)\, f^a_\ell(r)\, dr \Big\} \ , \qquad (9.37)$$

and similarly for M_+ with $\cos\bar{\theta}$ replaced by $\sin\bar{\theta}\, e^{i\varphi}$. Since we are interested in total cross sections, the direction of

the outgoing electron constitutes a degeneracy in the problem and may be integrated out. For convenience we shall continue to designate the dipole elements as M_z and M_+ even after integration over all final electron directions (i.e. over $d\hat{k}_b$). One obtains then

$$|M_+|^2 = (4\pi)^3 e^2 \sum_{\ell=0}^{\infty} \{(2\ell+1)\,(|I(\ell-1,\ell)\,h_+(\ell-1,\ell)|^2 + |I(\ell+1,\ell)\,h_+(\ell+1,\ell)|^2) - [(2\ell+1)(2\ell-3)]^{1/2} \times I(\ell-1,\ell)\,h_+^*(\ell+1,\ell)\,I(\ell-1,\ell-2)\,h_+(\ell-1,\ell-2) - [(2\ell+1)(2\ell+5)]^{1/2}\,I(\ell+1,\ell)\,h_+^*(\ell+1,\ell) \times I(\ell+1,\ell+2)\,h_+(\ell+1,\ell+2)\}, \qquad (9.38)$$

and

$$|M_z|^2 = (4\pi)^3 e^2 \sum_{\ell=0}^{\infty} \{(2\ell+1)\,(|I(\ell-1,\ell)\,h_z(\ell-1,\ell)|^2 + |I(\ell+1,\ell)\,h_z(\ell+1,\ell)|^2) - [(2\ell+1)(2\ell-3)]^{1/2} \times I(\ell-1,\ell)\,h_z^*(\ell-1,\ell)\,I(\ell-1,\ell-2)\,h_z(\ell-1,\ell-2) - [(2\ell+1)(2\ell+5)]^{1/2}\,I(\ell+1,\ell)\,h_z^*(\ell+1,\ell) \times I(\ell+1,\ell+2)\,h_z(\ell+1,\ell+2)\}, \qquad (9.39)$$

where

$$I(\ell - 1,\ell) = \int_0^\infty f^b_{\ell-1}(r)\, f^a_\ell(r)\, r\, dr\,, \qquad (9.40)$$

and where

$$h_+(\ell - 1,\ell) = \iint Y^*_{\ell-1,1}(\theta,\varphi) \sin\theta\, e^{i\varphi}\, Y_{\ell,0}(\theta,\varphi) \sin\theta\, d\theta\, d\varphi\,, \qquad (9.41)$$

$$h_z(\ell - 1,\ell) = \iint Y^*_{\ell-1,0}(\theta,\varphi) \cos\theta\, Y_{\ell,0}(\theta,\varphi) \sin\theta\, d\theta\, d\varphi\,; \qquad (9.42)$$

these are given in Table XXV. Substitution of the expressions

TABLE XXV

$$h_+(\ell - 1,\ell) = -\left[\frac{\ell(\ell - 1)}{(2\ell + 1)(2\ell - 1)}\right]^{1/2}$$

$$h_+(\ell + 1,\ell) = \left[\frac{(\ell + 1)(\ell + 2)}{(2\ell + 1)(2\ell + 3)}\right]^{1/2}$$

$$h_z(\ell - 1,\ell) = \frac{\ell}{[(2\ell + 1)(2\ell - 1)]^{1/2}}$$

$$h_z(\ell + 1,\ell) = \frac{(\ell + 1)}{[(2\ell + 1)(2\ell + 3)]^{1/2}}$$

from Table XXV into Eqs. (9.38) and (9.39) yields

$$|\vec{M}|^2 = (4\pi)^3 e^2 \sum_{\ell=0}^{\infty} \ell \left\{ |I(\ell - 1,\ell)|^2 + |I(\ell,\ell - 1)|^2 \right\}. \qquad (9.43)$$

At this point it is necessary to consider the detailed nature of the radial functions defined in Eqs. (9.32) and (9.33). In the case where $\Psi(\vec{r}_1,\vec{r}_2)$ is given the simple product form of Eq. (9.9), the static Hartree approximation results, and $f_\ell^a(r_2)$ is easily shown to satisfy (in Slater atomic units)

$$\left\{ \frac{d^2}{dr_2^2} + k_a^2 - \frac{\ell(\ell+1)}{r_2^2} - 2 \int |\psi_{1s}(\vec{r}_1)|^2 \frac{d\vec{r}_1}{r_{12}} \right\} f_\ell^a(r_2) = 0 , \tag{9.44}$$

where the asymptotic condition becomes, from Eq. (8.12),

$$f_\ell^a(r_2) \sim \frac{1}{k_a} \sin (k_a r_2 - \ell\pi/2 + \eta_\ell^a) . \tag{9.45}$$

Chandrasekhar[57] treated this problem numerically, and obtained values for the continuous absorption coefficient of H^- which were later shown to be somewhat too large. It was pointed out by Ohmura and Ohmura[58] that, since exchange and correlation effects are found to be important to the bound state of H^-, they may also be significant in the free state determination. They then suggested an approach in which only the asymptotic form of $f_0(r)$ is used in calculating the dipole matrix element. This of course includes the phase shift $\eta_0(k)$, which can be made to include such effects as exchange and electronic correlation. Matrix elements determined in this manner were compared, using the static Hartree phase shifts, with the numerically determined matrix elements and

found to agree within $\simeq$ 1% throughout the energy range of consideration. Using more accurate phase shifts, considerably improved absorption coefficients were obtained with regard to solar opacity measurements. In the above technique only s- and p-waves (i.e., $\ell = 0$ and $\ell = 1$) were considered and the phase shift for $\ell = 1$ was taken to be zero (i.e., Born approximation is used for p-wave); both are good assumptions for small energies.

In order to further examine the asymptotic approximation, the author considered a three-dimensional spherical potential-well problem. The well was assigned a depth k_o^2 and a radius a such that the resulting elastic scattering phase shifts agreed fairly well with those of electron-hydrogen scattering results. Since it is possible to solve such a problem exactly, matrix elements evaluated by the asymptotic approximation (i.e. asymptotic s-wave function and Born approximation for p-wave) could be compared directly with the correct results. We consider only the $\ell = 1$ term in Eq. (9.43); this assumption is valid for low energies and was used by Ohmura and Ohmura in their work. For incident energies between 2 and 6 eV, the error in $|\vec{M}|^2$ was found to lie between 0.3 and 2.0%, the larger of the two corresponding to 6 eV. It was also shown that by far the greatest source of error was not the asymptotic assumption for the s-wave, but the Born approximation for the p-wave (i.e. the assumption that $\eta_1 = 0$). This is quite easy to understand, since

the asymptotic form for the s-wave deviates from the true wave function only in a small region where the potential is still effective, i.e. where r is still rather small, while the neglect of the p-wave phase shift has a cumulative effect on the dipole matrix element. One concludes, then, that the above approximations are well within the desired accuracy. Details of this investigation will be presented in Appendix I.

Incorporating the approximations discussed above, we find the s- and p-wave functions to be given by

$$f_o^b(r) = \frac{1}{k_b} \sin\,(k_b r + \eta_o^b)\ , \tag{9.46}$$

$$f_1^a(r) = \frac{1}{k_a} \left\{ \cos\, k_a r - \frac{\sin k_a r}{k_a r} \right\} \tag{9.47}$$

Thus from Eq. (9.43), we have that (keeping only the $\ell = 1$ term)

$$|\vec{M}|^2 = \frac{(4\pi)^3}{k_a^2 k_b^2} \left\{ \left| \int_o^\infty \sin\,(k_b r + \eta_o^b) \left[\cos\, k_a r - \frac{\sin k_a r}{k_a r} \right] r\, dr \right|^2 \right.$$

$$\left. + \left| \int_o^\infty \sin\,(k_a r + \eta_o^a) \left[\cos\, k_b r - \frac{\sin k_b r}{k_b r} \right] r\, dr \right|^2 \right\} . \tag{9.48}$$

Carrying out the elementary integrations, one obtains

$$|\vec{M}|^2 = \frac{4(4\pi)^3}{(k_a^2 - k_b^2)^4} \left\{ k_a^2 \frac{\sin^2 \eta_o^b}{k_b^2} + k_b^2 \frac{\sin^2 \eta_o^a}{k_a^2} \right\} . \tag{9.49}$$

Relating η_o to the s-wave partial cross section by

$$\sigma_o(k) = \frac{4\pi}{k^2} \sin^2 \eta_o(k) \ , \tag{9.50}$$

we obtain

$$|\vec{M}|^2 = \frac{64\ \pi^2}{(k_a^2 - k_b^2)^4} (k_a^2\ \sigma_o^b + k_b^2\ \sigma_o^a) \ . \tag{9.51}$$

Emission Spectrum

In calculating the dipole matrix element, the continuum function representing the outgoing electron was normalized to a plane wave of unit amplitude at infinity. In order to obtain the energy per unit time of frequency ν emitted in a process where electrons go off with momenta in the range k_b, $k_b + dk_b$, we multiply by the final electron state density

$$\frac{k_b^2\ dk_b}{(2\pi)^3} \ , \tag{9.52}$$

or, in terms of the kinetic energy,

$$\frac{\sqrt{2}\ m^{3/2}}{(2\pi)^3\ \hbar^3} E_b^{1/2}\ dE_b \ . \tag{9.53}$$

Now, combining Eqs. (9.53), (9.51) and (9.28), we have

$$dS_\nu = 64\ \pi^2 \left(\frac{64\ \pi^4 e^2 \nu^4}{3c^3} \right) \left(\frac{\sqrt{2}\ m^{3/2}}{(2\pi)^3 \hbar^3} \right) \frac{E_b^{1/2}\ dE_b}{(k_a^2 - k_b^2)^4}$$

$$\times\ (k_a^2\ \sigma_o^b + k_b^2\ \sigma_o^a)$$

$$= \frac{4\sqrt{2}\,\alpha_f}{3\pi c^2 m^{3/2}} E_b^{1/2}\, dE_b\, (E_a\, \sigma_o^b + E_b\, \sigma_o^a)\,, \qquad (9.54)$$

where α_f is the fine structure constant ($\alpha_f = 7.29720 \times 10^{-3}$). Using the energy conservation relation

$$h\nu = E_a - E_b\,, \qquad (9.55)$$

we can write[59]

$$dS_\nu = \left(\frac{4\sqrt{2}\,\alpha_f}{3\pi}\right)\frac{1}{c^2}\left(\frac{E_a}{m}\right)^{3/2}\left(1 - \frac{h\nu}{E_a}\right)^{1/2}\left[\sigma_o^b + \left(1 - \frac{h\nu}{E_a}\right)\sigma_o^a\right] d(h\nu)\,, \qquad (9.56)$$

where we are thinking of a particular incident energy E_a (i.e. $|dE_b| = d(h\nu)$). In Eq. (9.56), the units are clearly erg-cm^3-sec^{-1}; thus one may interpret dS_ν as the emitted energy per sec per cm^3 of frequency ν, $\nu + d\nu$ per incident electron per hydrogen atom.

Since in discharges of various types and luminous regions of a shock, one does not have a mcnoenergetic beam of electrons, but rather a distribution (to a good approximation Maxwell-Boltzmann) described by an electron temperature T, it is necessary to weight dS_ν accordingly and integrate over all incident energies greater than $h\nu$. Thus, the fraction of electrons having kinetic energies in the range E, E + dE at temperature T is given by

$$f(E,T)\,dE = \frac{2}{\sqrt{\pi}}\,(kT)^{-3/2}\,e^{-E/kT}\,E^{1/2}\,dE\,, \qquad (9.57)$$

and we have

$$dS_\nu(T) = \left(\frac{8\sqrt{2}\,\alpha_f}{3(\pi m)^{3/2}c^2}\right)(kT)^{-3/2}\,d(h\nu)\left\{\int_{h\nu}^{\infty} e^{-E/kT}\left(1-\frac{h\nu}{E}\right)^{1/2}\right.$$

$$\left. x\;\sigma_o^b\,E^2\,dE + \int_{h\nu}^{\infty} e^{-E/kT}\left(1-\frac{h\nu}{E}\right)^{3/2}\sigma_o^a\,E^2\,dE\right\}. \qquad (9.58)$$

We have obtained an expression for the emitted power spectrum which now depends on the detailed nature of the particle interaction only through the s-wave partial cross sections corresponding to the initial and final kinetic energies. Firsov[59] and Hundley[60], who were investigating emission from electron collisions with heavy atoms, assume at this point that $\sigma_o^a = \sigma_o^b = \text{const.}$, and factor this out of the integrals, thereby obtaining the result that the radiated energy is proportional to the elastic scattering cross section. Clearly such an assumption is invalid in the case of hydrogen.

Electron-Hydrogen, Elastic Scattering Cross Sections

As was mentioned earlier, elastic scattering of electrons and hydrogen atoms at low energies is quite complicated since the continuum wave function of the electron strongly penetrates the atom (viz. s-waves most important), considerably distorting the atomic charge cloud, and exchange effects

are significant. A considerable amount of work has been done in connection with electron-hydrogen elastic scattering, including calculations[61,62] and laboratory measurements.[66,67]

Since high accuracy is really not warranted in this investigation, it was assumed satisfactory to fit an approximate curve to the s-wave partial cross sections given by Bransden et al.[68] It was found that a satisfactory fit could be made with the sum of a rapidly decaying and a slowly decaying exponential of the form

$$\sigma(E) = A(e^{-\alpha E} + Be^{-\beta E}) , \qquad (9.59)$$

where $\alpha = .1471\ eV^{-1}$, $\beta = 1.8382\ eV^{-1}$, $B = 2.5$, and $A = 20\ \pi a_o^2$. A comparison of $\sigma(E)$ from Eq. (9.59) and as given by Bransden et al. is given in Table XXVI. The agreement is satisfactory for our purposes.

TABLE XXVI

THE ELASTIC CROSS SECTION $\sigma_o(E)$ AS GIVEN BY BRANSDEN ET AL. AND BY EQ. (9.59)

k^2 units of 13.6 eV	σ_o Bransden et al.	σ_o Approximate
0.0025	63.8	66.9
0.01	53.6	58.7
0.05	32.5	32.4
0.1	23.0	20.5
0.2	15.0	13.7
0.3	11.0	11.0
0.4	8.5	8.99
0.6	6.0	6.02
0.8	4.0	4.04
1.0	2.7	2.70

Integration over the Boltzmann Distribution

From Eqs. (9.58) and (9.59) we obtain

$$dS_\nu(T) = \left(\frac{8\sqrt{2}\,\alpha_f}{3(\pi m)^{3/2}c^2} \right) (kT)^{3/2} A\, d(h\nu) \left\{ (1 + e^{\alpha h\nu}) g_2(\alpha,\nu) \right.$$

$$\left. + B(1 + e^{\beta h\nu})\, g_2(\beta,\nu) - g_1(\alpha,\nu) - B g_1(\beta,\nu) \right\} , \quad (9.60)$$

where[69]

$$g_1(\alpha,\nu) = \frac{h\nu}{(kT)^3} \int_{h\nu}^{\infty} E \left(1 - \frac{h\nu}{E}\right)^{1/2} e^{-(\alpha+1/kT)E}\, dE$$

$$= a_o^3\, e^{-a} \int_o^{\infty} [\xi(\xi + 1)]^{1/2}\, e^{-a\xi}\, d\xi$$

$$= \frac{a_o^3}{2a}\, e^{-a/2}\, K_1(a/2) , \quad (9.61)$$

and

$$g_2(\alpha,\nu) = \frac{1}{(kT)^3} \int_{h\nu}^{\infty} E^2 \left(1 - \frac{h\nu}{E}\right)^{1/2} e^{-(\alpha+1/kT)E}\, dE$$

$$= a_o^3\, e^{-a} \int_o^{\infty} (\xi + 1)[\xi(\xi + 1)]^{1/2}\, e^{-a\xi}\, d\xi = -h\nu \frac{dg_1(\alpha,\nu)}{da}$$

$$= \frac{a_o^3}{2a^2}\, e^{-a/2} \left[(2 + a/2)\, K_1(a/2) + (a/2)\, K_o(a/2) \right] , \quad (9.62)$$

with

$$a_o = \frac{h\nu}{kT} ,$$

and (9.63)

$$a = h\nu \left(\alpha + \frac{1}{kT} \right) .$$

The expressions for $g_1(\beta,\nu)$ and $g_2(\beta,\nu)$ are obtained from Eqs. (9.61) and (9.62) with α replaced by β and a replaced by b, where

$$b = h\nu \left(\beta + \frac{1}{kT} \right) . \tag{9.64}$$

The functions $K_o(a/2)$ and $K_1(a/2)$, of course, are the modified Bessel functions of the second kind of order zero and one, respectively.

Incorporating units such that we have n_e, n_H in 10^{17} cm^{-3}, λ in 10^3 A°, T in 10^4 °K, and A in πa_o^2, and employing the relationship

$$R = \frac{dn}{d\lambda} = n_e n_H \frac{1}{\lambda} \frac{dS_\nu(T)}{d(h\nu)} , \tag{9.65}$$

one finds for the number of photons per cm^3 per sec emitted per unit cm of wavelength to be given by

$$R_f = \left(\frac{dn}{d\lambda} \right)_f = (2.8539 \times 10^{22}) \frac{n_e n_H T^{3/2} A}{\lambda} G(\nu,T)$$

$$\times \text{ cm}^{-3} \text{ sec}^{-1} \text{ cm}^{-1} , \tag{9.66}$$

where $G(\nu,T)$ corresponds to the expression within the curly

brackets of Eq. (9.60). In these units, a is given by

$$a = \frac{1}{\lambda}\left(12.3946\ \alpha + \frac{14.3867}{T}\right),$$

and similarly for b, with α replaced by β.

It is important to observe that H^-, free-free emission increases linearly with N_e and quite strongly with temperature ($G(\nu,T)$ increases with T for smaller values of T).

In Tables XXVII and XXVIII are given rates of emission (i.e. number of photons emitted per cm^3 per sec per cm wavelength), calculated from Eq. (9.66). We should bear in mind, that in the above analysis it has been assumed that the p-wave phase shift is zero. This assumption is good for low energies, say $E \lesssim 8$ eV, but for $T = 100{,}000\ ^\circ K$, the electrons have an average thermal energy of ~ 10 eV, and the p-wave phase shift is no longer negligible. This could cause us to underestimate the emission somewhat. However, it is known that the phase shifts of Bransden et al.[68], which are used, somewhat overestimate the elastic cross section.[66] Thus, we might expect a partial cancellation of these two errors.

TABLE XXVII

CALCULATED VALUES OF THE RATE OF PHOTON EMISSION FROM FREE-FREE TRANSITIONS IN H^-

(units of $n_e n_H \times 10^{22}$ cm^{-3} sec^{-1} cm^{-1})

	T (10^4 °K)							
λ (10^3 A°)	1.0	1.5	2.0	2.5	3.0	3.5	4.0	4.5	5.0
2.0	.6723		21.01	41.49	65.00	89.15	112.4	134.0	153.5
2.5	1.733		27.69	48.24	69.71	90.41	109.5	126.5	141.4
3.0	3.059		31.65	50.89	69.90	87.53	103.3	117.1	129.0
3.5	4.399		33.66	51.25	68.00	83.15	96.47	107.9	117.7
4.0	5.603		34.41	50.39	65.21	78.41	89.85	99.61	107.8
4.5	6.612		34.39	48.90	62.13	73.77	83.77	92.22	99.26
5.0	7.417		33.90	47.13	59.04	69.42	78.27	85.71	91.88
5.5	8.037		33.14	45.26	56.06	65.41	73.35	79.98	85.45
6.0	8.498		32.23	43.39	53.26	61.76	68.94	74.92	79.83

TABLE XVIII

CALCULATED VALUES OF THE RATE OF PHOTON EMISSION FROM FREE-FREE TRANSITIONS IN H^-

(units of $n_e n_H \times 10^{22}$ cm^{-3} sec^{-1} cm^{-1})

	T (10^4 °K)									
λ (10^3 A°)	5.5	6.0	6.5	7.0	7.5	8.0	8.5	9.0	9.5	10.0
2.0	170.7	185.7	198.7	209.8	219.1	226.9	233.3	238.4	242.5	245.6
2.5	154.3	165.2	174.5	182.1	188.4	193.5	197.5	200.6	202.9	204.5
3.0	139.0	147.4	154.4	160.0	164.6	168.1	170.9	172.9	174.2	175.0
3.5	125.8	132.5	138.0	142.4	145.9	148.5	150.5	151.8	152.6	153.0
4.0	114.6	120.1	124.6	128.2	130.9	132.9	134.4	135.3	135.8	136.0
4.5	105.1	109.8	113.5	116.4	118.7	120.3	121.4	122.1	122.4	122.4
5.0	96.91	101.0	104.2	106.7	108.5	109.9	110.7	111.2	111.4	111.3
5.5	89.90	93.45	96.25	98.39	99.97	101.1	101.8	102.1	102.2	102.0
6.0	83.80	86.96	89.43	91.30	92.66	93.60	94.17	94.43	94.44	94.22

CHAPTER X

COMPARISON OF RADIATIVE PROCESSES

It is well known that the careful examination and interpretation of radiation emitted from a plasma can be an important tool for the determination of internal properties, such as electron density and temperature. Indeed, a multitude of techniques have been developed for extracting such information from various line intensities, widths, and contours, as well as relative intensities of different lines, and relative intensities of lines and adjacent regions of the continuum.[70,71] Several of these methods depend strongly on the presence of local thermodynamic equilibrium (LTE); this is to ensure that the relative populations of energy levels are related by the Boltzmann factors. It is known that under certain conditions, the populations vary significantly from a Boltzmann distribution,[72] and generally no simple relation exists between the electron temperature and the relative populations of bound and free states (e.g., the Saha equation is no longer applicable). In such cases it may be helpful to compare the measured continuum intensities with those calculated under a variety of conditions, and in such a way obtain an indication of the magnitudes of the electron temperature

and electron density.

Emission Spectrum

The tables given in Chapters VIII and IX were used to graph representative curves giving rates of emission corresponding to each of the four processes contributing to the continuum of hydrogen. In Figures 20 - 38 are given, on a semi-log plot, the rates of emission R (in units of $n^2 \times 10^{25}$ cm^{-3} sec^{-1} cm^{-1} wavelength, where n is the total particle density (i.e. $n = n_H + n_1$), in units of 10^{17} cm^{-3}) for the four processes: recombination (r), proton-electron bremsstrahlung (b), free-bound, H^- spectrum (fb) (See Appendix II), and free-free, H^- spectrum (ff). The curves corresponding to recombination (r) and bremsstrahlung (b) must still be multiplied by α^2, where α is the degree of ionization (i.e., $n_e = \alpha n$, $n_H = (1 - \alpha)n$, and the curves for free-bound (fb) and free-free (ff) must be multiplied by $\alpha(1 - \alpha)$. Alternatively, one may simply think of the recombination and bremsstrahlung curves as being given in units of $n_e^2 \times 10^{25}$ cm^{-3} sec^{-1} cm^{-1}, and those of free-bound and free-free emission in units of $n_e n_H \times 10^{25}$ cm^{-3} sec^{-1} cm^{-1}. The abscissa of each graph is scaled by the wavelength λ, given in units of 10^3 A°.

Because of the shifting of the ionization potential with electron density, the recombination emission has a somewhat complicated dependence on N_e. However, for moderate densities (i.e. $N_e \leq 10^{17}$), variation of the ionization

potential has a rather small effect. For comparison, curves have been given for four representative electron densities: $N_e = 10^{15}$, 10^{16}, 10^{17}, and 10^{18} cm^{-3} (i.e. $n_e = .01$, 0.1, 1.0, 10., respectively).

In Figures 39-46 are given, on a log-log plot, calculated values of rates of emission R (in units of 10^{25} cm^{-3} sec^{-1} cm^{-1} wavelength) for a total particle density of $N = 10^{17}$ cm^{-3} ($n = 1.0$) and several values of T, in terms of α, the degree of ionization. Figures 39, 41, 43, and 45 correspond to $\lambda = 3000°$ (λ below Balmer limit), and Figures 40, 42, 44, and 46 to $\lambda = 5000°$ (λ above Balmer limit). Curves are given for recombination (r), bremsstrahlung (b), free-bound (fb) (See Appendix II), free-free (ff), and the sum of the four processes, denoted by s. In order to investigate different total particle densities N (i.e. different pressures), one may scale the rates given in Figures 39 - 46 by n^2 (i.e. $N^2 \times 10^{-34}$); this is, of course, only approximate for the recombination curves, due to the shifting of the ionization potential with electron density, however, except for $N_e \gtrsim 10^{18}$, the error is small. The curves may easily be extended for higher degrees of ionization, by means of the tables in Chapters VIII and IX, and by recalling that

$$n_e n_1 \cong n_e^2 = \alpha^2 n^2 ,$$
$$n_e n_H = \alpha(1 - \alpha) n^2 . \qquad (10.1)$$

It should be mentioned, that the results given in

Figures 20 - 38 are in no way restricted to a pure hydrogen plasma. If other components are present, then in general the relation $n_e = n_i$ does not hold, and hence it is impossible to define an α satisfying Eq. (10.1), since charge neutrality may be maintained by means of ions of the other components as well as protons. In such cases, the contribution to the total emission, due to hydrogen, is obtained by multiplying the recombination (r) and bremsstrahlung (b) results by $n_e n_i$, where n_i gives the proton density, and the free-bound (fb) and free-free (ff) by $n_e n_H$.

Dependence on Electron Temperature and Electron Density

The emission from a highly ionized (say $\gtrsim 50\%$) hydrogen plasma is, of course, mainly due to recombination and proton-electron bremsstrahlung (Dissociation of H_2 is practically complete for temperatures of interest here.). Recombination is a rapidly decreasing function of temperature, as seen in Eq. (8.12), while bremsstrahlung increases with temperature over a certain range of T, due to the exponential dependence shown in Eq. (8.18). Bremsstrahlung is of considerably more importance beyond the Balmer series limit, where the recombination intensity has dropped off. (Recombination into the $n = 2$ state does not contribute to the emission for wavelengths beyond the Balmer series limit.), however for large temperatures it is quite significant on both sides of the limit.

In cases where the ratio n_e/n_H (i.e., $\alpha/(1 - \alpha)$

a purely hydrogenic plasma) is much less than unity, the effects of the negative hydrogen ion become important. The relative temperature dependence of the free-bound and the free-free processes is similar to that of recombination and bremstrahlung, the free-free emission becoming important at higher temperatures.

The Free-Bound H^- Continuum

In order to observe the free-bound continuum (affinity spectrum) (See Appendix II), it is necessary to maintain conditions such that the emission due to recombination and bremsstrahlung is weak (viz. high neutral density, but low degree of ionization). In a plasma possessing local thermal equilibrium, the neutral particle density, ion density, and the electron density are related by the Saha equation.[71,73]

$$\log_{10} \frac{n_e n_i}{n_H} = - \frac{5.050\ V_i}{T} + 1.5 \log_{10} T + 15.385 , \qquad (10.2)$$

where V_i is the ionization potential in volts, and where the total pressure is given by

$$P = P_n + P_i + P_e . \qquad (10.3)$$

In cases where $n_e = n_i$ (viz., a one-component plasma with no strong external fields), we have

$$\log_{10} \left(\frac{\chi^2}{1 - \chi^2} P \right) = \frac{-5.050\ V_i}{T} + 2.5 \log_{10} T - 6.5 , \qquad (10.4)$$

where

$$\chi = n_i/n = n_e/n \ .$$

One can see from Eq. (10.4), that low values of n_i and n_e are favored by large pressures, and consequently large neutral particle densities.

The appropriate conditions have been found to exist in high pressure, hydrogen-arc discharges at temperatures of the order 10,000 to 15,000 °K.[22] Lochte-Holtgreven and Nissen[74] found that in a water-cooled hydrogen arc at pressures of .4 to 1.0 atm. and temperatures of 10,000 to 12,000 °K, the observed continuum was, on the average, twice as strong as that due to recombination and bremsstrahlung alone. It was concluded that the free-bound, H^- continuum made up the difference, and in fact, theoretical calculations showed this to indeed be the case.[75] Several other similar experiments have been carried out involving pressures up to 1000 atm., in which case, the emission is very close to that of a black body.[22] At these higher pressures, the free-bound, H^- continuum is several times stronger than that of H.

It might be well to point out, that in the above work extensive use was made of the fact, that for cases where thermal equilibrium is present, the emission, and absorption coefficients are related by[22]

$$\frac{\epsilon_\nu}{K_\nu} = B_\nu(T) \ , \qquad (10.5)$$

where $B_\nu(T)$ is the Planck function, and is given by

$$B_\nu(T) = \frac{2h\nu^3}{c^2} (e^{h\nu/kT} - 1)^{-1} . \qquad (10.6)$$

This is Kirchoff's radiation law, and is simply a statement of thermal equilibrium of the particles. It is important to realize that Eq. (10.5) does not require thermodynamic equilibrium of the radiation itself (i.e., need not have black-body radiation). The relation given by Eq. (10.5) is quite useful, since extensive calculations of absorption coefficients are available;[24] however, one must be certain that the system is in thermal equilibrium.

Suitable conditions for the observation of the H^- continuum have also been obtained by Weber[76] in a diaphragm-type shock tube, filled with a H-Kr mixture in the low-pressure section and pure hydrogen in the high-pressure section. The discontinuity at the Balmer limit was found to be 25%, which is in approximate agreement with theory; in the absence of any H^- continuum, the intensity would jump by a factor of 30. The measurements were made behind the reflected shock wave, where the temperature was approximately 8600°K, and the densities were found to be: $N_e = 4.8 \times 10^{16}$, $N_H = 8.3 \times 10^{18}$, $N_{H^+} = 3.9 \times 10^{15}$, $N_{H^-} = 1.45 \times 10^{14}$, $N_{Kr} = 1.66 \times 10^{19}$, and $N_{Kr^+} = 4.4 \times 10^{16}$ cm^{-3}. The contribution from free-free transitions in H^- was of course assumed to be negligible because of the low temperature.

The Free-Free Continuum

Of the four processes discussed in this work, the

most difficult to observe is clearly that corresponding to free-free transitions in H^-. Quite unlike the affinity spectrum, where appropriate conditions can be realized in an equilibrium situation, the free-free, H^- continuum is important only in cases where the electron temperature is high (e.g. 25,000-50,000 °K) and the ion density low. Probably, only in cases of non-thermal equilibrium, can such conditions be met.

Hamberger,[77] in a study of intensity modulation of Balmer light from a high-frequency discharge, obtained conditions conducive to the appearance of the free-free, H^- continuum. At low pressures (~ .2 mm Hg), rather high electron temperatures result from the acceleration of the electrons in the rf field, while the electron density remains low. Typical conditions are given by: P = 0.2 mm Hg, $N_H = 10^{16}$ cm^{-3}, $N_e = 10^{12}$ cm^{-3}, where the electron temperature was estimated to vary between 3 and 9 eV, at 1.5×10^6 cps. Although no measurements were made on the continuum, it was observed to be relatively strong.[78] From the above discussion, we would conclude that, under these conditions, recombination and proton-electron bremsstrahlung contribute practically nothing to the continuum, which is then almost entirely due to free-bound and free-free transitions in H^-, with the free-free emission being somewhat the stronger of the two.

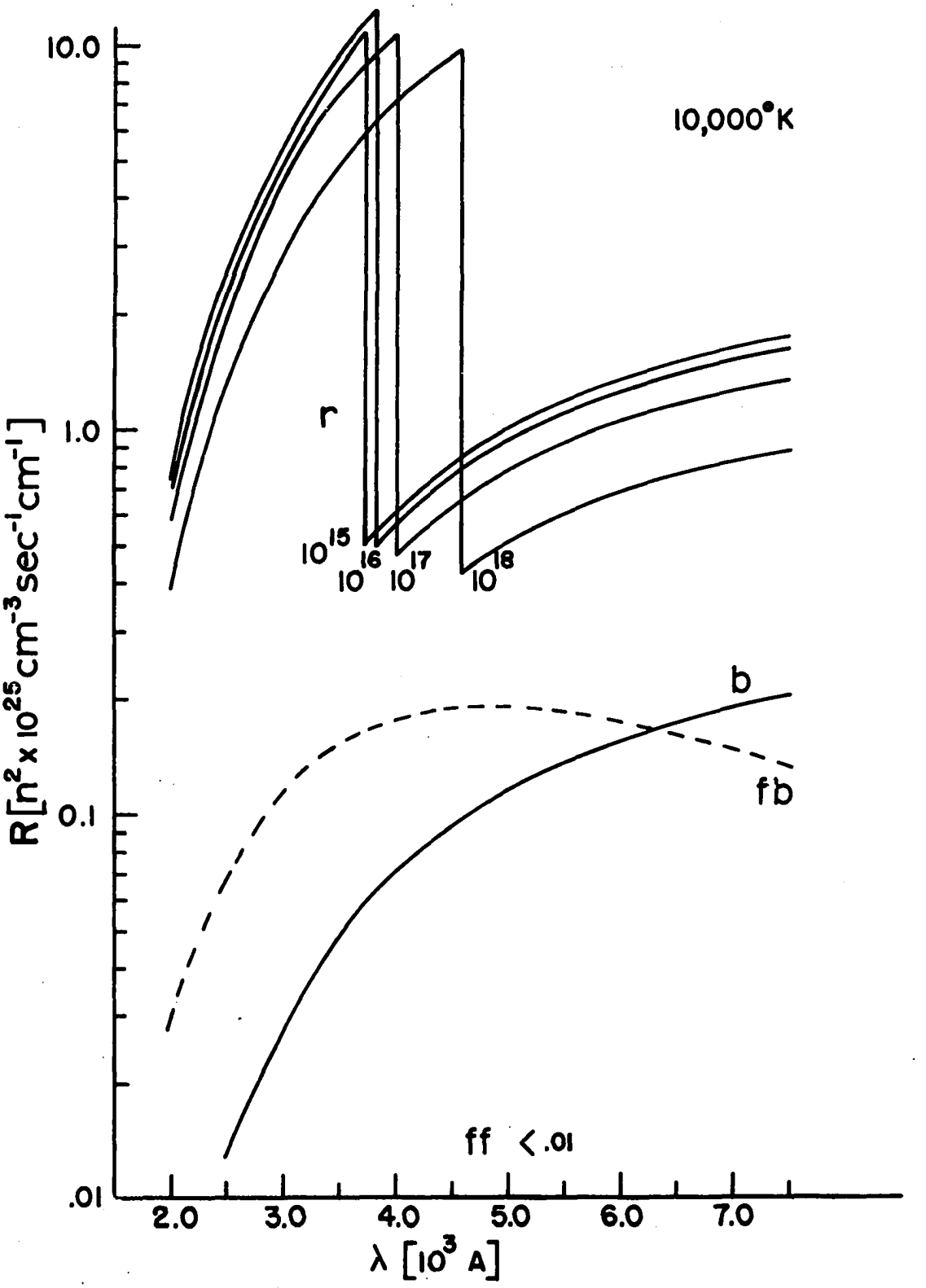

Figure 20. Continuum Spectrum, T = 10,000°K.

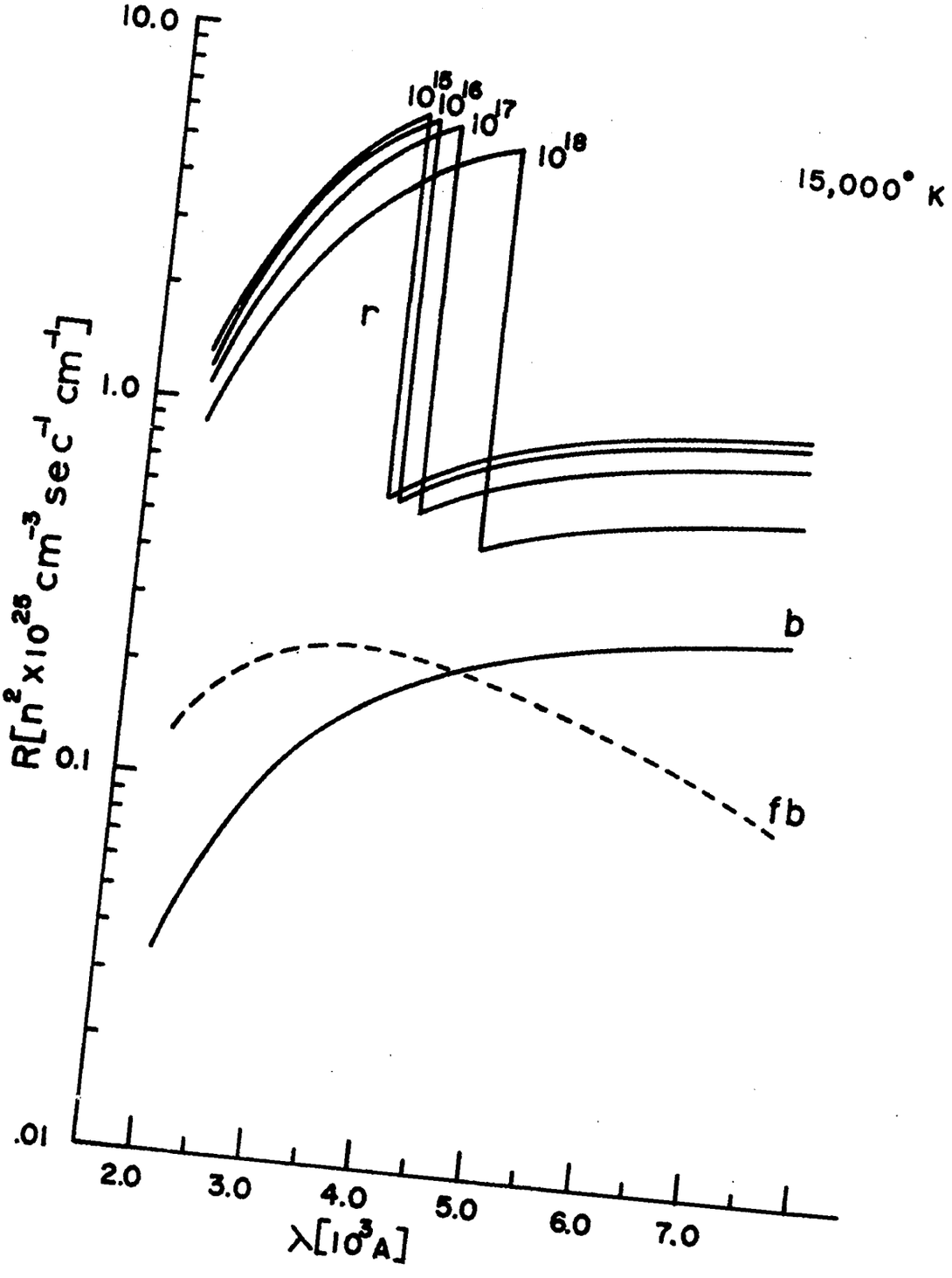

Figure 21. Continuum Spectrum, T = 15,000°K.

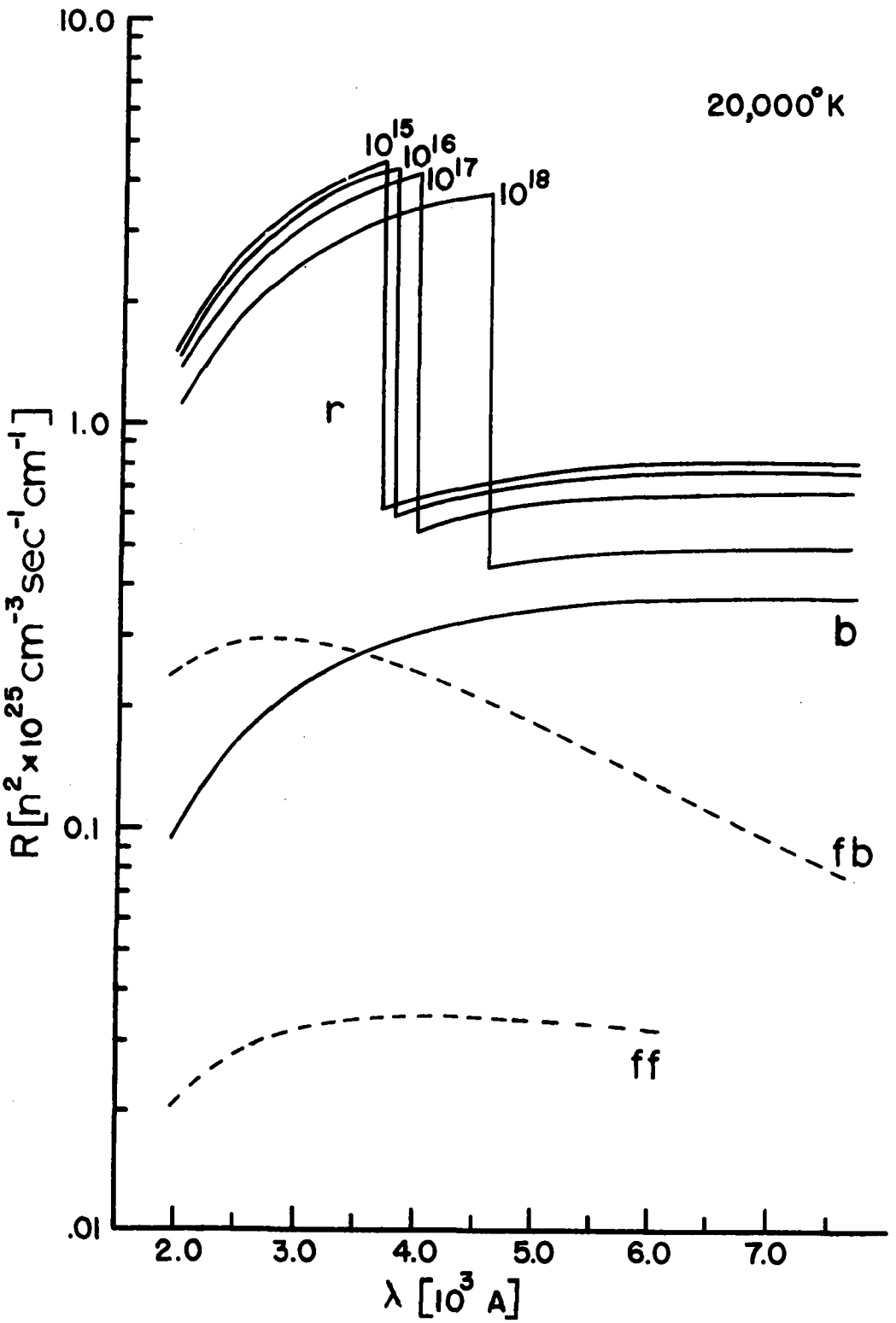

Figure 22. Continuum Spectrum, T = 20,000°K.

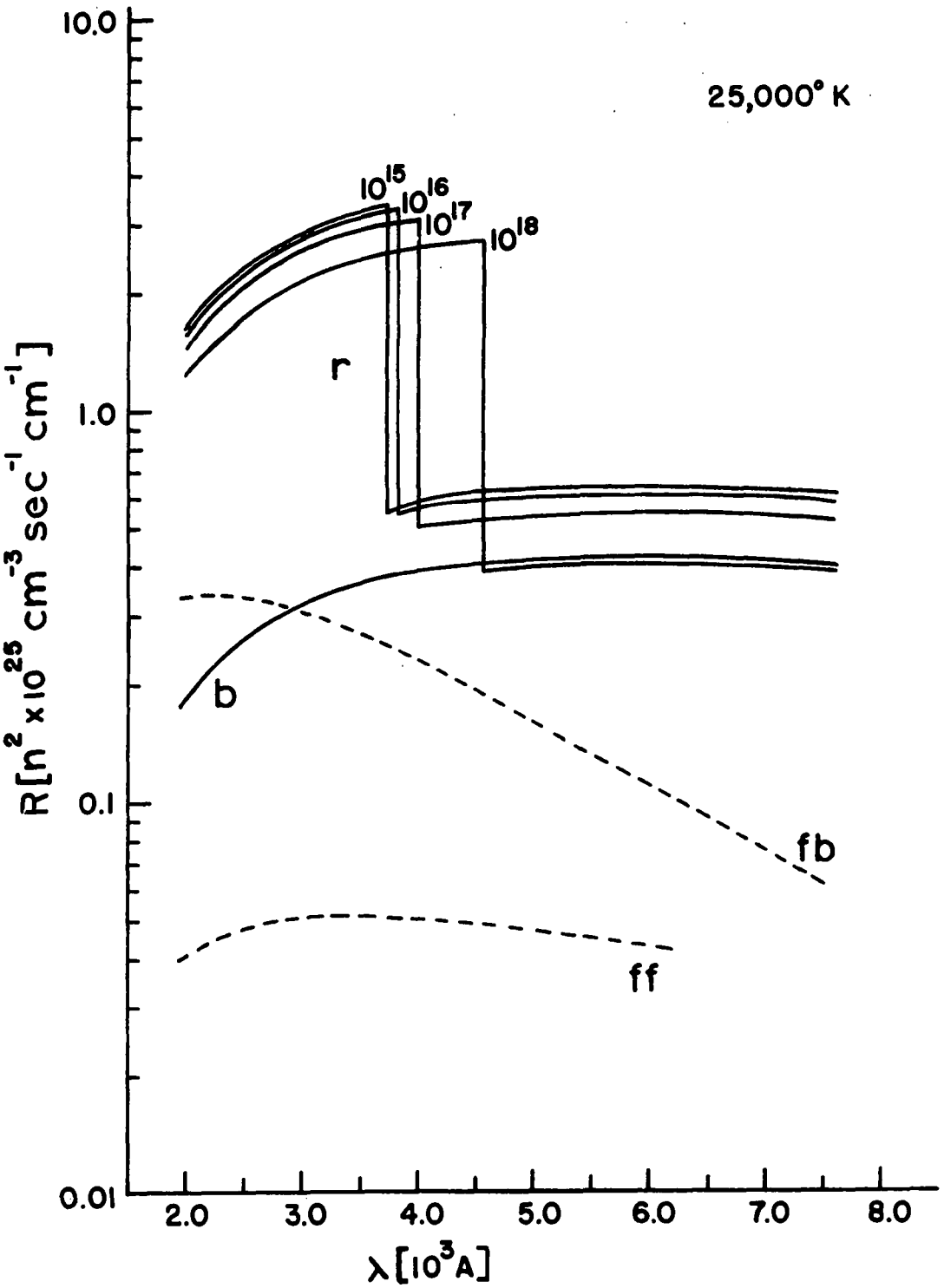

Figure 23. Continuum Spectrum, T = 25,000°K.

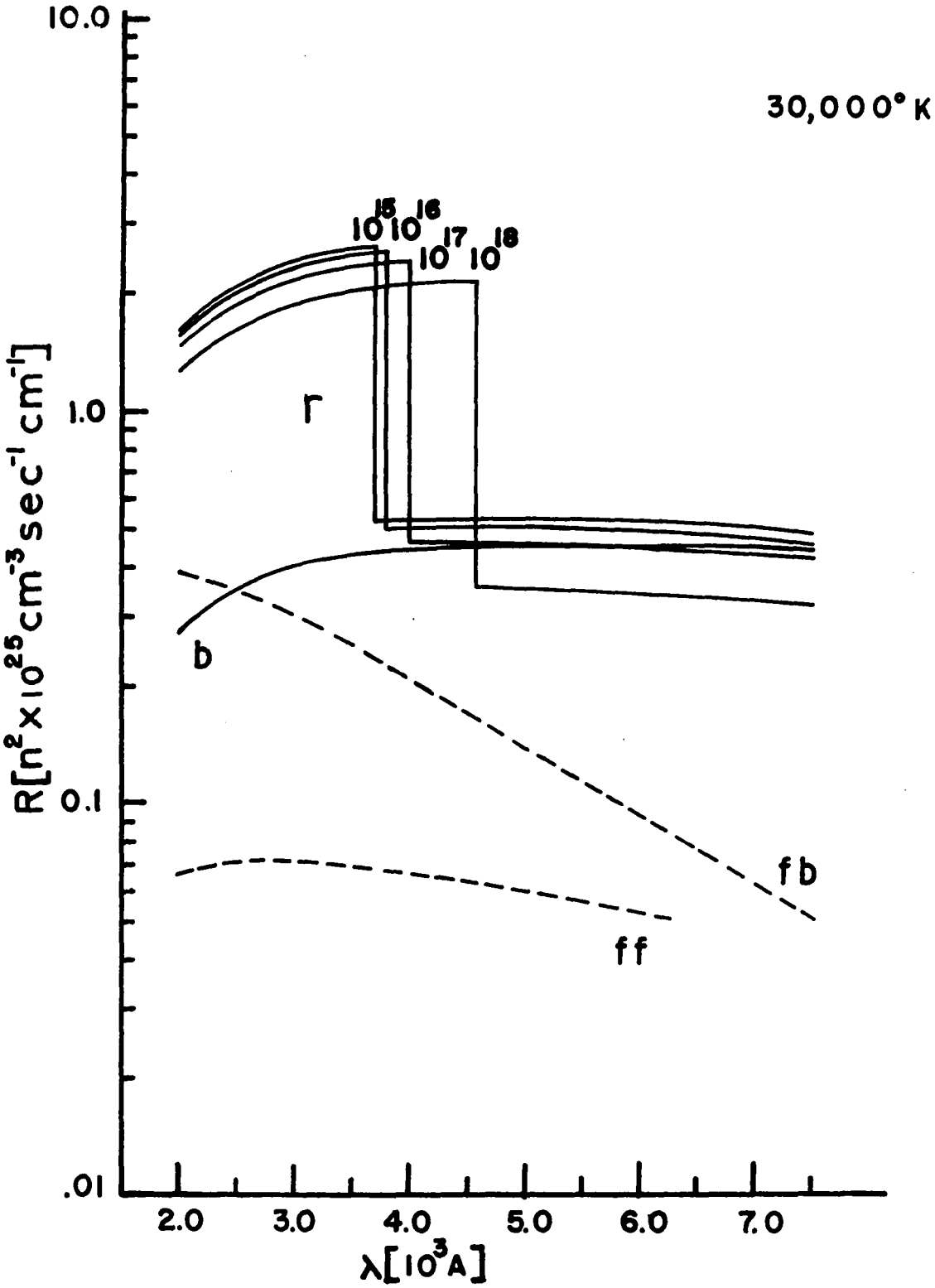

Figure 24. Continuum Spectrum, T = 30,000° K.

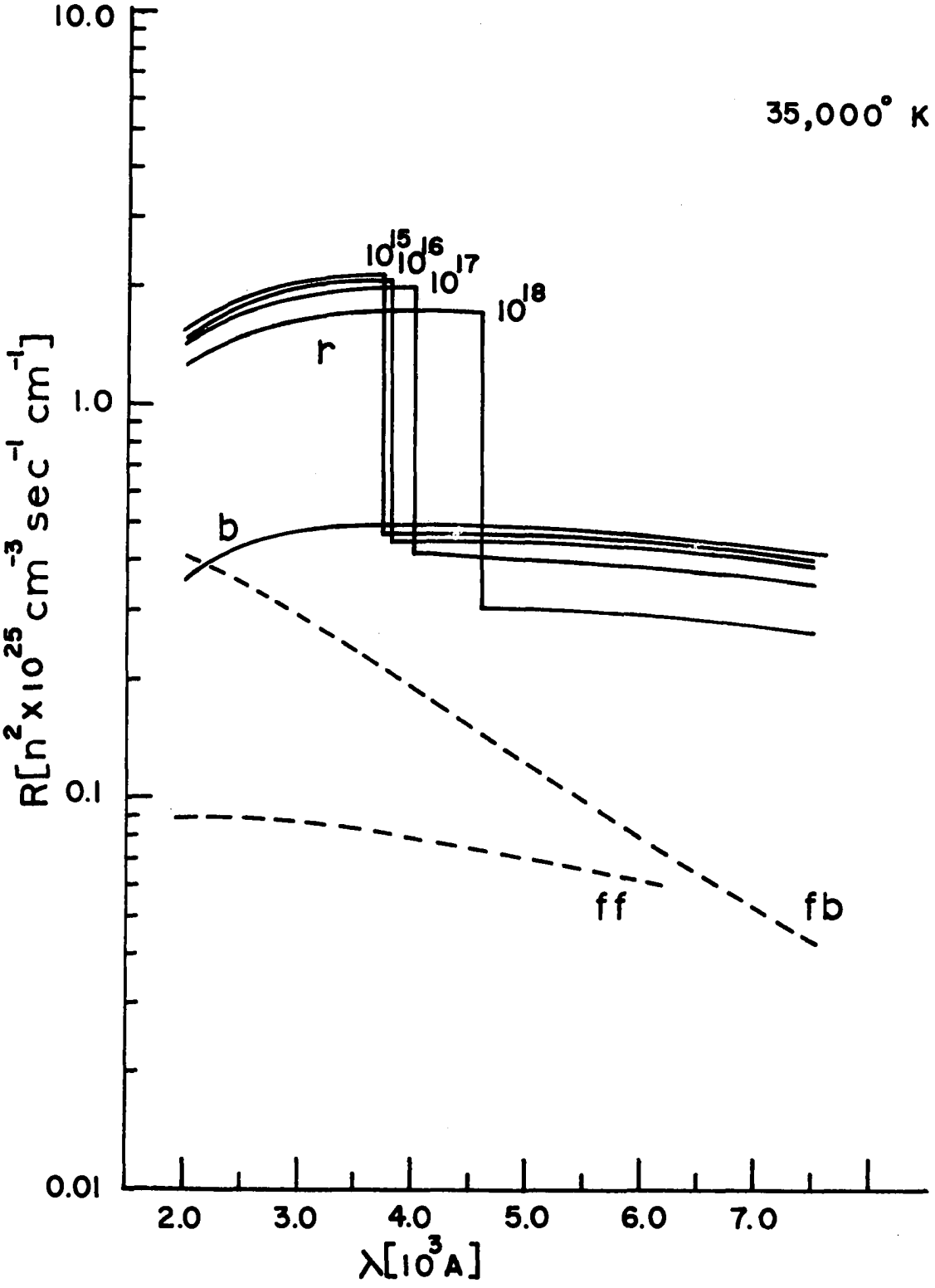

Figure 25. Continuum Spectrum, T = 35,000°K.

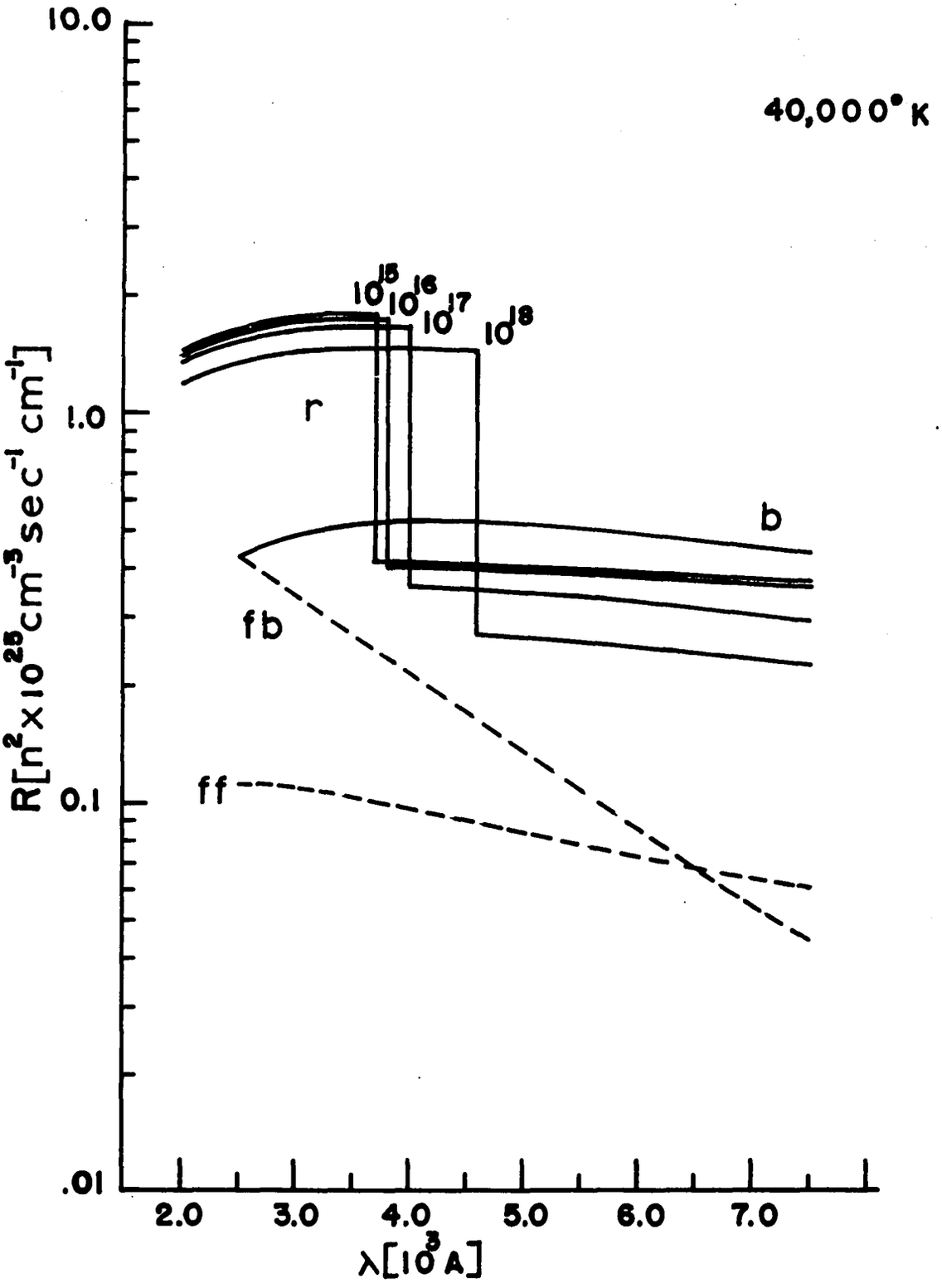

Figure 26. Continuum Spectrum, T = 40,000°K.

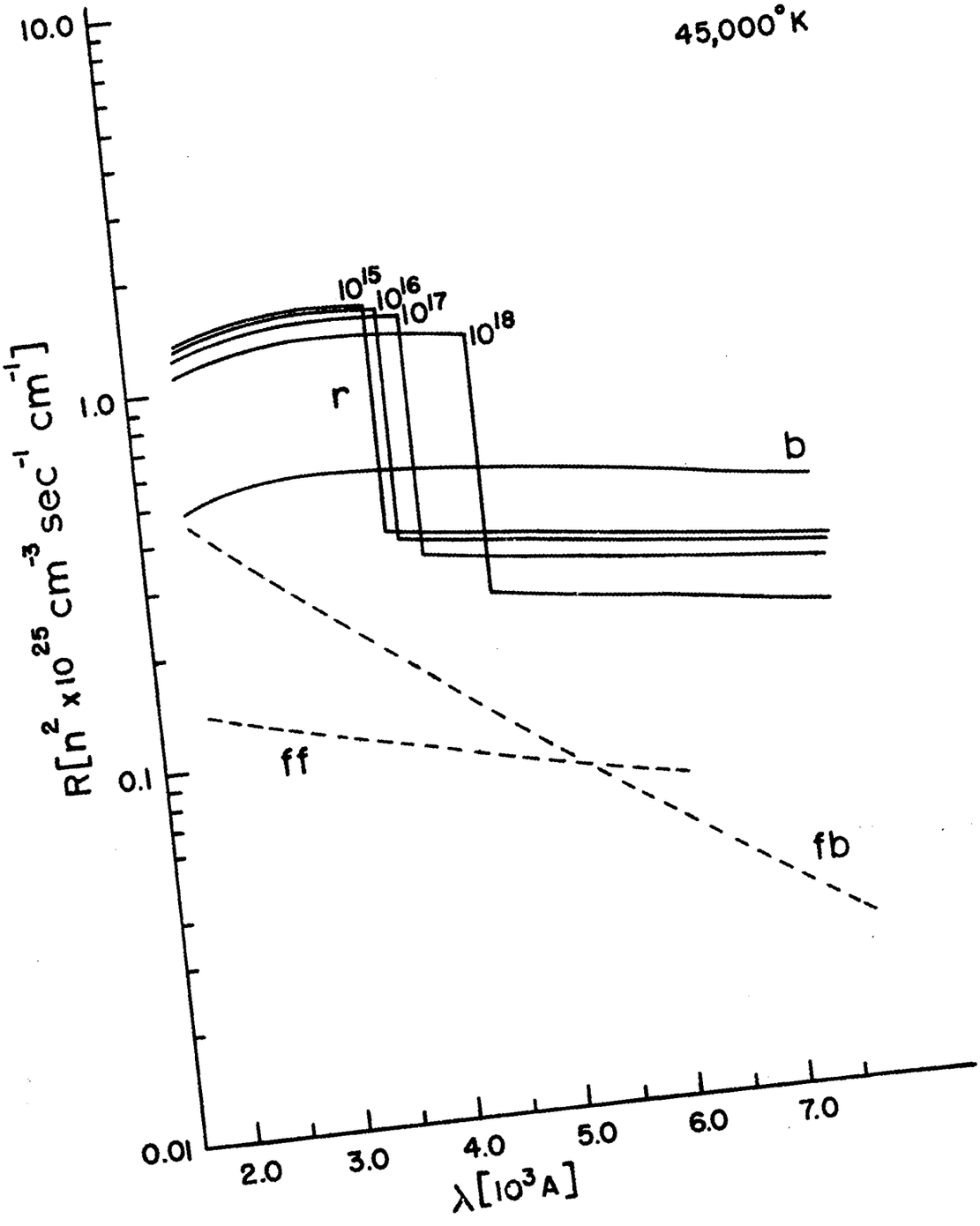

Figure 27. Continuum Spectrum, T = 45,000°K.

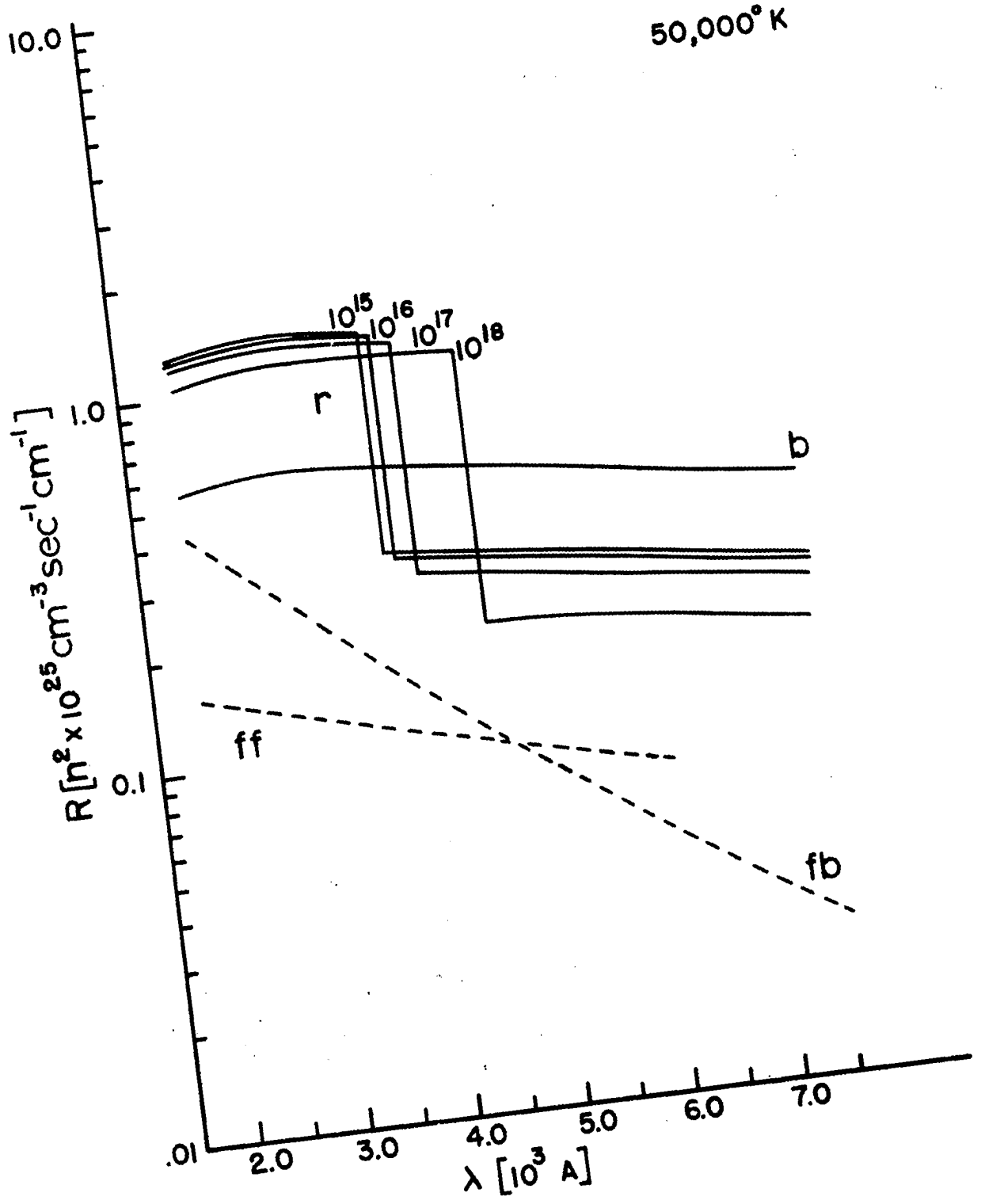

Figure 28. Continuum Spectrum, T = 50,000° K.

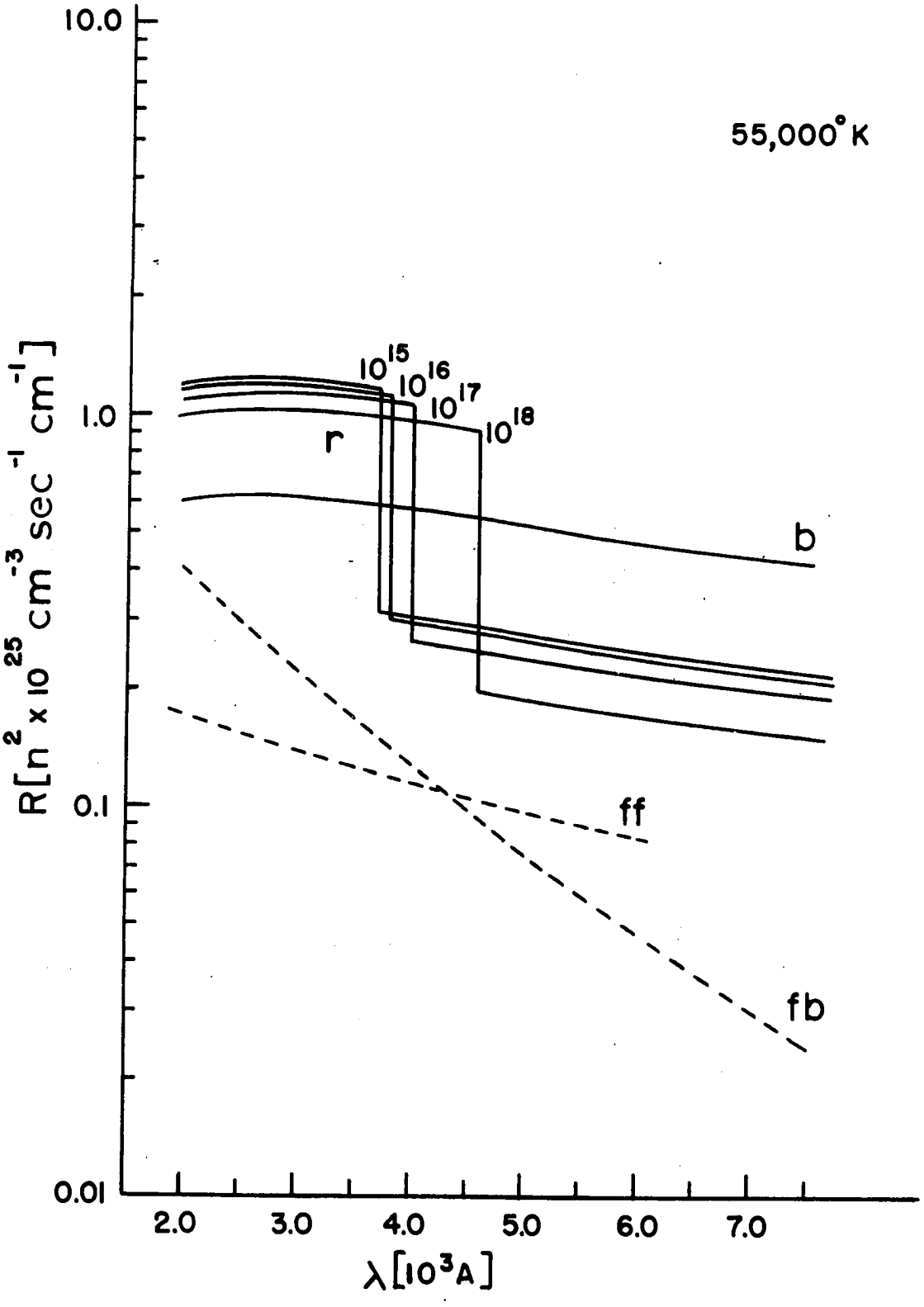

Figure 29. Continuum Spectrum, T = 55,000°K.

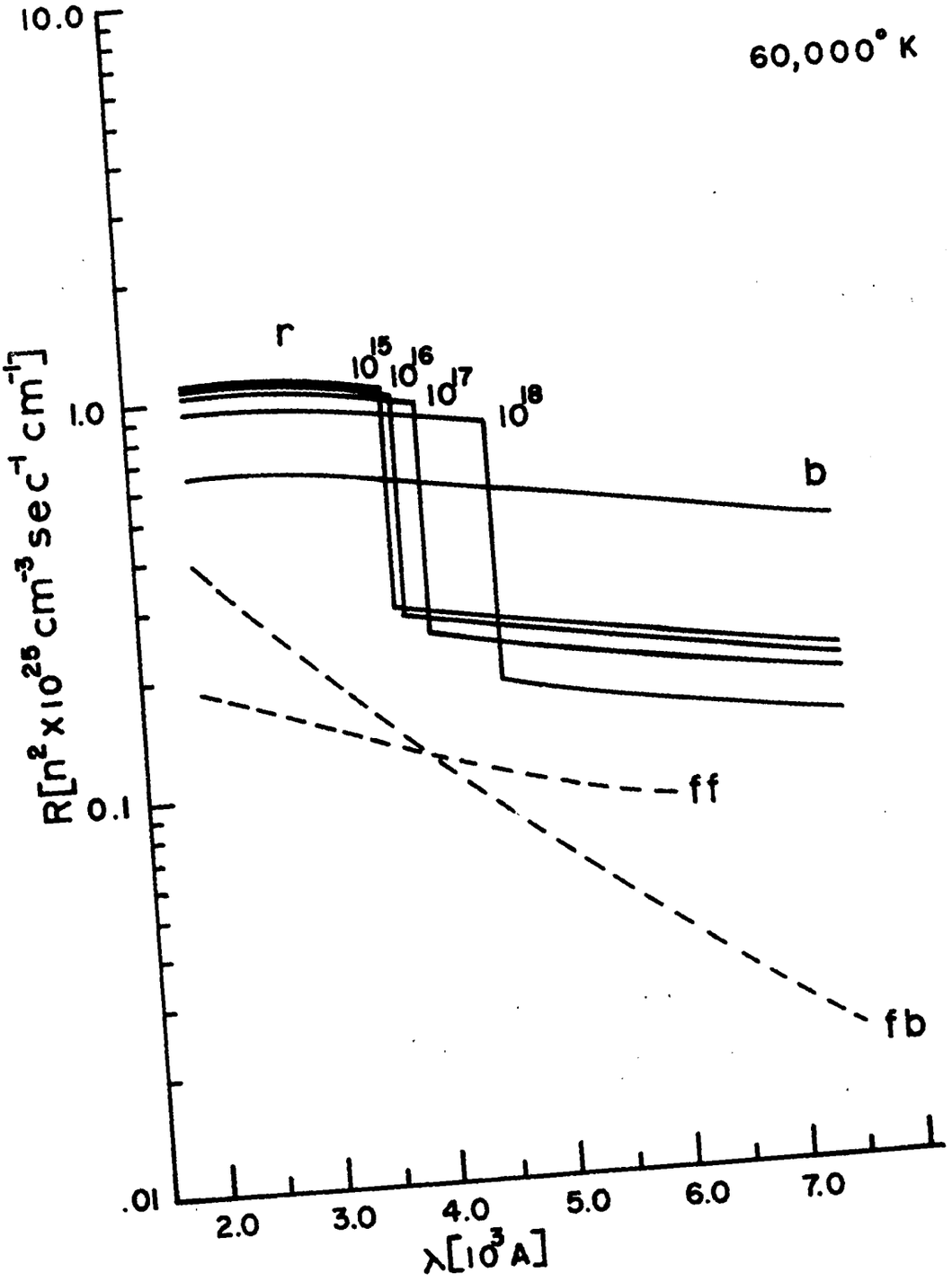

Figure 30. Continuum Spectrum, T = 60,000° K.

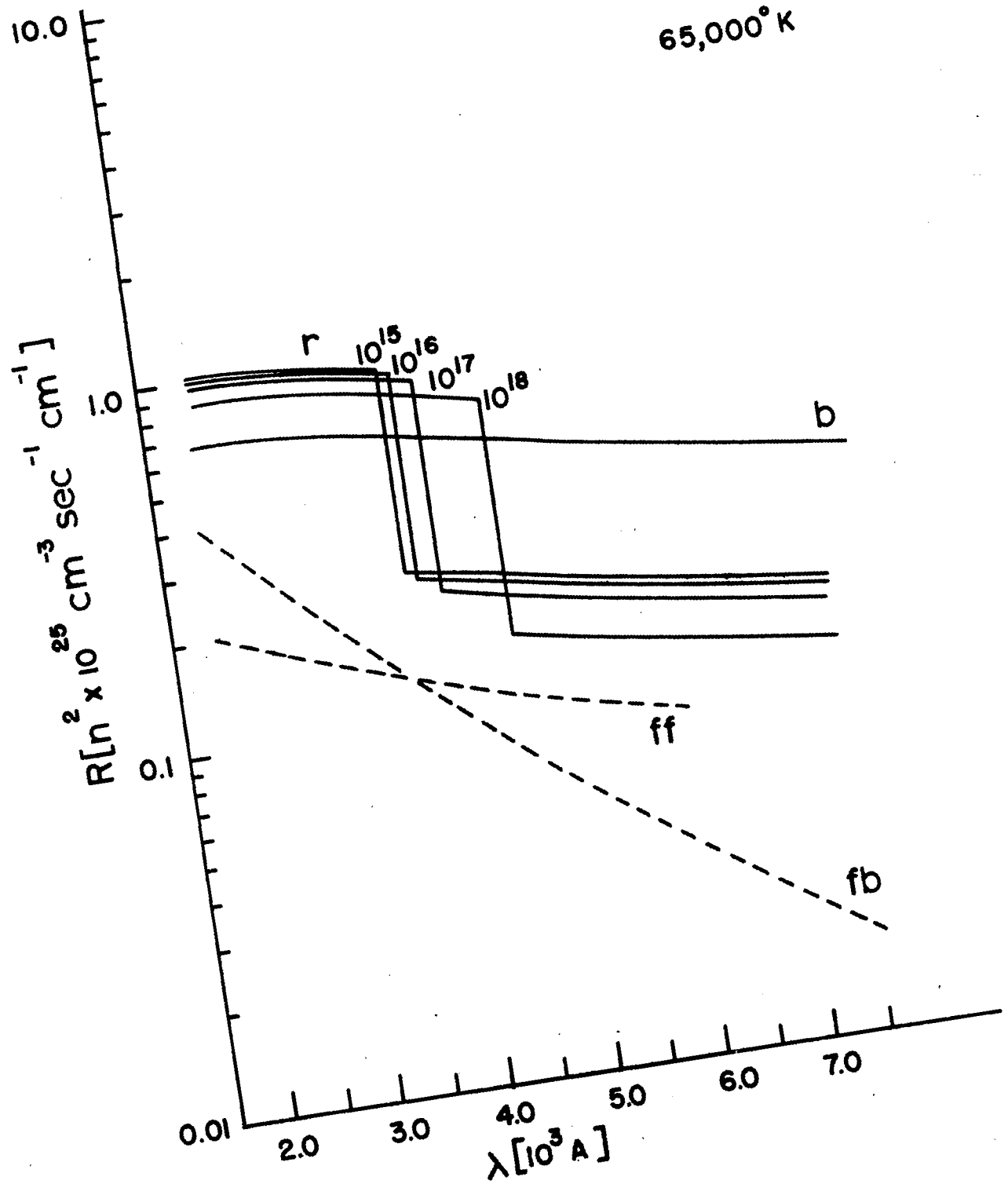

Figure 31. Continuum Spectrum, T = 65,000° K.

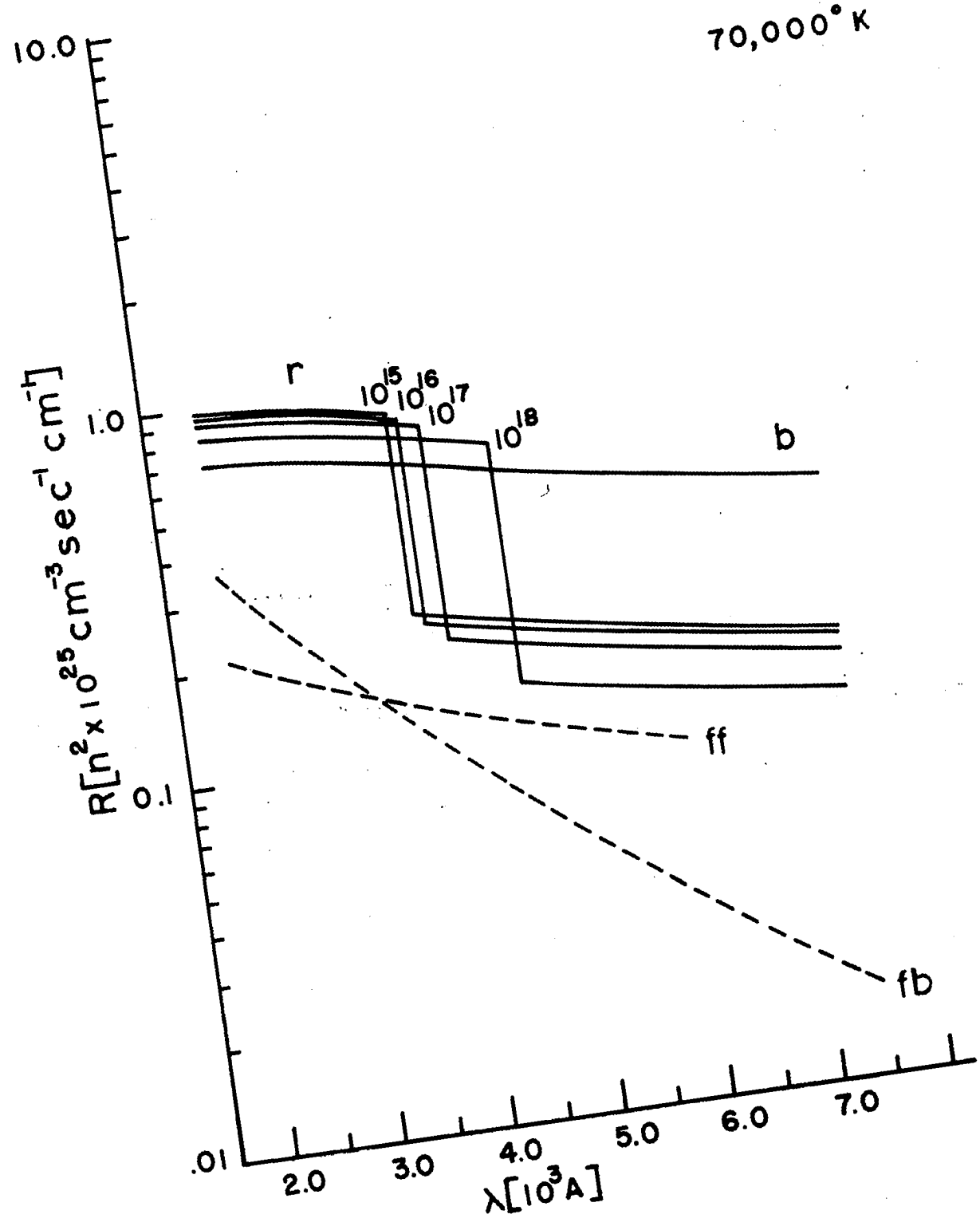

Figure 32. Continuum Spectrum, T = 70,000° K.

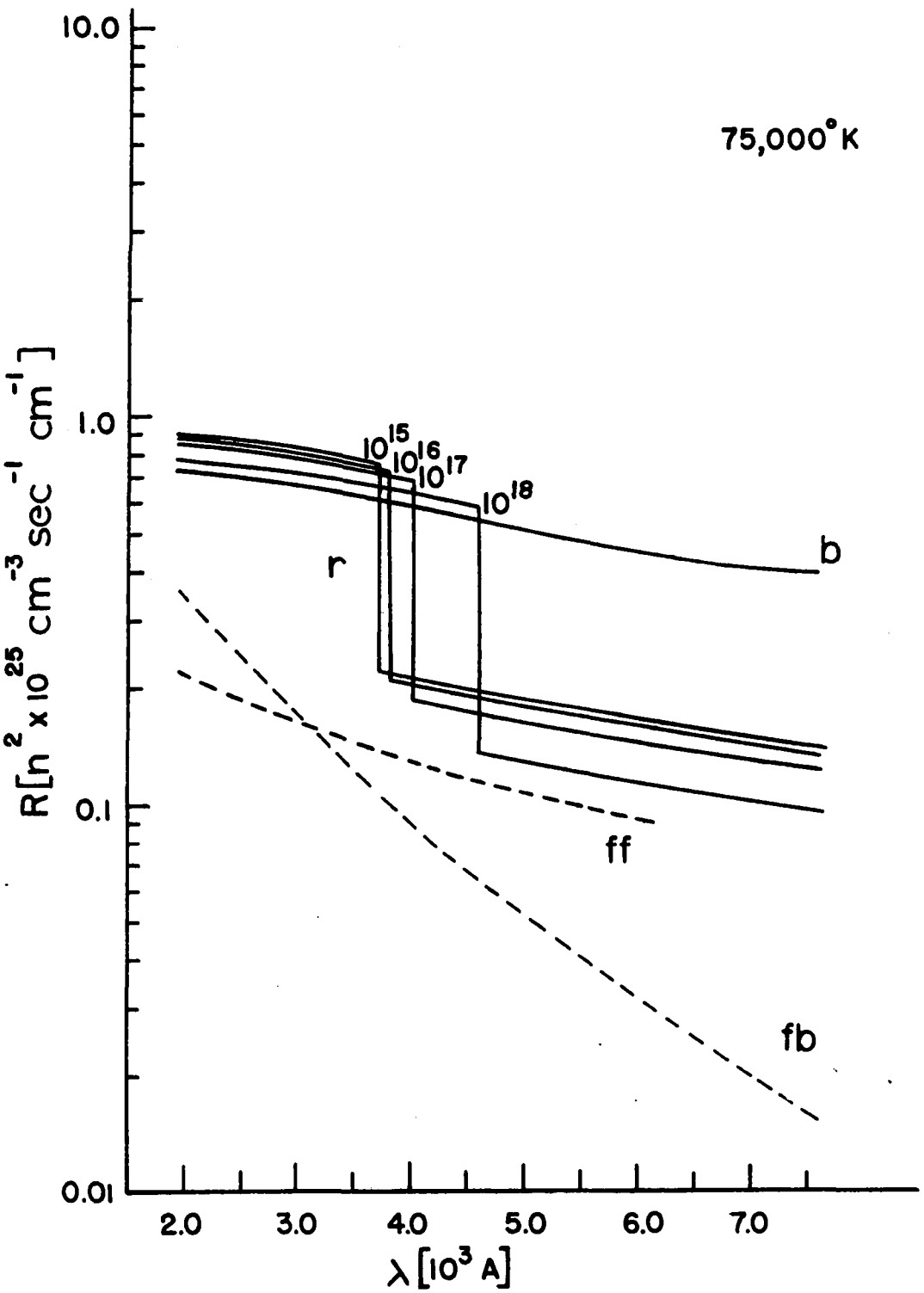

Figure 33. Continuum Spectrum, T = 75,000°K.

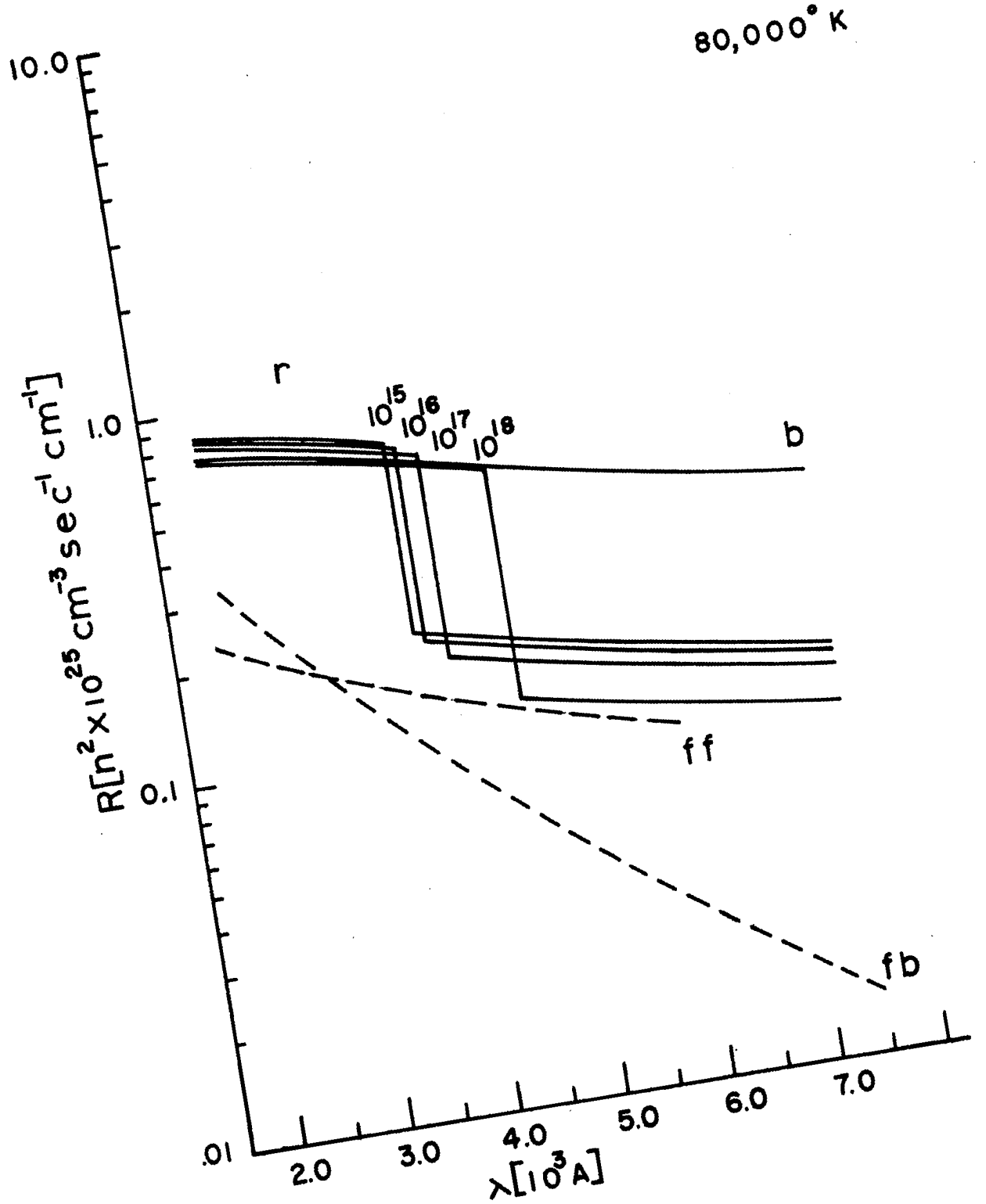

Figure 34. Continuum Spectrum, T = 80,000° K.

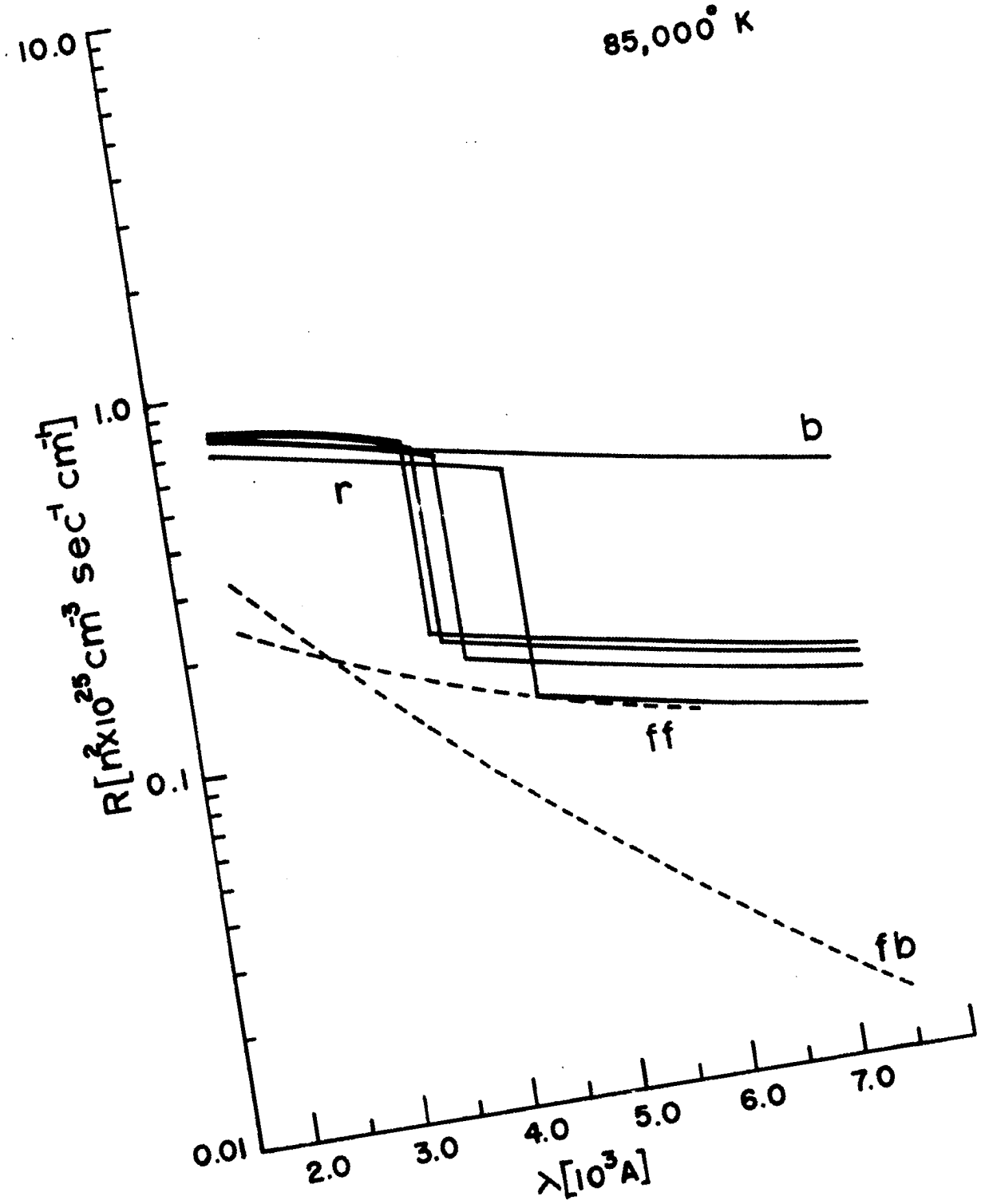

Figure 35. Continuum Spectrum, T = 85,000° K.

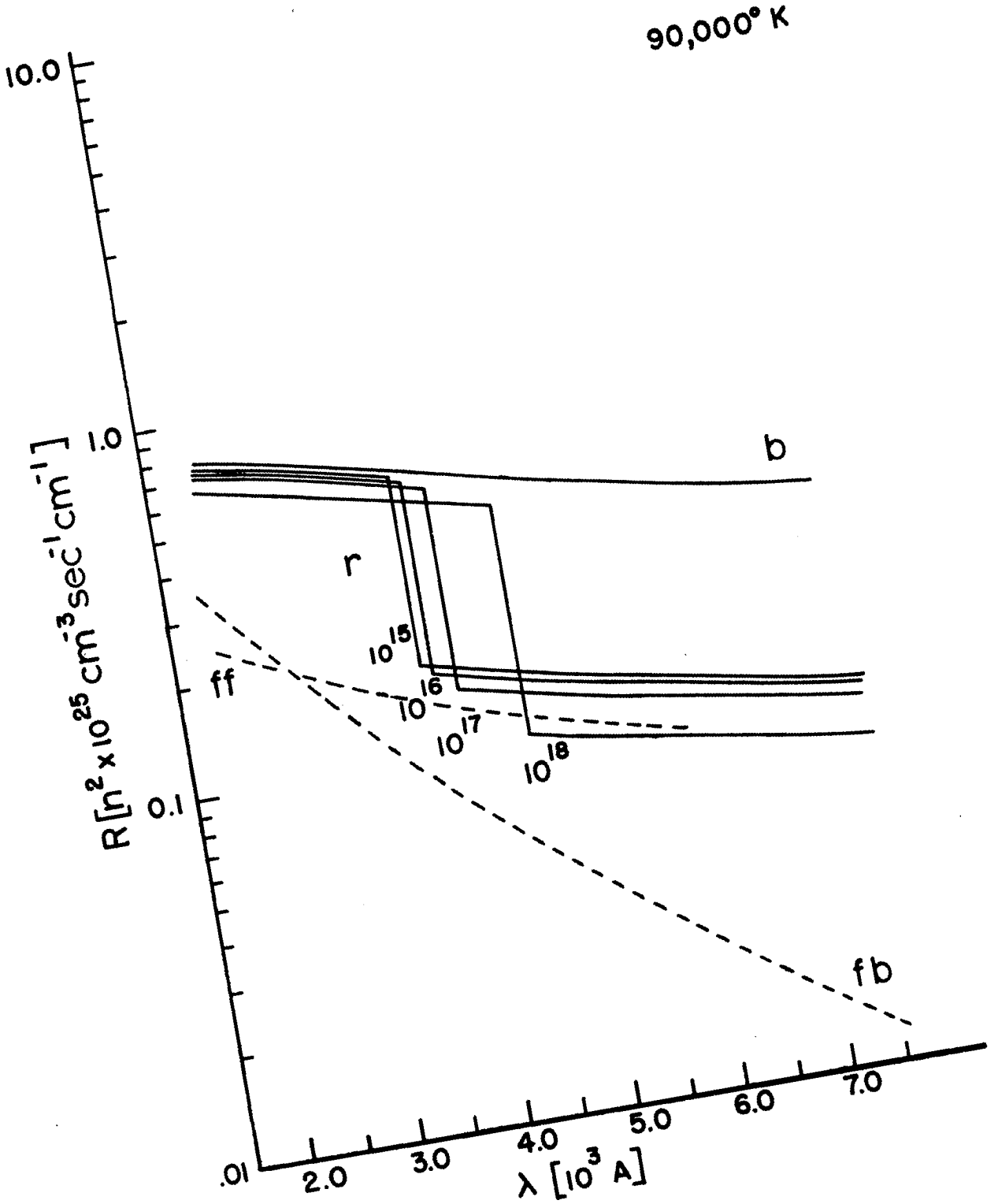

Figure 36. Continuum Spectrum, T = 90,000° K.

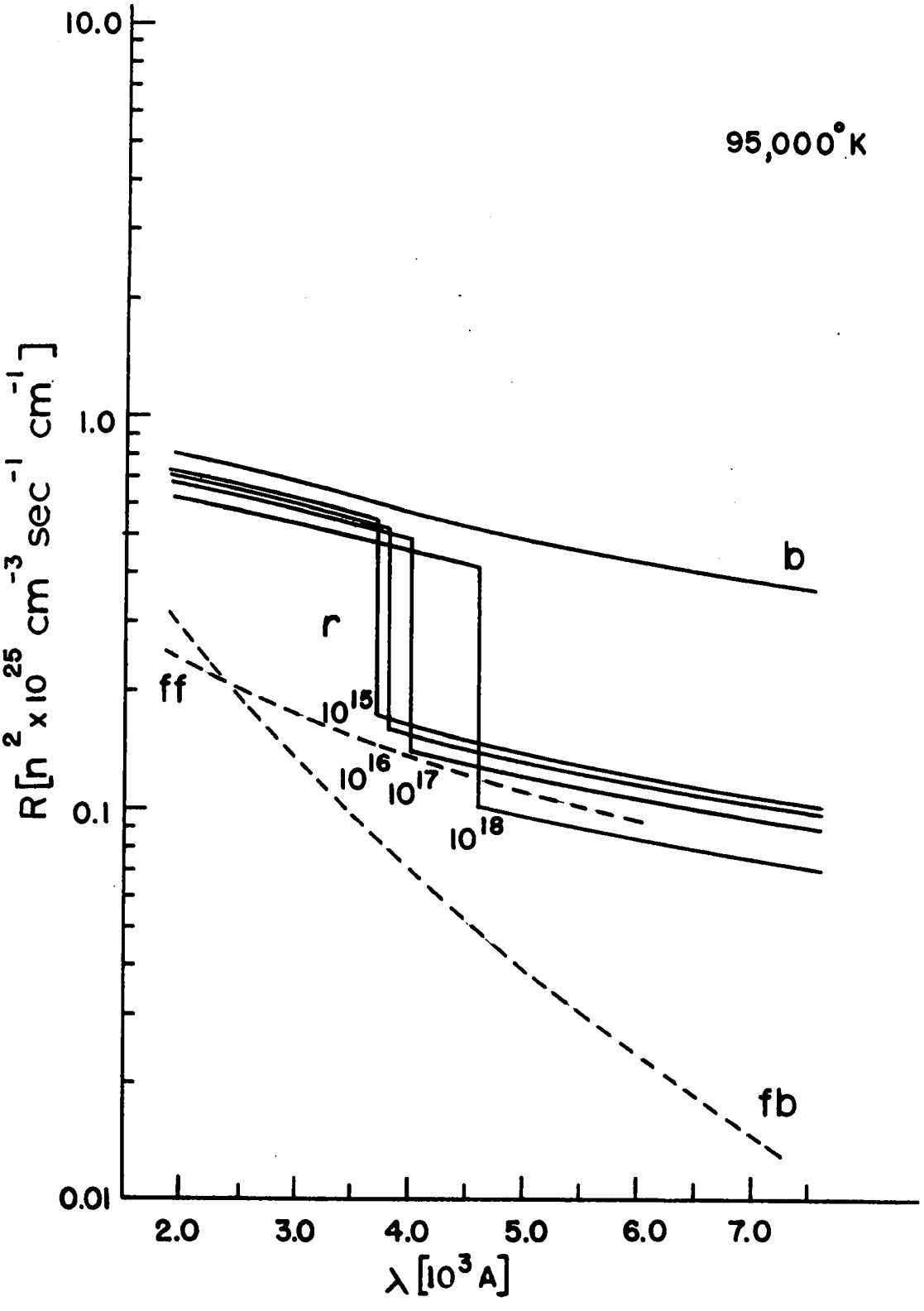

Figure 37. Continuum Spectrum, T = 95,000°K.

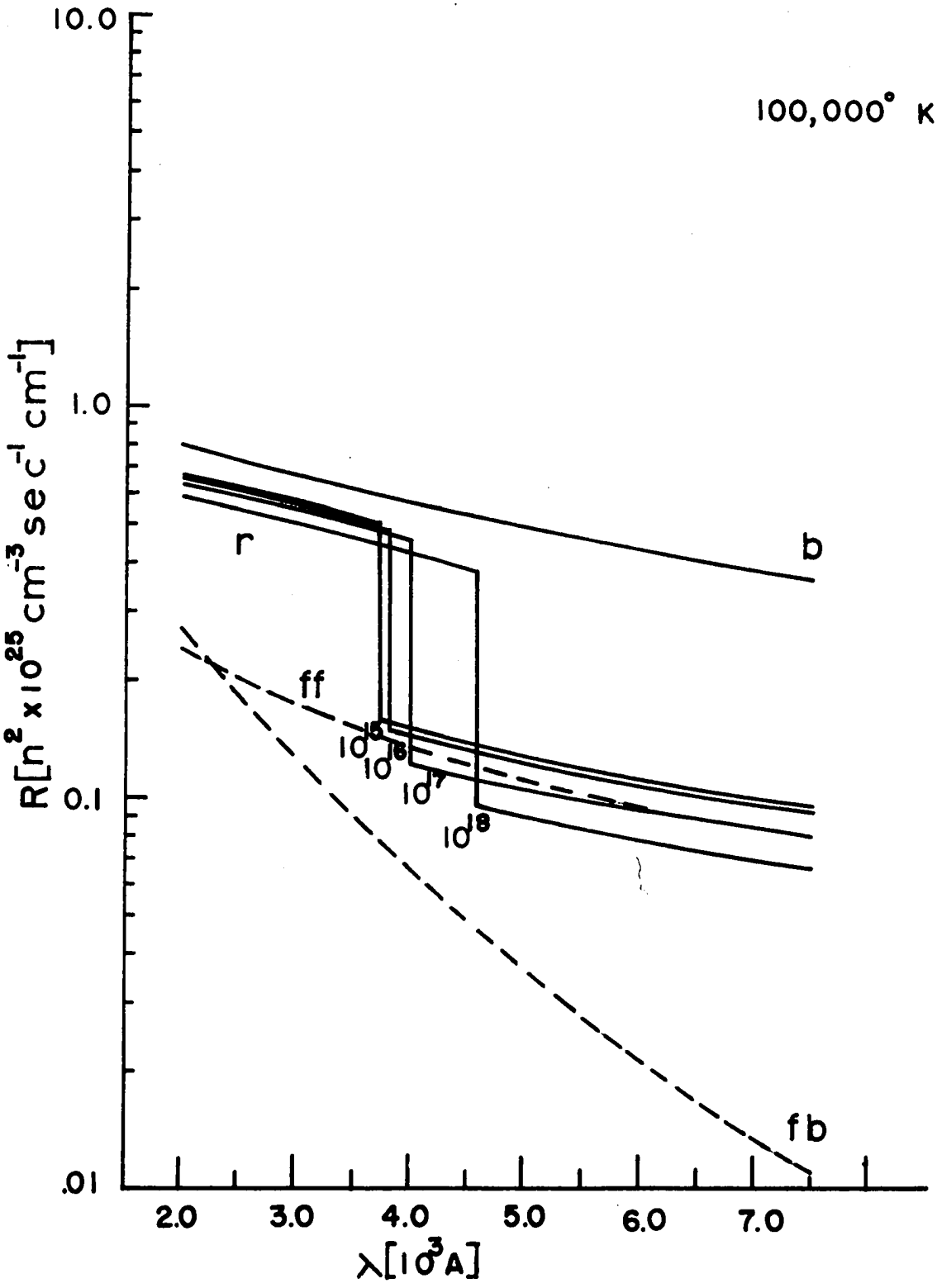

Figure 38. Continuum Spectrum, T = 100,000°K.

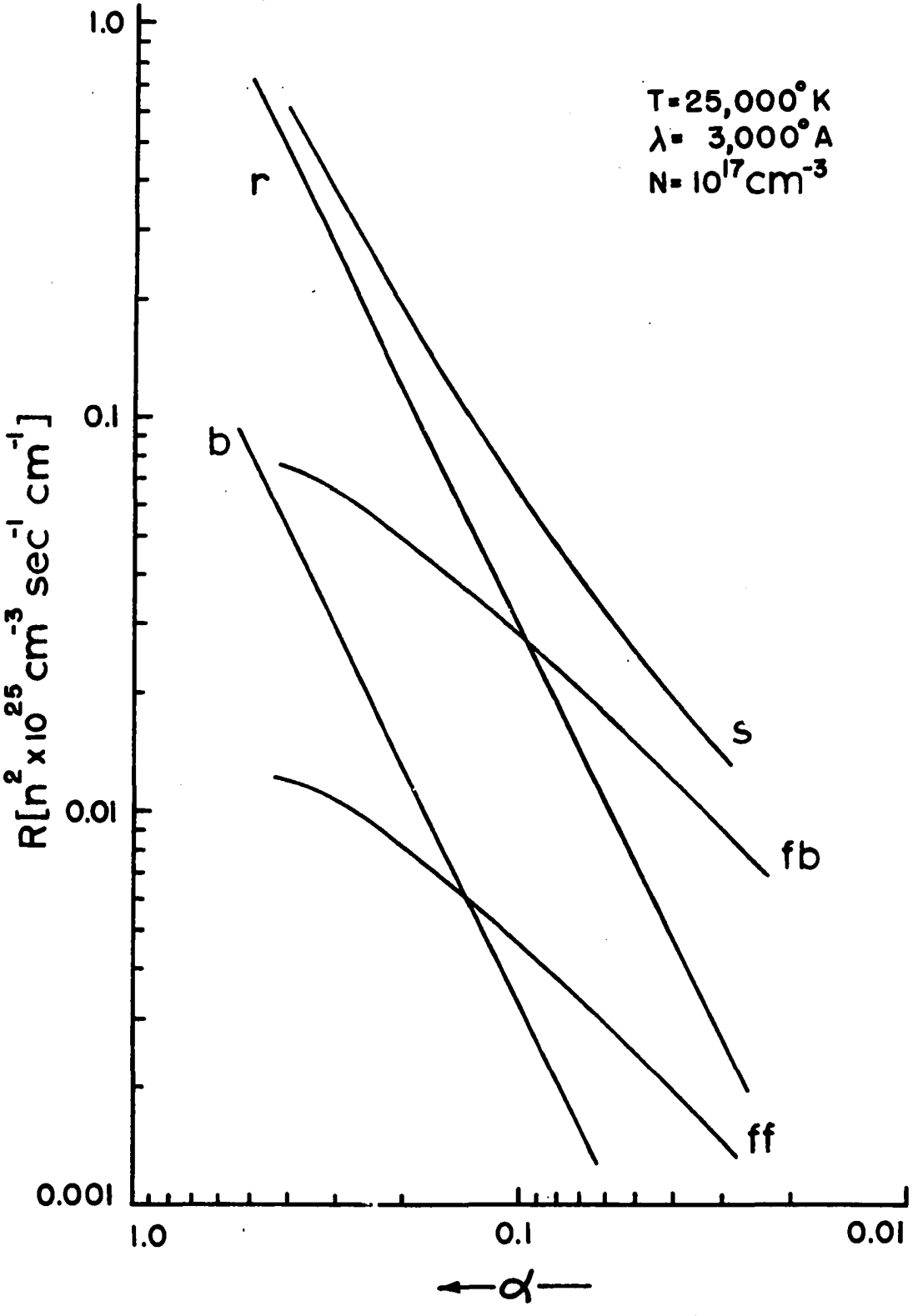

Figure 39. Continuum Emission for λ = 3000 A°, T = 25,000°K.

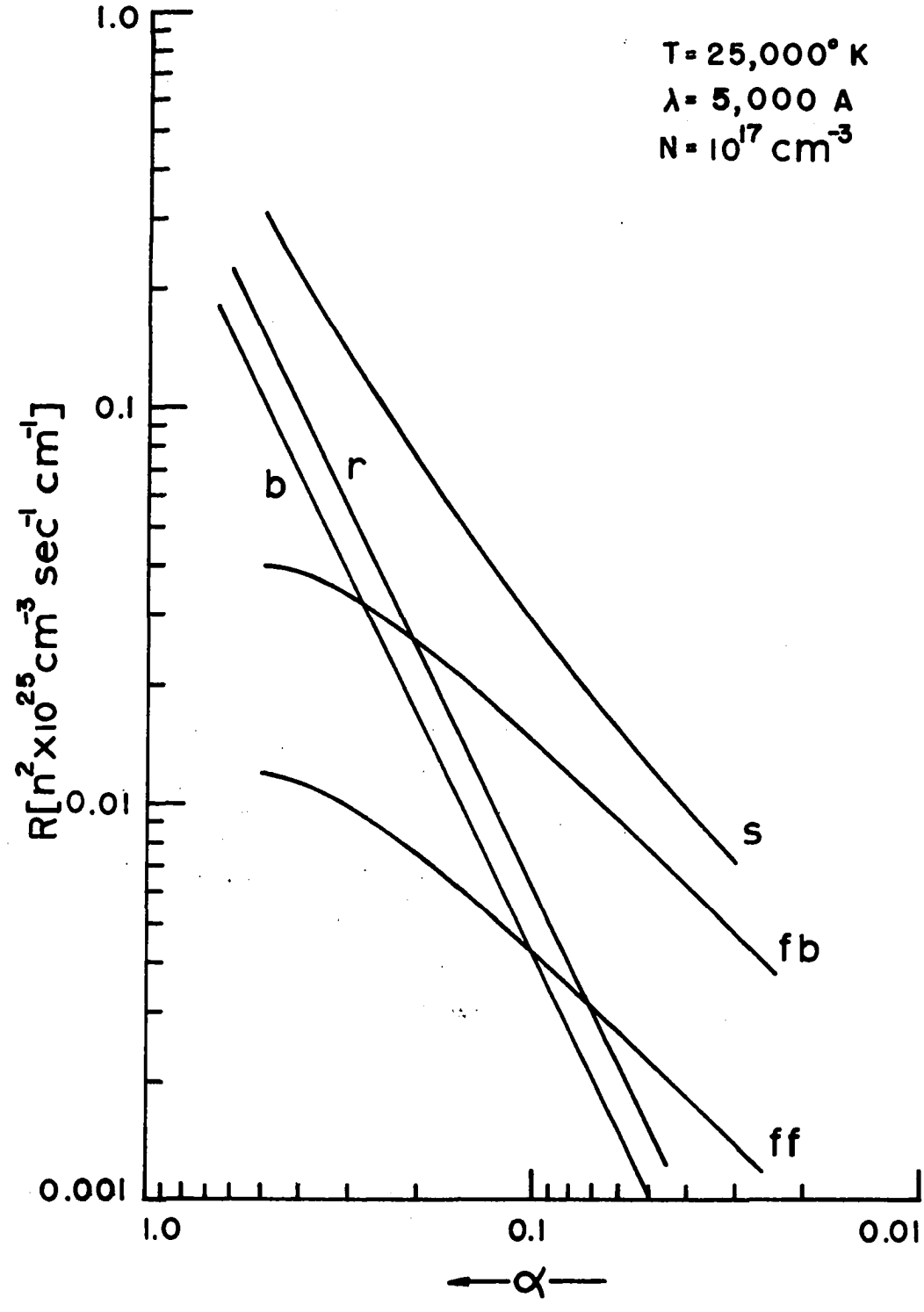

Figure 40. Continuum Emission for λ = 5000 A°, T = 25,000°K.

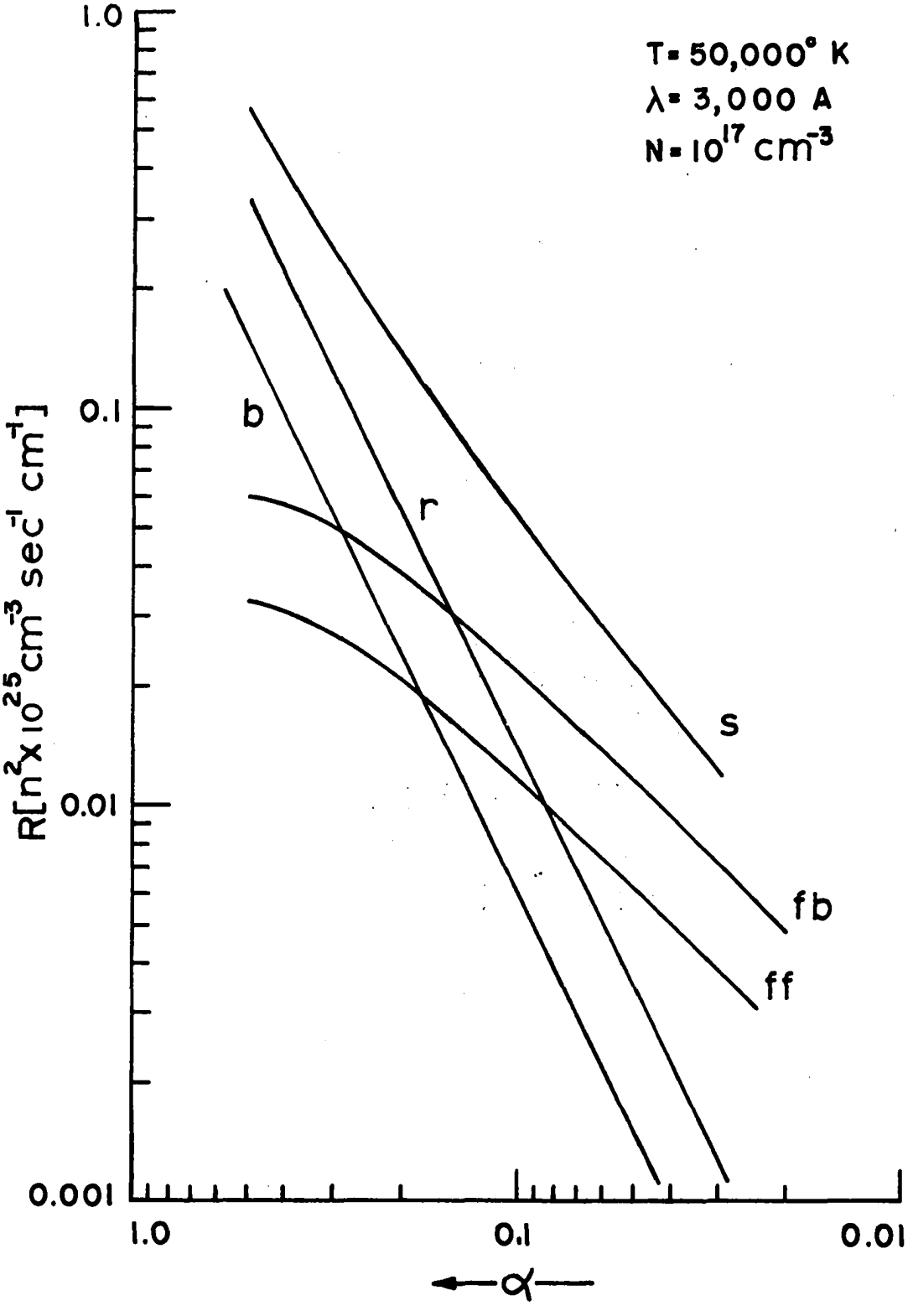

Figure 41. Continuum Emission for λ = 3000 A°, T = 50,000°K.

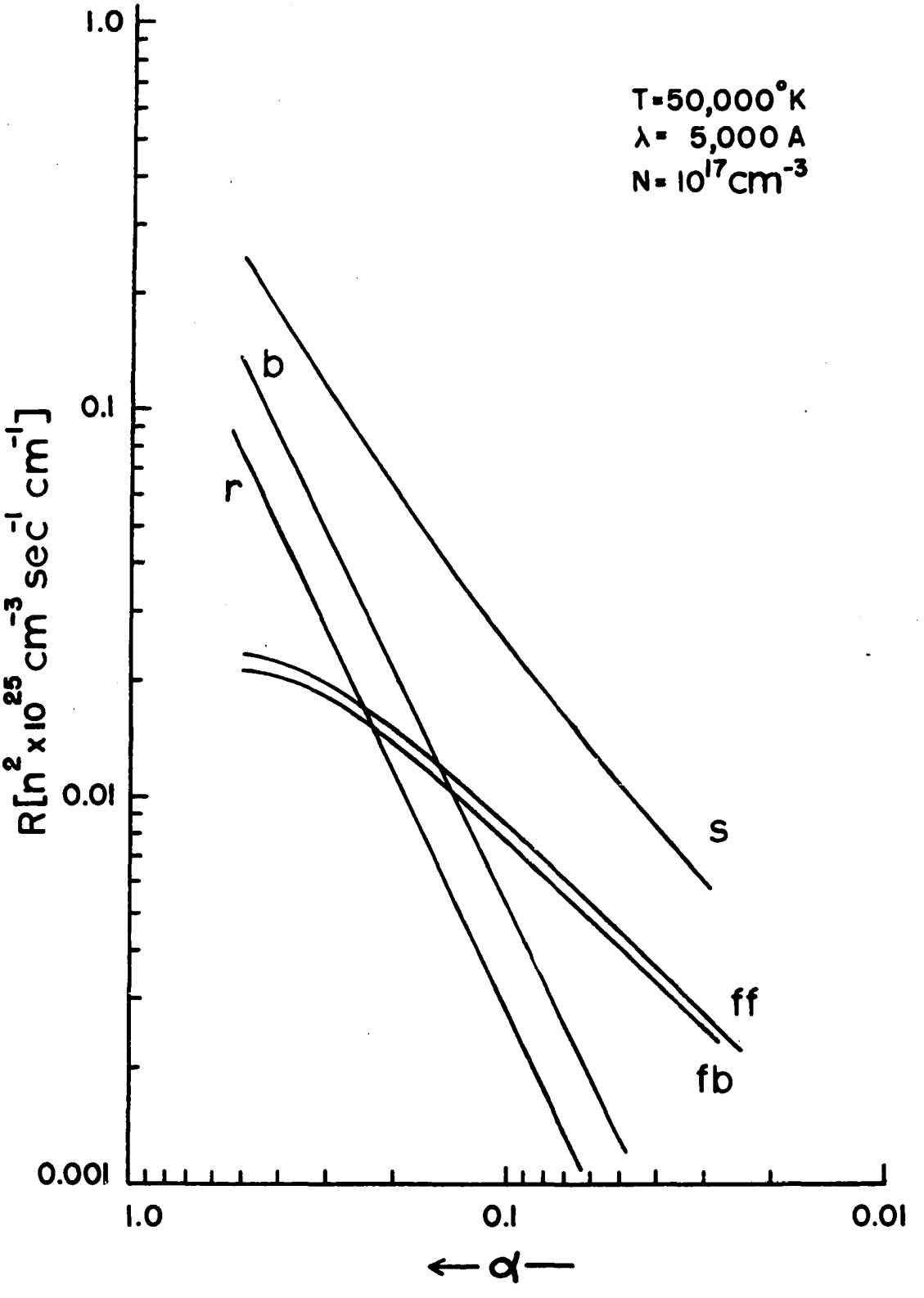

Figure 42. Continuum Emission for λ = 5000 A°, T = 50,000°K.

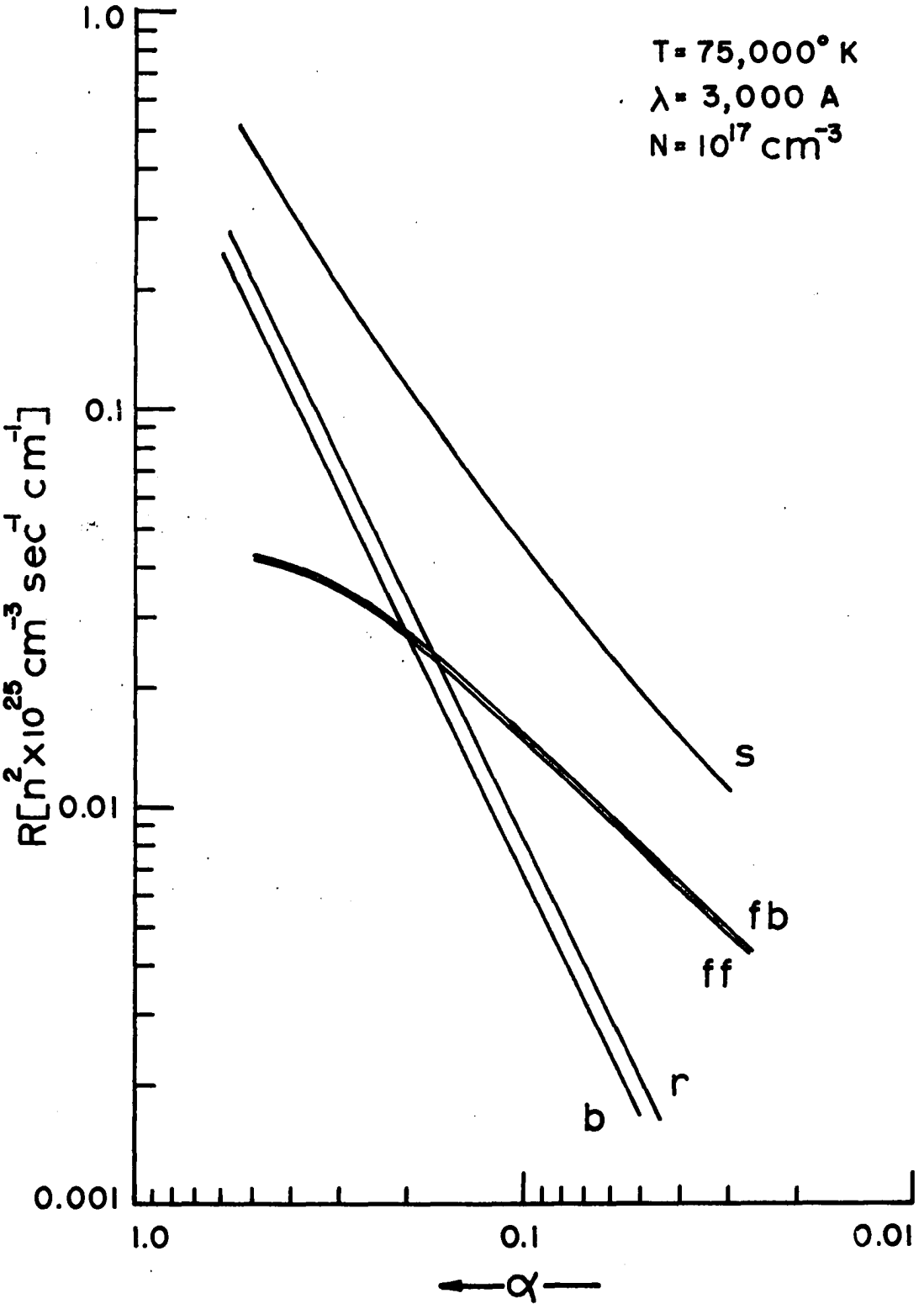

Figure 43. Continuum Emission for λ = 3000 A°, T = 75,000°K.

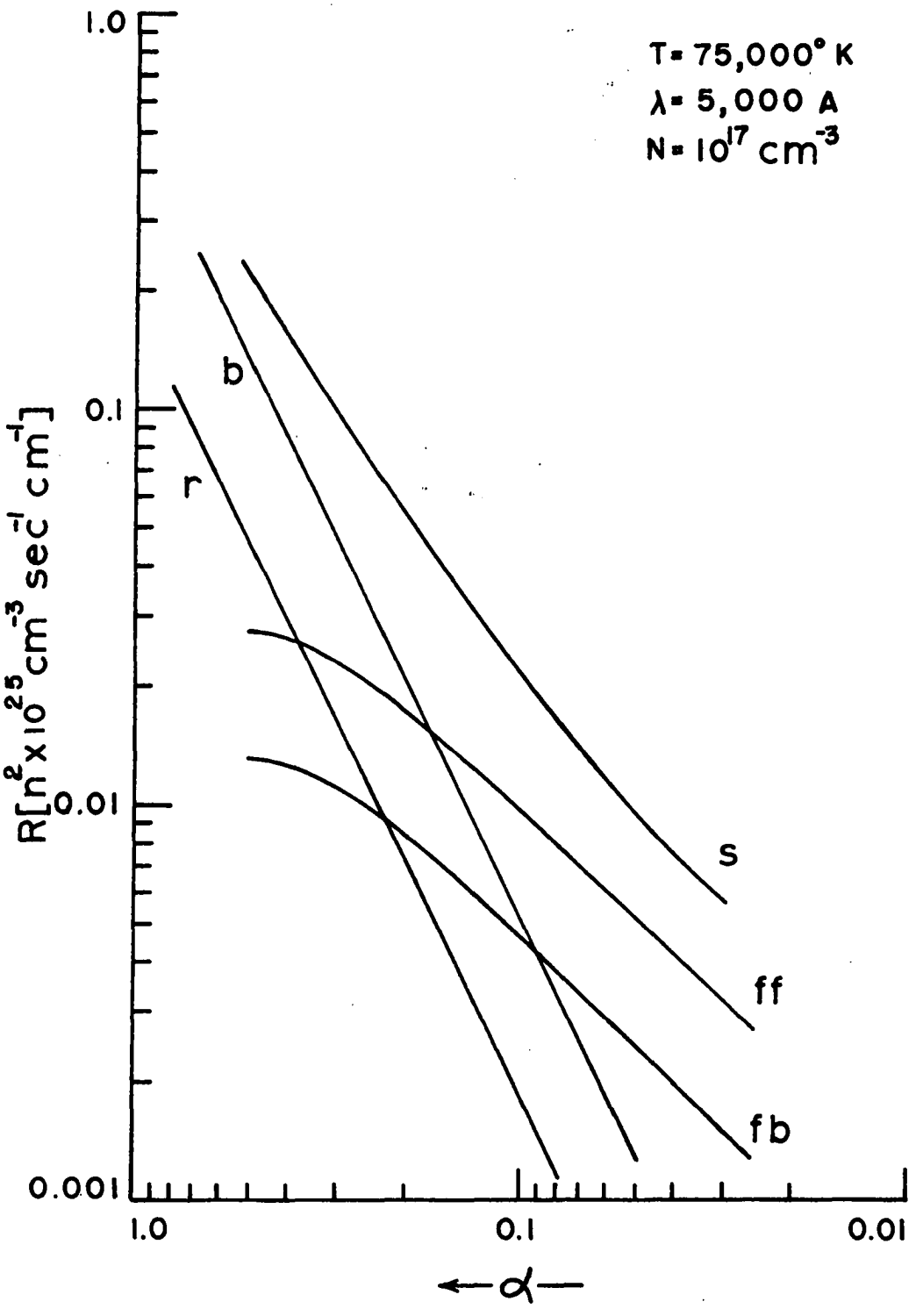

Figure 44. Continuum Emission for λ = 5000 A°, T = 75,000°K.

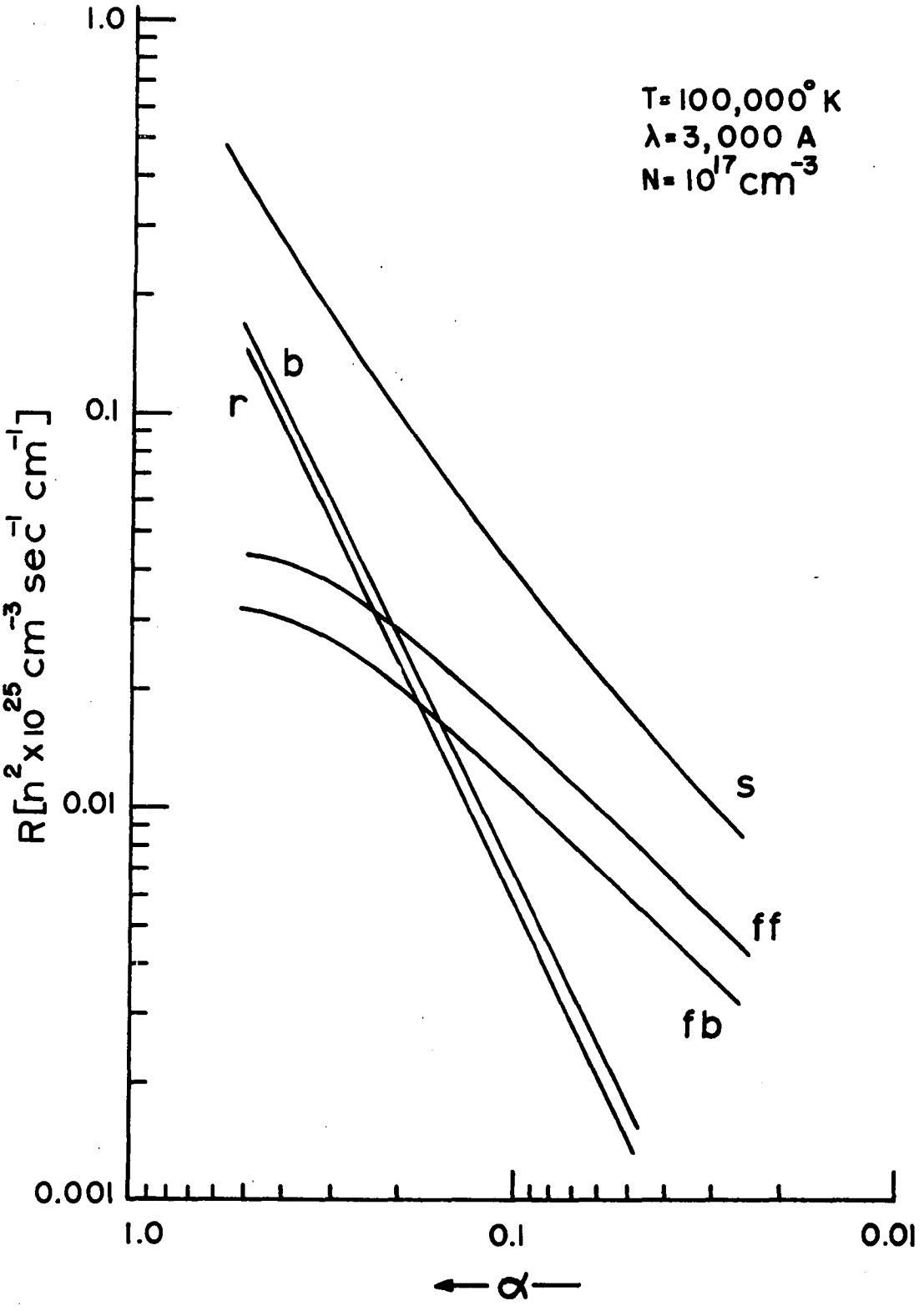

Figure 45. Continuum Emission for λ = 3000 A°, T = 100,000°K.

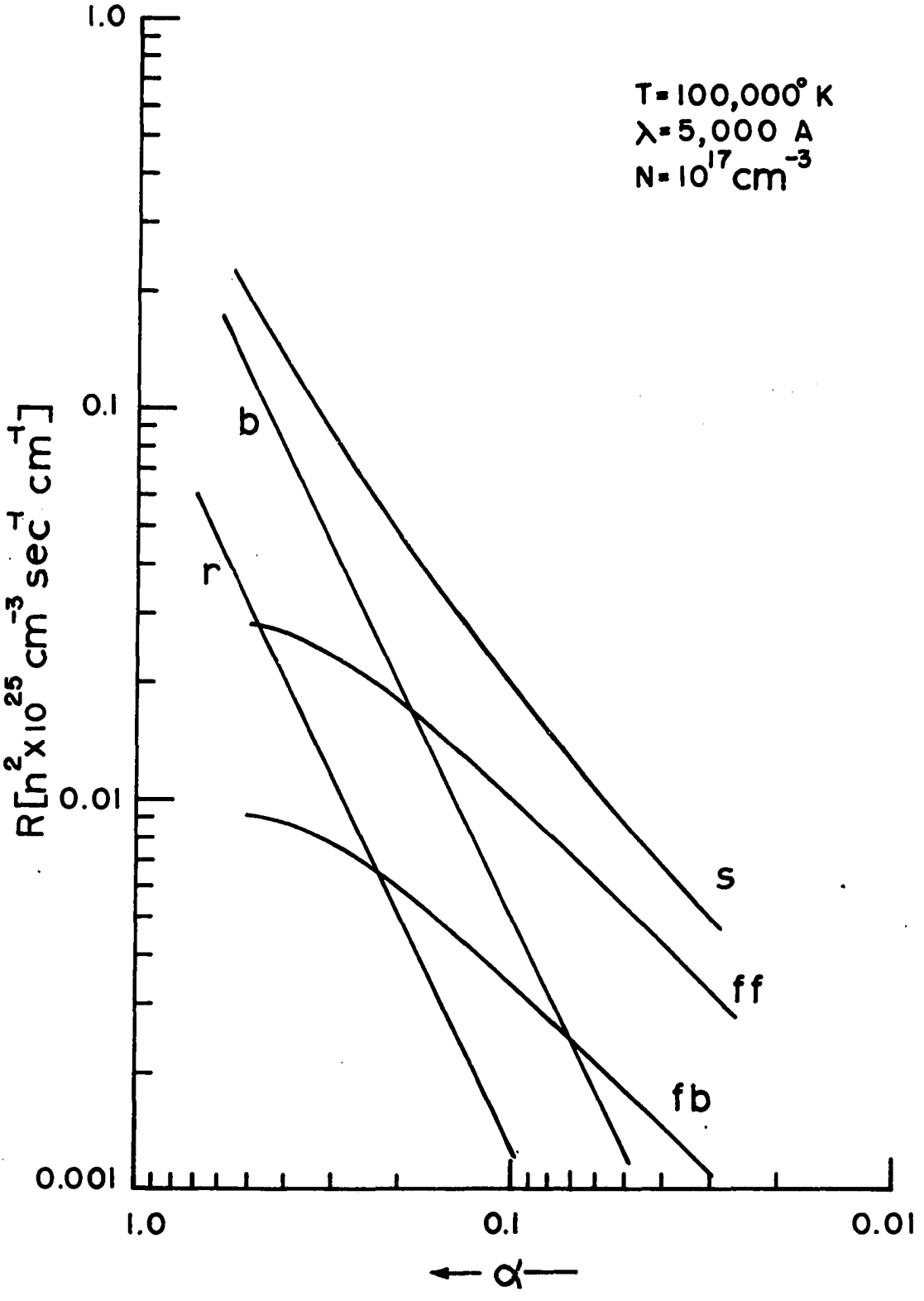

Figure 46. Continuum Emission for λ = 5000 A°, T = 100,000°K.

CHAPTER XI

TRANSITIONS BETWEEN FINE-STRUCTURE LEVELS IN MERCURY RESULTING FROM ELECTRON IMPACT

The careful analysis of gas discharge, or electron beam experiments requires accurate knowledge of transition probabilities between different levels, as well as population densities of these levels. Because of the great number of simultaneously occurring processes, determination of these quantities is extremely difficult. In cases where free electrons are present, these electrons may collide with atoms causing excitation (collision of the first kind), or they may collide with atoms in excited states causing de-excitation (collision of the second kind), neither process involving the absorption or emission of radiation. Cross sections for these processes are necessary for a complete description of the experiments.[79,80]

In mercury, the ground state is 6^1S_0 corresponding to the configuration $5d^{10}6s^2$. In the triplet system, as a result of the spin-orbit interaction, the first excited configuration $5d^{10}6s(^3S)6p$ produces three states 6^3P_0, 6^3P_1, and 6^3P_2, corresponding to J = 0, 1, 2, respectively; these are identified in Figure 47. As a result of the strong spin-

orbit interaction, there is some mixing between the states

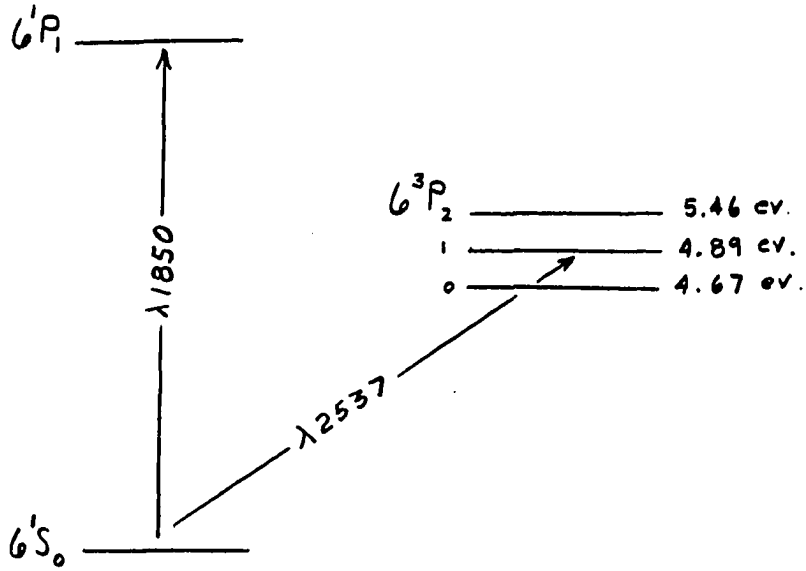

Figure 47. Energy Levels of Mercury

6^3P_1 and 6^1P_1 (i.e., S is not a completely good quantum number).[81] Consequently, the transition $6^3P_1 \rightarrow 6^1S_0$ is optically allowed, and produces the familiar 2537 A° resonance line of mercury. The levels 6^3P_0 and 6^3P_2, which are also populated by electron impact, are metastable, and do not contribute directly to the radiation field. However, collision-induced transitions between these states and 6^3P_1 can alter the population densities and in such a way influence the radiation. We wish to calculate approximate cross sections for such transitions.

Wave Functions for the $6^3P_{0,1,2}$ States of Mercury

Because of the extreme complexity of this atom, it is

approximated here by a helium-like, two-electron system. The antisymmetric basis functions for sharp spin, and orbital angular momentum (S = L = 1) are well known to be given by

$$\psi_{1m1m_s} = \frac{1}{\sqrt{2}} \left[\psi_{6pm}(1)\psi_{6s}(2) - \psi_{6pm}(2)\psi_{6s}(1) \right] \varphi_{1m_s}(1,2), \tag{11.1}$$

where

$$\begin{aligned} \psi_{6s}(1) &= R_{6s}(r_1)\, Y_{oo}(\hat{r}_1) , \\ \psi_{6pm}(1) &= R_{6p}(r_1)\, Y_{1m}(\hat{r}_1) , \end{aligned} \tag{11.2}$$

and where $\varphi_{1m_s}(1,2)$ is a member (corresponding to S = 1) of an orthonormal set of basis functions in a two-particle spin space. The radial functions in Eq. (11.2) will be discussed below.

Since the total angular momentum $\vec{J} = \vec{L} + \vec{S}$ is a constant of motion, wave functions accurately representing the system may be chosen to be eigenfunctions of the operators J^2 and J_z. Such functions are easily obtained by means of the Clebsch-Gordan coupling scheme, namely[82]

$$\Psi_{LSJM} = \sum_{mm_s} C^{LSJ}_{mm_sM}\, \psi_{LmSm_s} . \tag{11.3}$$

These functions are tabulated in Table XXIX in terms of ψ_{LmSm_s} (written as ψ_{mm_s}) for the special case L = S = 1. It should be mentioned that no singlet-triplet mixing is shown for the J = 1 state. Penney[83] has considered this and found the

TABLE XXIX

EIGENFUNCTIONS Ψ_{LSJM} IN TERMS OF $LmSm_s$ BASIS FUNCTIONS (WRITTEN AS ψ_{mm_s}) FOR L = S = 1

J = 2

$$\Psi_{1122} = \psi_{11}$$

$$\Psi_{1121} = \frac{1}{\sqrt{2}} (\psi_{10} + \psi_{01})$$

$$\Psi_{1120} = \frac{1}{\sqrt{6}} (\psi_{1-1} + 2\psi_{00} + \psi_{-11})$$

$$\Psi_{112-1} = \frac{1}{\sqrt{2}} (\psi_{0-1} + \psi_{-10})$$

$$\Psi_{112-2} = \psi_{-1-1}$$

J = 1

$$\Psi_{1111} = \frac{1}{\sqrt{2}} (\psi_{10} - \psi_{01})$$

$$\Psi_{1110} = \frac{1}{\sqrt{2}} (\psi_{1-1} - \psi_{-11})$$

$$\Psi_{111-1} = \frac{1}{\sqrt{2}} (\psi_{0-1} - \psi_{-10})$$

J = 0

$$\Psi_{1100} = \frac{1}{\sqrt{3}} (-\psi_{00} + \psi_{1-1} + \psi_{-11})$$

mixing to be small. In any case, if exchange is ignored in the scattering problem, then this singlet part will make no contribution to the cross section, and its effect will merely be to change the normalization of the bound-state function slightly.

Radial Functions

The radial functions R_{6s} and R_{6p} from Eq. (11.2) may be expected to be rather complicated nodal functions. Hartree,[84] by means of a self-consistent-field analysis, obtained a numerical result for the ground state function. Improved ground-state functions have been found, incorporating the relativistic correction,[85] and calculations have been carried out for several excited states of mercury, in particular the states: 6p, 6d, 7s, 7p, and 7d.[86]

In this preliminary investigation, we assume that the functions R_{6s} and R_{6p} do not differ much in the region of space important to the scattering problem. Also, we know from the discussions in Chapters I and III, that partial waves corresponding to large values of ℓ are sensitive only to the asymptotic form of the off-diagonal matrix elements. For $^3P_J \rightarrow {}^3P_{J'}$ transitions, it will be shown that these matrix elements behave asymptotically as

$$U(^3P_J, {}^3P_{J'}) \sim \frac{1}{r^3} \langle 6p | r^2 | 6p \rangle \ . \qquad (11.4)$$

Thus for large ℓ, one would expect good results if an

approximate function could be found for R_{6p} which would give accurate values for $\langle 6p|r^2|6p\rangle$. However, it is anticipated that for a problem involving matrix elements which behave as shown in Eq. (11.4), the dominant partial wave will probably correspond to smaller values of ℓ, say $\ell = 1$, or 2. Thus, the chosen radial functions should behave properly in a region somewhat closer to the nucleus of the mercury atom.

With this in mind, a rough calculation of $\bar{r}$ was made, using Hartree's SCF function;[84] it was found that

$$\bar{r}_H = \langle R^H_{6s}|r|R^H_{6s}\rangle \simeq 3.44\ a_o\ . \qquad (11.5)$$

As a first trial function then, we consider the Slater nodeless orbital[87]

$$R_n = \frac{1}{\sqrt{(2n)!}}\left(\frac{2Z}{n}\right)^{n+\frac{1}{2}} r^{n-1}\, e^{\frac{-zr}{n}}\ , \qquad (11.6)$$

where $n \leq$ principal quantum number, the particular value depending on the size of the quantum number, and where the expectation value of r is given by

$$\bar{r}_s = \frac{n(2n+1)}{2Z}\ . \qquad (11.7)$$

In the case of R_{6s} and R_{6p}, a reasonable choice is $n = 4$.[87] Then, equating $\bar{r}_s$ from Eq. (11.7) with $\bar{r}_H$ from Eq. (11.5), we obtain

$$\frac{18}{Z} = 3.44 ,$$

and

$$Z = 5.233 , \tag{11.8}$$

The corresponding normalized radial function is given as

$$R_{6s} = R_{6p} = (.378)\ r^3\ e^{-1.308r} . \tag{11.9}$$

This function is compared with that determined by Hartree in Figure 48. (The solid curve is the Hartree function and the dashed curve, the approximate function given in Eq. 11.9.) Agreement is seen to be satisfactory in the region surrounding $\overline{r}$.

Electron-Collision Problem

We now consider the problem of a free electron incident upon this two-electron system. The hamiltonian is given (in Hartree a.u.) by

$$H = -\frac{1}{2}\left(\nabla_1^2 + \nabla_2^2 + \nabla^2\right) - 2\left(\frac{1}{r_1} + \frac{1}{r_2}\right) + V(\vec{r}_1, \vec{r}_2, \vec{r}) ,$$

where

$$V(\vec{r}_1, \vec{r}_2, \vec{r}) = -\frac{2}{r} + \frac{1}{|\vec{r} - \vec{r}_1|} + \frac{1}{|\vec{r} - \vec{r}_2|} . \tag{11.10}$$

In the approximation where exchange is ignored, the total wavefunction describing a continuum state of the three-electron system, where the atom was initially assumed to be in the state $6^3P_{J'M'}$, is assumed to have the form[1]

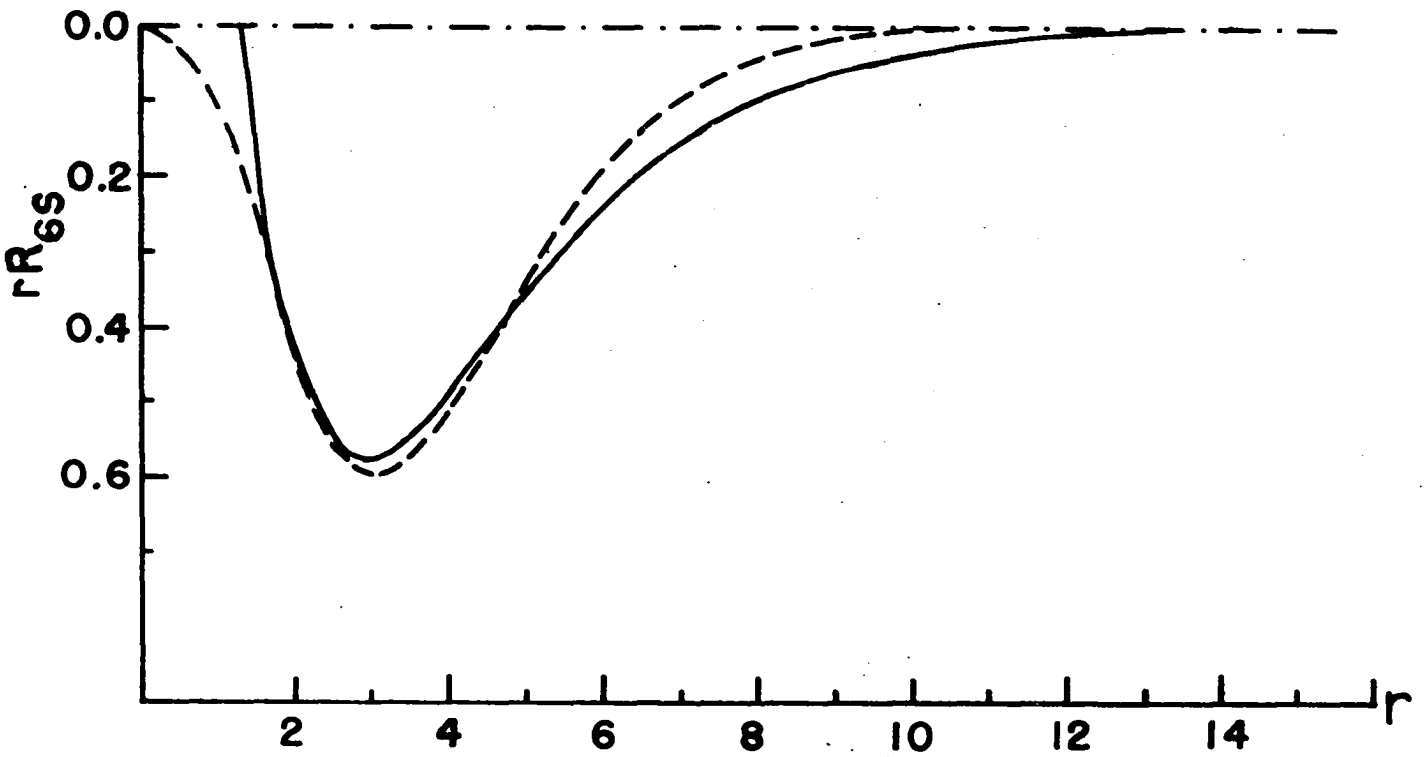

Figure 48. Comparison of r R_{6s} Calculated by Hartree's Function (solid curve) and a Nodeless Orbital (dashed curve).

$$\Psi(J'M'|\vec{r},\vec{r}_1,\vec{r}_2) = \sum_{J,M} F_{JM}\ (J'M'|\vec{r})\ \Psi_{11JM}(\vec{r}_1,\vec{r}_2)\ . \qquad (11.11)$$

In Eq. (11.11), angular momentum coupling between the atom and the incident electron has been neglected. Schrödinger's equation becomes (in Slater a.u.)

$$[\nabla^2 + k_J^2 - U(JM,JM)]\ F_{JM}(\vec{r}) = \sum_{J'M'}{}' U(JM,J'M')\ F_{J'M'}(\vec{r})\ , \qquad (11.12)$$

where

$$U(JM,J'M') = 2 \iint \Psi^*_{11JM}(\vec{r}_1,\vec{r}_2)\ V(\vec{r}_1,\vec{r}_2,\vec{r})\ \Psi_{11J'M'}(\vec{r}_1,\vec{r}_2)$$
$$\times\ d\vec{r}_1\ d\vec{r}_2\ d\sigma_{12}\ ,$$

$$= -\frac{4}{r}\,\delta(JM,J'M') + 4 \iint \Psi^*_{11JM}(\vec{r}_1,\vec{r}_2)\ \frac{1}{|\vec{r} - \vec{r}_1|}\ \Psi_{11J'M'}(\vec{r}_1,\vec{r}_2)$$
$$\times\ d\vec{r}_1\ d\vec{r}_2\ d\sigma_{12}\ , \qquad (11.13)$$

where $d\sigma_{12}$ represents the volume element in spin space.

Evaluation of the matrix elements from Eq. (11.13), using the functions given in Table XXIX, is straight-forward, and one finds

$$U(JM,J'M') = 2[y_o(6s^2|r) + y_o(6p^2|r) - \frac{2}{r}\ ]\ \delta(JM,J'M')$$
$$+ U_{JM,J'M'}\ , \qquad (11.14)$$

where

$$y_o(6s^2|r) = \int_o^\infty R_{6s}^2 (r_1) \frac{r_1^2\, dr_1}{r_>} ,$$

$$y_o(6p^2|r) = \int_o^\infty R_{6p}^2 (r_1) \frac{r_1^2\, dr_1}{r_>} , \qquad (11.15)$$

and where the matrix $U_{JM,J'M'}$ is given in Table XXX. The entries in this table must all be multiplied by the common factor

$$\frac{2\sqrt{\pi}}{5\sqrt{5}} y_2 (6p^2|r) , \qquad (11.16)$$

where

$$y_2(6p^2|r) = \int_o^\infty R_{6p}^2(r_1) \frac{r_<^2\, r_1^2\, dr_1}{r_>^3} . \qquad (11.17)$$

One has the asymptotic relation

$$y_2(6p^2|r) \sim \frac{1}{r^3} \int_o^\infty R_{6p}^2(r_1)\, r_1^4\, dr_1 . \qquad (11.18)$$

Two-Channel Approximation

The angular dependence of the functions U(JM,J'M') makes solution of the coupled partial differential equations given in Eq. (11.12) extremely difficult. In view of the nature of the approximations already introduced, it is reasonable to seek only an approximate solution. Recalling that in time-dependent perturbation theory, transition probabilities

TABLE XXX

THE MATRIX $U_{JM,J'M'}$

All entries should be multiplied by $(2\sqrt{\pi}/5\sqrt{5})\ y_2\ (6p^2|r)$.

		J' = 0	J' = 1		
		M' = 0	M' = 1	M' = 0	M' = -1
J = 0	M = 0	0	0	0	0
	M = 1	0	Y_{20}	$\sqrt{3}\ Y_{2-1}$	$\sqrt{6}\ Y_{2-2}$
J = 1	M = 0	0	$-\sqrt{3}\ Y_{21}$	$-2\ Y_{20}$	$-\sqrt{3}\ Y_{2-1}$
	M = -1	0	$\sqrt{6}\ Y_{22}$	$\sqrt{3}\ Y_{21}$	Y_{20}

J' = 2

	M' = 2	M' = 1	M' = 0	M' = -1	M' = -2
J = 0, M = 0	$-2\sqrt{2}\ Y_{22}$	$-2\sqrt{2}\ Y_{21}$	$-2\sqrt{2}\ Y_{20}$	$-2\sqrt{2}\ Y_{2-1}$	$-2\sqrt{2}\ Y_{2-2}$
M = 1	$-\sqrt{6}\ Y_{21}$	$-3\ Y_{20}$	$-3\ Y_{2-1}$	$-\sqrt{6}\ Y_{2-2}$	0
(J = 1) M = 0	$2\sqrt{3}\ Y_{22}$	$\sqrt{3}\ Y_{21}$	0	$-\sqrt{3}\ Y_{2-1}$	$-2\sqrt{3}\ Y_{2-2}$
M = -1	0	$\sqrt{6}\ Y_{22}$	$3\ Y_{21}$	$3\ Y_{20}$	$\sqrt{6}\ Y_{2-1}$

TABLE XXX (continued)

		J' = 2				
		M' = 2	M' = 1	M' = 0	M' = -1	M' = -2
J = 2	M = 2	$-2\ Y_{20}$	$-\sqrt{6}\ Y_{2-1}$	$-2\ Y_{2-2}$	0	0
	M = 1	$\sqrt{6}\ Y_{21}$	Y_{20}	$-Y_{2-1}$	$-\sqrt{6}\ Y_{2-2}$	0
	M = 0	$-2\ Y_{22}$	Y_{21}	$2Y_{20}$	Y_{2-1}	$-2\ Y_{2-2}$
	M = -1	0	$-\sqrt{6}\ Y_{22}$	$-Y_{21}$	Y_{20}	$\sqrt{6}\ Y_{2-1}$
	M = -2	0	0	$-2Y_{22}$	$-\sqrt{6}\ Y_{21}$	$-2\ Y_{20}$

are proportional to the absolute squares of the perturbation matrix elements,[63] we consider the angularly independent functions given (for $J \neq J'$) by

$$U(J,J') = \left\{ \frac{1}{2J'+1} \sum_{M,M'} |U(JM,J'M')|^2 \right\}^{1/2} . \qquad (11.19)$$

The factor $(2J'+1)^{-1}$, and the sum over M' are introduced to take into consideration the averaging over initial degenerate states, while the sum over M is related to the summing over all final degenerate states. For the transitions $^3P_1 \rightarrow {}^3P_2$ and $^3P_0 \rightarrow {}^3P_2$, we find

$$U(2,1) = U_{21} = \frac{\sqrt{6}}{5} y_2(6p^2|r) , \qquad (11.20)$$

and

$$U(2,0) = U_{20} = \frac{2\sqrt{2}}{5} y_2(6p^2|r) . \qquad (11.21)$$

The diagonal matrix elements in cases of close coupling usually have a rather slight effect on the partial cross sections, at least for large values of ℓ. For instance, in a case where exact resonance is valid, the partial cross sections for a two-channel problem are proportional to $\sin^2(\eta_\ell - \delta_\ell)$ as shown in Eq. (1-23). The phase shifts η_ℓ and δ_ℓ are determined from the functions $F_0 + F_n$ and $F_0 - F_n$, respectively. These functions satisfy differential equations differing only in the sign of the off-diagonal element (see Eq. 1.20). We now make the approximation of averaging the

diagonal elements over θ,φ, thus retaining only the spherically symmetric part common to all J,M, namely

$$U(JM,JM) = 2y_o(6s^2|r) + 2y_o(6p^2|r) - \frac{4}{r} . \quad (11.22)$$

The functions $y_o(6s^2|r)$ and $y_o(6p^2|r)$ are found to contain pure 1/r terms, causing U(JM,JM) to behave exponentially.

Incorporating the matrix elements given in Eqs. (11.20), (11.21), and (11.22), we are able to reduce the problem to one of two channels. The corresponding differential equations are given for the transition $6^3P_1 \rightarrow 6^3P_2$ by

$$\begin{aligned} (v^2 + k_1^2 - U_{11})F_1(\vec{r}) &= U_{12}F_2(\vec{r}) \\ (v^2 + k_2^2 - U_{22})F_2(\vec{r}) &= U_{21}F_1(\vec{r}) , \end{aligned} \quad (11.23)$$

where, according to Eqs. (11.19) and (11.22), $U_{11} = U_{22}$ and $U_{12} = U_{21}$. Considering the closeness of the levels (see Figure 47), we make the additional assumption that $k_1 = k_2$. With these simplifications, one may easily decouple Eqs. (11.23), obtaining

$$(v^2 + k_1^2 - U_{11} \mp U_{12})F^{\pm}(\vec{r}) = 0 , \quad (11.24)$$

where

$$F^{\pm}(\vec{r}) = F_1(\vec{r}) \pm F_2(\vec{r}) . \quad (11.25)$$

Because of the spherical symmetry of the matrix elements, $F^{\pm}(\vec{r})$ may be expanded in the form

$$F^{\pm}(\vec{r}) = \frac{1}{r} \sum_{l} i^{l} (2l + 1) e^{i\eta_l^{\pm}} P_l(\cos \theta) F_l^{\pm}(r) , \qquad (11.26)$$

and Eqs. (11.24) reduced to

$$\left(\frac{d^2}{dr^2} + k^2 - \frac{l(l + 1)}{r^2} - U_{11} \mp U_{12} \right) F^{\pm}(r) = 0 . \qquad (11.27)$$

Since, according to Eq. (11.18) the matrix elements fall off faster than $1/r^2$ for large r, the phase shifts $\eta_l^{\pm}$ may be determined from the asymptotic relation

$$F_l^{\pm}(r) \sim \left(\frac{\pi r}{2k} \right)^{\frac{1}{2}} \left[\cos \eta_l^{\pm} J_{l+\frac{1}{2}}(kr) + (-1)^{l} \sin \eta_l^{\pm} J_{-l-\frac{1}{2}}(kr) \right] \qquad (11.28)$$

$$\sim \frac{1}{k} \sin (kr - l\pi/2 + \eta_l^{\pm}) . \qquad (11.29)$$

The expression (11.28) is valid when the matrix elements are much smaller than $l(l + 1)/r^2$, while (11.29) holds only for very large values of r (for $l > 0$) such that the matrix elements and $l(l + 1)/r^2$ are negligible compared to k^2. Clearly, for numerical work, (11.28) is the more practical of the two.

Solution of the Differential Equations

Because of the complexity of the matrix elements, it is necessary to apply numerical methods in order to obtain

solutions of Eq's. (11.27). A technique devised specifically for second-order, linear equations is that of Numerov.[88]

In the Numerov method, it is first necessary to obtain solutions of the equations at two points, say $F_\ell^\pm(r_o)$ and $F_\ell^\pm(r_1)$. Application of the method of Frobenius to Eq's. (11.27) shows that for small r,

$$F_\ell^\pm(r) = A^\pm \, r^{\ell+1} \, , \tag{11.30}$$

where $A^\pm$ is an arbitrary constant (may be chosen equal to unity); this equation holds so long as the matrix elements increase no faster than $1/r^2$. Once solutions at two points are found, the general solution may be built up by means of the relation

$$F_\ell^\pm(r_{j+1}) = \left[1 - \frac{1}{12}(\delta r)^2 f_{j+1}^\pm \right]^{-1} \left\{ \left[2 + \frac{5}{6}(\delta r)^2 f_j^\pm \right] F_\ell^\pm(r_j) - \left[1 - \frac{1}{12}(\delta r)^2 f_{j-1}^\pm \right] F_\ell^\pm(r_{j-1}) \right\} , \tag{11.31}$$

where

$$f_j^\pm = - \left[k^2 - \frac{\ell(\ell+1)}{r_j^2} - U_{11} \mp U_{12} \right] , \tag{11.32}$$

and where

$$\delta r = r_{j+1} - r_j \, .$$

The phase shifts are then obtained by matching the numerically determined function to the bessel function

combination in Eq. (11.28) for two values of r, say r_a and r_b, large enough so that Eq. (11.28) is valid. Then defining the ratios

$$K^{\pm} = F_{\ell}^{\pm}(r_a)/F_{\ell}^{\pm}(r_b) , \qquad (r_a > r_b) \qquad (11.33)$$

we obtain

$$\tan \eta_{\ell}^{\pm} = (-1)^{\ell+1} \left\{ \frac{K^{\pm} P_{\ell+\frac{1}{2}}(kr_b) - P_{\ell+\frac{1}{2}}(kr_a)}{K^{\pm} P_{-\ell-\frac{1}{2}}(kr_b) - P_{-\ell-\frac{1}{2}}(kr_a)} \right\} , \qquad (11.34)$$

where

$$P_{\ell+\frac{1}{2}}(kr) = \left(\frac{\pi kr}{2} \right)^{\frac{1}{2}} J_{\ell+\frac{1}{2}}(kr) . \qquad (11.35)$$

The partial cross section is then given (in units of πa_o^2) by

$$Q_{\ell} = \frac{1}{k^2} (2\ell + 1) \sin^2 (\eta_{\ell}^{+} - \eta_{\ell}^{-}) . \qquad (11.36)$$

Bethe I Approximation

We have found that for large values of ℓ, the weak coupling approximation is justified, and also only asymptotic parts of the matrix elements are significant. Thus, a comparison of the Bethe I, and two-channel approximations gives some indication of the strength of coupling and the importance of accurate matrix elements.

The Bethe I approximation for this type of transition simply reduces to the Born I approximation for a schematic

model possessing the off-diagonal matrix element

$$U' = \frac{BC}{r^3} , \tag{11.37}$$

where according to Eqs. (11.20) and (11.21), B is given by

$$U_{12} = By_2(6p^2|r) , \tag{11.38}$$

and C by

$$y_2(6p^2|r) \sim \frac{C}{r^3} , \tag{11.39}$$

or

$$C = \int_0^\infty R_{6p}^2(r)\, r^4\, dr = 13.218 . \tag{11.40}$$

The Bethe I partial cross section is easily found to be given by

$$Q_\ell^{B'I} = \frac{\pi}{k_o^2} (\pi BC)^2 \, (I_\ell^{B'I})^2 , \tag{11.41}$$

where

$$I_\ell^{B'I} = \int_0^\infty J_{\ell+\frac{1}{2}}(k_o r)\, J_{\ell+\frac{1}{2}}(k_n r)\, \frac{dr}{r^2} , \tag{11.42}$$

with

$$k_n^2 = k_o^2 - \frac{2m}{\hbar^2} (E_n - E_o) .$$

Under the assumption of exact resonance (i.e., $k_o = k_n = k$), one finds[9]

$$I_\ell^{B'I} = \int_o^\infty \left[J_{\ell+\frac{1}{2}}(kr)\right]^2 \frac{dr}{r^2}$$

$$= \frac{k}{\pi} \frac{1}{\ell(\ell+1)} , \quad \ell \neq 0 . \qquad (11.43)$$

Hence, from Eq. (11.40) we have, in units of πa_o^2 ,

$$Q_\ell^{B'I} = (BC)^2 \frac{2\ell+1}{\ell^2(\ell+1)^2} , \qquad \ell \neq 0 . \qquad (11.44)$$

It is interesting to observe that $Q_\ell^{B'I}$ is independent of the kinetic energy of the incident electron. We should, then, expect this to be true of the two-channel cross sections for large values of ℓ.

Exact-Resonance Results

The solution of Eqs. (11.27), and determination of the partial cross sections have been carried out for the $6^3P_1 \rightarrow 6^3P_2$ transition in mercury, where the off-diagonal matrix element was taken to be that given by Eq. (11.20). Because of the long-range character of U_{12}, it was necessary to carry the solution out to rather large values of r before attempting to determine the phase shifts by matching with the bessel function combination in Eq. (11.28). Resulting two-channel and B'I cross sections are given in Table XXXI

TABLE XXXI

PARTIAL CROSS SECTIONS (UNITS OF πa_o^2) FOR THE $6^3P_1 \rightarrow 6^3P_2$ TRANSITION IN MERCURY IN THE TWO-CHANNEL, AND BETHE I EXACT-RESONANCE, APPROXIMATIONS

ℓ \ k^2	.05	.10	.15	.20	.25	.30	B'I
0	16.40	9.51	4.83	2.76	1.76	1.23	
1	27.96	16.06	17.97	14.28	8.33	5.02	31.45
2	5.67	5.64	5.52	5.35	5.13	4.87	5.82
3	1.96	1.98	1.97	11.96	1.93	1.90	2.04
4	0.89	0.91	0.92	0.92	0.92	0.91	0.94

for several energies. As suggested earlier, the two-channel results are seen to approach those of B'I for large values of ℓ, and consequently become rather insensitive to the incident energy of the colliding electron. It is clear that within the accuracy of this preliminary investigation, B'I partial cross sections may be used for $\ell \geq 5$. Total cross sections may then be calculated; these are given in Table XXXII.

TABLE XXXII

TOTAL CROSS SECTIONS (UNITS OF πa_o^2) FOR THE $6^3P_1 \rightarrow 6^3P_2$ TRANSITION IN MERCURY IN THE TWO-CHANNEL, EXACT-RESONANCE, APPROXIMATION

k^2	.05	.10	.15	.20	.25	.30
Q	54.9	36.1	33.2	27.3	20.1	15.9

No direct measurements of these cross sections have yet been made. However, according to Yavorsky, Fahrikant has been able to deduce some results from Hg-discharge experiments.[18,89] These are quoted in Yavorsky's paper along with his Born-Oppenheimer results. (These results are given in terms of the effective cross section, which is gotten by multiplying the ordinary cross section by the atom density n at 1 mm Hg, and 0°C; usually $n = 3.56 \times 10^{16}$ cm^{-3}.) It may be seen that the results in Table XXXII are considerably larger than those quoted by Yavorsky; typical values obtained by Yavorsky are $Q \cong 19.7\ \pi a_o^2$ at $k^2 = 0.1$ and $Q \cong 16.9\ \pi a_o^2$ at $k^2 = 0.15$. However, considering the well-known inconsistencies of the Born-Oppenheimer method, and the lack of information regarding Fahrikant's data, comparison is rather difficult at this point. It should be pointed out, also, that the rather crude averaging procedure applied to the matrix elements, could indeed overestimate the resulting cross section.

APPENDIX I

FREE-FREE TRANSITIONS OF A PARTICLE IN A THREE-DIMENSIONAL POTENTIAL WELL

Calculation of the cross section for a free-free transition accompanied by the emission of radiation, was discussed in Chapter IX. It was shown that the continuum states could be described by functions of the form

$$\varphi(\vec{r}) = \frac{1}{r} \sum_{\ell=0}^{\infty} i^{\ell} (2\ell + 1)\, e^{i\eta_\ell}\, P_\ell \cos\theta\, f_\ell(r) \ ,$$

where

$$f_\ell(r) \sim \frac{1}{k} \sin\,(kr - \ell\pi/2 + \eta_\ell) \ .$$

The cross section, and hence the rate of emission, was found (as shown in Eq. (9.27)) to be proportional to the square of the dipole matrix element $\vec{M}$, and from Eq. (9.43), we have

$$|\vec{M}|^2 = (4\pi)^3\, e^2 \sum_{\ell=0}^{\infty} \ell \left\{ |I(\ell-1,\ell)|^2 + |I(\ell,\ell-1)|^2 \right\} \ ,$$

where

$$I(\ell-1,\ell) = \frac{1}{k_a k_b} \int_0^{\infty} \chi_{\ell-1}(k_b r)\chi_\ell(k_a r) r\, dr = \int_0^{\infty} f^b_{\ell-1}(r) f^a_\ell(r) r\, dr,$$

and where a and b refer to the initial and final states,

respectively; thus

$$h\nu = \frac{\hbar^2}{2m} (k_a^2 - k_b^2) .$$

In calculating the matrix elements for free-free transitions in H^-, an approximation was introduced, in which the asymptotic form, including the phase shift, was taken for the s-wave, and the $\ell = 1$ component of a plane wave was assumed for the p-wave (i.e., assume $\eta_1(k) = 0$); partial waves corresponding to $\ell > 1$ were not considered. It was indicated that for low energies, these approximations are valid. In order to partially examine the validity of the above approximations, we consider the corresponding matrix elements for a problem involving free-free transitions of a system consisting of a particle and three-dimensional potential well. Since this problem may be solved exactly, we are able to compare exact and approximate results.

Consider a particle of kinetic energy k^2 (a.u.), incident upon a potential well of depth k_o^2 (a.u.) and radius a, as shown in Figure a. We require continuum states of

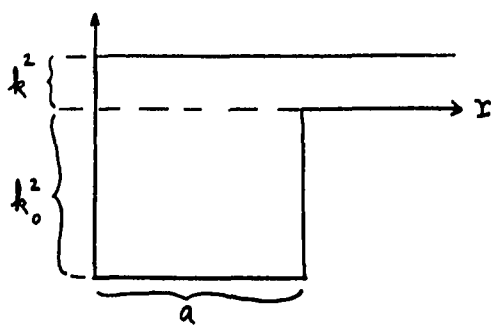

Figure a

the set of equations

$$\left(\frac{d^2}{dr^2} - \frac{\ell(\ell+1)}{r^2} + k'^2 \right) \chi_\ell(kr) = 0 \qquad (r < a) ,$$

$$\left(\frac{d^2}{dr^2} - \frac{\ell(\ell+1)}{r^2} + k^2 \right) \chi_\ell(kr) = 0 \qquad (r > a) ,$$

where

$$k'^2 = k^2 + k_o^2 .$$

Exact solutions for the case $\ell = 0$ are given by[1]

$$\chi_o^E(kr) = \begin{cases} A_o \sin(k'r) & (r < a) \\ \sin(kr + \eta_o) & (r > a) , \end{cases}$$

where the scattering phase shift η_o is given by

$$\eta_o = \tan^{-1}\left(\frac{k}{k'} \tan k'a \right) - ka ,$$

and the coefficient A_o, by

$$A_o = \left[\sin^2 k'a + \left(\frac{k'}{k} \right)^2 \cos^2 k'a \right]^{-1/2} .$$

The solutions for $\ell = 1$ are similarly found to be

$$\chi_1^E(kr) = \begin{cases} A_1 \sqrt{r}\, J_{3/2}(k'r) & (r < a) \\ \left(\frac{\pi kr}{2} \right)^{1/2} \left\{ \cos \eta_1 \, J_{3/2}(kr) - \sin \eta_1 \, J_{-3/2}(kr) \right\} & (r > a), \end{cases}$$

where

$$\eta_1 = \tan^{-1}\left\{ \frac{(3g_1 - 1)(2ka)^3}{24[1 - (ka)^2(g_1 - \frac{1}{2})]} \right\},$$

with

$$g_1 = (k'a \sin k'a)^{-1}\left[\frac{\sin k'a}{k'a} - \cos k'a \right],$$

and where

$$A_1 = \frac{\cos \eta_1 \, j_{3/2}(ka) - \sin \eta_1 \, j_{-3/2}(ka)}{j_{3/2}(k'a)},$$

with

$$j_{3/2}(ka) = \frac{\sin ka}{ka} - \cos ka ,$$

and

$$j_{-3/2}(ka) = \frac{-\cos ka}{ka} - \sin ka .$$

Solutions for $\ell > 1$ can easily be obtained[1], however they will not be necessary in this investigation. The asymptotic approximation for the s-wave solution amounts to assuming for all r, the relation

$$\chi_o^A(kr) = \sin (kr + \eta_o) \qquad (0 \leq r < \infty),$$

while the plane-wave approximation (i.e., Born approximation) for the p-wave is given by

$$\chi_1^B(kr) = \left(\frac{\pi kr}{2} \right)^{1/2} J_{3/2}(kr) \qquad (0 \leq r < \infty).$$

The following integrals may now be defined:

$$(Ea,Eb) = \int_0^\infty \chi_o^E(k_a r)\ \chi_1^E(k_b r)\ r\ dr\ ,$$

$$(Ea,Bb) = \int_0^\infty \chi_o^E(k_a r)\chi_1^B(k_b r)\ \ r\ dr\ ,$$

$$(Aa,Bb) = \int_0^\infty \chi_o^A(k_a r)\chi_1^B(k_b r)\ \ r\ dr\ ,$$

where clearly the first letters refer to the s-wave and the second to the p-wave. In order to examine error in particular regions of space, we append 1 for $0 \leq r < a$, and 2 for $a \leq r < \infty$, for example (Ea,Bb) = (Ea,Bb)1 + (Ea,Bb)2, and similarly for (Ea,Eb) and (Aa,Bb). The cross section, then is proportional to the sum of squares of matrix elements in the form

$$(EE) = (Ea,Eb)^2 + (Eb,Ea)^2\ ,$$

for the exact solution, and

$$(EB) = (Ea,Bb)^2 + (Eb,Ba)^2\ ,$$
$$(AB) = (Aa,Bb)^2 + (Ab,Ba)^2\ ,$$

for the two types of approximations.

The radius a, and the depth k_o^2 of the potential well

may be chosen so that the phase shifts agree, within a few percent, with those obtained by Chandrasekhar and Breen using the static-hartree-field approximation for H^-.[57] Such a choice of parameters gives $a = 1.0\ a_o$, and $k_o^2 = 2.3$ a.u. ($\sim$ 31 eV). In Tables A and B are given calculated values of (EE), (EB), (AB), and their percentage differences (always taken relative to the more exact of the two). The approximation used in Chapter IX corresponds to AB in this model calculation. It is seen from Tables A and B, that for low energies the error is rather small, and even for an electron energy of 12 eV the error is still less than 10%.

If we now recall the significance of the approximations, then it is clear that the agreement of (EE) and (EB) is a measure of the validity of assuming $\eta_1 = 0$ (i.e., plane wave component for p-wave), while the agreement of (EB) and (AB) indicates the validity of using the asymptotic form for the s-wave; the latter is quite obviously the better of the two approximations. This is easily understood, since the asymptotic approximation is in error only in the inner region ($0 \leq r < a$), which contributes little to the integrals, while the plane-wave assumption for $\ell = 1$ has a cumulative effect which is strongly felt in the outer region ($a \leq r < \infty$), which is most important to the integrals. This argument should also apply to H^-, since the potential seen by the electrons is short range and rapidly decaying (exponential in the static-hartree-field approximation).

TABLE A

CALCULATED VALUES OF (EE), (EB), (AB), AND PERCENTAGE DIFFERENCES FOR $a = 1.0\ a_o$ AND $k_o^2 = 2.3$ a.u.

E (eV)	λ (10^3A°)	(EE)	% (EE,EB)	(EB)	% (EB,AB)	(AB)	% (EE,AB)
2.0	10.	1151.	.3	1154.	0	1154.	.3
3.0	6.	325.4	.6	327.3	0	327.4	.6
	8.						
	10.	3167.	.6	3185.	0	3185.	.6
4.0	4.	108.5	1.0	109.6	0	109.6	1.0
	6.	666.8	.9	673.0	0	673.1	.9
	8.	2349.	.9	2370.	0	2370.	.9
	10.	6145.	.9	6202.	0	6202.	.9
5.0	4.	189.8	1.4	192.4	0	192.5	1.4
	6.	1124.	1.4	1140.	0	1140.	1.4
	8.	3883.	1.4	3936.	0	3936.	1.4
	10.	10021.	1.4	10161.	0	10162.	1.4
6.0	4.	291.5	1.9	297.1	0	297.2	1.9
	6.	1691.	1.9	1723.	0	1723.	1.9
	8.	5756.	2.0	5870.	0	5870.	2.0
	10.	14714.	2.0	15012.	0	15013.	2.0
7.0	2.	19.42	2.8	19.97	.1	20.00	2.8
	4.	413.3	2.6	423.9	0	424.1	2.6
	6.	2356.	2.6	2418.	0	2418.	2.6

TABLE B

CALCULATED VALUES OF (EE), (EB), (AB), AND PERCENTAGE DIFFERENCES FOR $a = 1.0\ a_o$ AND $k_o^2 = 2.3$ a.u.

E (eV)	λ (10^3A°)	(EE)	% (EE,EB)	(EB)	% (EB,AB)	(AB)	% (EE,AB)
8.0	2.	27.23	3.6	28.21	.1	28.24	3.7
	4.	553.0	3.4	571.8	0	572.0	3.4
	6.	3107.	3.5	3217.	0	3218.	3.5
10.0	2.	44.67	5.6	47.17	.1	47.24	5.7
	4.	876.6	5.7	926.2	0	926.5	5.7
	6.	4816.	6.0	5103.	0	5104.	6.0
12.0	2.	65.16	8.4	70.66	.1	70.76	8.6
	4.	1240.	9.0	1351.	0	1351.	9.0
	6.	6701.	9.4	7333.	0	7334.	9.4

In order to examine the sensitivity of the results with respect to the radius a and the depth k_o^2, several combinations were investigated for an intermediate energy of 4 eV. In Table C are given percentage differences of (EE), (EB), and (AB) for several choices of a and k_o^2. One concludes that for problems involving potentials of longer range, care should be taken in the treatment of the p-wave. In such cases, one should consider higher partial waves as well.

TABLE C

A COMPARISON OF (EE), (EB), AND (AB) FOR SEVERAL CHOICES OF THE RADIUS a AND DEPTH k_o^2

	λ (10^3 A°)	% (EE,EB)	% (EB,AB)	% (EE,AB)
($a_2 = 1.0$, $k_o^2 = 0.5$)	4.	6.5	.04	6.5
	10.	5.1	.01	5.1
($a_2 = 1.0$, $k_o^2 = 1.0$)	4.	4.3	.04	4.3
	10.	3.5	.01	3.5
($a_2 = 1.0$, $k_o^2 = 1.5$)	4.	3.0	.03	3.0
	10.	2.4	.01	2.4
($a_2 = 1.0$, $k_o^2 = 2.0$)	4.	1.8	.03	1.9
	10.	1.5	.01	1.5
($a_2 = 2.0$, $k_o^2 = 0.5$)	4.	24.	.54	25.
	10.	22.	.09	22.
($a_2 = 2.0$, $k_o^2 = 1.0$)	4.	5.8	.49	5.4
	10.	3.5	.08	3.6
($a_2 = 2.0$, $k_o^2 = 1.5$)	4.	19.	.43	19.
	10.	3.2	.07	3.3

APPENDIX II

IMPORTANT POINTS CONCERNING USE OF THE FIGURES AND TABLES

It is important to emphasize that great care must be taken in interpreting the figures and tables of Chapters VIII - X. In all cases, the free-bound and free-free gaunt factors for hydrogen have been taken as unity; this can give rise to error as high as 15% for the proton-electron bremsstrahlung emission (b). In Figures 20-38, the recombination (r) and proton-electron bremsstrahlung (b) curves must still be multiplied by $n_e n_i$ (or $\alpha^2 n^2$ in the case of a pure hydrogen plasma), while the free-bound H^- (fb) and the free-free H^- (ff) curves must be multiplied by $n_e n_H$ (or $\alpha(1 - \alpha)n^2$ in the case of a pure hydrogen plasma); n_e, n_i, and n represent the electron density, positive hydrogen ion density, and total particle density, all in units of 10^{17} cm^{-3}, and $n_i = \alpha n$.

One further, somewhat ambiguous, point remains. The attachment cross sections for free-bound transitions in H^-, which are given in Table XXI, are consistent with those given by Massey and Burhop,[53] and are used in Chapter IX to calculate the free-bound H^- (fb) rates of emission presented in

Tables XXII - XXIV and in the graphs of Chapter X. However, in checking the predicted free-bound absorption coefficients (temperature dependent) with those given by Griem,[71] one may see that our's are four times too large. The difference appears to stem from definition, and in our formulation arises with the introduction of γ in Eq. (9.2). In order to be consistent, it is necessary to reduce by four all free-bound H^- (fb) rates of emission appearing in the tables and figures. The S curves must be adjusted accordingly.

LIST OF REFERENCES

1. N. F. Mott and H. S. W. Massey, The Theory of Atomic Collisions (Oxford University Press, London, England, 1949), 2nd ed.

2. H. S. W. Massey, Handbuch der Physik, edited by S. Flügge (Springer-Verlag, 1956), Vol. 36, p. 233.

3. M. J. Seaton, "The Theory of Excitation and Ionization by Electron Impact", Atomic and Molecular Processes, edited by D. R. Bates (Academic Press, New York, 1962), p. 374.

4. See Reference 1, p. 146.

5. M. J. Seaton, Proc. Phys. Soc. (London) 77, 174 (1961).

6. D. R. Bates and A. Damgaard, Phil. Trans. Roy. Soc. London A 242, 842 (1949).

7. M. J. Seaton, Proc. Phys. Soc. (London) 68, 457 (1955).

8. See Reference 1, p. 107.

9. G. N. Watson, Theory of Bessel Functions (Cambridge University Press, London, England, 1944), 2nd ed., p. 404.

10. See Reference 1, p. 40.

11. A. Erdélyi, Higher Transcendental Functions, I. (McGraw-Hill, New York, 1953), p. 56.

12. H. S. W. Massey and C. B. O. Mohr, Proc. Roy. Soc. A 132, 605 (1931); Oppenheimer, Z. Physik 43, 27 (1927).

13. E. U. Condon and G. H. Shortley, The Theory of Atomic Spectra (Cambridge University Press, London, England, 1951), p. 175.

14. I. C. Percival and M. J. Seaton, Proc. Cambridge Phil. Soc. 53, 654 (1957).

15. See Reference 1, p. 149.

16. A. Salmona and M. J. Seaton, Proc. Phys. Soc. (London) 77, 617 (1961).

17. W. Christoph, Ann. Physik 23, 51 (1935); I. P. Zapesochnyi and L. L. Shimen, Optics and Spectrosc. 13, 355 (1962).

18. D. R. Bates, A. Fundaminsky, and H. S. W. Massey, Phil. Trans. Roy. Soc. London A 243, 93 (1950); G. Haft, Z. Physik 82, 73 (1933).

19. Uncoupled representation refers to the expansion of the total Wave function as a linear combination of products of the atomic wave functions and the colliding electron functions F. In the coupled representation, on the other hand, the wave function is expanded according to Eq. (3.3).

20. W. P. Allis and P. M. Morse, Z. Physik 70, 567 (1931); P. M. Morse, Rev. Mod. Phys. 4, 577 (1932).

21. R. G. Fowler, Electrically Energized Shock Tubes (University of Oklahoma Research Institute, Norman, Okla., 1963).

22. W. Finkelnberg and Th. Peters, Handbuch der Physik, edited by S. Flügge (Springer-Verlag, 1957), Vol. 28, p. 79.

23. R. Wildt, Astrophys. J. 89, 295 (1939).

24. L. M. Branscomb, "Photodetachment," Atomic and Molecular Processes, edited by D. R. Bates (Academic Press, New York, 1962), p. 100.

25. R. G. Fowler (private communication).

26. H. A. Bethe and E. E. Salpeter, Quantum Mechanics of One- and Two-Electron Atoms (Academic Press, New York, 1957), p. 322.

27. L. Spitzer, Physics of Fully Ionized Gases (Interscience, New York, 1956), p. 90.

28. D. H. Menzel and C. L. Pekeris, Mon. Not. Roy. Astron. Soc., 96, 77 (1935).

29. W. C. Karzas and R. Latter, Astrophys. J. Suppl. #55, 167 (1961).

30. P. J. Brussaard, and H. C. van de Hulst, Rev. Mod. Phys. 34, 307 (1962).

31. D. R. Inglis and E. Teller, Astrophys. J. 90, 439 (1939).

32. H. R. Griem, Phys. Rev. 128, 997 (1962).

33. J. Pomerantz, J. Quant. Spectrosc. Radiat. Transfer 1, 185 (1961).

34. G. Ecker, Z. Physik 148, 593 (1957); G. Ecker and W. Weizel, Ann. Phys. 17, 126 (1956); Z. Naturf. 129, 859 (1957); J. Brunner, Z. Physik 159, (1960).

35. W. Ecker and W. Kröll, Phys. Fluids 6, 62 (1963).

36. A. Unsöld, Z. Astrophys. 24, 355 (1948).

37. H. A. Kramers, Phil. Mag. 46, 836 (1923).

38. J. A. Gaunt, Proc. Roy. Soc. A 126, 654 (1930).

39. A. Sommerfeld, Ann. Physik 11, 257 (1931).

40. A. Sommerfeld and A. Maue, Ann. Physik 23, 589 (1935).

41. A. Sommerfeld, Atombau und Spectrallinien, Vol. II (Friedr. Vieweg und Sohn, Braunschweig, 1939), p. 558.

42. See Reference 26, p. 331.

43. H. A. Bethe, Z. Physik 57, 815 (1929).

44. E. A. Hylleraas, Z. Physik 60, 624 (1930).

45. H. S. W. Massey, Negative Ions (Cambridge University Press, Cambridge, England, 1950).

46. A. Unsöld, Physik Der Sternatmosphären (Springler-Verlag, Berlin), 2nd ed.

47. See Reference 26, p. 316.

48. See Reference 26, p. 154.

49. B. H. Armstrong, Phys. Rev. 131, 1132 (1963).

50. S. Geltman, Astrophys. J. 136, 935 (1962).

51. T. L. John, Mon. Not. Roy. Astron. Soc. 121, 41 (1960).

52. F. A. Milne, Phil. Mag. 47, 209 (1924).

53. H. S. W. Massey and E. H. S. Burhop, Electronic and Ionic Impact Phenomena (Oxford University Press, London, England, 1956), p. 334.

54. S. J. Smith and D. S. Burch, Phys. Rev. 116, 1125 (1959).

55. L. Nedelsky, Phys. Rev. 42, 641 (1932).

56. J. A. Wheeler and R. Wildt, Astrophys. J. 95, 281 (1942).

57. S. Chandrasekhar and F. H. Breen, Astrophys. J. 103, 41 (1946); 104, 430 (1946).

58. T. Ohmura and H. Ohmura, Astrophys. J. 131, 8 (1960); Phys. Rev. 121, 513 (1960).

59. O. B. Firsov and M. I. Chibisov, J. Exptl. Theoret. Phys. (U.S.S.R.) 12, 1235 (1961).

60. R. O. hundley, Rand Report RM-3334-ARPA (The Rand Corp., Santa Monica, Calif.)

61. B. L. Moiseiwitsch, "Elastic Scattering of Electrons", Atomic and Molecular Processes, edited by D. R. Bates (Academic Press, New York, 1962), p. 280.

62. P. G. Burke and K. Smith, Rev. Mod. Phys. 34, 458 (1962).

63. W. Heitler, The Quantum Theory of Radiation (Oxford University Press, London, England), 3rd ed.

64. See Reference 26, p. 324.

65. See Reference 26, p. 243.

66. R. H. Neynaber, L. L. Marino, E. W. Rothe, and S. M. Trujillo, Phys. Rev. 124, 135 (1961).

67. R. T. Brackmann, W. L. Fite, and R. H. Neynaber, Phys. Rev. 112, 1157 (1958).

68. B. H. Bransden, A. Dalgarno, T. L. John, and M. J. Seaton, Proc. Phys. Soc. (London) 71, 877 (1958).

69. A. Erdélyi, Tables of Integral Transorms, I. (McGraw-Hill, New York, 1954), p. 138.

70. W. Lochte-Holtgreven, "Production and Measurement of High Temperatures", Reports on Progress in Physics XXI, (The Physical Society, London, 1958), p. 312.

71. H. R. Griem, "Plasma Spectroscopy", Proceedings of the Fifth International Conference on Ionization Phenomena in Gases II (North-Holland, Amsterdam, 1962), p. 1857.

72. R. Wilson, J. Quant. Spectrosc. Radiat. Transfer 2, 477 (1962).

73. J. D. Cobine, Gaseous Conductors (Dover Publications, Inc., New York, 1958), p. 92.

74. W. Lochte-Holtgreven and W. Nissen, Z Physik 133, 126 (1952).

75. E. Vitense, Himmelswelt 56, 33 (1949); See Also Reference 22.

76. O. Weber, Z. Physik 152, 281 (1958).

77. S. Hamberger, Plasma Physics (Journal of Nuclear Energy Part C) 5, 73 (1963).

78. S. Hamberger (private communication).

79. A. C. G. Mitchell and M. W. Zemansky, Resonance Radiation and Excited Atoms, (Cambridge Press, London, England, 1961).

80. See Reference 53, Chapters I and II.

81. See Reference 53, p. 62.

82. J. C. Slater, Quantum Theory of Atomic Structure II, (McGraw-Hill, New York, 1960), p. 87.

83. W. G. Penney, Phys. Rev. 39, 467 (1932).

84. D. R. Hartree and W. Hartree, Proc. Roy. Soc. 149 A, 210 (1935).

85. D. F. Mayers, Proc. Roy. Soc. 241 A, 93 (1957).

86. B. Mishra, Proc. Cambridge Phil. Soc. 48, 511 (1952).

87. J. C. Slater, Phys. Rev. 36, 57 (1930).

88. D. R. Hartree, The Calculation of Atomic Structures, (John Wiley and Sons, New York, 1957), 71.

89. B. Yavorsky, J. Phys. U.S.S.R. 10, 476 (1946).